Outline

Surface, interface, and nanoscience—short introduction

Some surface concepts and techniques→why photoemission?

Synchrotron radiation: experimental aspects

Electronic structure—a brief review

The basic synchrotron radiation techniques: more details

→ --Instrumentation for PS

Core-level photoemission

Valence-level photoemission

Microscopy with photoemission

Electron Spectroscopy—A typical configuration

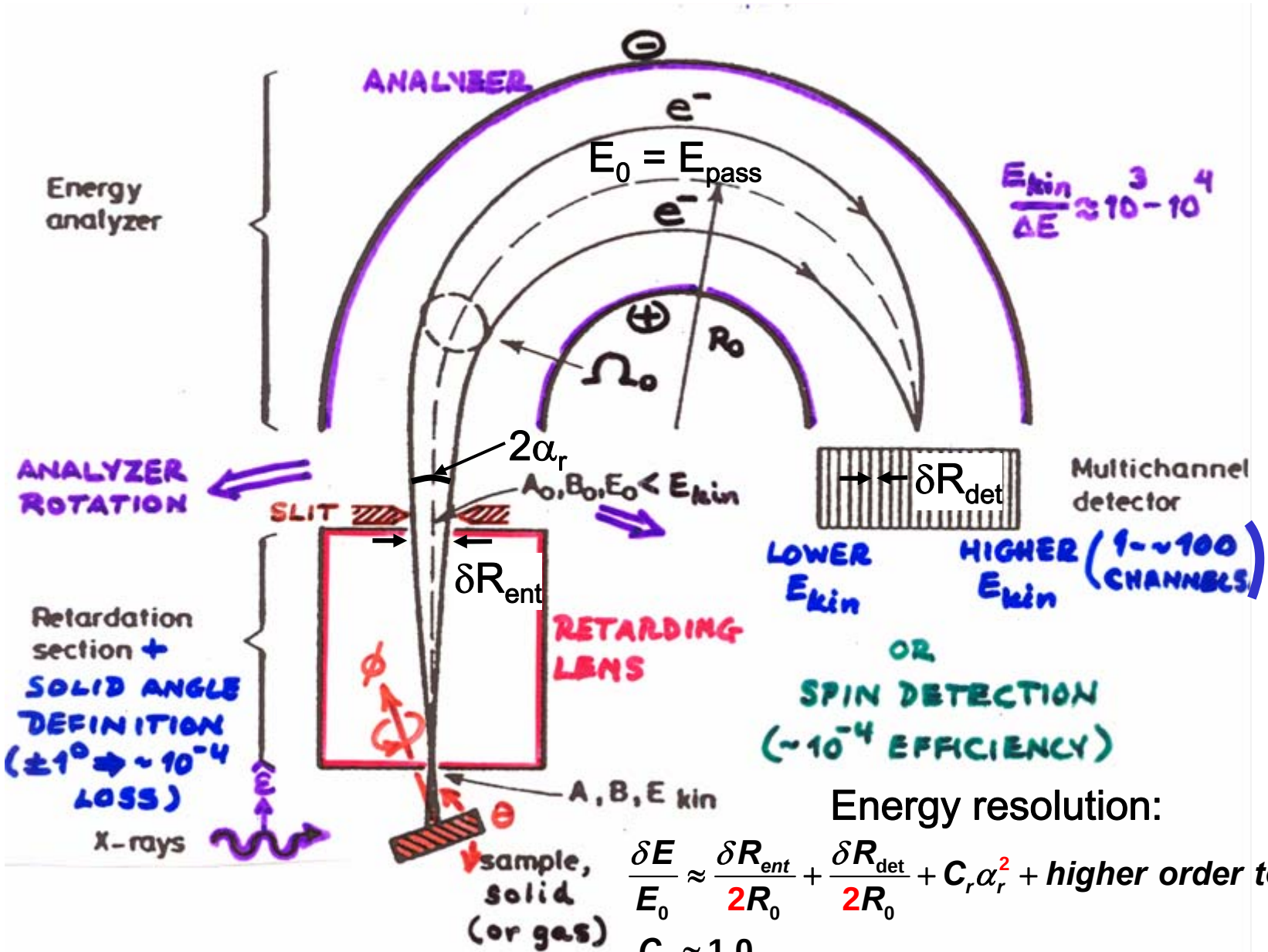

Energy resolution:

$$\frac{\delta E}{E_0} \approx \frac{\delta R_{ent}}{2R_0} + \frac{\delta R_{det}}{2R_0} + C_r \alpha_r^2 + \textit{higher order terms}$$

$$C_r \approx 1.0$$

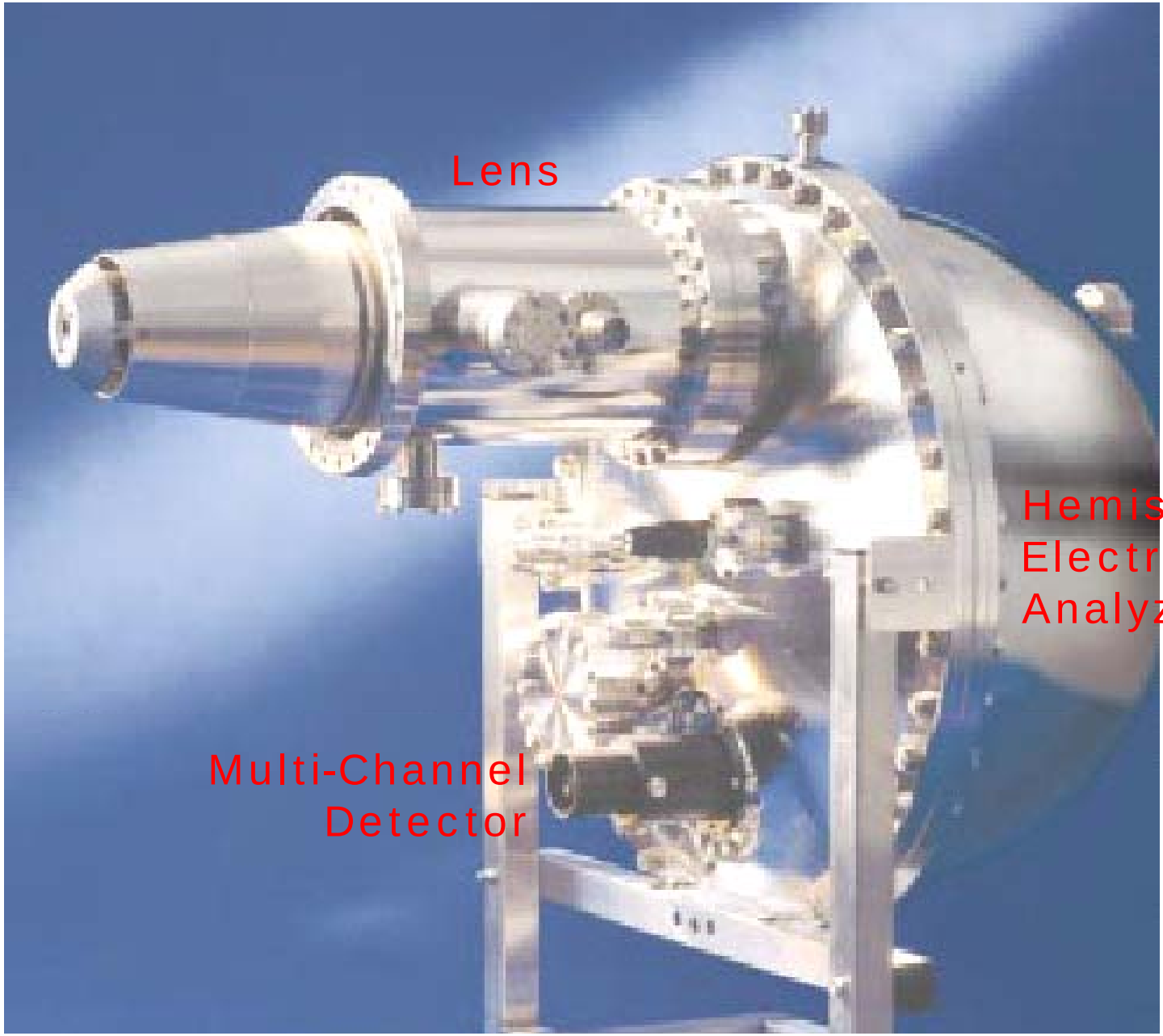

The Scienta R4000

MULTICHANNEL DETECTION GEOMETRIES

Multiple channeltrons: brute force

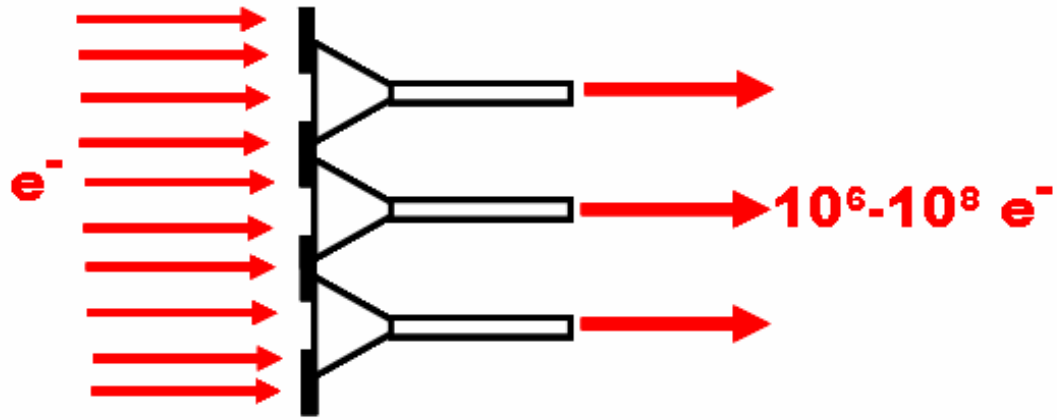

Up to ~ 1-5 MHz per channel

Microchannel plates (MCPs) and

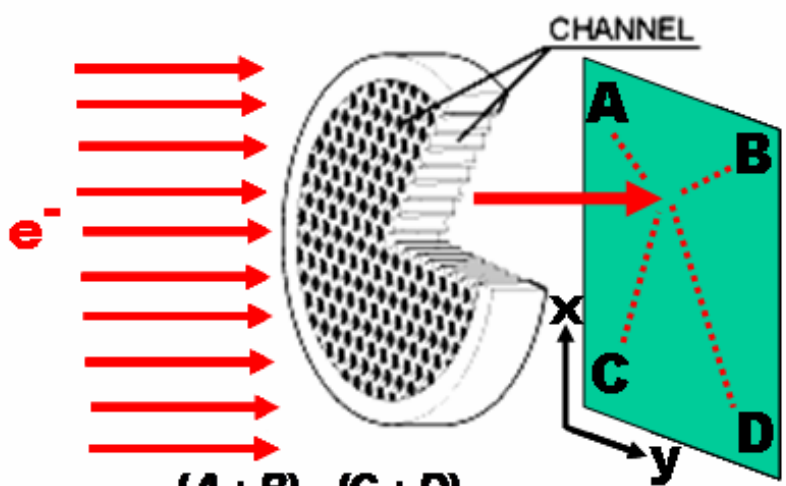

$$x = \frac{(A+B)-(C+D)}{A+B+C+D}$$

$$y = \frac{(B+D)-(A+C)}{A+B+C+D}$$

Resistive Anode—2D: Up to ~1 MHz

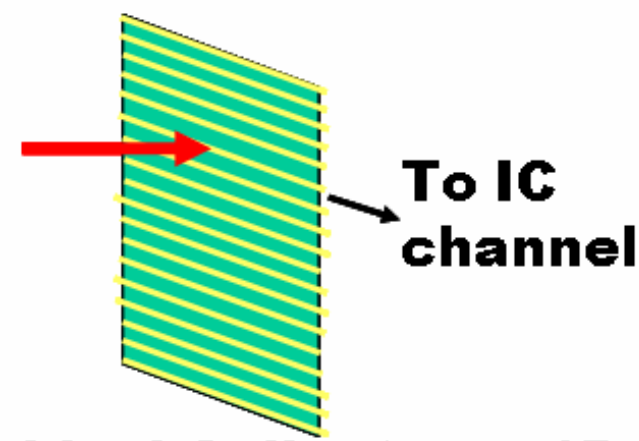

Individual Collectors—1D (Elettra and the ALS): Up to ~ 1GHz

The Microchannel Plate Electron (and Photon) Multiplier

Diam.
Down to 5
microns

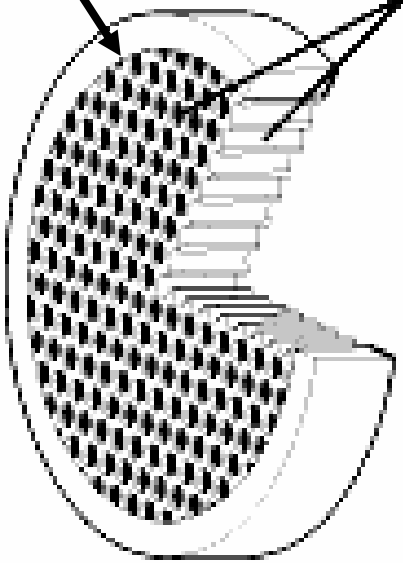

Pb-DOPED GLASS

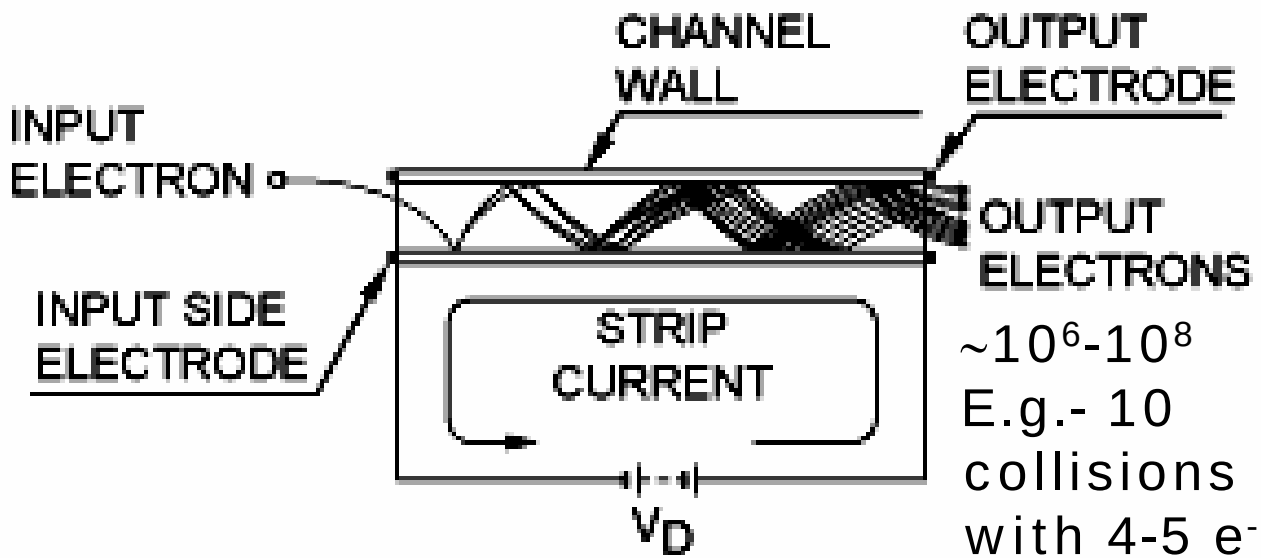

~10^6-10^8
E.g.- 10
collisions
with 4-5 e^-
each

The Next Generation: ALS High-Speed Detector

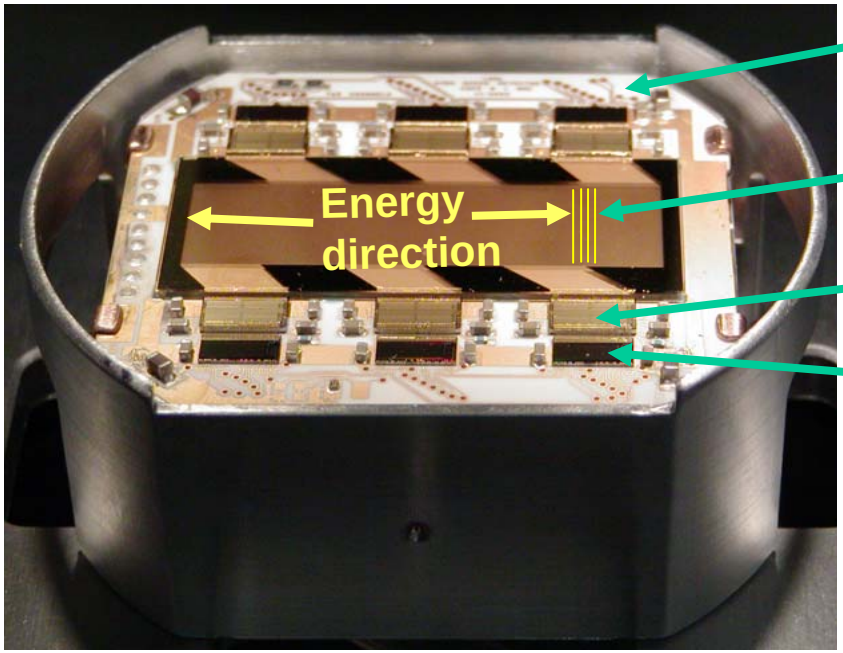

Ceramic substrate

768 collector strips

Amplifier/discriminator chip (CAFE-M) from HEP

Buffered multichannel counter chip (BMC)

Microchannel plates

e^-, $h\nu$

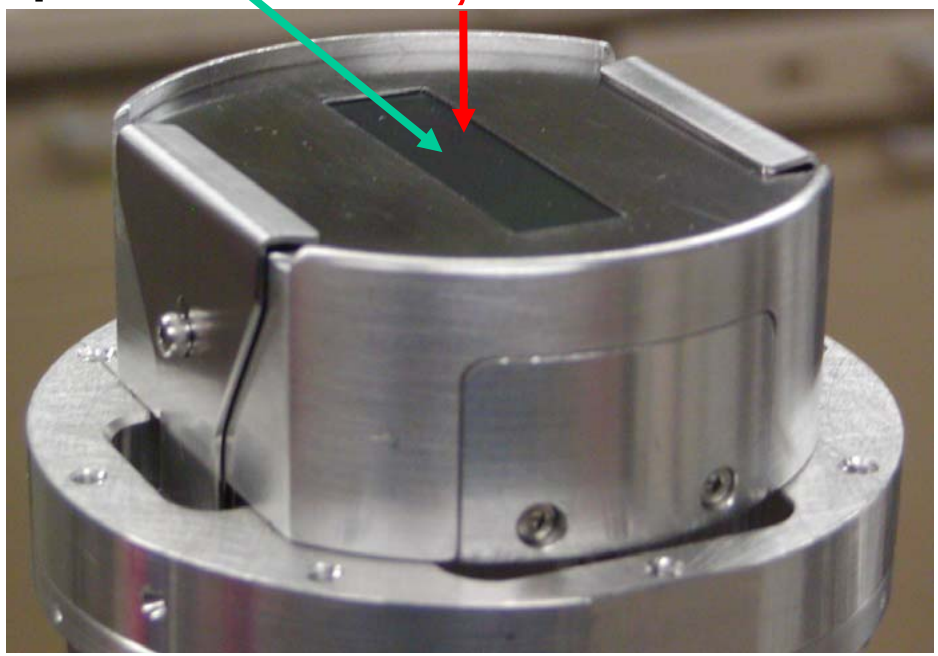

- Basic specifications:
  - 768 channels along one dimension
  - ~75 micron spatial resolution
  - >2 GHz overall linear count-rate→ 100-1000x faster than present
  - spectral readout in as little as 100 μs→ time-resolved measurements
  - programmable, robust
- Operating successfully since July, 2003

ALS High-Speed Detector--Some First Data: Photoelectron Diffraction

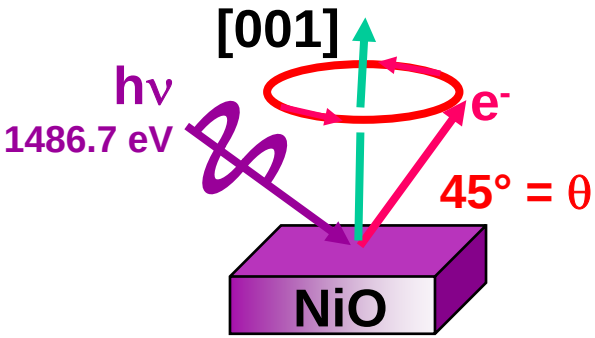

Ni 2p Spectrum

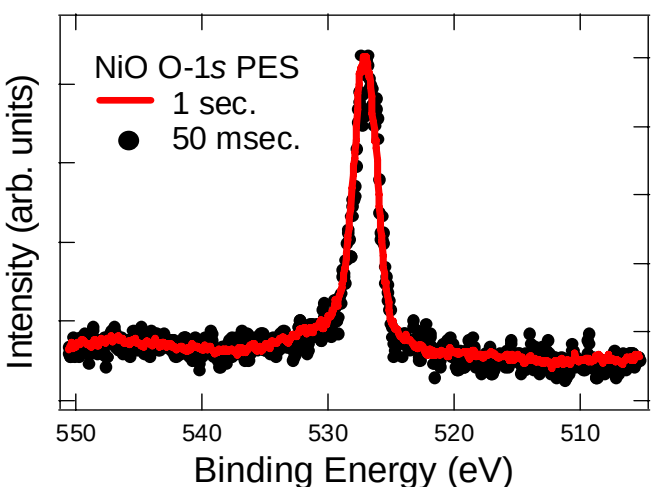

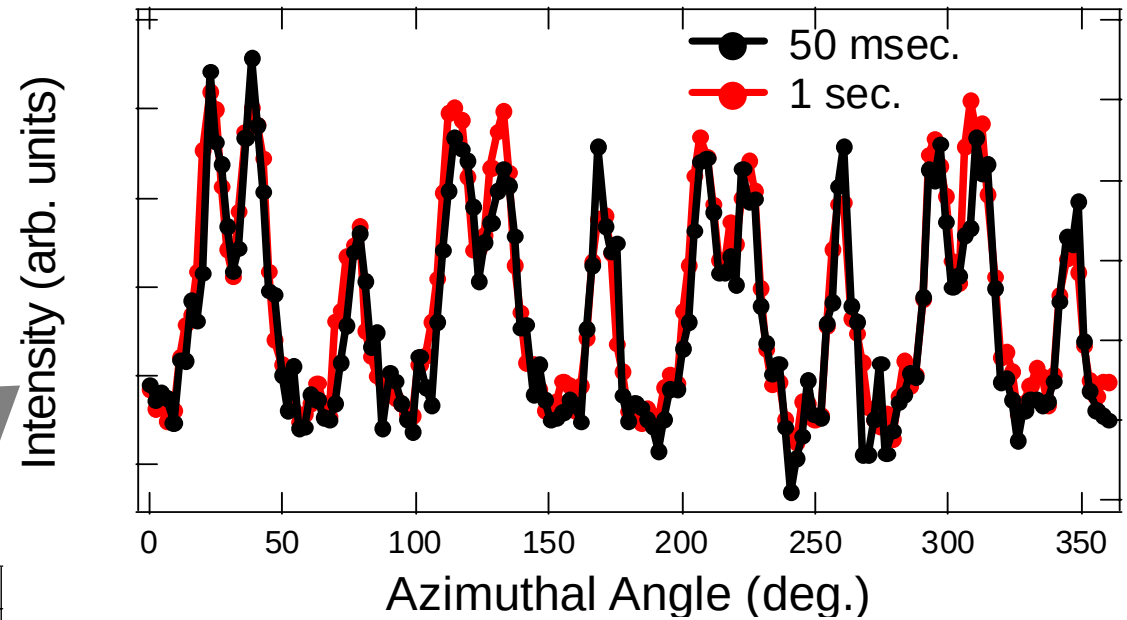

← Total 2 min. and 5min. →

→7 sec. without CPU process time and 200 microsec per spectrum with future improvement

The MicroMott Electron Spin Detector

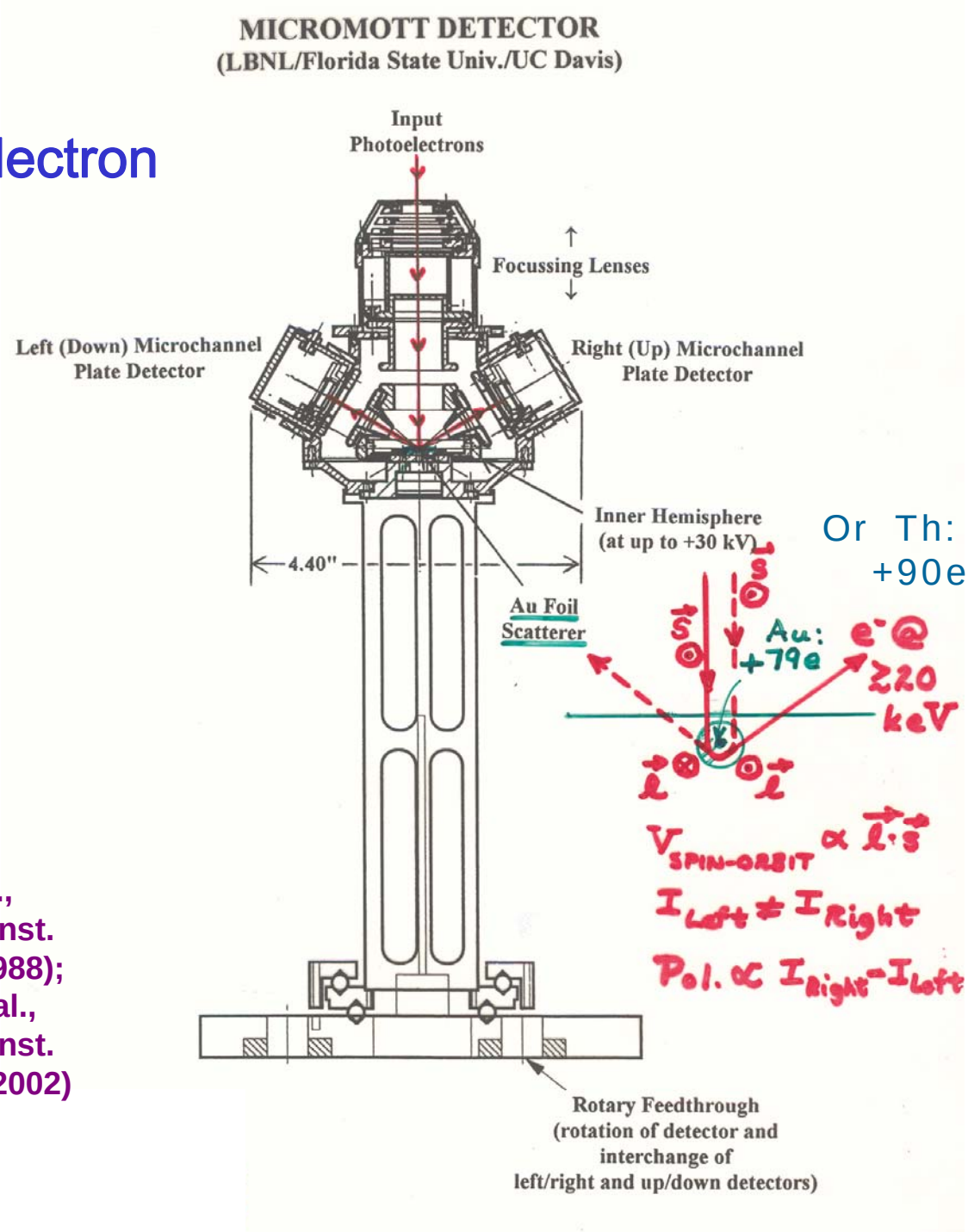

Tang et al., Rev. Sci. Inst. 59, 504 (1988); Huang et al., Rev. Sci. Inst. 73, 3778 (2002)

MULTI-TECHNIQUE PHOTOELECTRON SPECTROMETER/ DIFFRACTOMETER (MTSD)

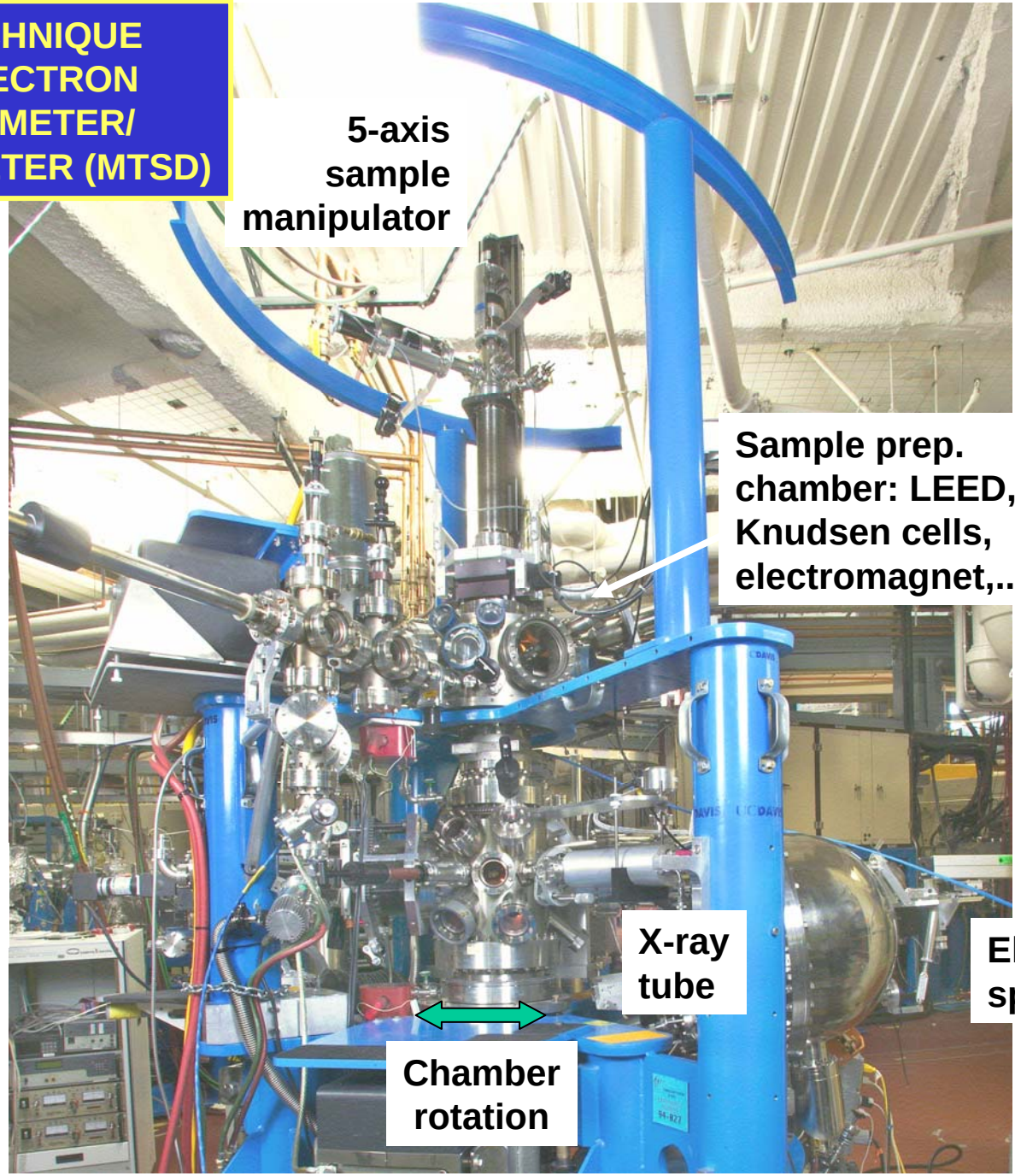

MULTI-TECHNIQUE SPECTROMETER/ DIFFRACTOMETER (APSD)

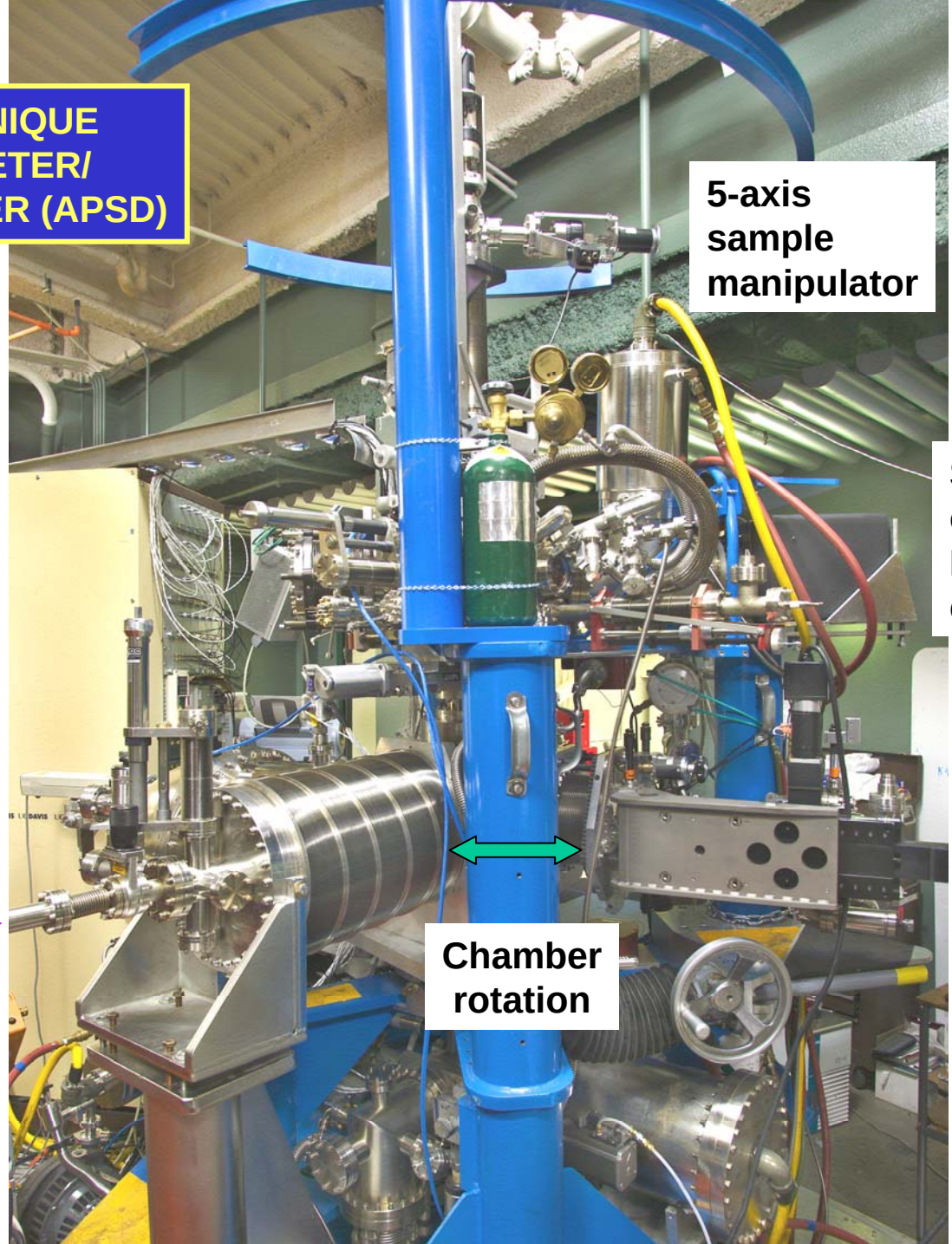

ALS
hν

φ spect

E_{kin}

Measuring Electron Binding Energies

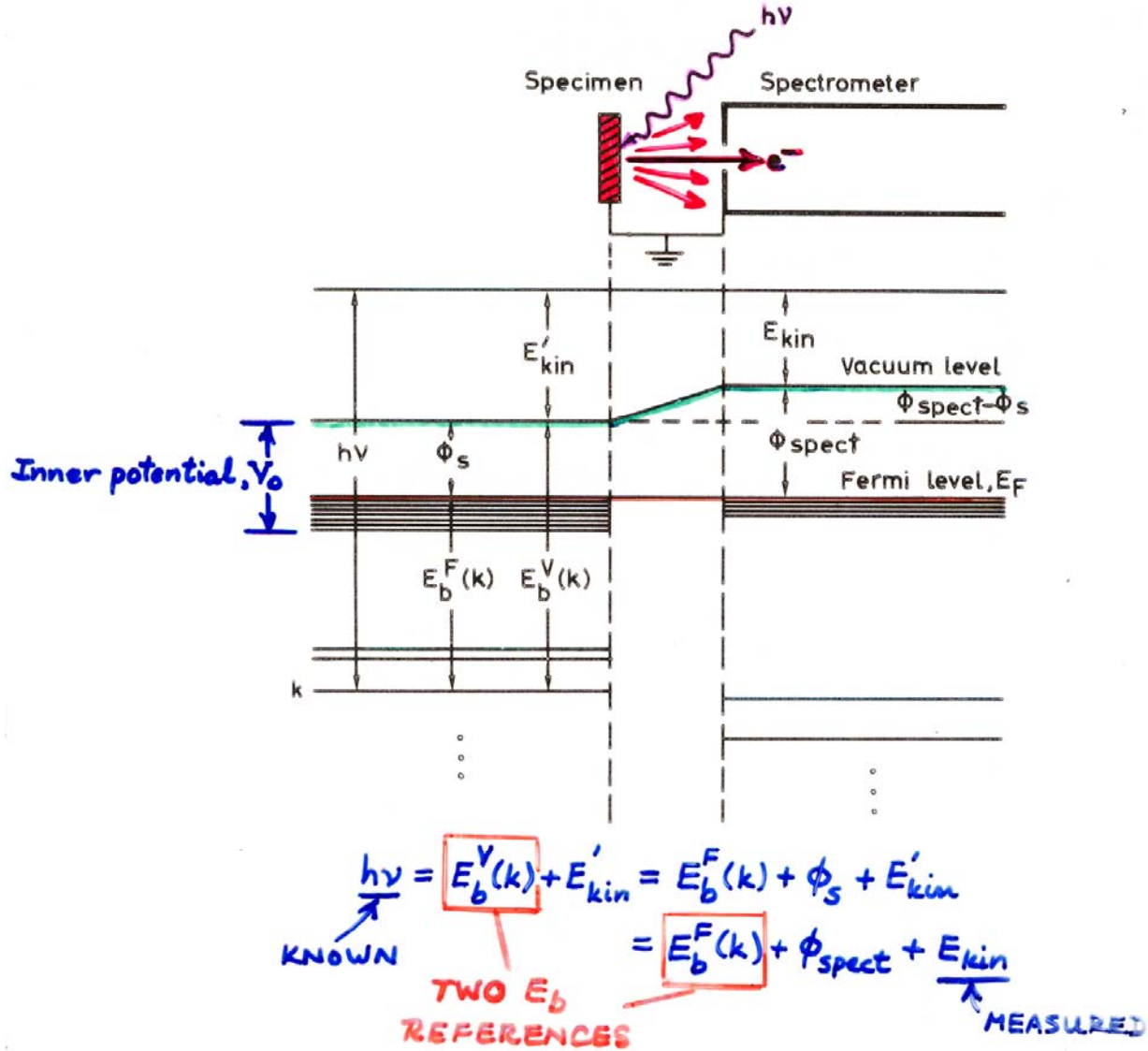

Figure 3 -- Energy level diagram for a metallic specimen in electrical equilibrium with an electron spectrometer. The closely spaced levels near the Fermi level E_F represent the filled portions of the valence bands in specimen and spectrometer. The deeper levels are core levels. An analogous diagram also applies to semiconducting or insulating specimens, with the only difference being that E_F lies somewhere between the filled valence bands and the empty conduction bands above.

"Basic Concepts of XPS"
Figure 3

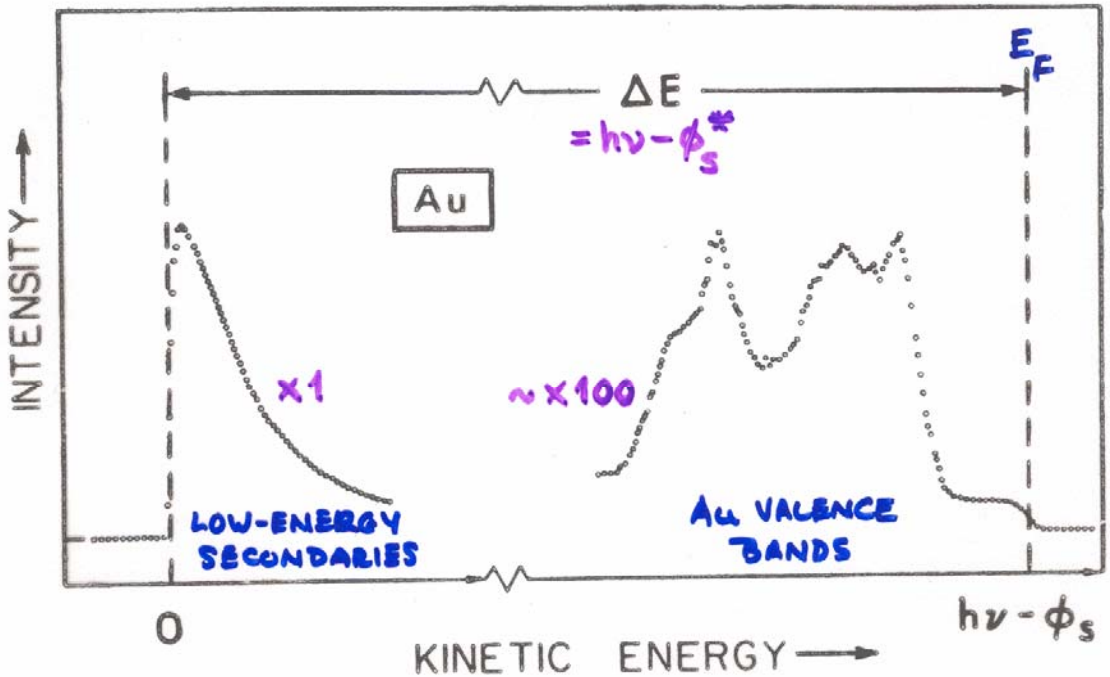

*PROVIDED $\phi_s > \phi_{spect}$ OR, IF $\phi_s < \phi_{spect}$, SAMPLE BIASSED NEGATIVELY BY $V_{BIAS} > \phi_{spect} - \phi_s$ (−)

Figure 4 -- Full XPS spectral scan for a polycrystalline Au specimen, showing both the cutoff of the secondary electron peak at zero kinetic energy and the high-energy cutoff for emission from levels at the metal Fermi level. The measureable distance ΔE thus equals $h\nu-\phi_s$, provided that suitable specimen biasing has been utilized. For this case, hν was 1253.6 eV and ϕ_s was 5.1 eV. (From Baer, reference 56).

"Basic Concepts of XPS"
Figure 3

Work functions of the Elements [eV]

After L. Ley and M. Cardona, "Photoemission in Solids", Springer 1979

Low

High

1 H -																	2 He -
3 Li 2.4	4 Be 1.5											5 B 4.5	6 C 4.7	7 N -	8 O -	9 F -	10 Ne -
11 Na 2.35	12 Mg 3.6											13 Al 4.25	14 Si 4.8	15 P -	16 S -	17 Cl -	18 Ar -
19 K 2.2	20 Ca 2.8	21 Sc 3.3	22 Ti 3.95	23 V 4.1	24 Cr 4.6	25 Mn 3.8	26 Fe 4.3	27 Co 4.4	28 Ni 4.5	29 Cu 4.4	30 Zn 4.2	31 Ga 4.0	32 Ge 4.8	33 As 5.1	34 Se 4.7	35 Br -	36 Kr -
37 Rb 2.2	38 Sr 2.35	39 Y 3.3	40 Zr 3.9	41 Nb 4.0	42 Mo 4.3	43 Tc -	44 Ru 4.6	45 Rh 4.75	46 Pd 4.8	47 Ag 4.3	48 Cd 4.1	49 In 3.8	50 Sn 4.4	51 Sb 4.1	52 Te 4.7	53 I -	54 Xe -
55 Cs 1.8	56 Ba 2.5	57 La 3.3	72 Hf 3.5	73 Ta 4.1	74 W 4.5	75 Re 5.0	76 Os 4.7	77 Ir 5.3	78 Pt 5.3	79 Au 4.3	80 Hg 4.5	81 Tl 3.7	82 Pb 4.0	83 Bi 4.4	84 Po -	85 At -	86 Rn -
87 Fr -	88 Ra -	89 Ac -															

58 Ce 2.7	59 Pr -	60 Nd -	61 Pm -	62 Sm -	63 Eu -	64 Gd -	65 Tb -	66 Dy -	67 Ho -	68 Er -	69 Tm -	70 Yb -	71 Lu -
90 Th 3.3	91 Pa -	92 U 3.3	93 Np	94 Pu	95 Am	96 Cm	97 Bk	98 Cf	99 Es	100 Fm	101 Md	102 No	103 Lr

Electron Work Functions of the Elements

From the CRC-Handbook, 73rd edition (1993)

Element	Surface crystallographic orientation	Work function (eV)
Ag	polycrystalline	4.26
	(100)	4.64
	(110)	4.52
	(111)	4.74
Al	polycrystalline	4.28
	(100)	4.41
	(110)	4.06
	(111)	4.24
As		3.75
Au	polycrystalline	5.1
	(100)	5.47
	(110)	5.37
	(111)	5.31
B		4.45
Ba		2.7
Be		4.98
Bi		4.22
C		5.0

Depends on surface orientation

Measuring Electron Binding Energies: Charging Effects For Insulators

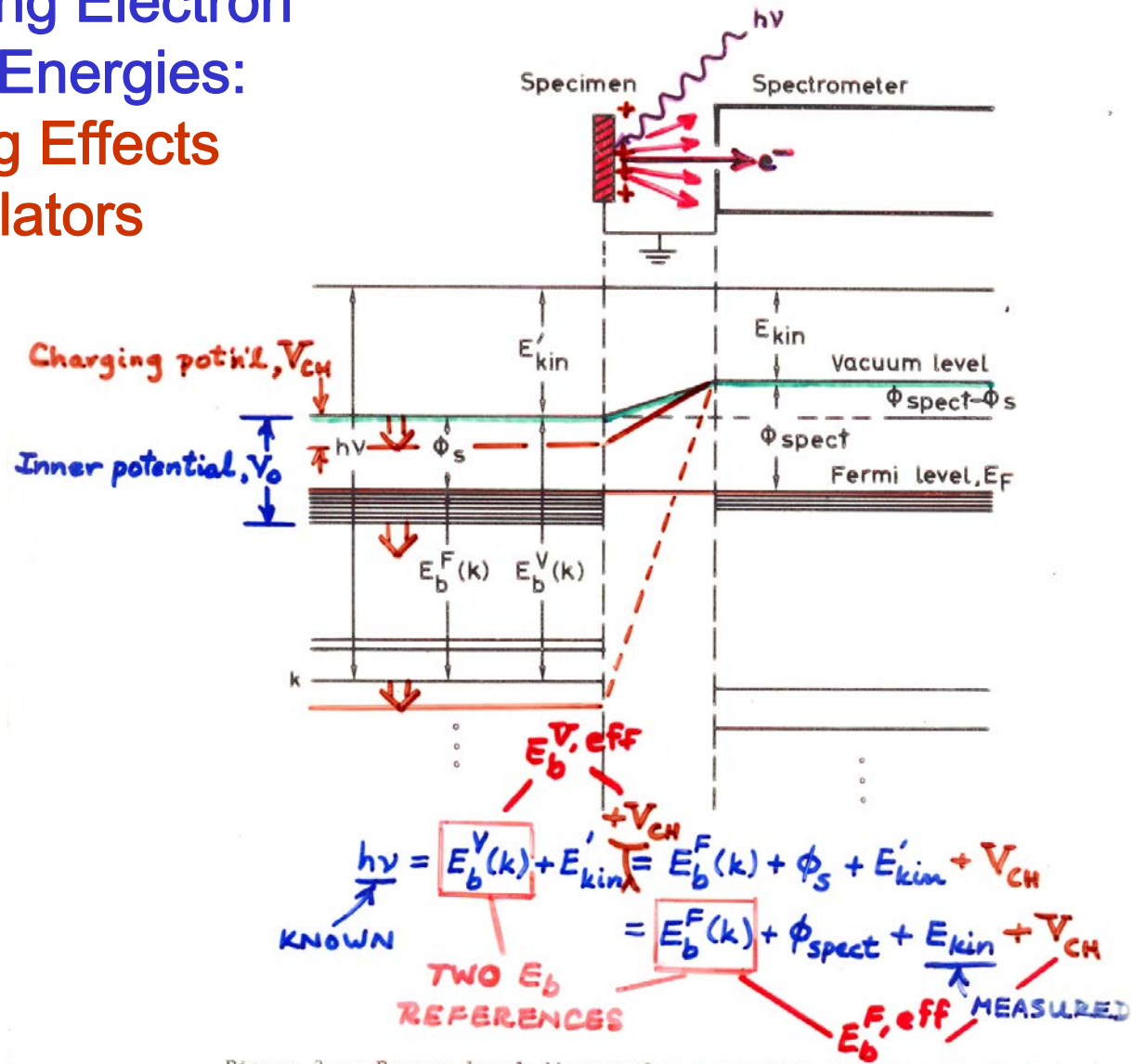

Figure 3 -- Energy level diagram for a metallic specimen in electrical equilibrium with an electron spectrometer. The closely spaced levels near the Fermi level E_F represent the filled portions of the valen bands in specimen and spectrometer. The deeper levels are core levels. An analogous diagram also applies to semiconducting or insulating specimens, with the only difference being that E_F lies somewhere between the filled valence bands and the empty conduction bands above.

"Basic Concepts of XPS" Figure 3

BEST CURRENT SOLUTION TO AN OLD PROBLEM: CHARGING IN INSULATORS

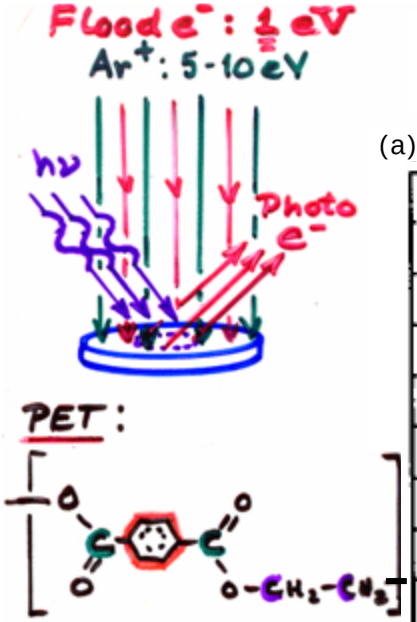

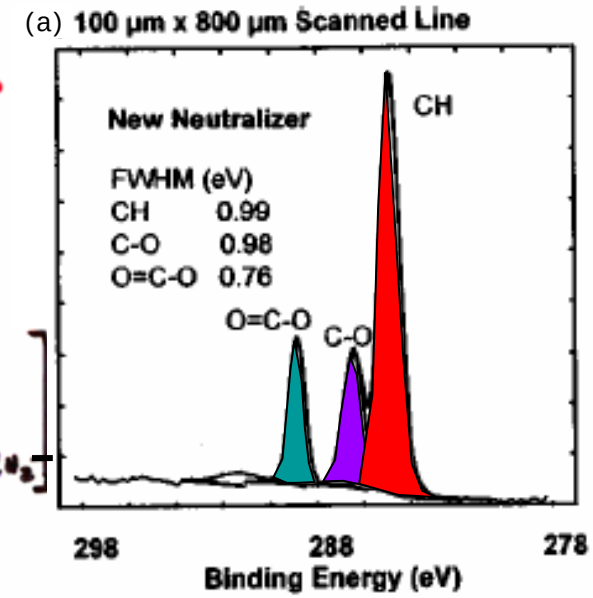

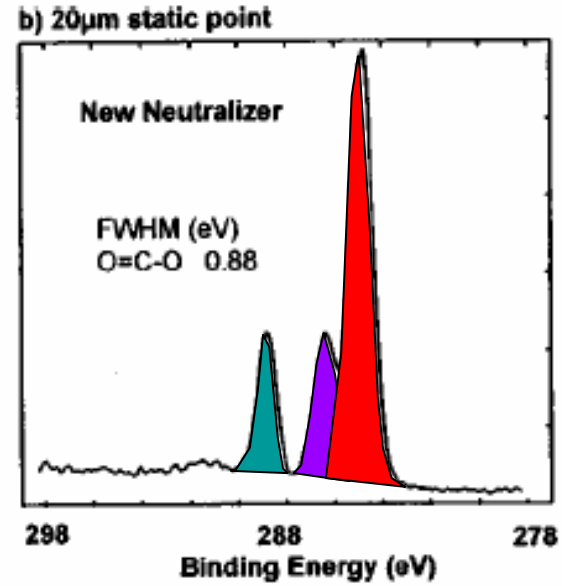

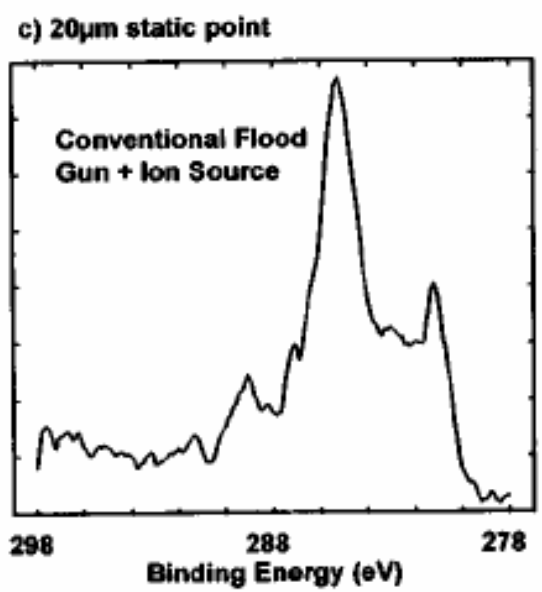

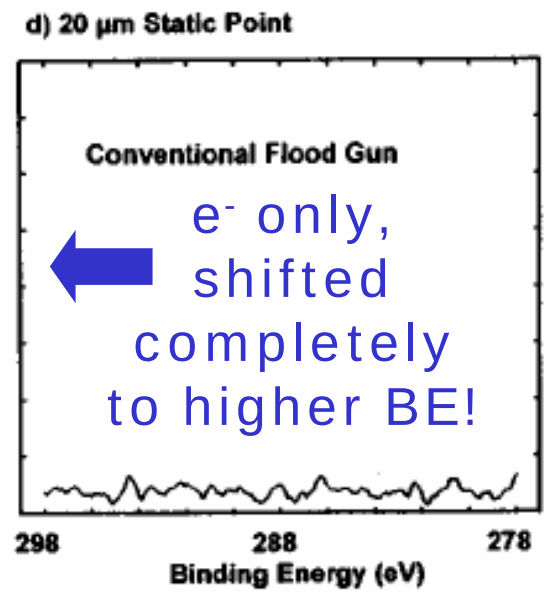

e^- only, shifted completely to higher BE!

P. LARSON, M. KELLY, J. VAC. SCI. TECH. 16, 3483 ('98)

One-Electron Picture of Photoemission from a Surface

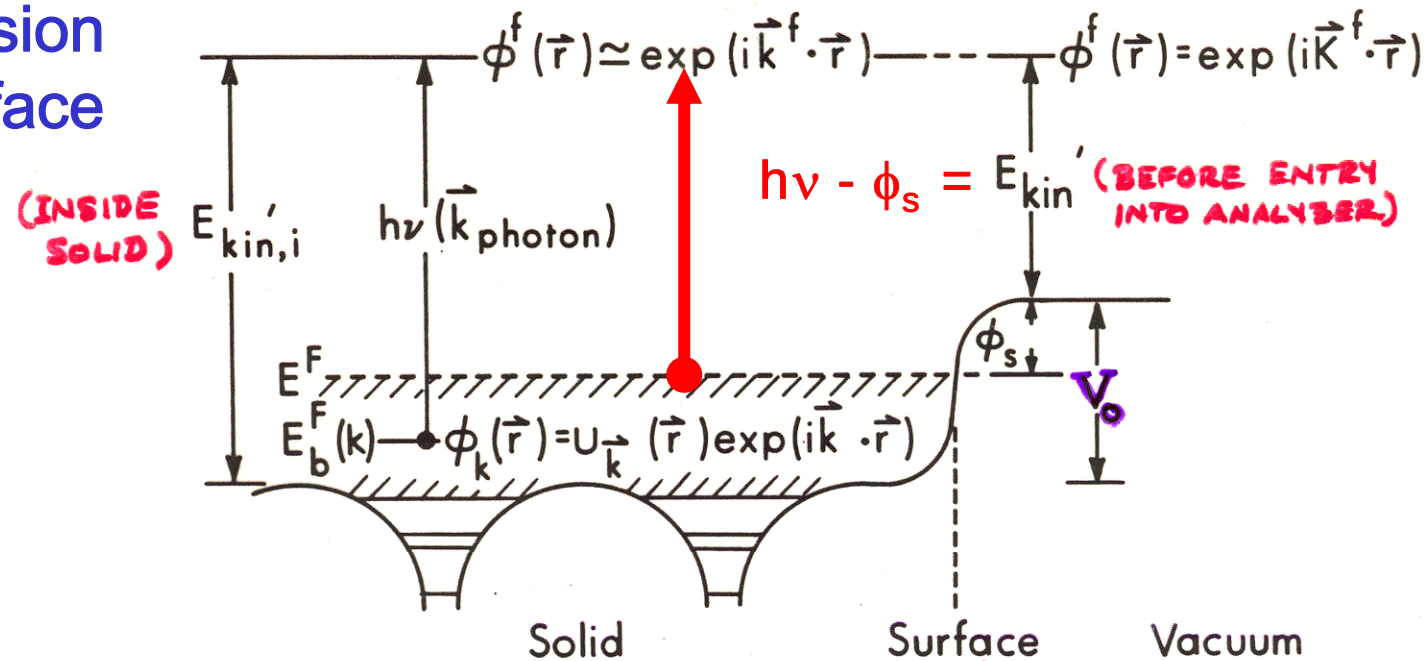

(1) $$E_{kin,i}' = h\nu - E_b^F(k) + V_o - \phi_s \simeq \frac{\hbar^2 (k^f)^2}{2m}$$

(2) $$E_{kin}' = E_{kin,i}' - V_o = \frac{\hbar^2 (K^f)^2}{2m}$$

(3) $$\vec{k} + \vec{k}_{photon} + \vec{g} = \vec{k}^f$$

$$\vec{k}_{photon} \equiv \vec{k}_{h\nu}$$

One-Electron Picture of Photoemission from a Surface

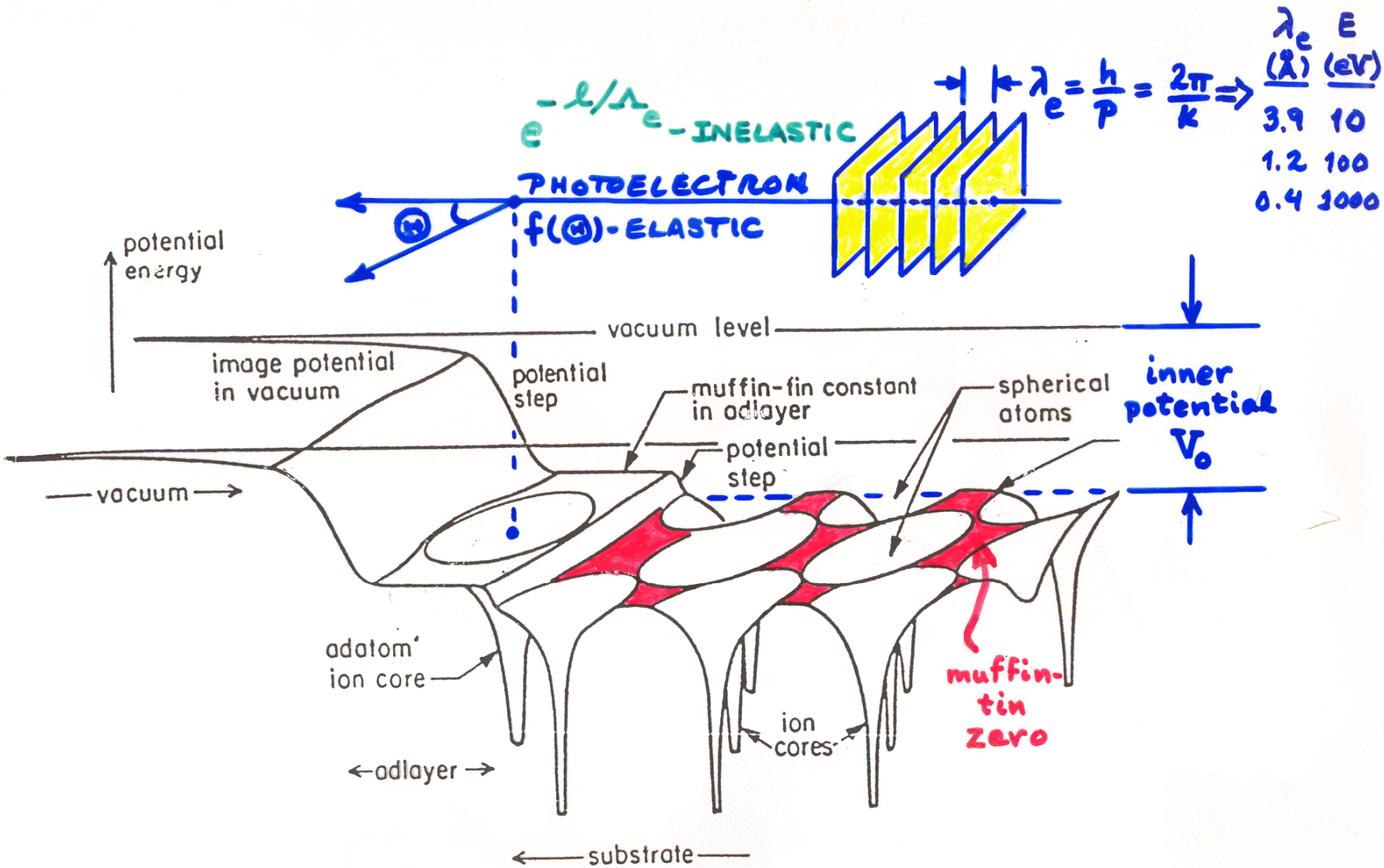

CALCULATION OF V_0 FOR AN IDEAL METAL

Fig. 4.2. Electron density profile at a jellium surface for two choices of the background density, r_s (Lang & Kohn, 1970).

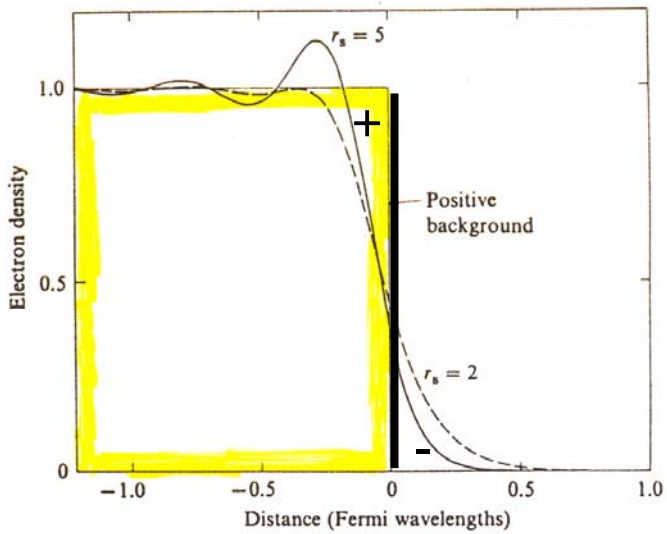

$Q = CV_{retard}$

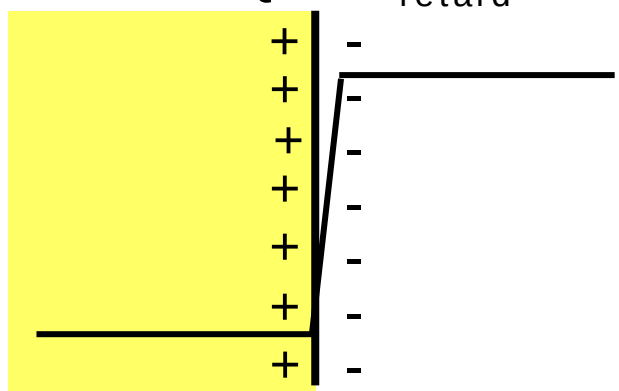

Fig. 4.3. Electrostatic potential, $v(z)$, and total effective one-electron potential, $v_{eff}(z)$, near a jellium surface (Lang & Kohn, 1970).

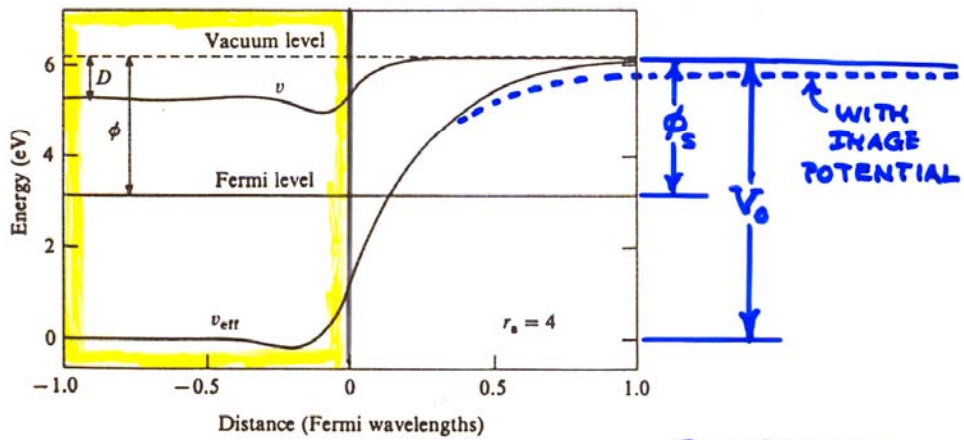

ZANGWILL, "SURFACE PHYSICS"

The electronic structure of a transition metal—fcc Cu

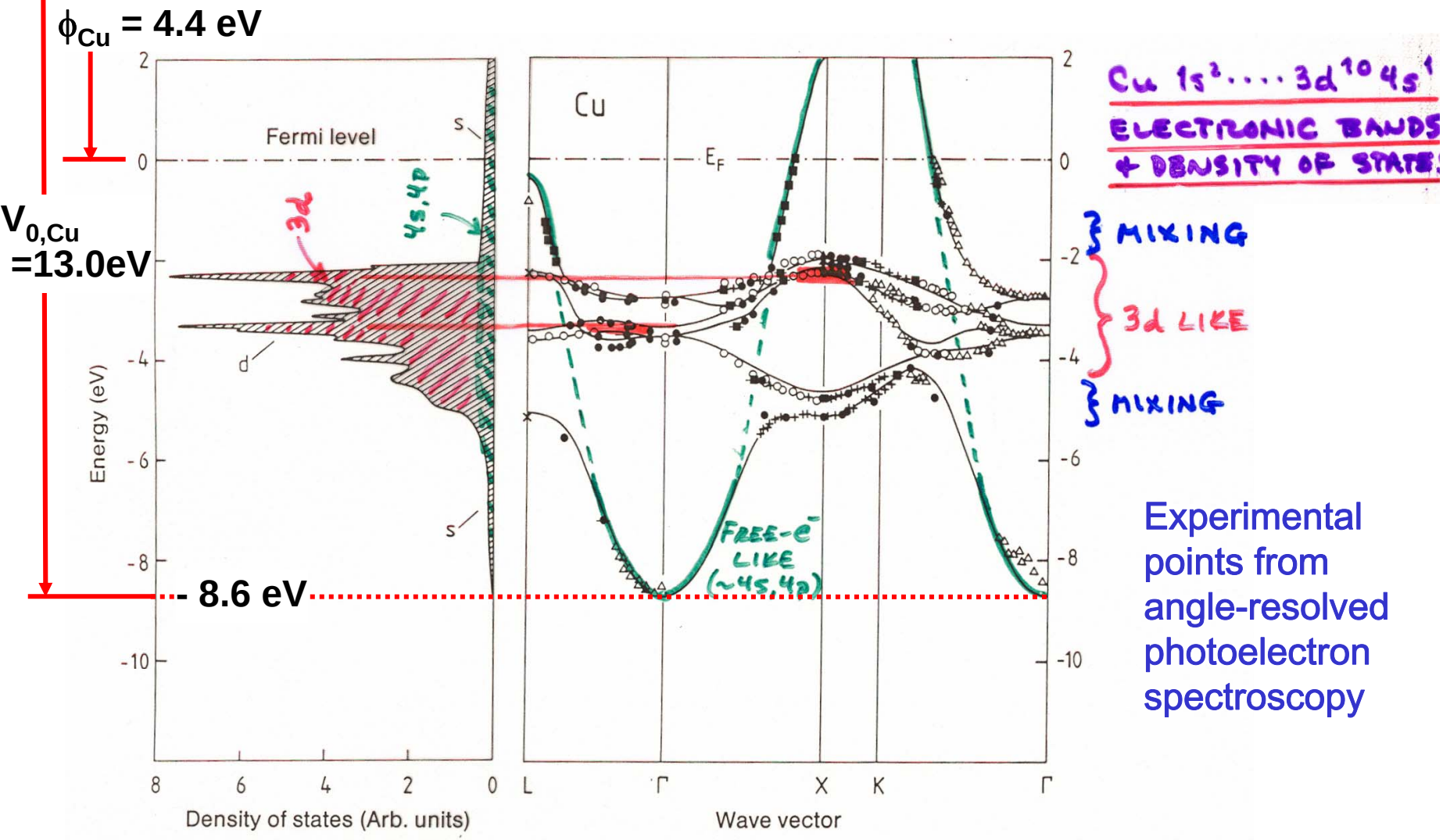

Experimental points from angle-resolved photoelectron spectroscopy

Fig. 7.12. Bandstructure $E(k)$ for copper along directions of high crystal symmetry (*right*). The experimental data were measured by various authors and were presented collectively by Courths and Hüfner [7.4]. The full lines showing the calculated energy bands and the density of states (*left*) are from [7.5]. The experimental data agree very well, not only among themselves, but also with the calculation

Outline

Surface, interface, and nanoscience—short introduction

Some surface concepts and techniques→photoemission

Synchrotron radiation: experimental aspects

Electronic structure—a brief review

The basic synchrotron radiation techniques

Core-level photoemission:
peak intensities and surface analysis

Valence-level photoemission

Microscopy with photoemission

CALCULATING INTENSITIES IN PHOTOELECTRON SPECTRA

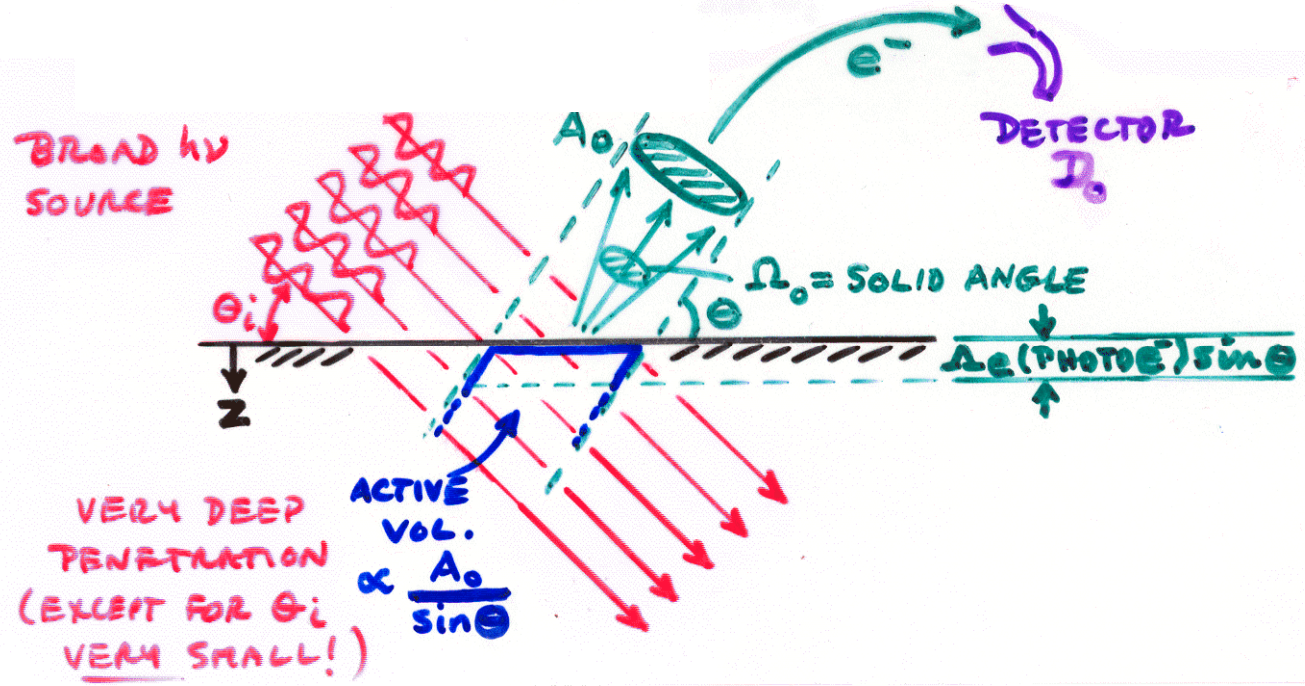

$$\text{INTENSITY} \propto \left[\begin{array}{c}\text{INCIDENT}\\ \text{EXCITING}\\ \text{FLUX}\end{array}\right] \cdot \left[\begin{array}{c}\text{DENSITY OF}\\ \text{ATOMS EX-}\\ \text{CITED}\end{array}\right] \cdot \left[\begin{array}{c}\text{ACTIVE}\\ \text{VOLUME}\end{array}\right] \cdot$$

$$\left(\frac{\text{NO.}}{\text{CM}^2\text{-SEC}}\right) \qquad \left(\frac{\text{NO.}}{\text{CM}^3}\right) \qquad (\text{CM}^3)$$

$$\left[\begin{array}{c}\text{"CROSS}\\ \text{SECTION"}\\ \text{PER ATOM}\\ \text{FOR EXCITATION}\\ \text{INTO ANALYZER}\end{array}\right] \cdot \left[\begin{array}{c}\text{PROBABILITY}\\ \text{FOR}\\ \text{NO-LOSS}\\ \text{ESCAPE}\end{array}\right] \cdot \left[\begin{array}{c}\text{PROBABILITY}\\ \text{FOR}\\ \text{DETECTION}\\ \text{IN}\\ \text{ANALYZER}\end{array}\right]$$

$$(\text{CM}^2) \qquad = e^{-z/\Lambda_e \sin\theta} \qquad \equiv D_0$$

CALCULATION OF PHOTOELECTRON INTENSITIES—THE 3-STEP MODEL

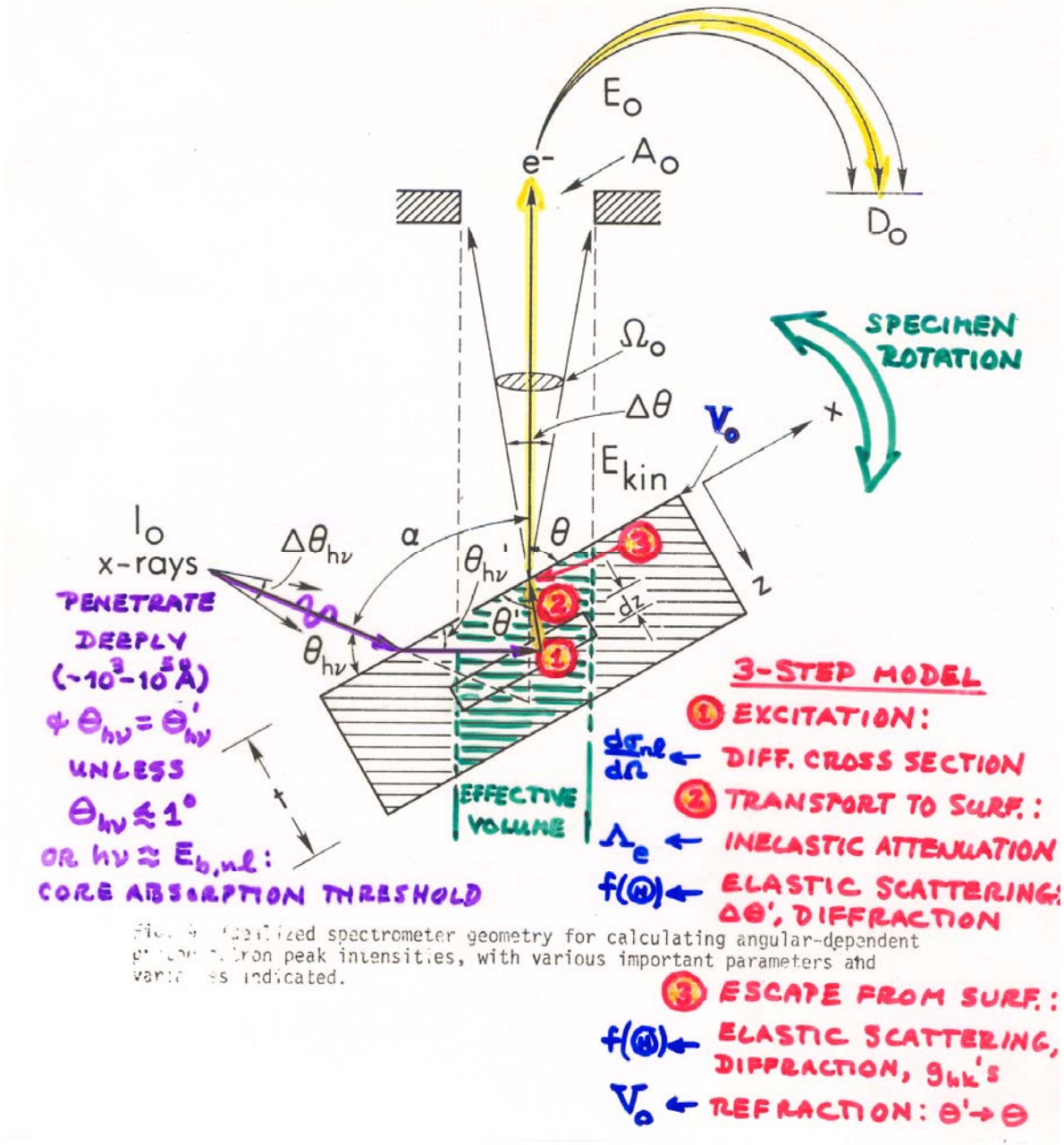

Fig. 9 Idealized spectrometer geometry for calculating angular-dependent photoelectron peak intensities, with various important parameters and variables indicated.

PHOTOELECTRON INTENSITIES FOR SOME USEFUL CASES

(a) Semi-infinite specimen, atomically clean surface, peak k with $E_{\mathrm{kin}} \equiv E_k$:

$$N_k(\theta) = I_0 \Omega_0(E_k) A_0(E_k) D_0(E_k) \rho \; \mathrm{d}\sigma_k/\mathrm{d}\Omega \; \Lambda_e(E_k) \quad (115)$$

(NO θ DEP.)

This case corresponds to an optimal measurement on a homogeneous specimen for which no surface contaminant layer is present.

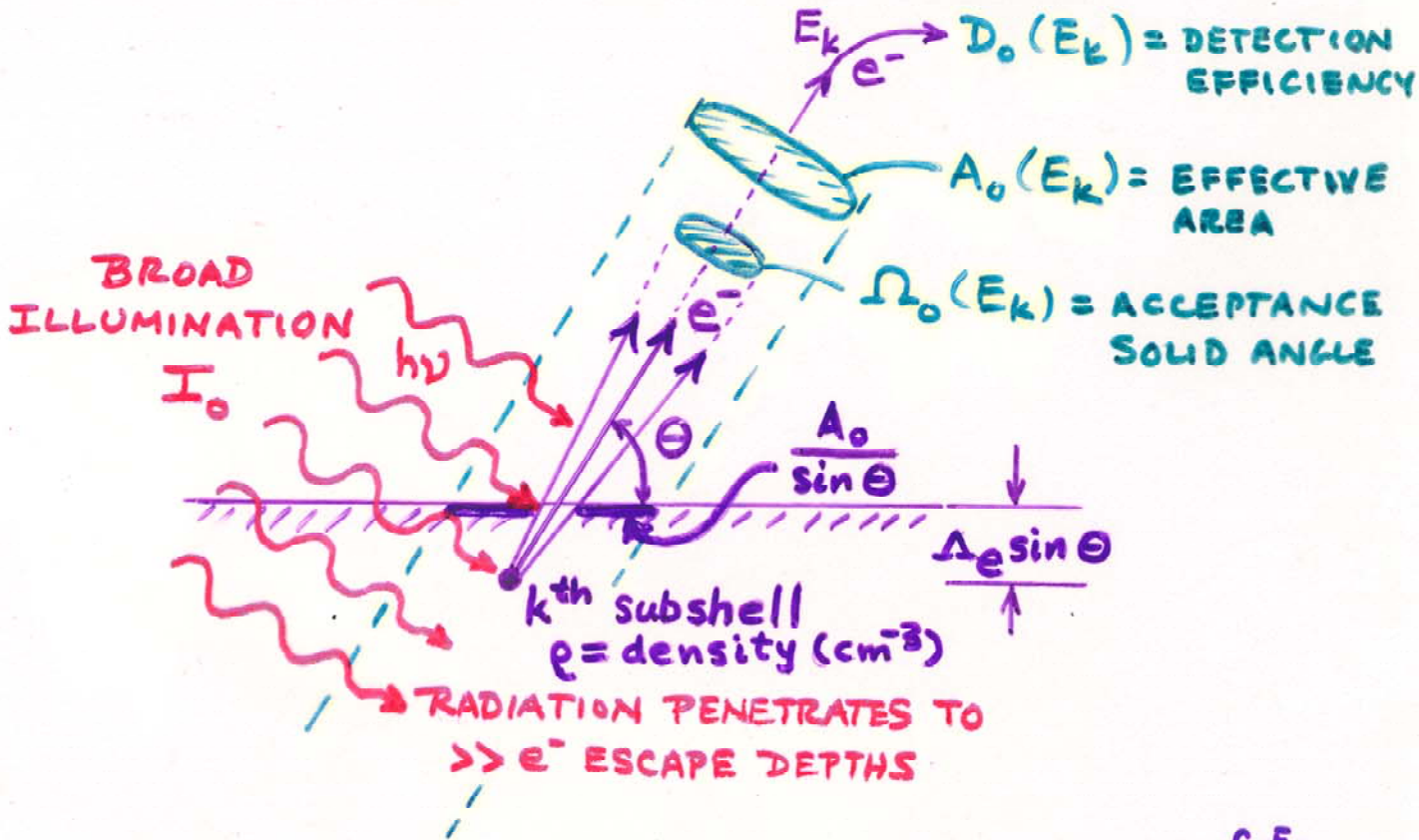

C.F.
"BASIC CONCEPTS OF XPS"
IN ELECTRON SPECT...
BRUNDLE, BAKER, EDS., '78

(b) Specimen of thickness t, atomically clean surface, peak k with $E_{\text{kin}} \equiv E_k$:

$$N_k(\theta) = I_0 \Omega_0(E_k) A_0(E_k) D_0(E_k) \rho \; \mathrm{d}\sigma_k/\mathrm{d}\Omega \; \Lambda_e(E_k) \times [1 - \exp(-t/\Lambda_e(E_k) \sin\theta)] \qquad (116)$$

Here, the intensity of a peak originating in a specimen of finite thickness is predicted to increase with decreasing θ.

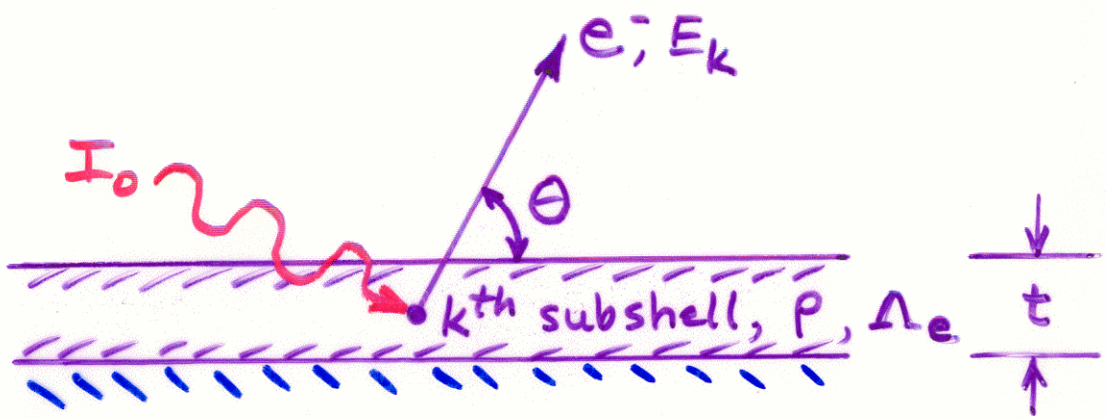

(c) Semi-infinite substrate with uniform overlayer of thickness t - Peak k from substrate with $E_{kin} \equiv E_k$:

$$N_k(\theta) = I_0 \Omega_0(E_k) A_0(E_k) D_0(E_k) \rho \, d\sigma_k/d\Omega \, \Lambda_e(E_k) \times \exp(-t/\Lambda_e'(E_k) \sin\theta) \qquad (117)$$

Peak l from overlayer with $E_{kin} \equiv E_l$:

$$N_l(\theta) = I_0 \Omega_0(E_l) A_0(E_l) D_0(E_l) \rho' \, d\sigma_l/d\Omega \, \Lambda_e'(E_l) \times [1 - \exp(-t/\Lambda_e'(E_l) \sin\theta)] \qquad (118)$$

where

$\Lambda_e(E_k)$ = an attenuation length in the substrate

$\Lambda_e'(E_k)$ = an attenuation length in the overlayer

ρ = an atomic density in the substrate

ρ' = an atomic density in the overlayer.

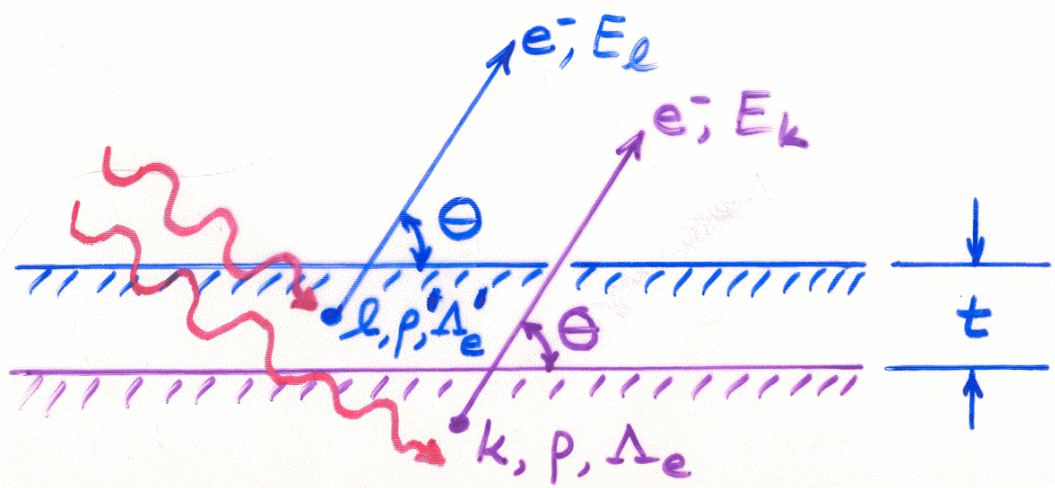

(d) Semi-infinite substrate with a non-attenuating overlayer at fractional monolayer coverage—Peak k from substrate: Eq. (115).

Peak l from overlayer:

$$N_l(\theta) = I_0 \Omega_0(E_l) A_0(E_l) D_0(E_l)\, s'(\mathrm{d}\sigma_l/\mathrm{d}\Omega)(\sin\theta)^{-1} \tag{120a}$$

Overlayer/substrate ratio:

$$\frac{N_l(\theta)}{N_k(\theta)} = \frac{\Omega_0(E_l) A_0(E_l) D_0(E_l) s'(\mathrm{d}\sigma_l/\mathrm{d}\Omega)}{\Omega_0(E_k) A_0(E_k) D_0(E_k) s\ \mathrm{d}\sigma_k/\mathrm{d}\Omega\ (\Lambda_e(E_k)\sin\theta/d)}$$

$$= \left[\frac{s'}{s}\right] \cdot \frac{D_0(E_l)\Omega_0(E_l) A_0(E_l)(\mathrm{d}\sigma_l/\mathrm{d}\Omega) d}{D_0(E_k)\Omega_0(E_k) A_0(E_k)\ \mathrm{d}\sigma_k/\mathrm{d}\Omega\ \Lambda_e \sin\theta} \tag{120b}$$

with

s' = the mean surface density of atoms in which peak l originates in cm^{-2}

s = the mean surface density of substrate atoms in $\mathrm{cm}^{-2} \equiv \rho_s$

s'/s = the fractional monolayer coverage of the atomic species in which peak l originates

d = the mean separation between layers of density s in the substrate (calculable from s/ρ).

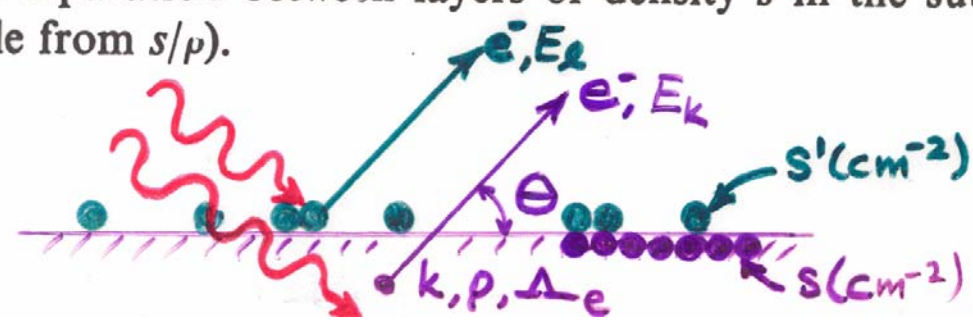

Table 4 Density and atomic concentration

The data are given at atmospheric pressure and room temperature, or at the stated temperature in deg K. (Crystal modifications as for Table 3.)

Atomic radius = r_{MT} = 0.5 n-n dist.

Average surface density = $\rho_S = (\rho_V)^{2/3}$

H 4K																	He 2K
0.088																	0.205 (at 37 atm)
Li 78K	Be											B	C	N 20K	O	F	Ne 4K
0.542	1.82											2.47	3.516	1.03			1.51
4.700	12.1											13.0	17.6				4.36
3.023	2.22												1.54			1.44	3.16
Na 5K	Mg											Al	Si	P	S	Cl 93K	Ar 4K
1.013	1.74											2.70	2.33			2.03	1.77
2.652	4.30											6.02	5.00				2.66
3.659	3.20											2.86	2.35			2.02	3.76
K 5K	Ca	Sc	Ti	V	Cr	Mn	Fe	Co	Ni	Cu	Zn	Ga	Ge	As	Se	Br 123K	Kr 4K
0.910	1.53	2.99	4.51	6.09	7.19	7.47	7.87	8.9	8.91	8.93	7.13	5.91	5.32	5.77	4.81	4.05	3.09
1.402	2.30	4.27	5.66	7.22	8.33	8.18	8.50	8.97	9.14	8.45	6.55	5.10	4.42	4.65	3.67	2.36	2.17
4.525	3.95	3.25	2.89	2.62	2.50	2.24	2.48	2.50	2.49	2.56	2.66	2.44	2.45	3.16	2.32		4.00
Rb 5K	Sr	Y	Zr	Nb	Mo	Tc	Ru	Rh	Pd	Ag	Cd	In	Sn	Sb	Te	I	Xe 4K
1.629	2.58	4.48	6.51	8.58	10.22	11.50	12.36	12.42	12.00	10.50	8.65	7.29	5.76	6.69	6.25	4.95	3.78
1.148	1.78	3.02	4.29	5.56	6.42	7.04	7.36	7.26	6.80	5.85	4.64	3.83	2.91	3.31	2.94	2.36	1.64
4.837	4.30	3.55	3.17	2.86	2.72	2.71	2.65	2.69	2.75	2.89	2.98	3.25	2.81	2.91	2.86	3.54	4.34
Cs 5K	Ba	La	Hf	Ta	W	Re	Os	Ir	Pt	Au	Hg 227	Tl	Pb	Bi	Po	At	Rn
1.997	3.59	6.17	13.20	16.66	19.25	21.03	22.58	22.55	21.47	19.28	14.26	11.87	11.34	9.80	9.31		
0.905	1.60	2.70	4.52	5.55	6.30	6.80	7.14	7.06	6.62	5.90	4.26	3.50	3.30	2.82	2.67	—	—
5.235	4.35	3.73	3.13	2.86	2.74	2.74	2.68	2.71	2.77	2.88	3.01	3.46	3.50	3.07	3.34		
Fr	Ra	Ac															
		10.07															
—	—	2.66															
		3.76															

Density in g cm^{-3} (10^3kg m^{-3}) ⟶

Concentration in 10^{22} cm^{-3} (10^{28} m^{-3}) ⟶

Nearest-neighbor distance, in Å (10^{-10}m) ⟶

Ce	Pr	Nd	Pm	Sm	Eu	Gd	Tb	Dy	Ho	Er	Tm	Yb	Lu
6.77	6.78	7.00		7.54	5.25	7.89	8.27	8.53	8.80	9.04	9.32	6.97	9.84
2.91	2.92	2.93	—	3.03	2.04	3.02	3.22	3.17	3.22	3.26	3.32	3.02	3.39
3.65	3.63	3.66		3.59	3.96	3.58	3.52	3.51	3.49	3.47	3.54	3.88	3.43
Th	Pa	U	Np	Pu	Am	Cm	Bk	Cf	Es	Fm	Md	No	Lr
11.72	15.37	19.05	20.45	19.81	11.87								
3.04	4.01	4.80	5.20	4.26	2.96	—	—	—	—	—	—	—	—
3.60	3.21	2.75	2.62	3.1	3.61								

Surface sensitivity enhancement for grazing exit angles

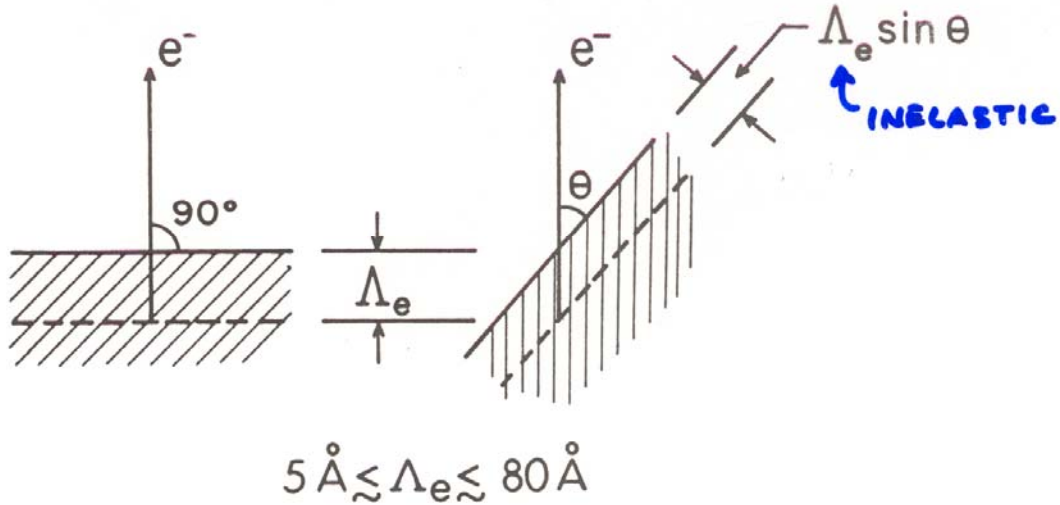

Fig. 5. Illustration of the basic mechanism producing surface sensitivity enhancement for low electron exit angles θ. The average depth for no-loss emission as measured perpendicular to the surface is $\Lambda_e \sin\theta$.

E.g.- $\Lambda_e = 28$ Å in Au(s) at 1400 eV

	θ	Mean Depth	No. layers
"BULK" →	90°	28 Å	~9
"SURFACE" →	10°	~4.4 Å	~1.5

... BUT REFRACTION AT SURFACE AND ELASTIC SCATTERING CAN REDUCE SURFACE ENHANCEMENT, ESP. AT LOW $\theta \lesssim 30°$

Surface sensitivity enhancement for grazing exit angles

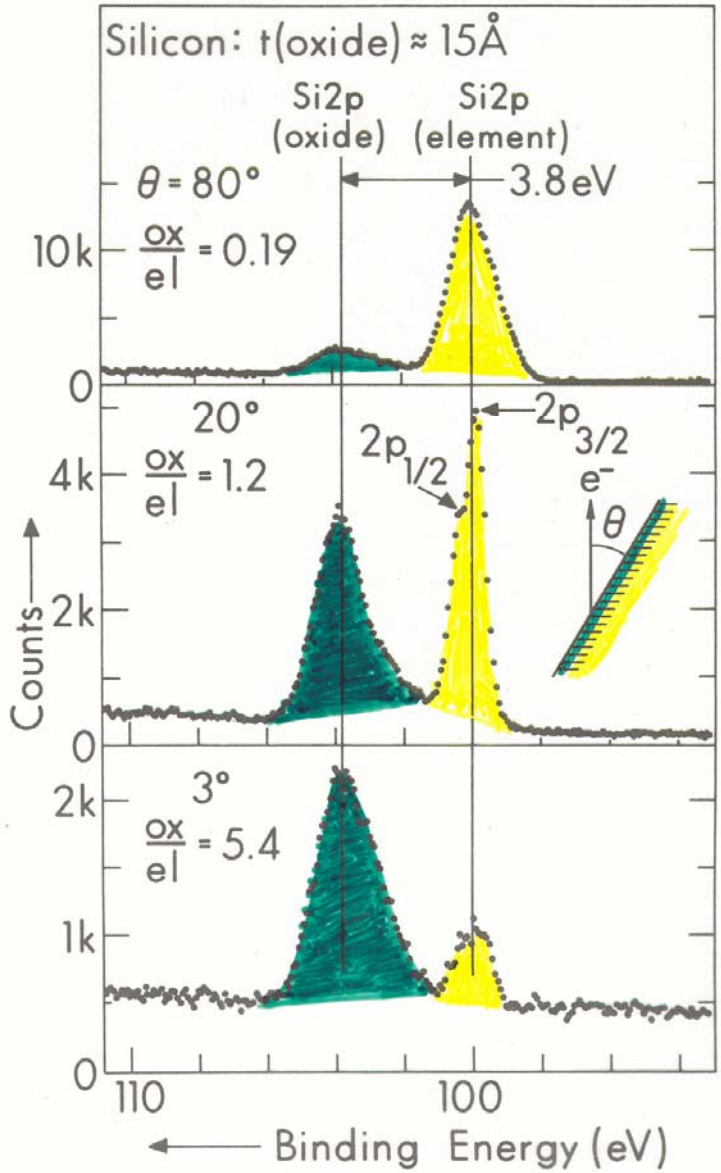

Fadley, Progress in Surface Science, 16, 275 ('84)

Fig. 7. Si2p spectra at three electron exit angles for a Si specimen with a 15-Å thick oxide overlayer. Note the complete reversal of the relative intensities of oxide and element between high and low θ. (From Hill et al., ref. (19).)

Surface sensitivity enhancement for grazing exit angles

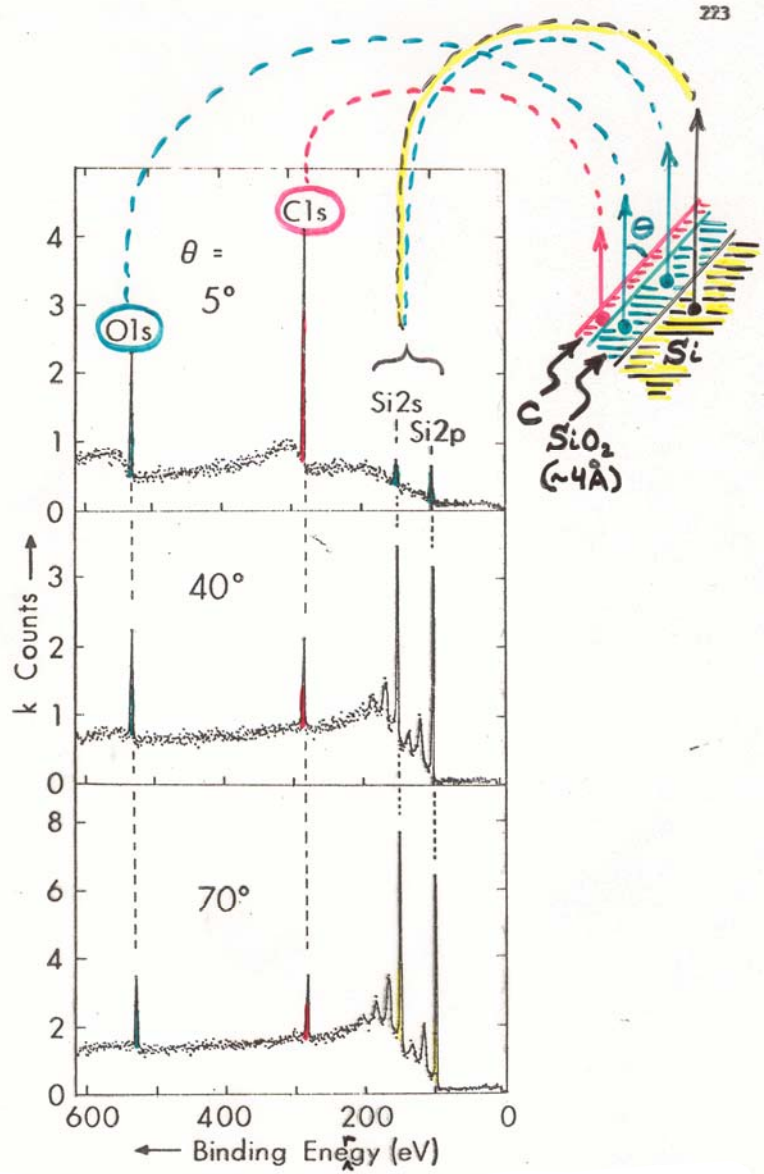

Figure 44 -- Broad-scan core spectra at low and high exit angles for a Si specimen with a thin oxide overlayer (~ 4Å) and an outermost carbon contaminant overlayer approximately 1-2 monolayers in thickness. The Cls and Ols signals are markedly enhanced in relative intensity at low θ due to the general effect presented in Figure 43. (From Fadley, reference 17.)

CALCULATION OF PHOTOELECTRON INTENSITIES—THE 3-STEP MODEL

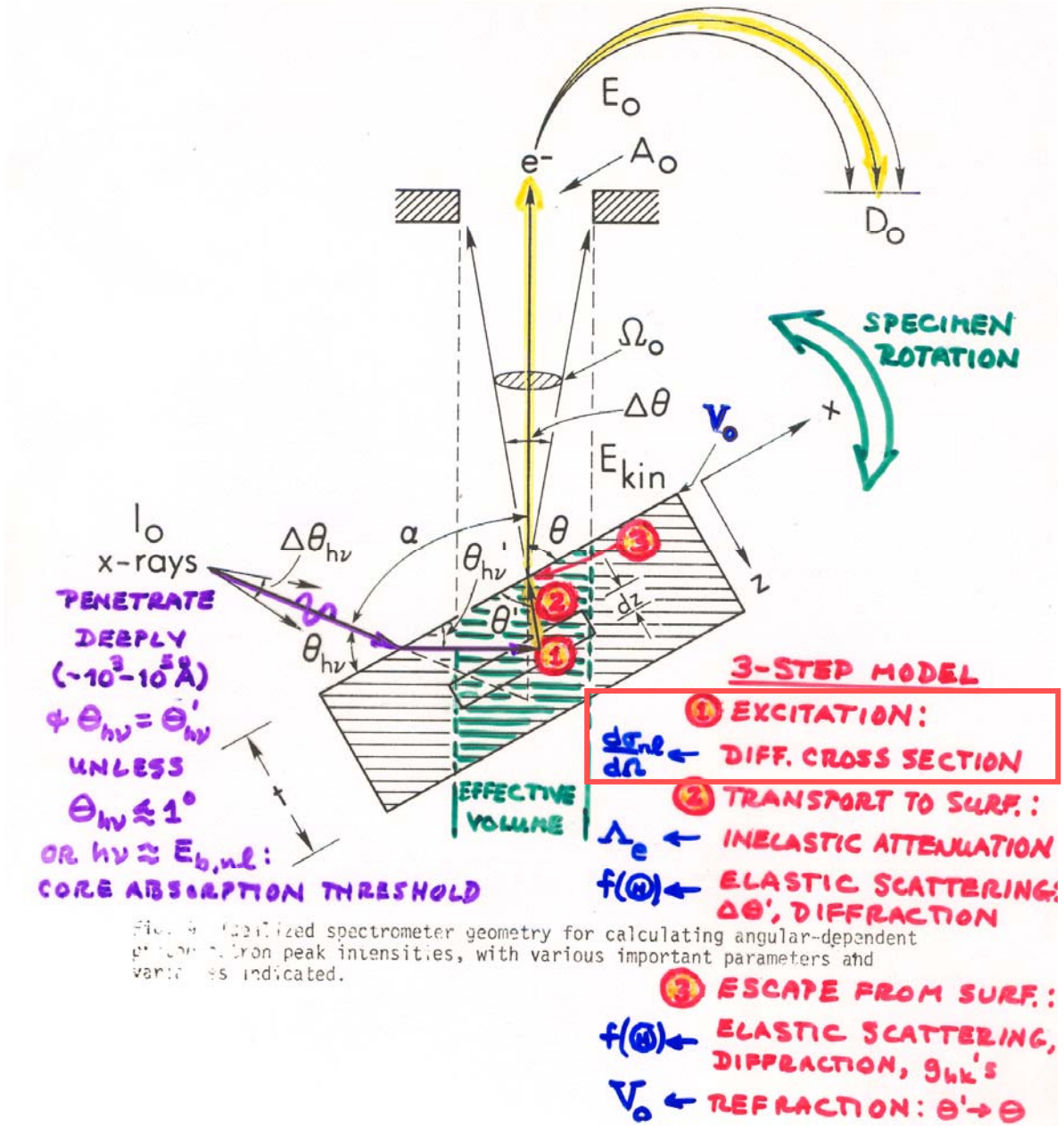

Fig. 9 Idealized spectrometer geometry for calculating angular-dependent photoelectron peak intensities, with various important parameters and variables indicated.

PHOTOELECTRON EMISSION – BASIC MATRIX ELEMENTS + SELECTION RULES:

- **ATOMIC-LIKE (LOCALIZED) STATES ⇒ CORE:**

$$\varphi_i(\vec{r}) = \varphi_{n_i l_i m_i}(r,\theta,\phi) = R_{n_i l_i}(r)\, Y_{l_i m_i}(\theta,\phi) \begin{cases} \alpha(\sigma) = m_{si} = +½ = \uparrow \\ \beta(\sigma) = m_{si} = -½ = \downarrow \end{cases}$$

PLUS SPIN:

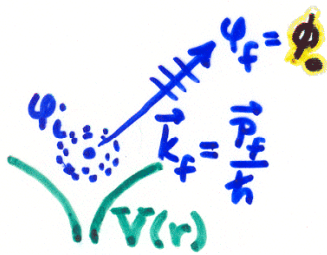

$$\varphi_f(\vec{r},\vec{k}_f) = \varphi_{E_f}(\vec{r},\vec{k}_f) \begin{cases} \alpha(\sigma) \\ \beta(\sigma) \end{cases}$$

PHASE SHIFT OF l_f WAVE IN $V(r)$

$$= 4\pi \sum_{l_f, m_f} i^{l_f} e^{-i\delta_{l_f}} Y^*_{l_f m_f}(\theta_{k_f}, \phi_{k_f})\, Y_{l_f m_f}(\theta,\phi)\, R_{E_f, l_f}(r) \begin{cases} \alpha(\sigma) \\ \beta(\sigma) \end{cases}$$

DIPOLE APPROX.: INT. $\propto |\langle \varphi_f | \hat{\varepsilon}\cdot\vec{r} | \varphi_i \rangle|^2 = |\hat{\varepsilon}\cdot\langle \varphi_f | \vec{r} | \varphi_i \rangle|^2 \Rightarrow$

- $\Delta l = l_f - l_i = \pm 1$ TWO CHANNELS
- $\Delta m = m_f - m_i = 0, \pm 1$ LINEAR POLARIZ.
- $\Delta m = \pm 1$, CIRCULAR POLARIZATION

$\Delta m_s = m_{sf} - m_{si} = 0$!

EQUIVALENT WITHIN CONSTANT FACTOR ($\vec{r} \leftrightarrow \vec{p} \leftrightarrow \vec{\nabla} V(r)$)

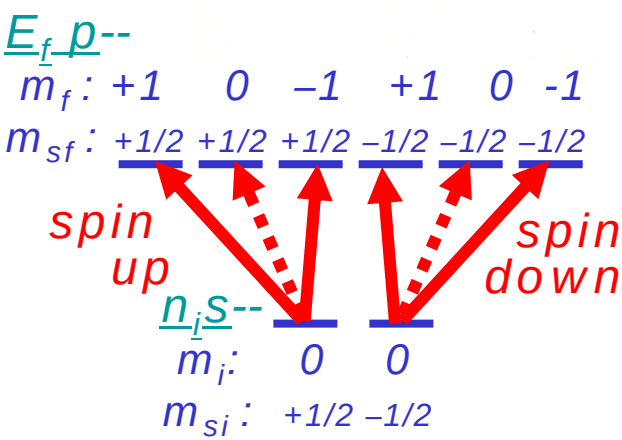

FOR A GIVEN $n_i l_i m_i m_{si}$: SUM OVER DEGENERATE INITIAL STATES $m_i m_{si}$ AND AVERAGE OVER FINAL STATES $E_f\, l_f m_f m_{sf}$ ACCESSED FROM EACH m_i TO YIELD DIFFERENTIAL SUBSHELL PHOTOELECTRIC CROSS SECTION :

$$d\sigma_{n_i l_i} / d\Omega$$

$\propto$ PROBABILITY PER UNIT SOLID ANGLE OF EXCITING ONE ELECTRON FROM SUBSHELL $n_i l_i$ INTO THE DIRECTION k_f

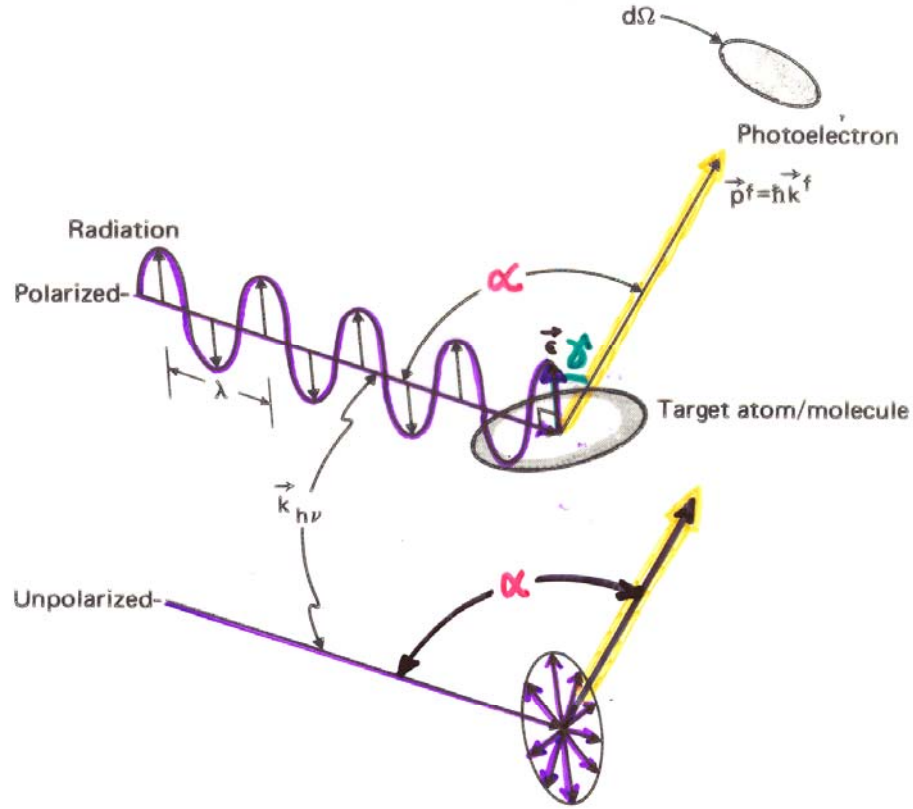

FOR ATOMIC-LIKE EMISSION:

LIN. POLARIZED: $$\frac{d\sigma_{n\ell}(E_f)}{d\Omega} = \frac{\sigma_{n\ell}(E_f)}{4\pi}\left[1 + \beta_{n\ell}(E^f)\left(\frac{3}{2}\cos^2\gamma - \frac{1}{2}\right)\right]$$

UNPOLARIZED: $$\frac{d\sigma_{n\ell}(E_f)}{d\Omega} = \frac{\sigma_{n\ell}(E_f)}{4\pi}\left[1 + \frac{1}{2}\beta_{n\ell}(E^f)\left(\frac{3}{2}\sin^2\alpha - 1\right)\right]$$

Figure 7 -- General geometry for defining the differential cross section $d\sigma/d\Omega$, showing both polarized and unpolarized incident radiation. The polarization vector $\vec{e}$ is parallel to the electric field $\vec{E}$ of the radiation. In order for the dipole approximation to be valid, the radiation wave length λ should be much larger than typical target dimensions (that is, the opposite of what is shown here).

WITH:

$\sigma_{n\ell}$ = TOTAL CROSS SECTION

$\beta_{n\ell}$ = ASYMMETRY PARAMETER

$\sigma_{n\ell}$, $\beta_{n\ell}$ TABULATIONS IN: GOLDBERG ET AL., J. ELECT. SPECT. & YEH, LINDAU, AT. NUC. DATA 22, 1 ('85) & 21, 285 ('91)

TOTAL SUBSHELL CROSS SECTION: $\int_{4\pi} \frac{d\sigma_{nl}}{d\Omega} d\Omega =$

$$\sigma_{nl}(E^f) = \frac{4\pi\alpha_0 a_0^2}{3}(h\nu)[lR_{l-1}^2(E^f) + (l+1)R_{l+1}^2(E^f)]$$

= SUM OVER ALL m_l, m_s IN SUBSHELL nl

RADIAL MATRIX ELEMENTS TO $l \pm 1$ CHANNELS:

$$R_{l\pm1}(E^f) = \int_0^\infty R_{nl}(r) r R_{E^f,\, l\pm1}(r) r^2\, dr = \int_0^\infty P_{nl}(r) r P_{E^f,\, l\pm1}(r)\, dr$$

DIFFERENTIAL CROSS SECTION: UNPOLARIZED

$$\frac{d\sigma_{nl}}{d\Omega}(E^f) = \frac{\sigma_{nl}}{4\pi}[1 - \tfrac{1}{2}\beta_{nl}(E^f)P_2(\cos\alpha)]$$

$$= \frac{\sigma_{nl}}{4\pi}[1 + \tfrac{1}{2}\beta_{nl}(E^f)(\tfrac{3}{2}\sin^2\alpha - 1)]$$

$$= A + B\sin^2\alpha$$

ASYMMETRY PARAMETER:

TERM FOR $l \pm 1$ INTERFERENCE

$$\beta_{nl}(E^f) = \frac{\{l(l-1)R_{l-1}^2(E^f) + (l+1)(l+2)R_{l+1}^2(E^f) - 6l(l+1)R_{l+1}(E^f)R_{l-1}(E^f)\cos[\delta_{l+1}(E^f) - \delta_{l-1}(E^f)]\}}{(2l+1)[lR_{l-1}^2(E^f) + (l+1)R_{l+1}^2(E^f)]}$$

$\delta_{l\pm1}(E^f)$ = CONTINUUM ORBITAL PHASE SHIFTS IN ATOMIC POTENTIAL $V(r)$

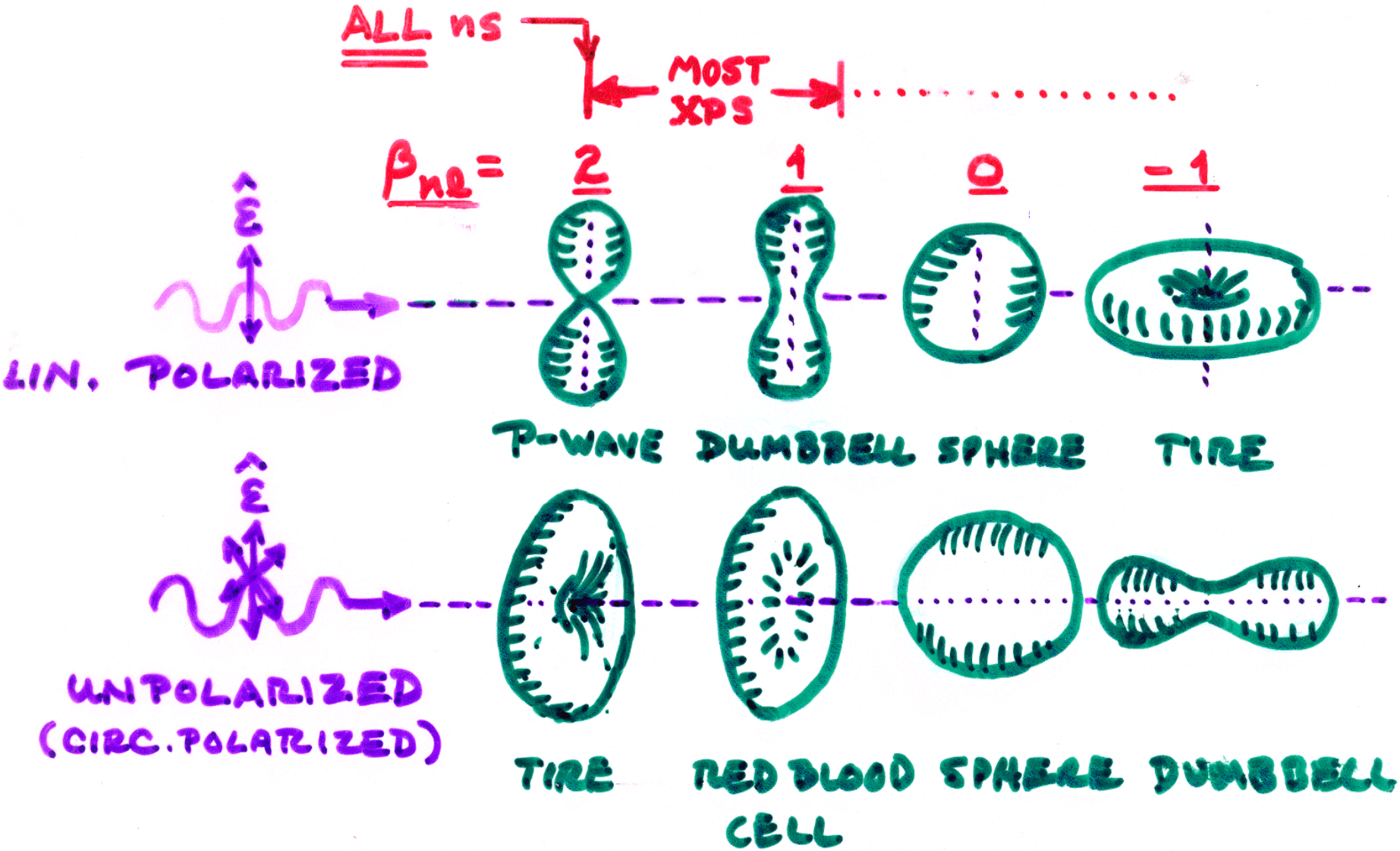

RANGE OF SHAPES OF $\frac{d\sigma}{d\Omega}$

GRAPH I. Atomic Subshell Photoionization Cross Sections for 0–1500 eV, $1 \leqslant Z \leqslant 103$

See page 6 for Explanation of Graphs

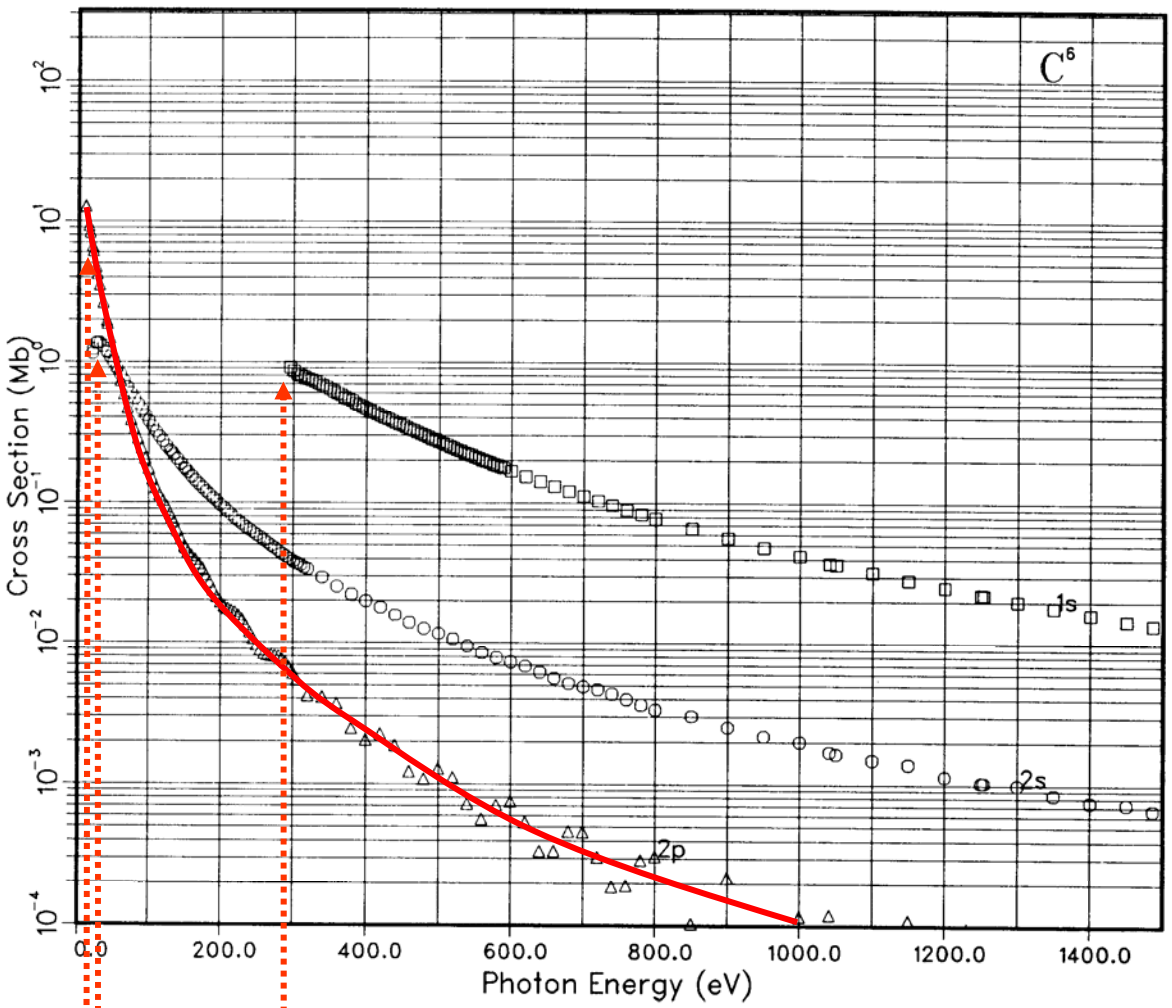

Plus other Examples from Yeh and Lindau in Sec. 1.5 of X-Ray Data Booklet, and plots for all elements at: http://ulisse.elettra.trieste.it/elements/WebElements.html

WebCrossSections - Microsoft Internet Explorer

File Edit View Favorites Tools Help

Back Search Favorites Media

Address http://ulisse.elettra.trieste.it/elements/WebElements.html Go Links

Search Web Mail My Yahoo! Games Yahoo! Personals LAUNCH Sign In

Media

Atomic Calculation of Photoionization Cross-Sections and Asymmetry Parameters

This periodic table interface was developed to easily acces the calculated atomic cross sections for photoionization and the related asymmetry parameters. The data are taken from: J.J. Yeh, *Atomic Calculation of Photoionization Cross-Sections and Asymmetry Parameters,* Gordon and Breach Science Publishers, Langhorne, PE (USA), 1993 and from J.J. Yeh and I.Lindau, *Atomic Data and Nuclear Data Tables*, **32**, 1-155 (1985). The data shown here are those calculated in the dipole length approximation.

This is a beta version: comments are welcome.

Group	1	2	3	4	5	6	7	8	9	10	11	12	13	14	15	16	17	18
	1A	2A	3B	4B	5B	6B	7B	8B			1B	2B	3A	4A	5A	6A	7A	8A
Period																		
1	1 H																	2 He
2	3 Li	4 Be											5 B	6 C	7 N	8 O	9 F	10 Ne
3	11 Na	12 Mg											13 Al	14 Si	15 P	16 S	17 Cl	18 Ar
4	19 K	20 Ca	21 Sc	22 Ti	23 V	24 Cr	25 Mn	26 Fe	27 Co	28 Ni	29 Cu	30 Zn	31 Ga	32 Ge	33 As	34 Se	35 Br	36 Kr
	37	38	39	40	41	42	43	44	45	46	47	48	49	50	51	52	53	54

Internet

Graph - Microsoft Internet Explorer

File Edit View Favorites Tools Help

Back Search Favorites Media

Address http://ulisse.elettra.trieste.it/elements/mnu_elem.cgi?ACTION=SHOWGRAPH&ELEMENT=c&C0=1s&C1=2p&C2=2s

Go Links

Search Web Mail My Yahoo! Games Yahoo! Personals LAUNCH Sign In

Media

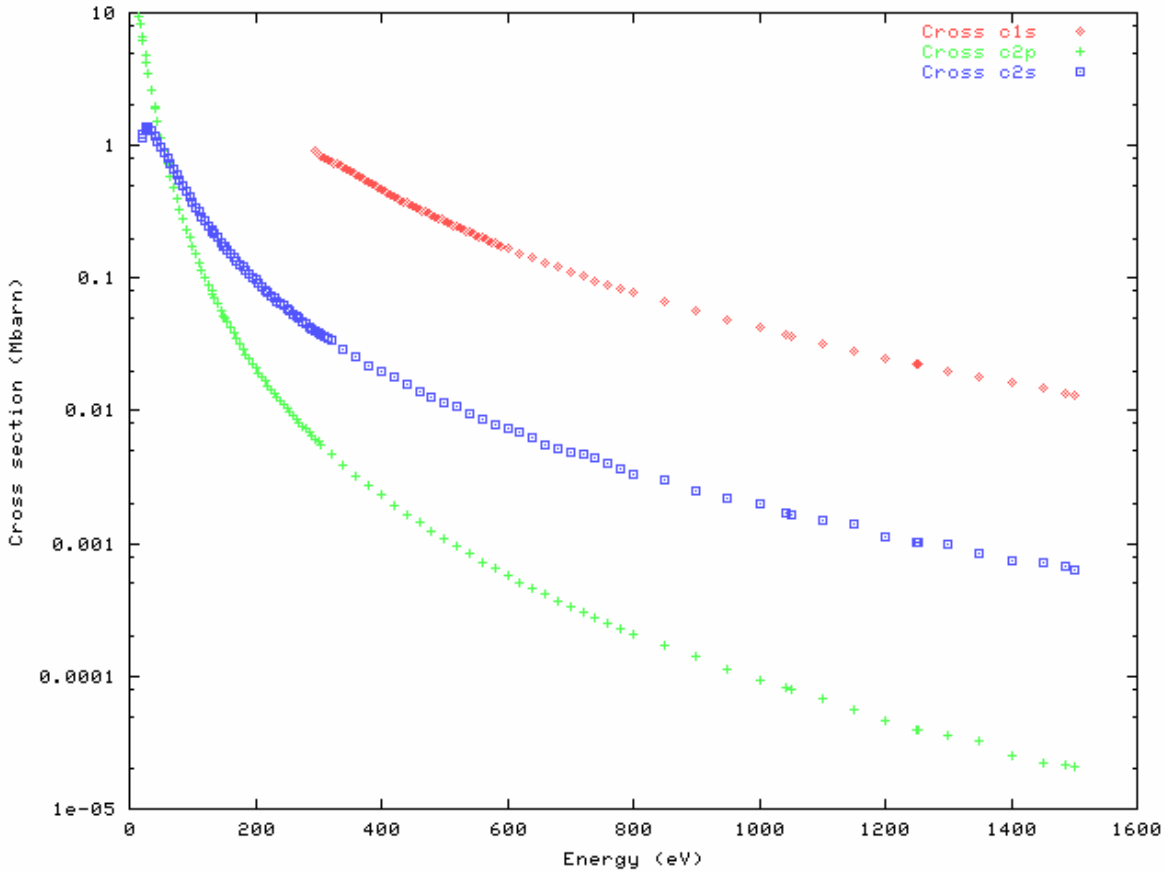

Done

Internet

Start

11:17 AM

GRAPH I. Atomic Subshell Photoionization Cross Sections for 0–1500 eV, $1 \leq Z \leq 103$

See page 6 for Explanation of Graphs

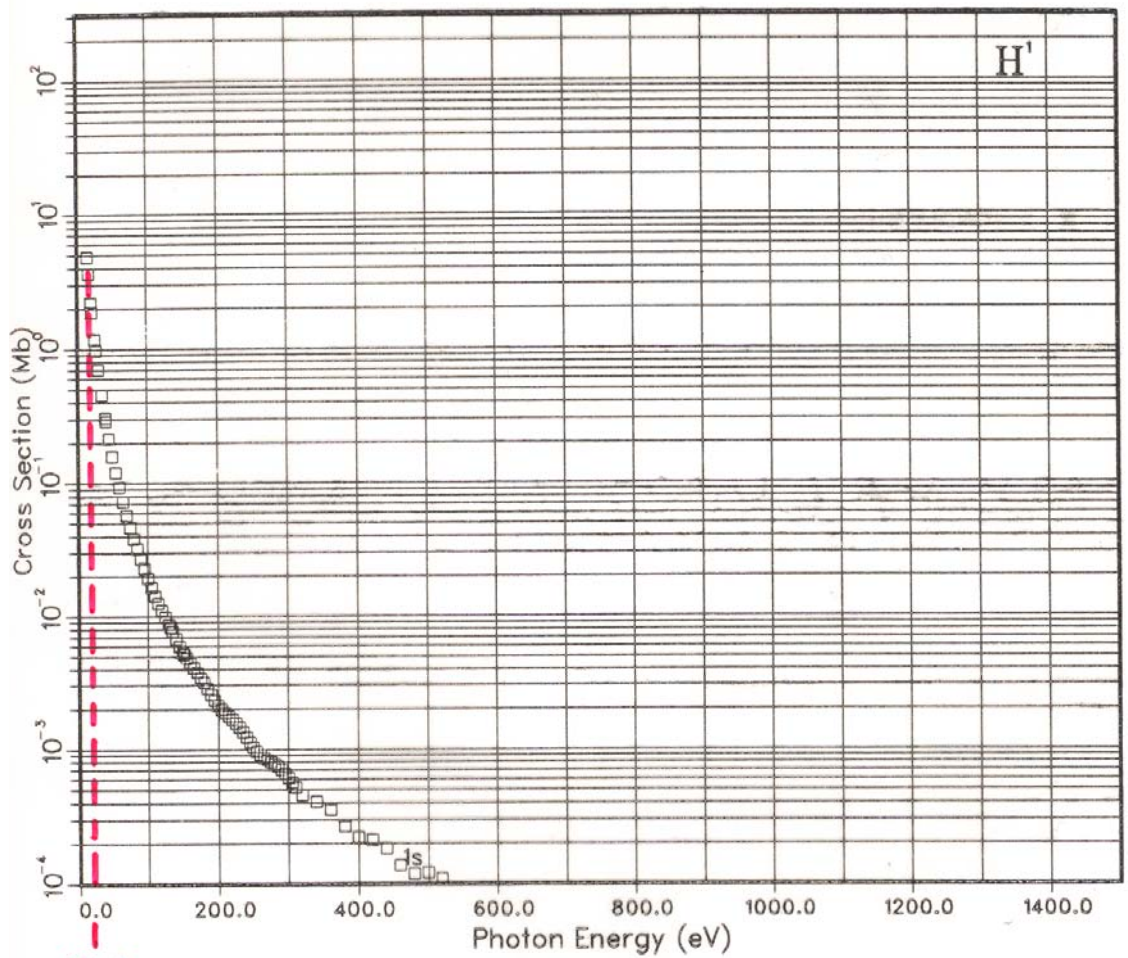

13.6 eV = THRESHOLD FOR e^- EMISSION

H binding energies(eV) are:

1s(1) 13.6050

GRAPH I. Atomic Subshell Photoionization Cross Sections for 0–1500 eV, $1 \leq Z \leq 103$

See page 6 for Explanation of Graphs

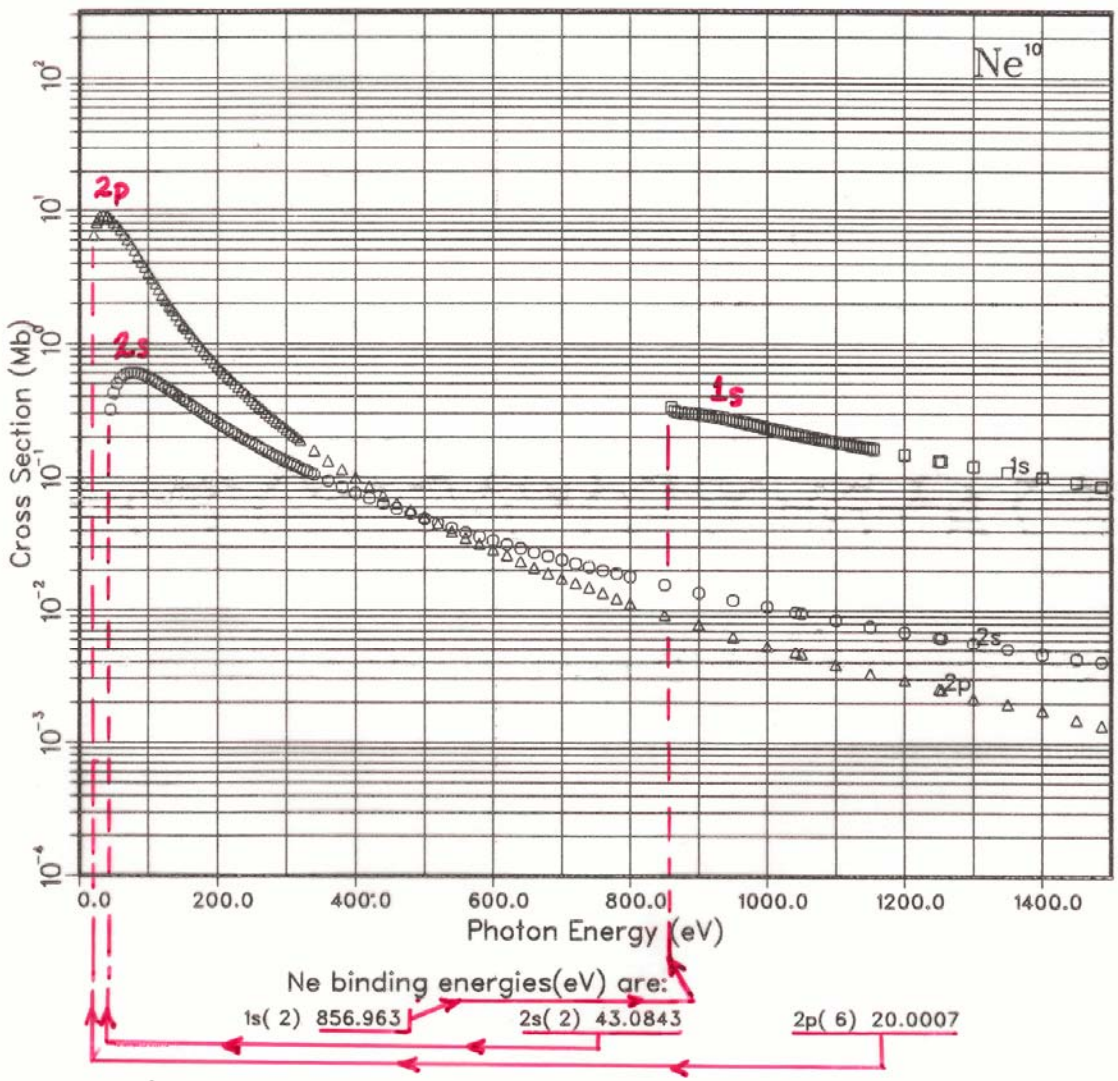

GRAPH I. Atomic Subshell Photoionization Cross Sections for 0–1500 eV, $1 \leq Z \leq 103$

See page 6 for Explanation of Graphs

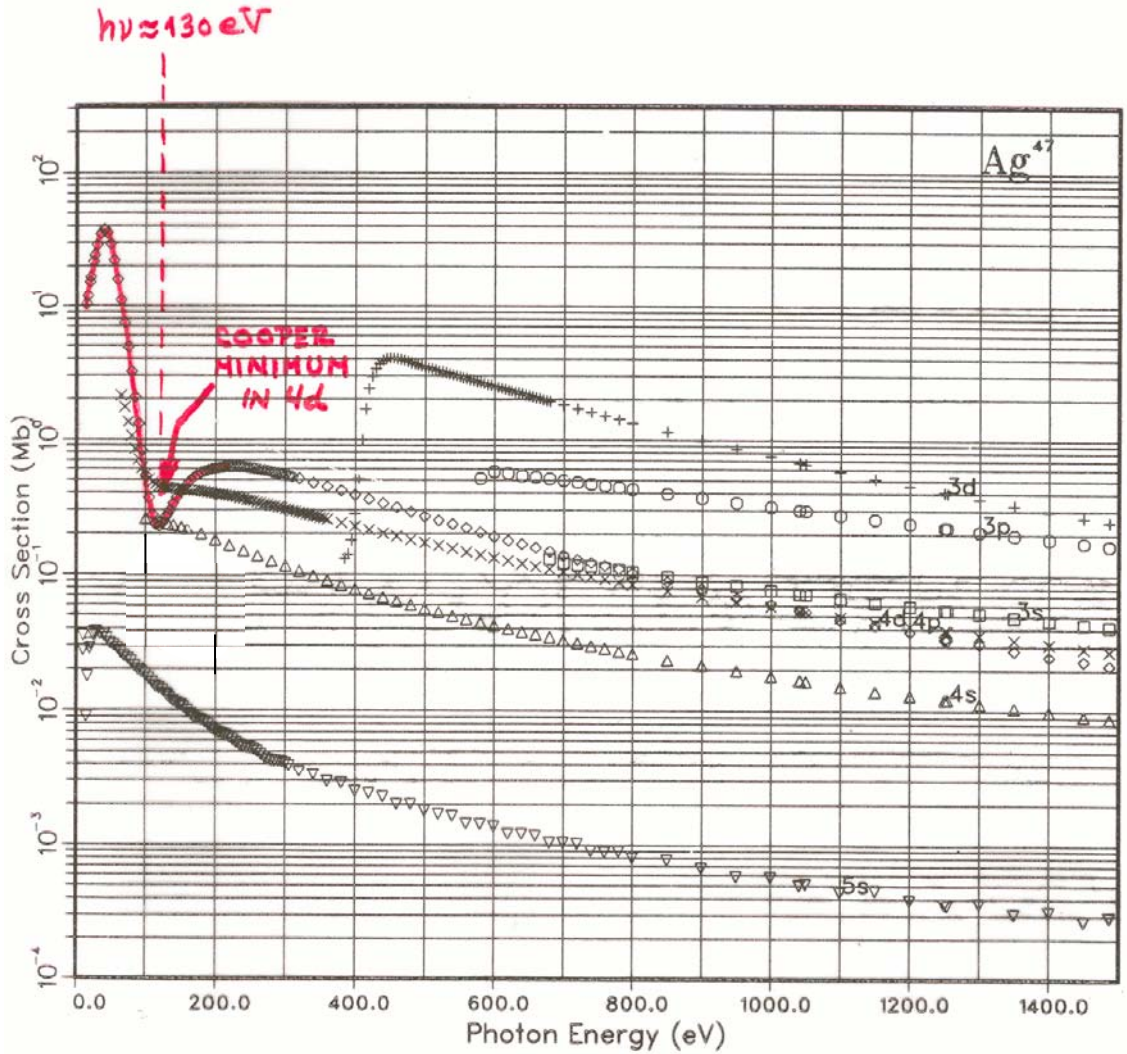

Ag binding energies(eV) are:

1s(2) 24693.5	2s(2) 3591.17	2p(6) 3352.94
3s(2) 665.102	3p(6) 567.203	4s(2) 94.2146
3d(10) 384.360	4p(6) 62.9041	4d(10) 12.6499
5s(1) 6.42700		

COOPER MINIMUM IN Ag 4d (Z = 47) CROSS SECTION : Expt. & Theory

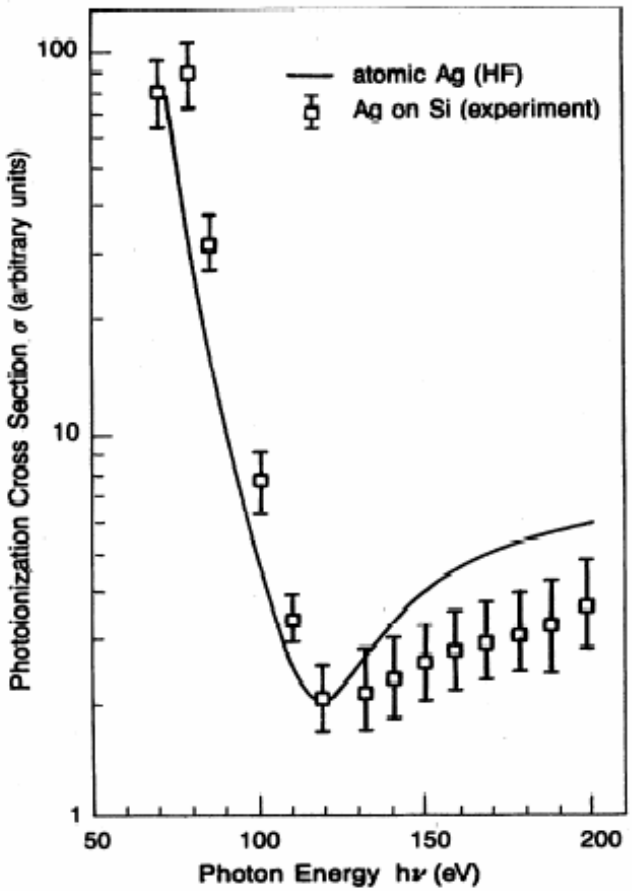

FIG. 5. Partial photoionization cross section for 4*d* electrons of Ag in logarithmic scale. Our experimental data for the Ag/Si interface (squares) are compared with the Hartree-Fock results for atomic Ag by Yeh and Lindau (solid line). Note that our experimental data are normalized at the minimum to the theoretical value.

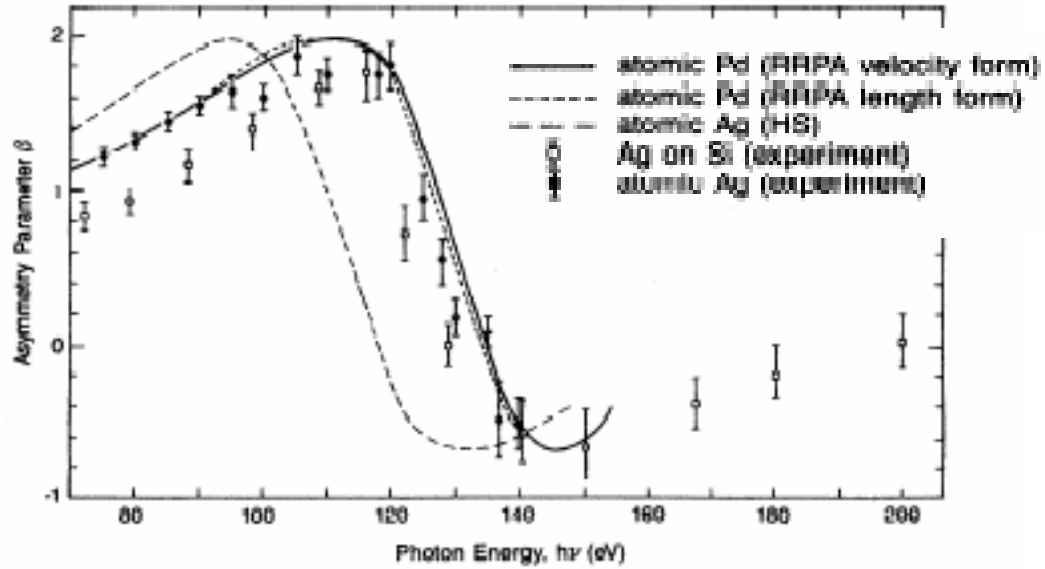

FIG. 6. Asymmetry parameter for 4*d* electrons of Ag. Our experimental data for the Ag/Si interface (squares) are compared with the data for atomic Ag (circles), the RRPA prediction for atomic Pd by Radojevic and Johnson (solid line, velocity form; short-dashed line, length form), and the HS calculations for atomic Ag by Manson (long-dashed line).

M. Ardehali et al., Phys. Rev. B 39, 8107 (1989)

COOPER MINIMUM IN In 4d (Z = 49) CROSS SECTION—Radial Matrix Element Variation

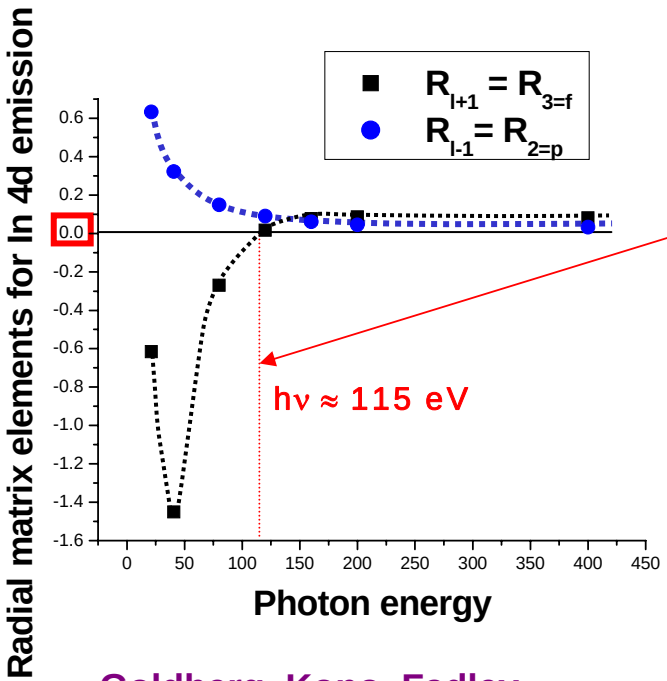

Goldberg, Kono, Fadley
J. Elect. Spect. 21, 285 ('81)

GRAPH I. Atomic Subshell Photoionization Cross Sections for 0–1500 eV, 1 ≤ Z ≤ 103
See page 6 for Explanation of Graphs

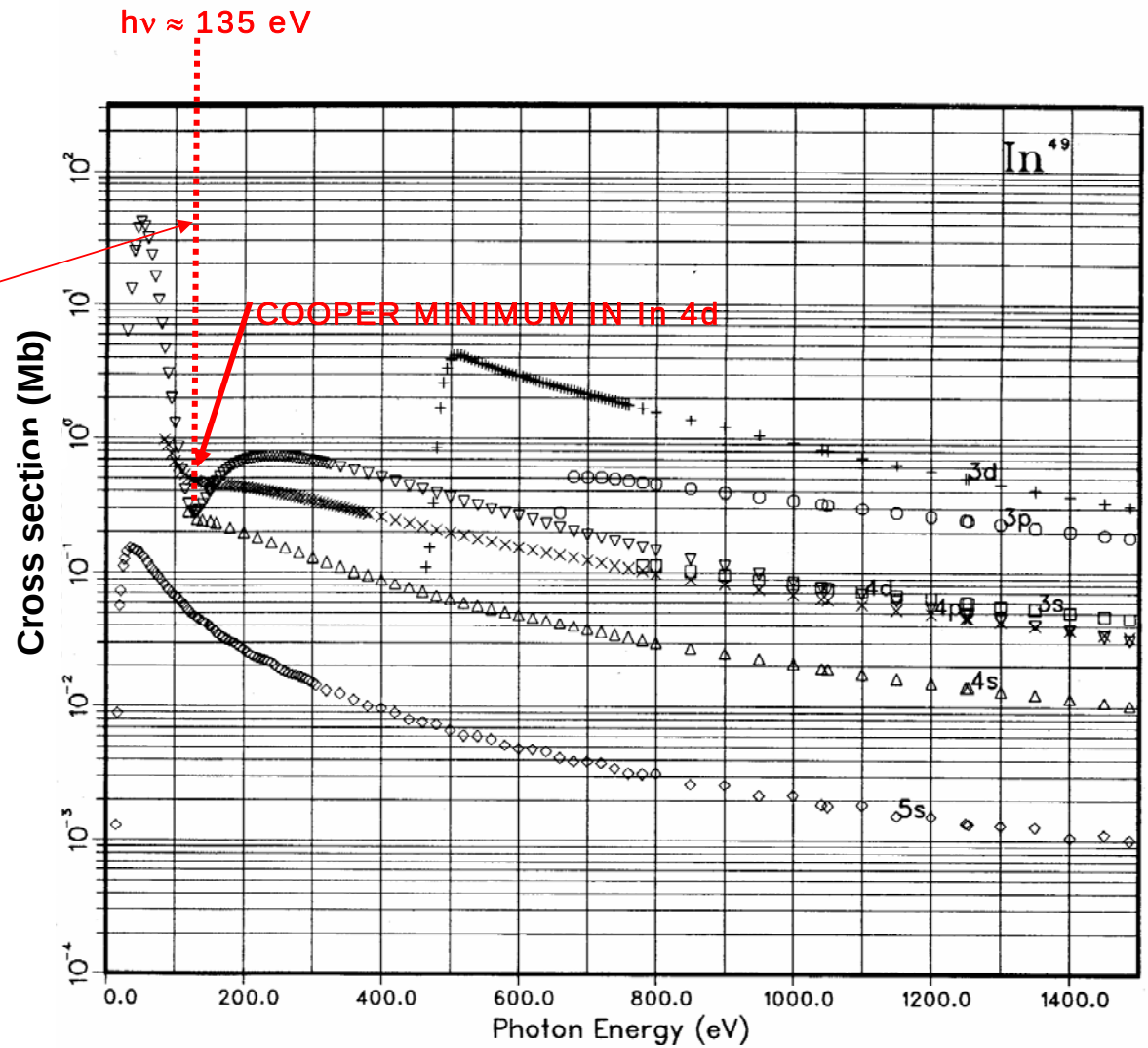

In binding energies(eV) are:

1s(2) 26971.5	2s(2) 3983.01	2p(6) 3731.41
3s(2) 764.232	3p(6) 659.286	4s(2) 118.953
3d(10) 462.909	4p(6) 84.0558	5s(2) 10.1384
4d(10) 26.2168	5p(1) 4.69781	

ATOMIC + NUCLEAR DATA TABLES 32, 45 (1985)

GRAPH I. Atomic Subshell Photoionization Cross Sections for 0–1500 eV, $1 \leq Z \leq 103$

See page 6 for Explanation of Graphs

THEORETICAL ATOMIC CROSS SECTIONS: ENTIRE PERIODIC TABLE

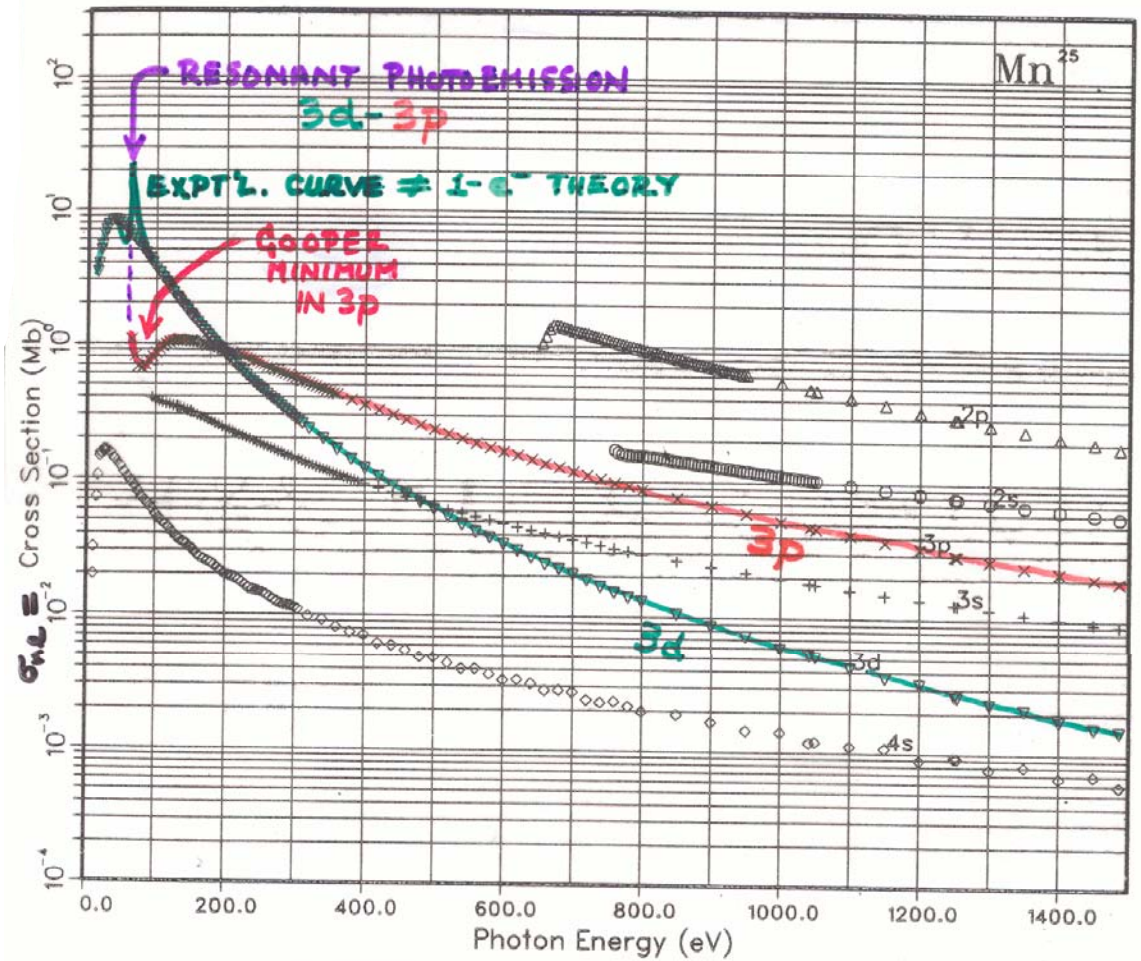

Mn binding energies(eV) are:

1s(2) 6455.26	2s(2) 755.155	2p(6) 653.681
3s(2) 90.8814	3p(6) 60.9150	4s(2) 7.14671
3d(5) 12.0486		

Single-atom resonant photoemission:

Ex. – Mn atom: Mn3d emission, resonance with Mn3p

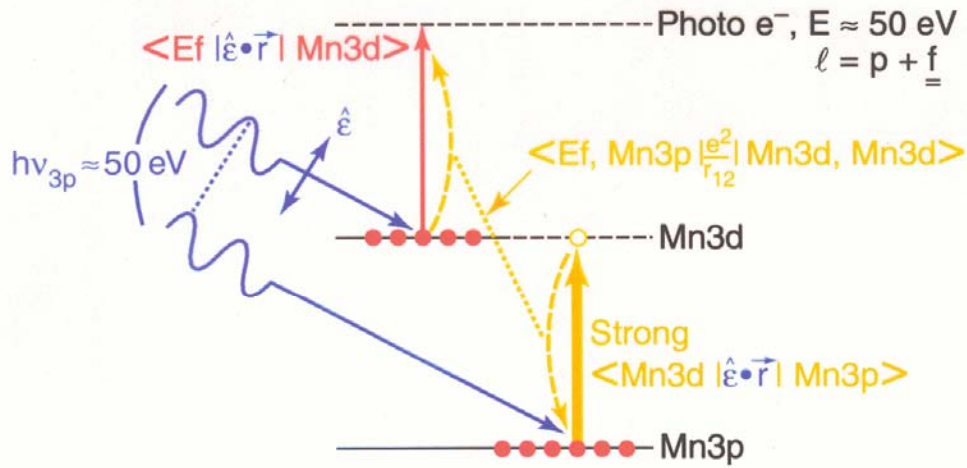

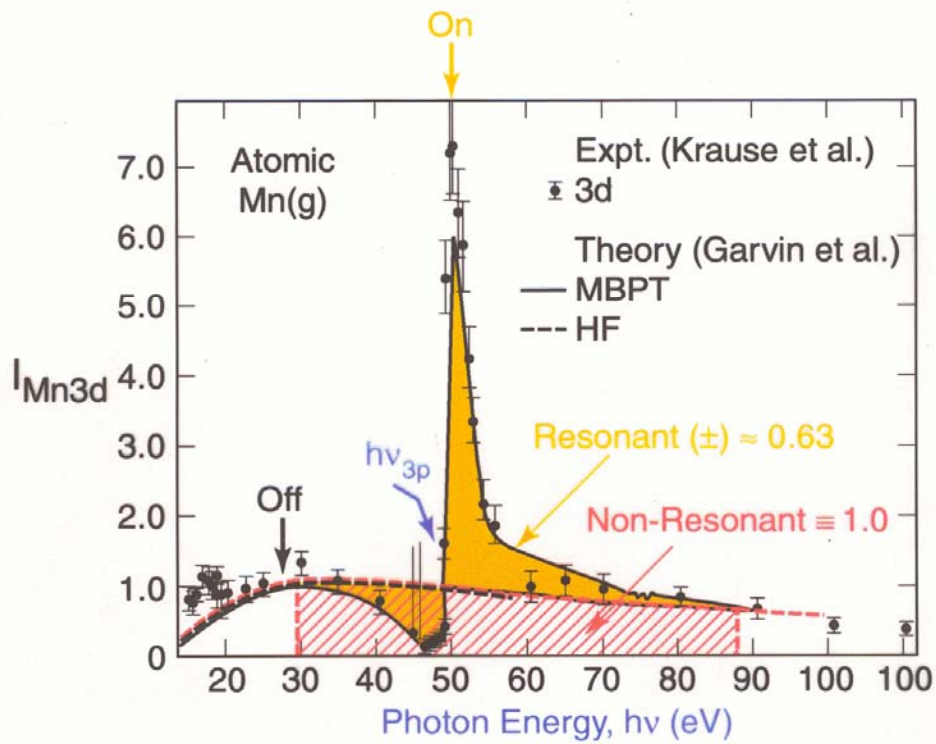

SINGLE-ATOM RESONANT PHOTOEMISSION:

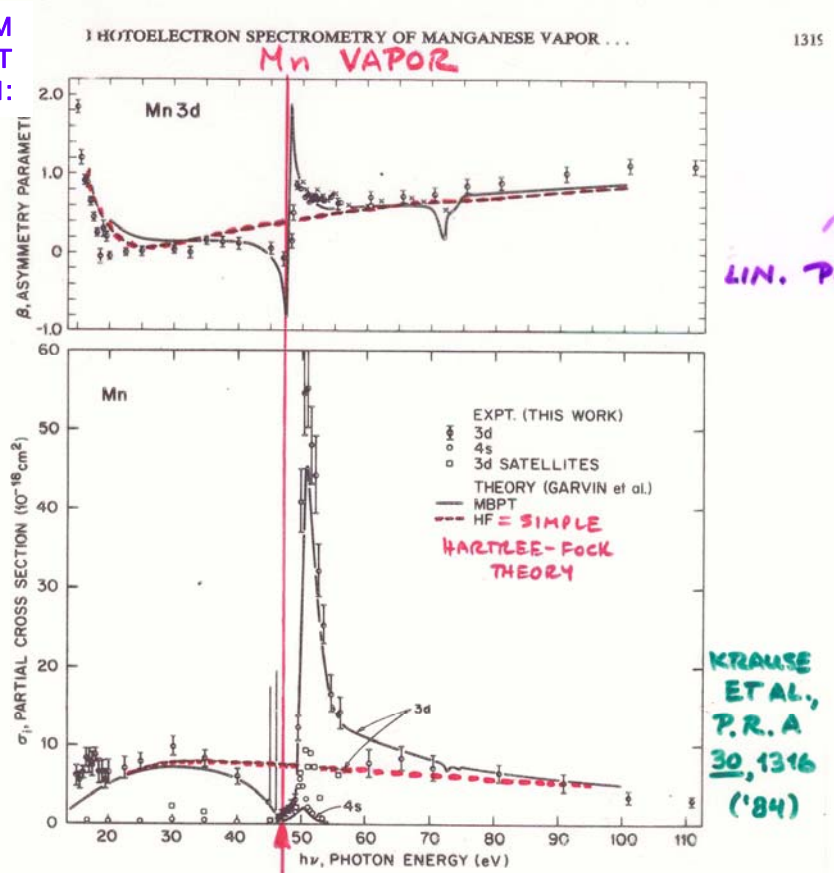

KRAUSE ET AL., P.R.A 30, 1316 ('84)

FIG. 2. Angular distribution parameter β of $3d$ photoelectrons (upper panel) and partial cross sections of $4s$, $3d$ and satellite peaks (lower panel). Crosses (×) for β are from Ref. 3, theory from Ref. 6. The resonance near 50 eV is due to the $3p \rightarrow 3d$ excitation into the partially filled $3d$ subshell of Mn.

$h\nu = E_b^V(Mn\,3p)$

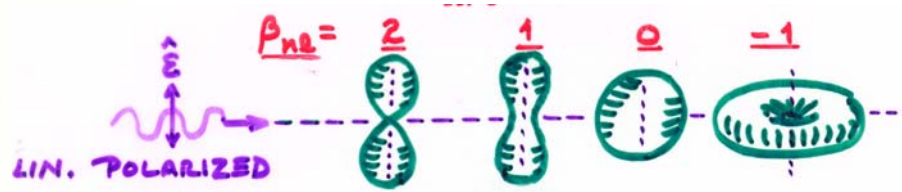

RESONANT PROCESS:

IF $h\nu \approx E_b$ OF $n\ell'$ SUBSHELL INSIDE OF $n\ell$ SUBSHELL OF INTEREST (E.G., 3p FOR 3d), TWO "CHANNELS" COUPLE -

USUAL 3d: $Mn^0 \ldots 3s^2 3p^6 3d^5 4s^2 \xrightarrow{h\nu} Mn^+ \ldots 3s^2 3p^6 3d^4 4s^2$ + PHOTOELECTRON

RESONANT 3p: $Mn^0 \ldots 3s^2 3p^6 3d^5 4s^2 \xrightarrow{h\nu} Mn^0 \ldots 3s^2 3p^5 3d^6 4s^2$

$\xrightarrow[\text{ZATION}]{\text{AUTOIONI-}} Mn^+ \ldots 3s^2 3p^6 3d^4 4s^2$ + ELECTRON @ SAME E_{KIN} AS PHOTOELECTRON

(≈ AUGER)

COUPLING MUCH ENHANCES CROSS SECTION

MATRIX ELEMENTS IN THE SOFT X-RAY SPECTROSCOPIES: DIPOLE LIMIT

- ***Photoelectron spectroscopy/photoemission:***

$$I \propto \left| \hat{e} \bullet \langle \varphi_f(1) | \vec{r} | \varphi_i(1) \rangle \right|^2$$

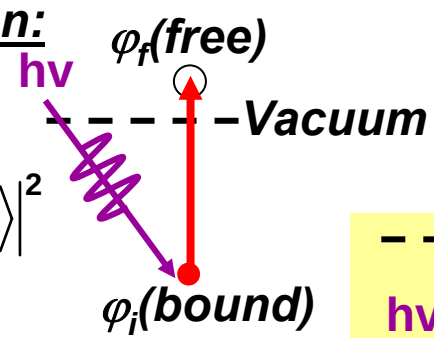

- ***Near-edge x-ray absorption:***

$$I \propto \left| \hat{e} \bullet \langle \varphi_f(1) | \vec{r} | \varphi_i(1) \rangle \right|^2$$

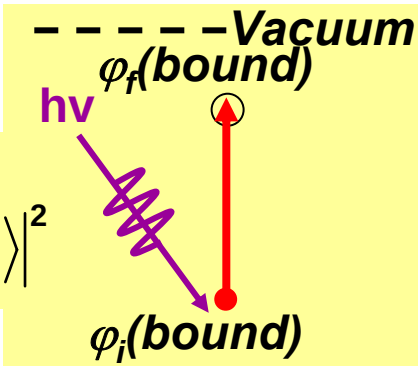

- ***Auger electron emission:***

$$I \propto \left| \langle \varphi_f(1)\varphi_1(2) | \frac{e^2}{r_{12}} | \varphi_3(1)\varphi_2(2) \rangle - \langle \varphi_1(1)\varphi_f(2) | \frac{e^2}{r_{12}} | \varphi_3(1)\varphi_2(2) \rangle \right|^2$$

Direct

Exchange

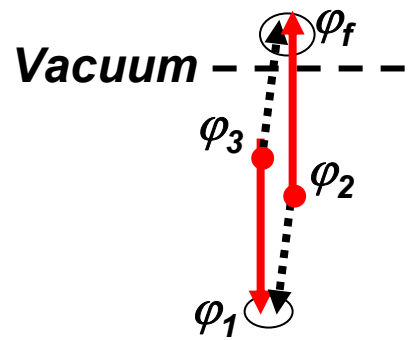

- ***X-ray emission:***

$$I \propto \left| \hat{e} \bullet \langle \varphi_f(1) | \vec{r} | \varphi_i(1) \rangle \right|^2$$

MATRIX ELEMENTS IN THE SOFT X-RAY SPECTROSCOPIES: RESONANT EFFECTS

- ***Resonant photoemission:***

$$I \propto \left| \langle \varphi_f(1) | \hat{e} \bullet \vec{r} | \phi_i(1) \rangle + \sum_m \langle \varphi_f(1)\varphi_1(2) | \frac{e^2}{r_{12}} | \varphi_i(1)\varphi_m(2) \rangle \langle \varphi_m(1) | \hat{e} \bullet \vec{r} | \varphi_1(1) \rangle \right|^2 \times \delta(h\nu - (E_m - E_1))$$

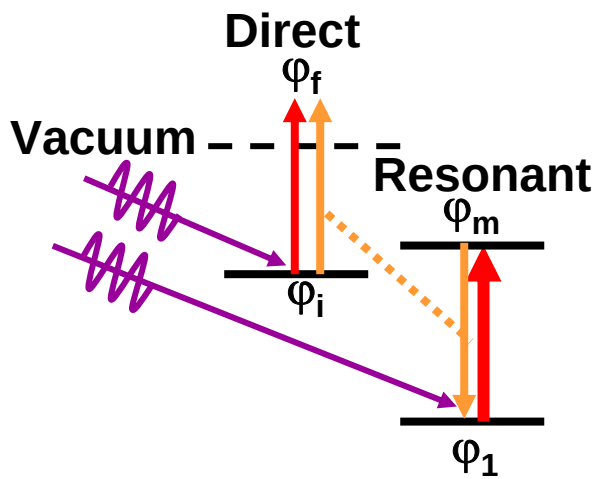

- ***Resonant inelastic x-ray scattering:***

$$I \propto \sum_f \left| \sum_m \frac{\langle \Psi_f(N) | \hat{e} \bullet \vec{r} | \Psi_m(N) \rangle \langle \Psi_m(N) | \hat{e} \bullet \vec{r} | \Psi_i(N) \rangle}{h\nu + E_i(N) - E_m(N) - i\Gamma} \right|^2 \times \delta(h\nu - (E_m(N) - E_i(N)))$$

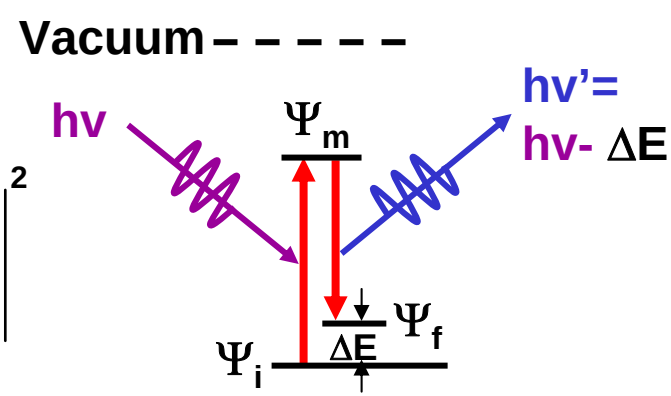

Multi-Atom Resonant Photoemission

Microscopic Q.M. picture

Ex. – MnO(001): O1s emission, resonance with $Mn2p_{3/2}$

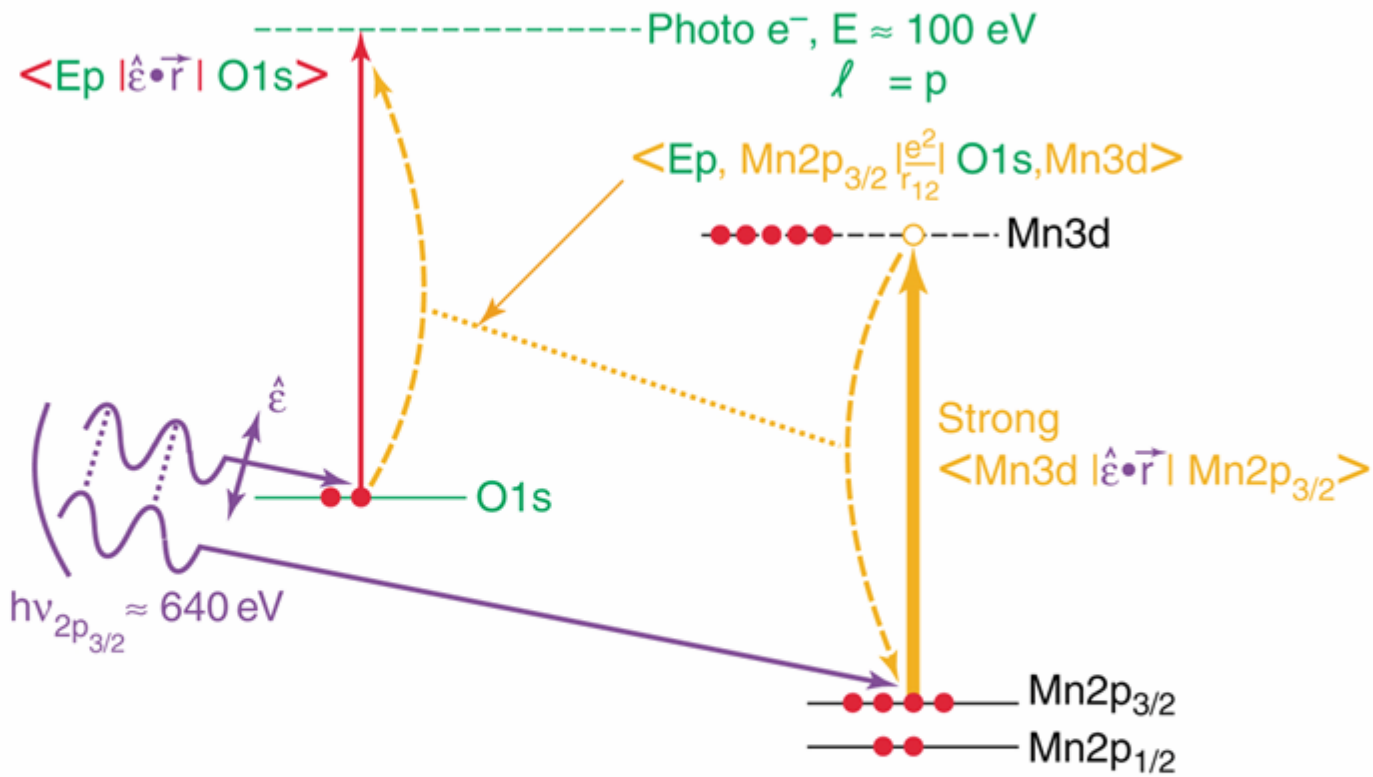

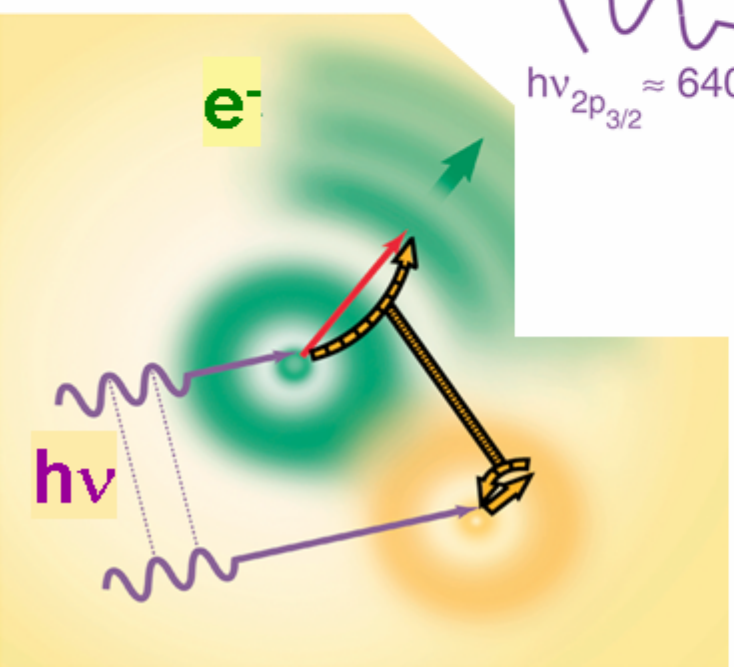

Kay et al.,
Science 281, 679 ('98);
Corrected picture in
PRB 61, 5119 ('01)←

Multi-Atom Resonant Photoemission—O 1s emission from NiO(001)

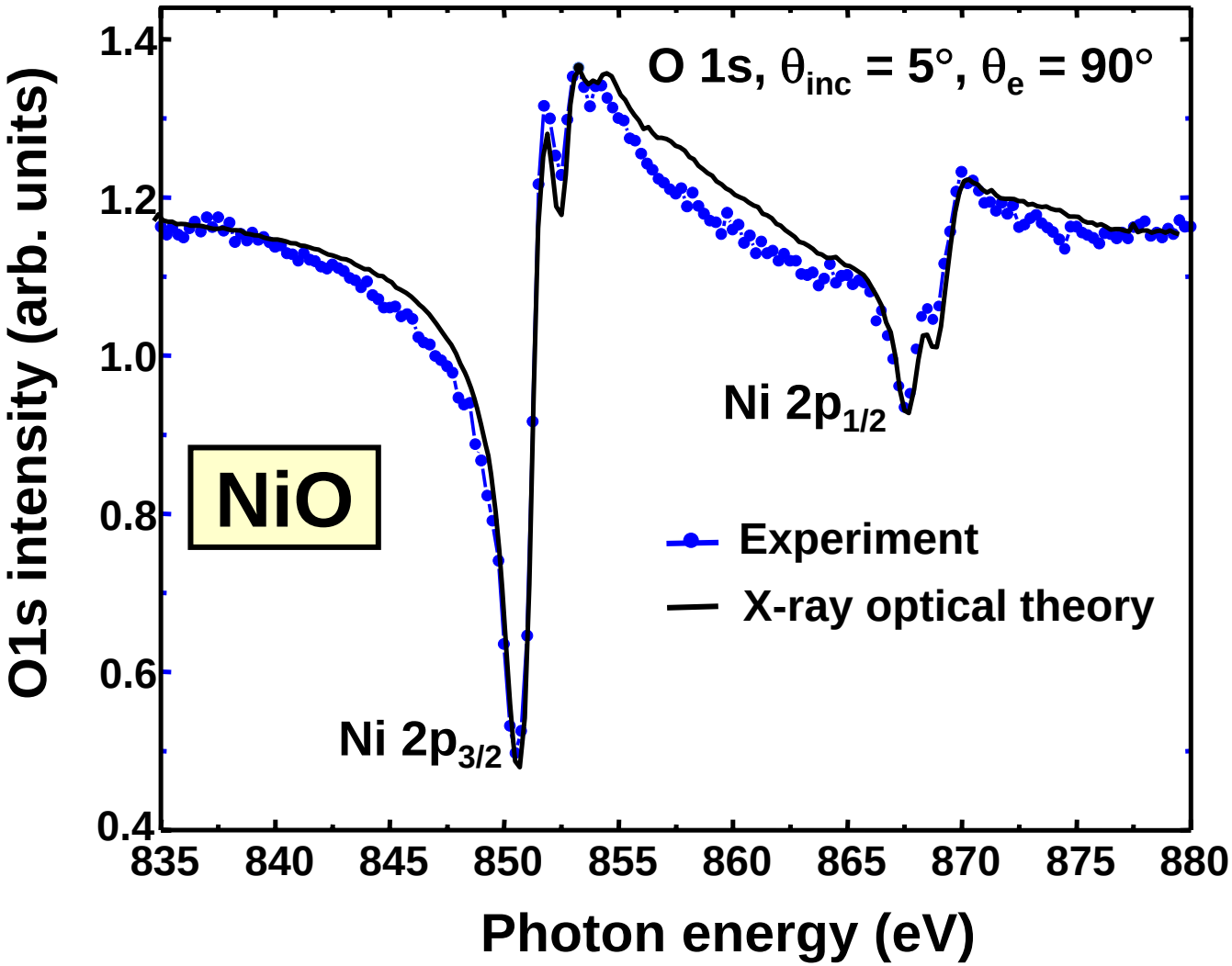

More later

Mannella et al., to be published

Differential cross section in the non-dipole approximation

The differential cross section for photoionization of randomly oriented target atoms by 100% linearly polarized photons has the form:

$$\frac{d\sigma}{d\Omega} = \left(\frac{\sigma}{4\pi}\right)\left[\underbrace{1+\beta\, P_2(\cos\alpha)}_{\text{DIPOLE}} + \underbrace{\left(\delta+\gamma\cos^2\alpha\right)\sin\alpha\cos\phi}_{\text{NON-DIPOLE}}\right]$$

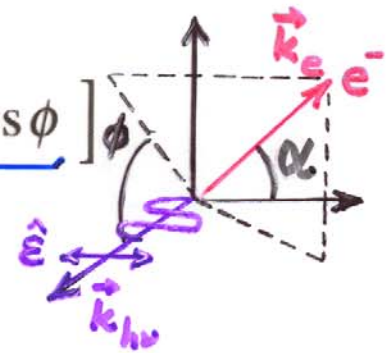

with:

$$P_2(\cos\alpha) = \frac{1}{2}\left(3\cos^2\alpha - 1\right)$$

σ: angle integrated cross section

β: electron anisotropy parameter

γ: non-dipole electron anisotropy parameter

δ: non-dipole electron anisotropy parameter

$$\exp(i\vec{k}_{h\nu}\cdot\vec{r}) = \underbrace{1}_{\text{DIPOLE}} + \underbrace{i\vec{k}_{h\nu}\cdot\vec{r} - \tfrac{1}{2}(\vec{k}_{h\nu}\cdot r)^2 + \cdots}_{\text{NON-DIPOLE}}$$

Krause et al.
Lindle et al.
Krässig et al.

$k_{h\nu} = 2\pi/\lambda_{h\nu} = 0.75$ Å^{-1} @ 1.49 keV $\rightarrow k_{h\nu} \cdot [\langle r_{nl}\rangle \approx 1$ Å$] \approx 0.75$—Non-dipole imp?

0.075 Å^{-1} @ 149 eV $\rightarrow k_{h\nu} \cdot [\langle r_{nl}\rangle \approx 1$ Å$] \approx 0.075$—Dipole ~OK

BEYOND THE DIPOLE APPROXIMATION?

FREE-ATOM DIFFERENTIAL CROSS SECTIONS

(KRAUSE, PHYS. REV. 177, 151 ('69)

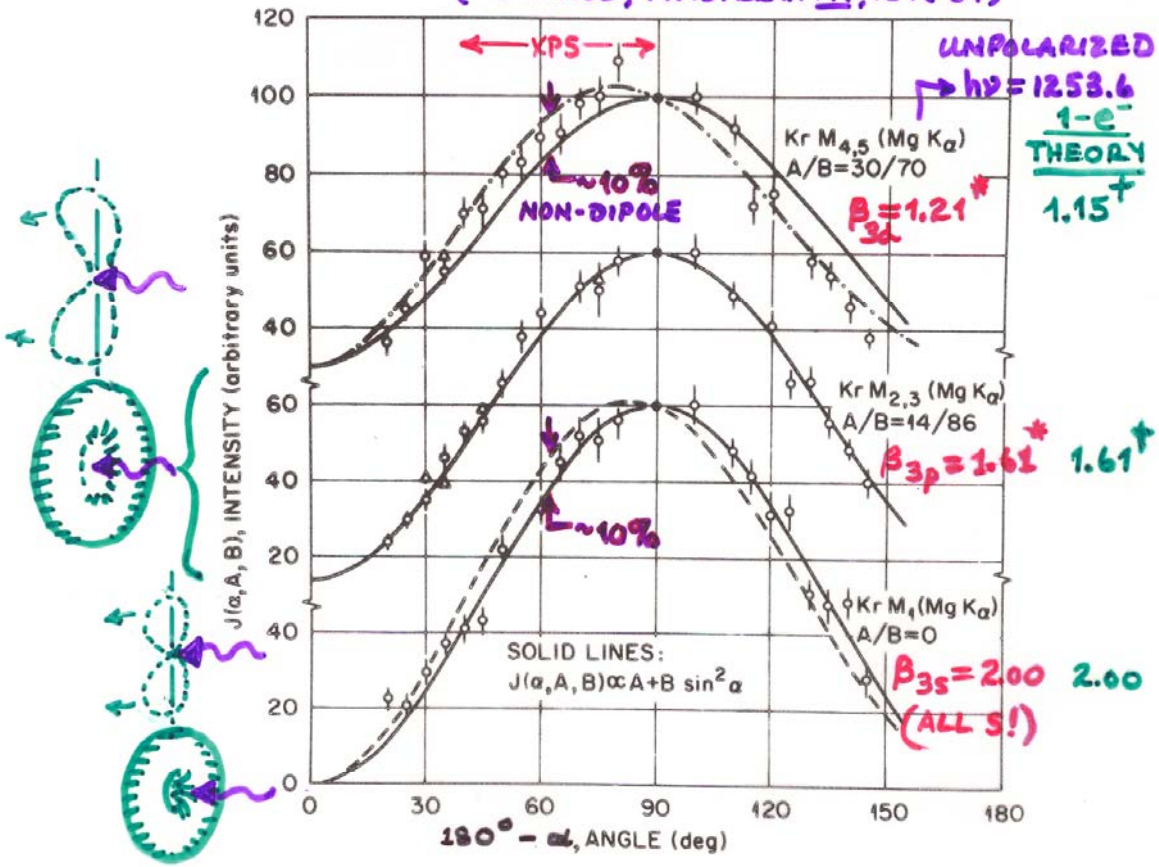

Figure 10 -- Experimental angular distributions of 3s (= M_1), 3p (= $M_{2,3}$), and 3d (= $M_{4,5}$) photoelectrons excited from gaseous Kr with MgKα X-rays. The curves represent least-squares fits to the data points of a relationship of the form of Equation (93), in which A and B were treated as empirical constants. (From Krause, reference 142.)

* FROM: $\beta_{n\ell} = \frac{4B}{(3A+2B)} = \frac{4}{(3A/B+2)}$

NEAR EQ. 93; FADLEY, "BASIC CONCEPTS OF XPS"

+ FROM YEH & LINDAU TABLES

"Basic Concepts of XPS"
Figure 10

Non-dipole effects in 2p emission from Ne

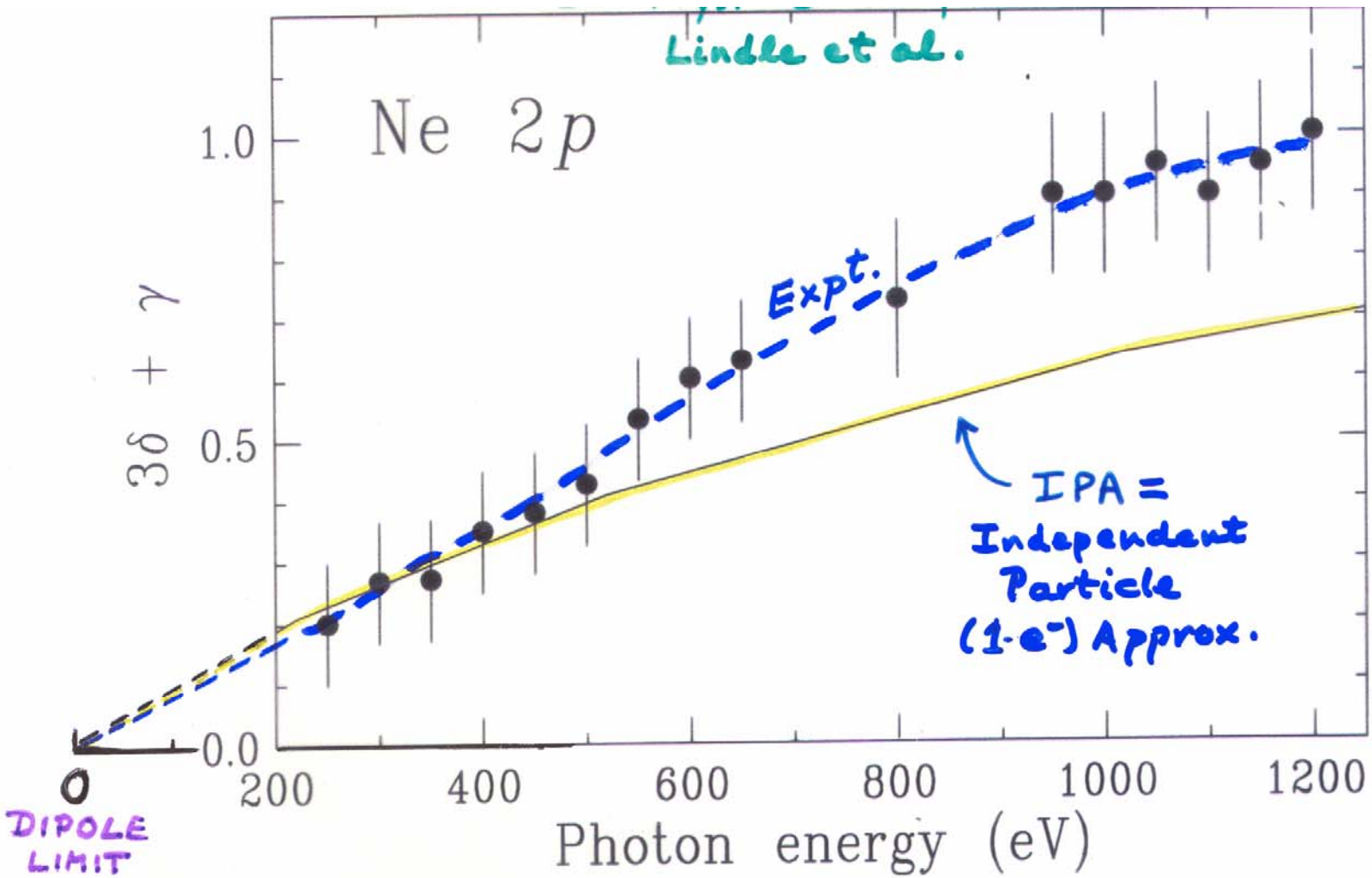

+ see Phys. Rev. Lett. 78, 4553 ('97): Lindle et al.
" " " 75, 4736 ('95): Krässig et al.

CALCULATION OF PHOTOELECTRON INTENSITIES—THE 3-STEP MODEL

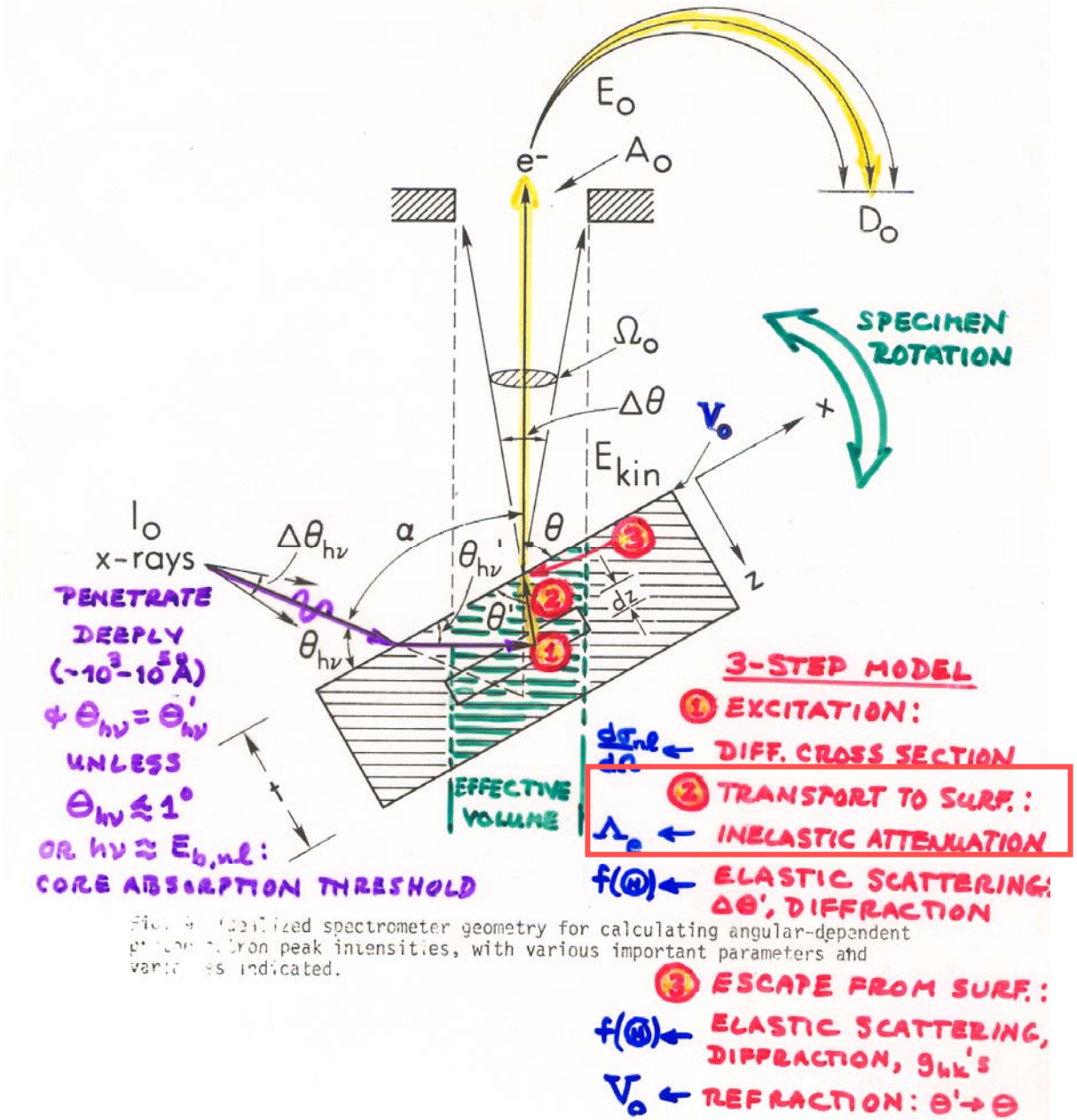

Fig. 9 Idealized spectrometer geometry for calculating angular-dependent photoelectron peak intensities, with various important parameters and variables indicated.

Why are electrons so useful as probes of surfaces?

Most up-to-date collection of experimental data: NIST Electron Effective-Attenuation-Length Database—http://www.nist.gov/srd/nist82.htm

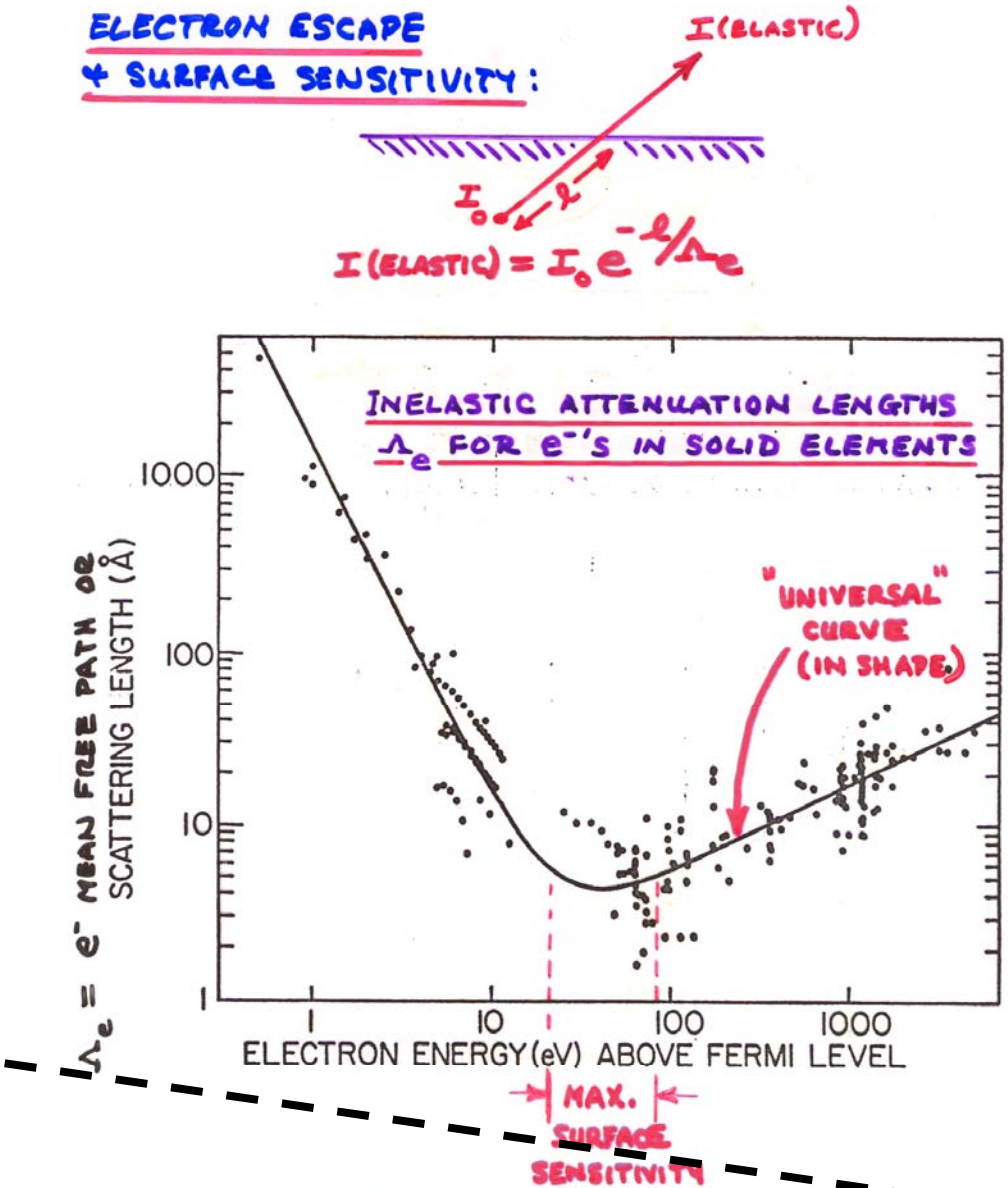

COMPILATIONS: Seah + Dench, Surf. Int. Anal. 1, 2 (1979)
Tanuma, Powell, + Penn, Surf. Int. Anal. 17, 911 + 927 (1991); 21, 165 (1994)
Powell + Jablonski, J. Phys. Chem. Ref. Data 28, 19 (1999); Surf. Int. Anal. 29, 108 (2000)

Inelastic mean free paths in solids

Database of experimental and theoretically estimated mean free paths at http://www.nist.gov/srd/webguide/nist71/71imfp.htm#elements

Plus estimation with the TPP-2M (TPP-2) formula of Tanuma, Powell, Penn:

Web calculation for elements from: http://www.ss.teen.setsunan.ac.jp/e-imfp2.html

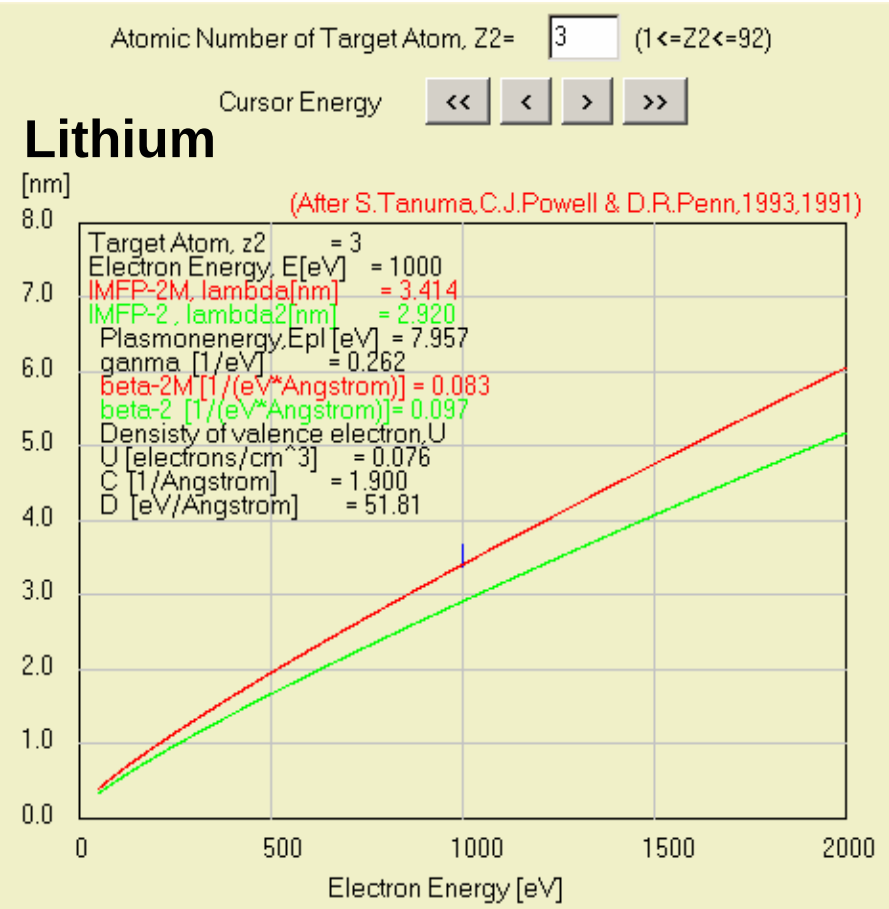

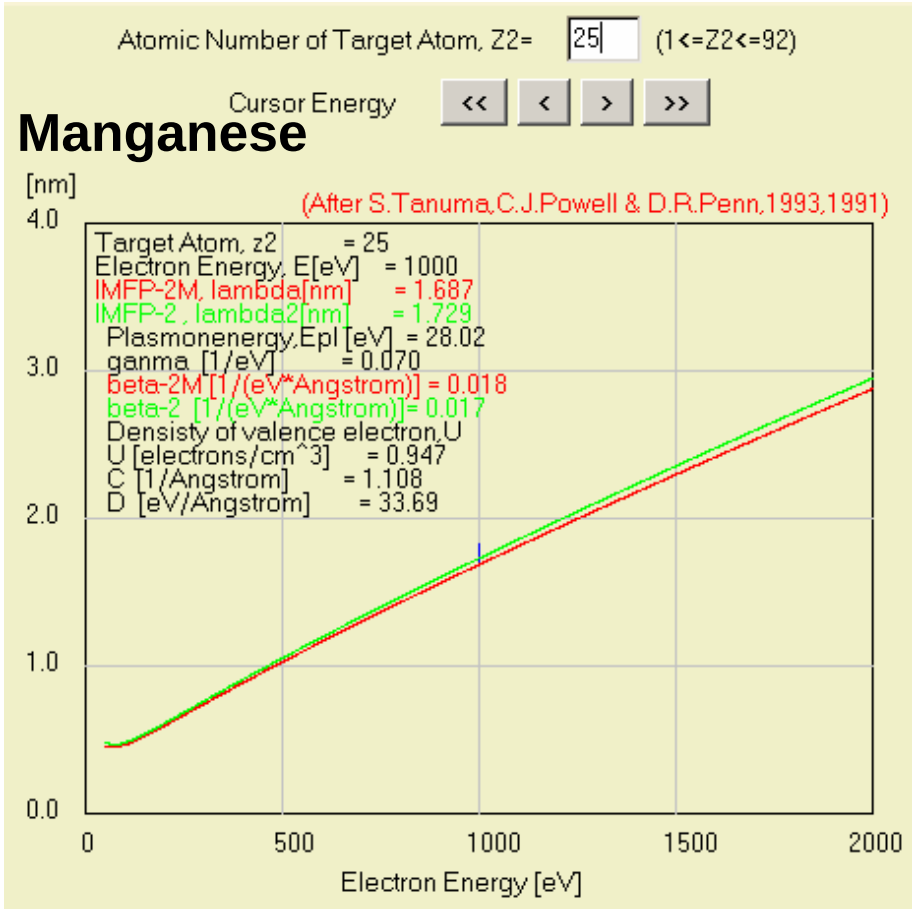

Inelastic mean free paths in solids

Estimation from the TPP-2M formula: any compound

$$\Lambda_e \approx \lambda = \frac{E}{E_p^2[\beta \ln(\gamma E) - (C/E) + (D/E^2)]}$$

where

$$\beta = -0.10 + 0.944/(E_p^2 + E_g^2)^{1/2} + 0.069\rho^{0.1}$$

$$\gamma = 0.191\rho^{-0.50}$$

$$C = 1.97 - 0.91U$$

$$D = 53.4 - 20.8U$$

$$U = N_v\rho/M = E_p^2/829.4$$

and $E_p = 28.8\,(N_v\rho/M)^{1/2}$ is the free-electron plasmon energy (in eV), ρ is the density (in g cm^{-3}), N_v is the number of valence electrons per atom (for an element) or molecule (for a compound), M is the atomic or molecular weight, and E_g is the bandgap energy (in eV). These equations are collectively known as the TPP-2M equation.

Tanuma, Powell, Penn, Surf. Interface Anal. 21, 165 (1994)

CALCULATION OF PHOTOELECTRON INTENSITIES—THE 3-STEP MODEL

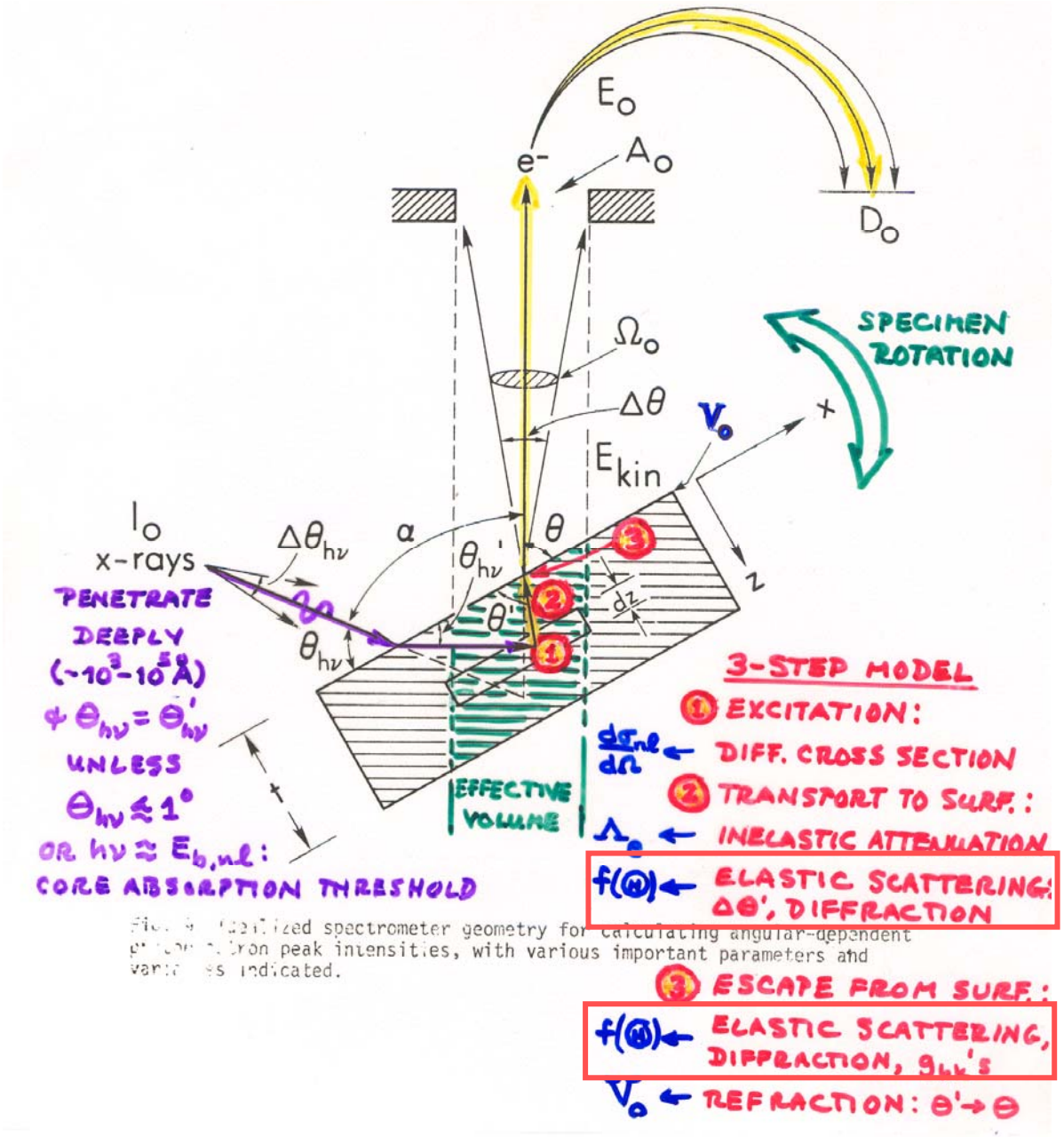

Fig. 9 Idealized spectrometer geometry for calculating angular-dependent photoelectron peak intensities, with various important parameters and variables indicated.

Varying surface sensitivity for lower electron takeoff angles

Simplest interpretation:

Average emission depth = $\Lambda_{inelastic} \sin\theta_{takeoff}$

How valid?

$E_{kin} \approx$ 500-1000 eV

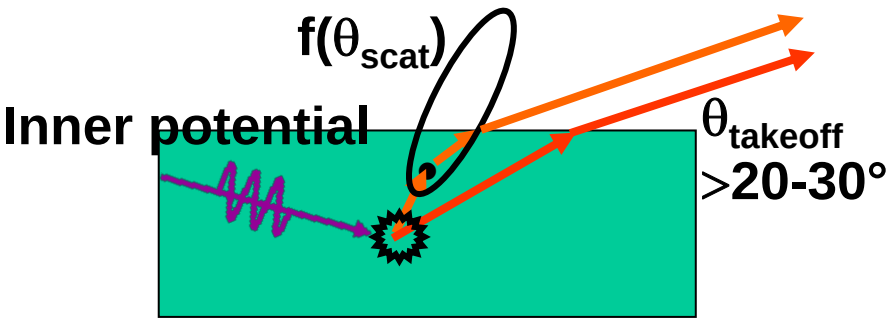

E.g.: A. Jablonski and C. J. Powell, J. Vac. Sci. Tech. A 21, 274 (2003):

→ Mean Emission Depth (MED) more relevant than $\Lambda_{inelastic}$

EFFECTS OF ELASTIC SCATTERING ON ANGULAR DISTRIBUTIONS: POLYCRYSTALLINE OR AMORPHOUS SAMPLE

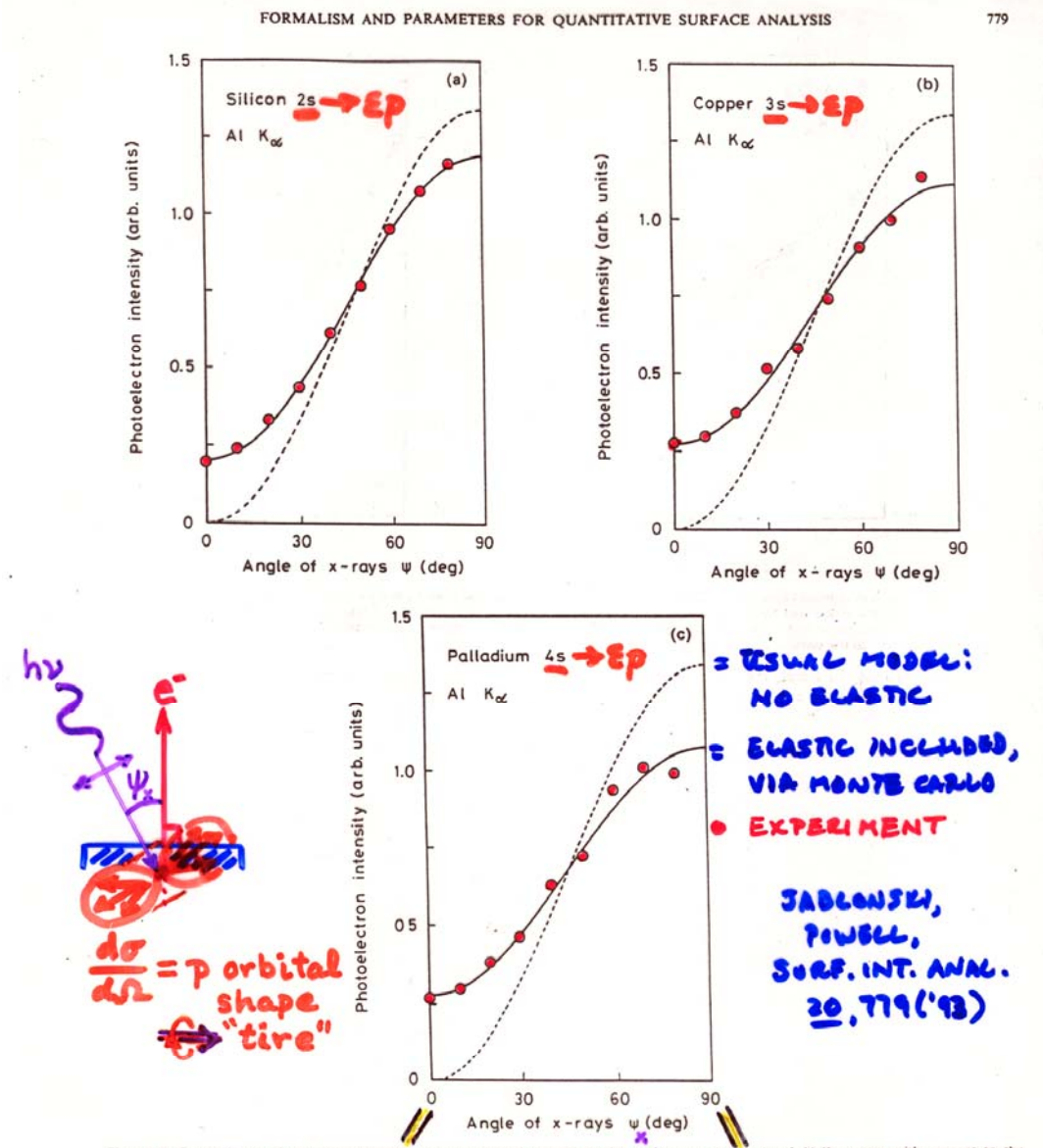

Figure 4. Dependence of the photoelectron intensity emitted normal to the surface on the angle of Al Kα x-rays with respect to the direction of analysis. Circles and solid line: Monte Carlo calculations accounting for elastic collisions of photoelectrons; dashed line: result of common simple formalism of XPS in which elastic collisions are neglected. (a) Silicon 2s photoelectrons; (b) copper 3s photoelectrons; (c) palladium 4s photoelectrons. (Taken from Ref. 20).

Intensity increased by elastic scattering

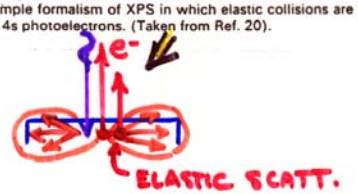

Intensity decreased by elastic scatt.

Varying surface sensitivity for lower electron takeoff angles

Simplest interpretation:

Average emission depth = $\Lambda_{inelastic} \sin\theta_{takeoff}$

How valid?

$E_{kin} \approx$ 500-1000 eV

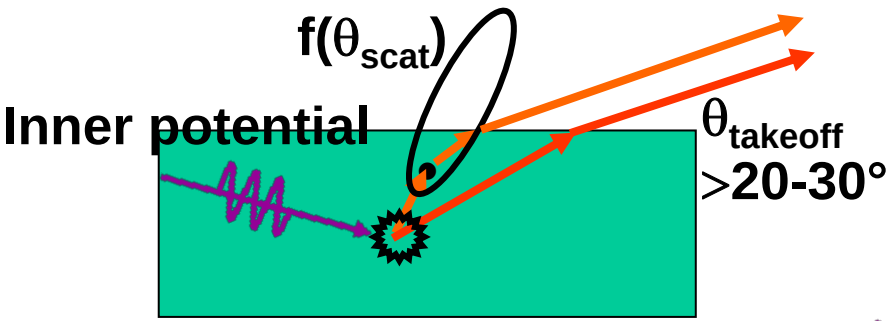

E.g.: A. Jablonski and C. J. Powell, J. Vac. Sci. Tech. A 21, 274 (2003):
→ Mean Emission Depth (MED) more relevant than $\Lambda_{inelastic}$

$E_{kin} \approx$ 10,000 eV

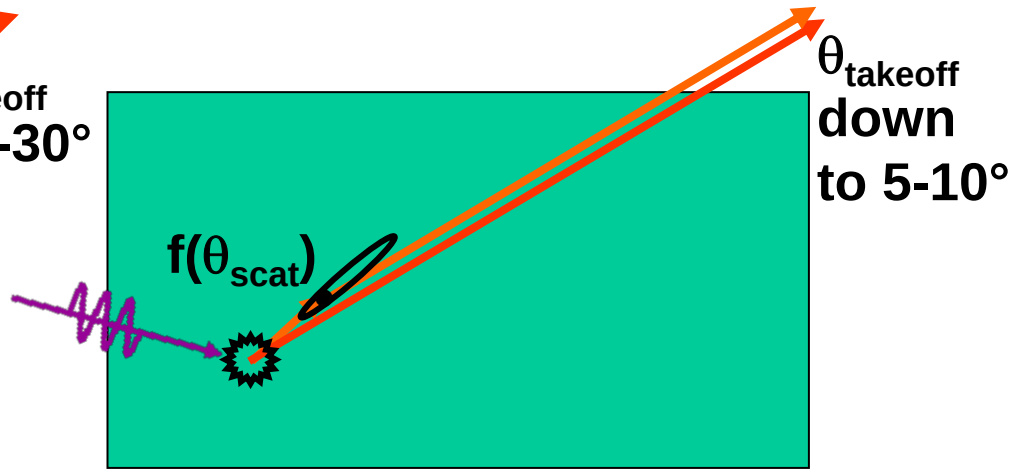

Simpler analysis

Cleaner bulk & surface distinction

C. J. Powell, W. Werner et al., priv. comm.;
C.S.F., Nucl. Inst. & Meth. A 547, 24 (2005)

CALCULATION OF PHOTOELECTRON INTENSITIES—THE 3-STEP MODEL

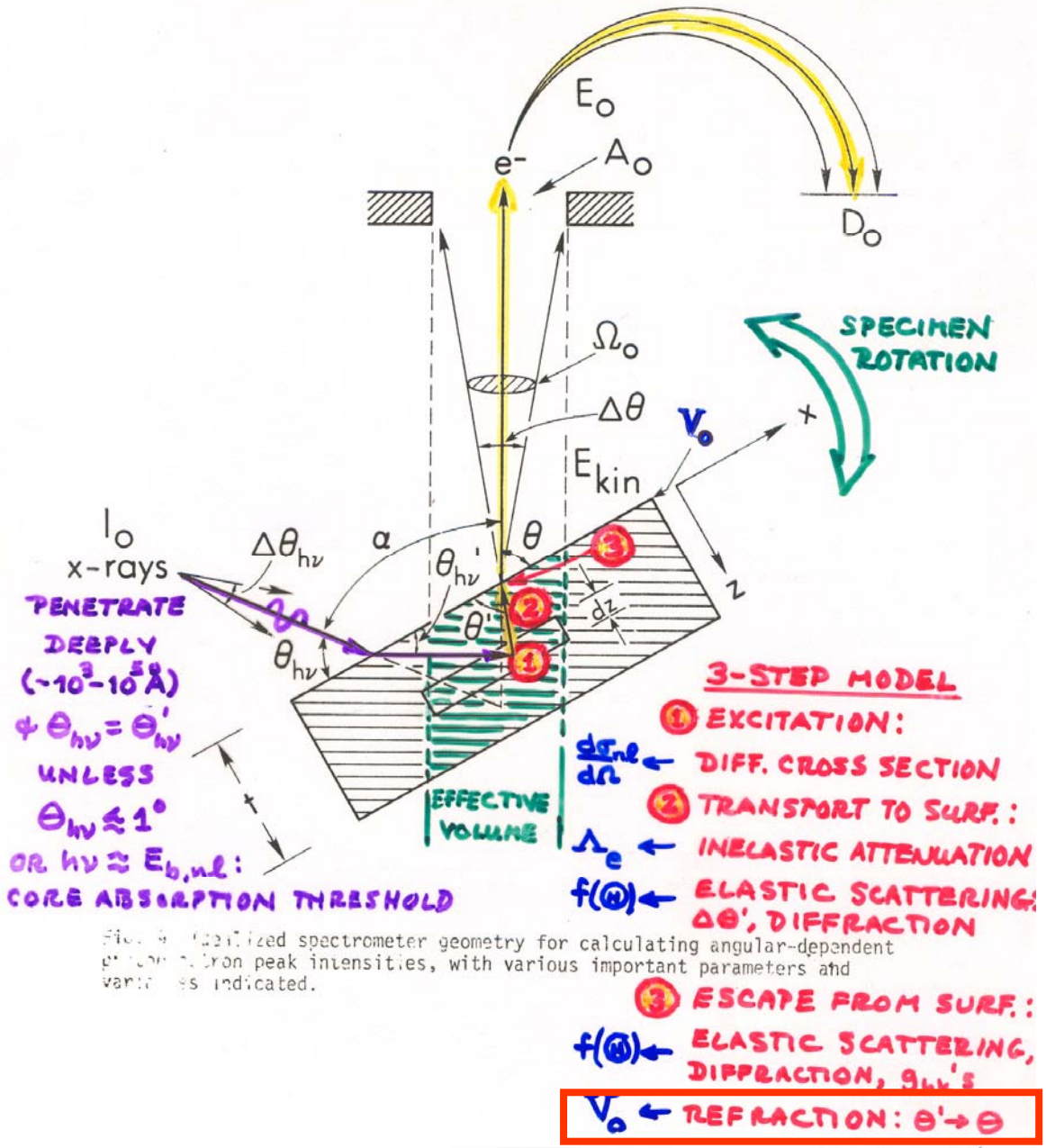

Fig. 9 Idealized spectrometer geometry for calculating angular-dependent photoelectron peak intensities, with various important parameters and variables indicated.

Electron Refraction at the Surface Due to the Inner Potential

$$\theta = \tan^{-1}\left[\sqrt{\sin^2\theta' - \frac{V_o}{E_{kin}}} \Big/ \cos\theta'\right]$$

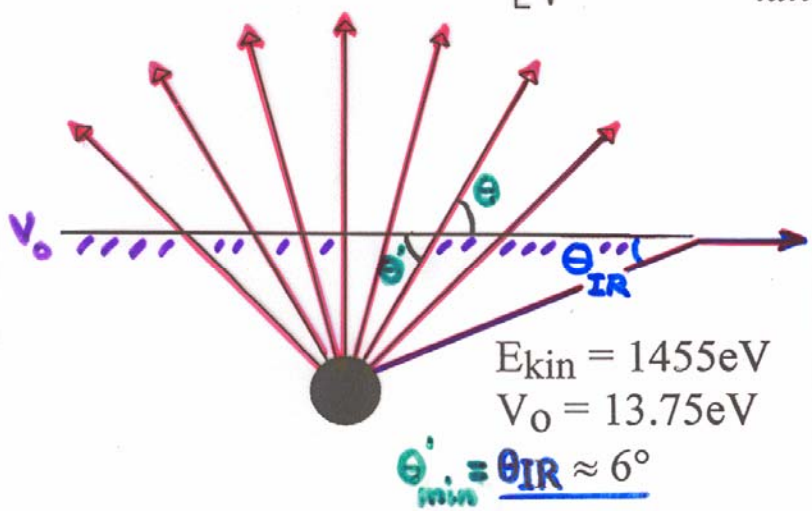

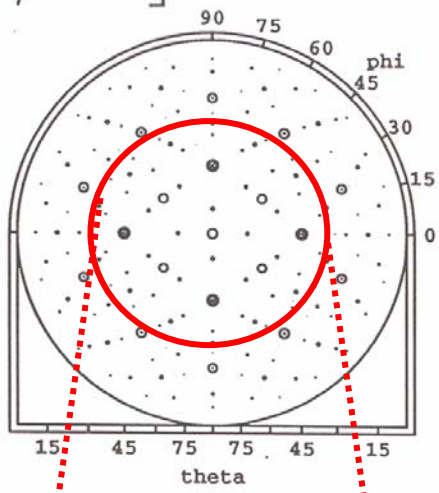

Observed Low-Index Directions Above W(110)

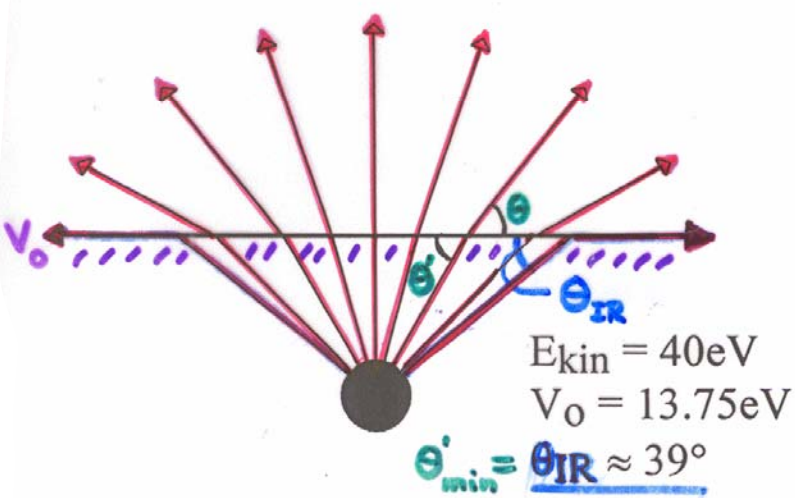

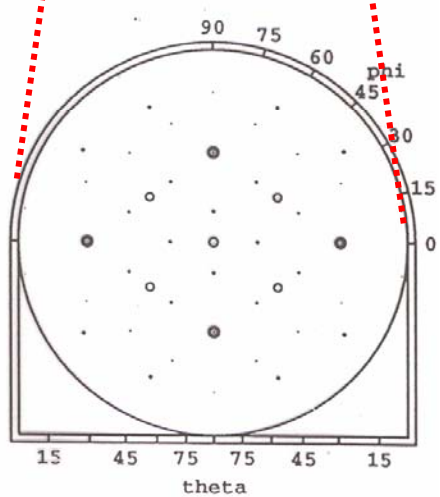

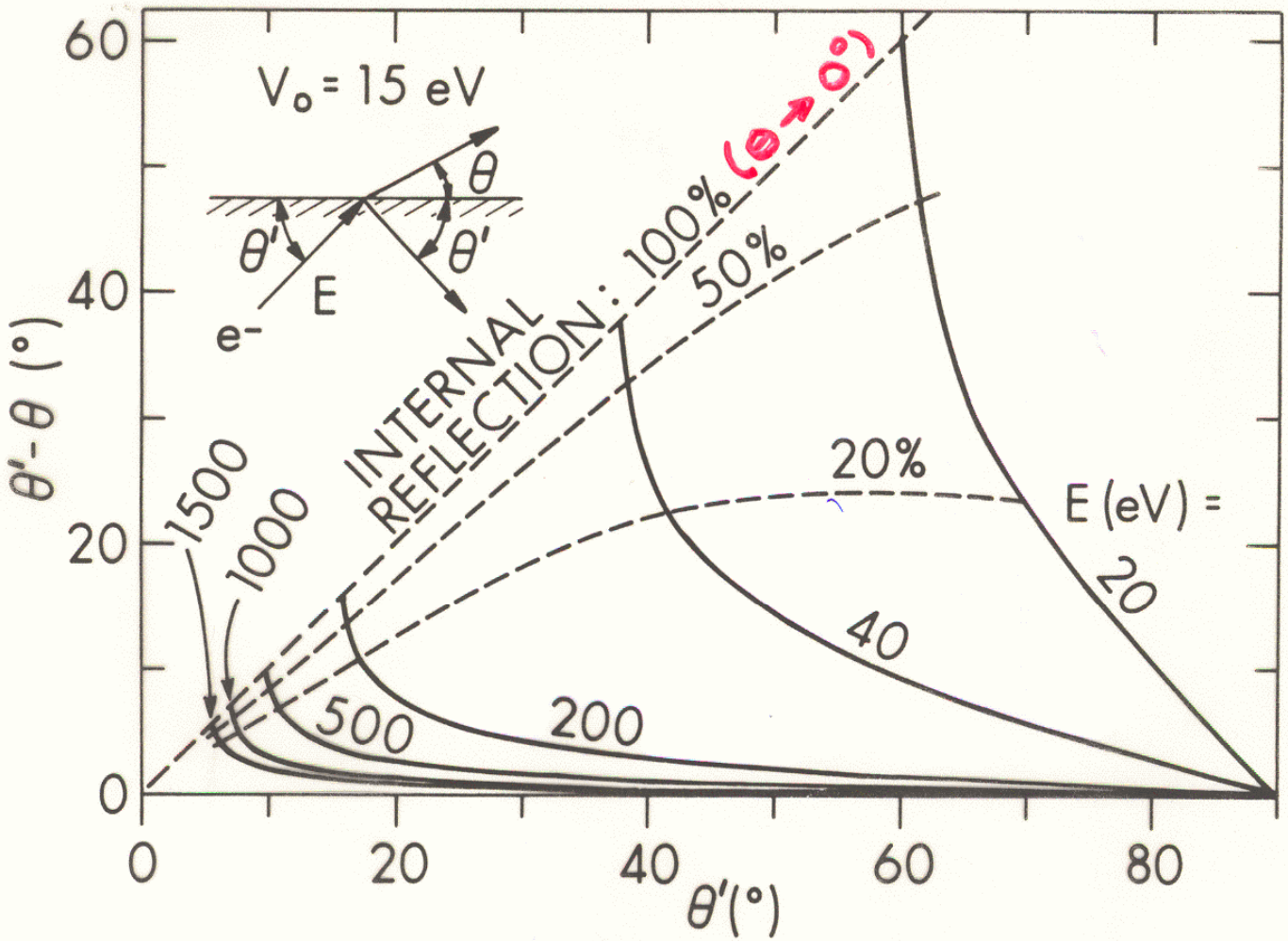

Fig. 14. Calculation of electron refraction effects for different electron kinetic energies and a typical V_0 value of 15eV. The degree of refraction is indicated by the difference θ' (internal) — θ (external) Contours of equal probablility of internal reflection are also shown. (From ref. (5).)

Surface sensitivity enhancement for grazing exit angles

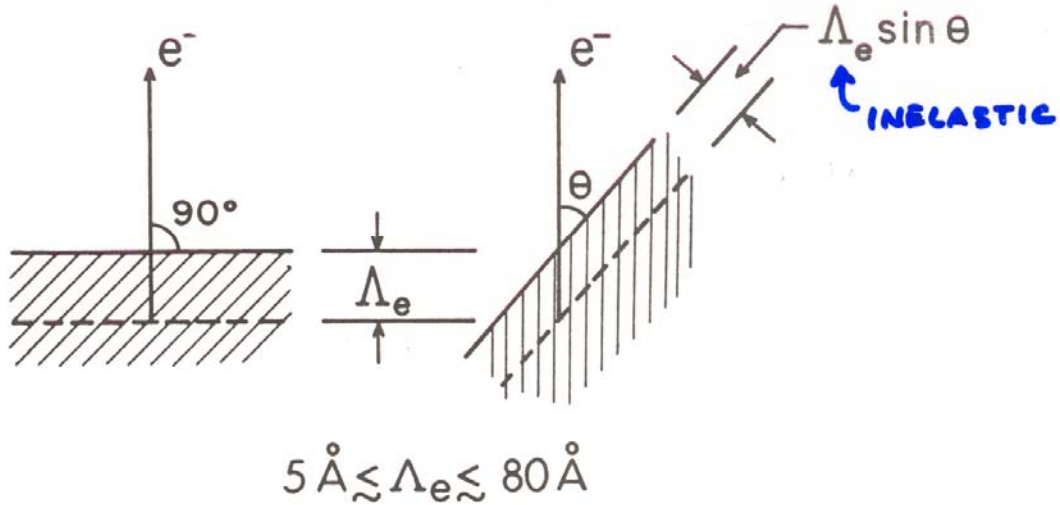

Fig. 5. Illustration of the basic mechanism producing surface sensitivity enhancement for low electron exit angles θ. The average depth for no-loss emission as measured perpendicular to the surface is $\Lambda_e \sin\theta$.

E.g.- $\Lambda_e = 28$ Å in Au(s) at 1400 eV

	θ	Mean Depth	No. layers
"BULK" →	90°	28 Å	~9
"SURFACE" →	10°	~4.4 Å	~1.5

... BUT REFRACTION AT SURFACE AND ELASTIC SCATTERING CAN REDUCE SURFACE ENHANCEMENT, ESP. AT LOW $\theta \lesssim 30°$

∴ BEST QUANTITATIVE ANALYSIS FOR RANGE 20-30° ≤ θ ≤ 90°

Outline

Surface, interface, and nanoscience—short introduction

Some surface concepts and techniques→photoemission

Synchrotron radiation: experimental aspects

Electronic structure—a brief review

The basic synchrotron radiation techniques
+Instrumentation for PS and XES

Core-level photoemission:
photoelectron diffraction

Valence-level photoemission

Microscopy with photoemission

Some basic measurements:

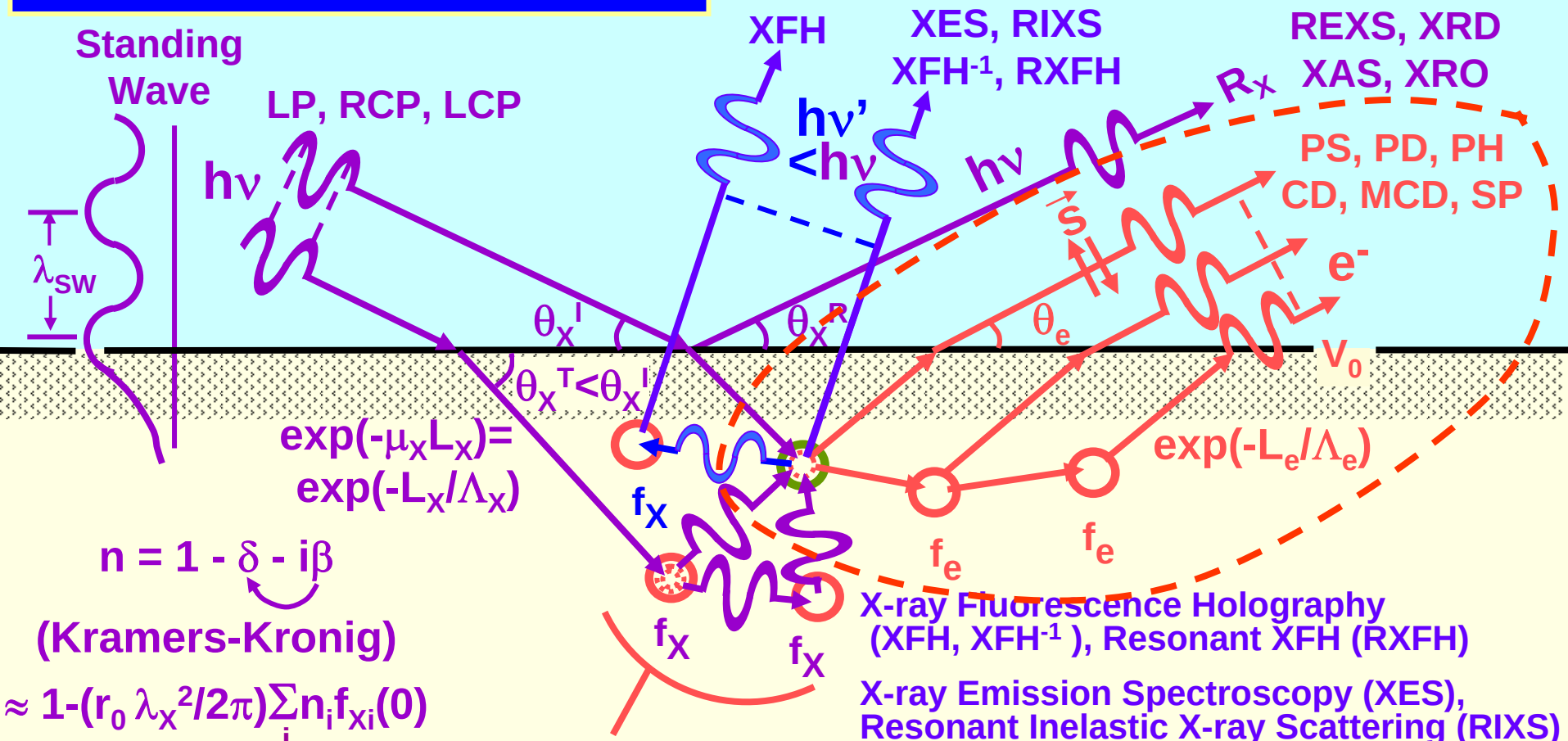

$n = 1 - \delta - i\beta$

(Kramers-Kronig)

$\approx 1-(r_0 \lambda_X^2/2\pi)\sum_i n_i f_{Xi}(0)$

$\mu_X = 4\pi\beta/\lambda_X$

$\theta_X^R = \theta_X^I$

$\lambda_{SW} = \lambda_X/(2\sin\theta_X^I)$

$\theta_{CRIT}^I = (2\delta)^{1/2}$

Multi-atom resonant photoemission (MARPE)

X-ray Fluorescence Holography (XFH, XFH^{-1}), Resonant XFH (RXFH)

X-ray Emission Spectroscopy (XES), Resonant Inelastic X-ray Scattering (RIXS)

Resonant Elastic X-ray Scattering (REXS)

X-Ray Diffraction (XRD)

X-ray Absorption Spectroscopy (XAS)

X-Ray Optical measurements (XRO)

Photoelectron Spectroscopy (PS), Diffraction (PD), Holography (PH)
+ Circular Dichroism (CD), Magnetic CD (MCD), Spin Polarization (SP)

CALCULATION OF PHOTOELECTRON INTENSITIES—THE 3-STEP MODEL

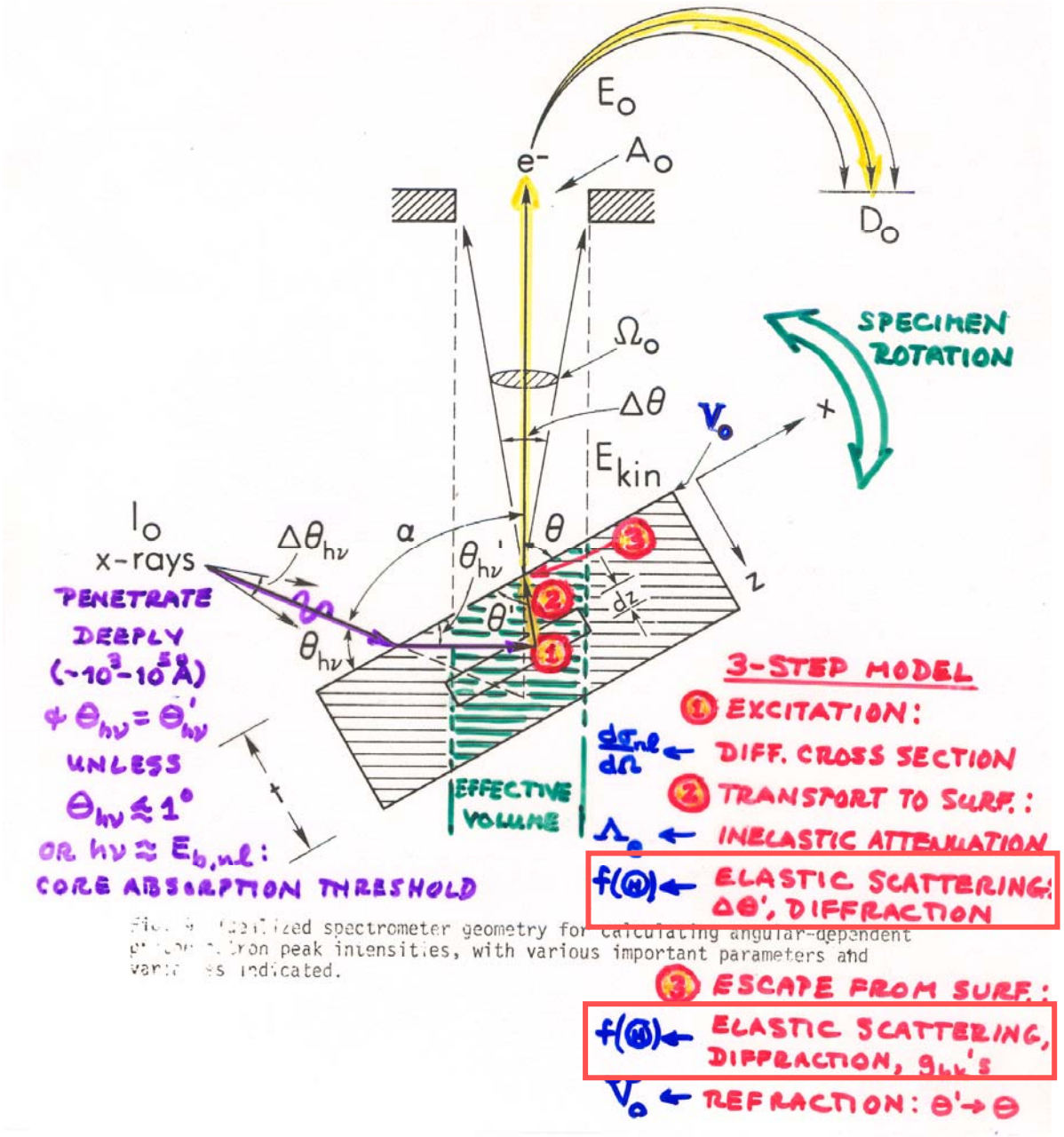

Fig. 9 Idealized spectrometer geometry for calculating angular-dependent photoelectron peak intensities, with various important parameters and variables indicated.

PHOTOELECTRON DIFFRACTION AND HOLOGRAPHY

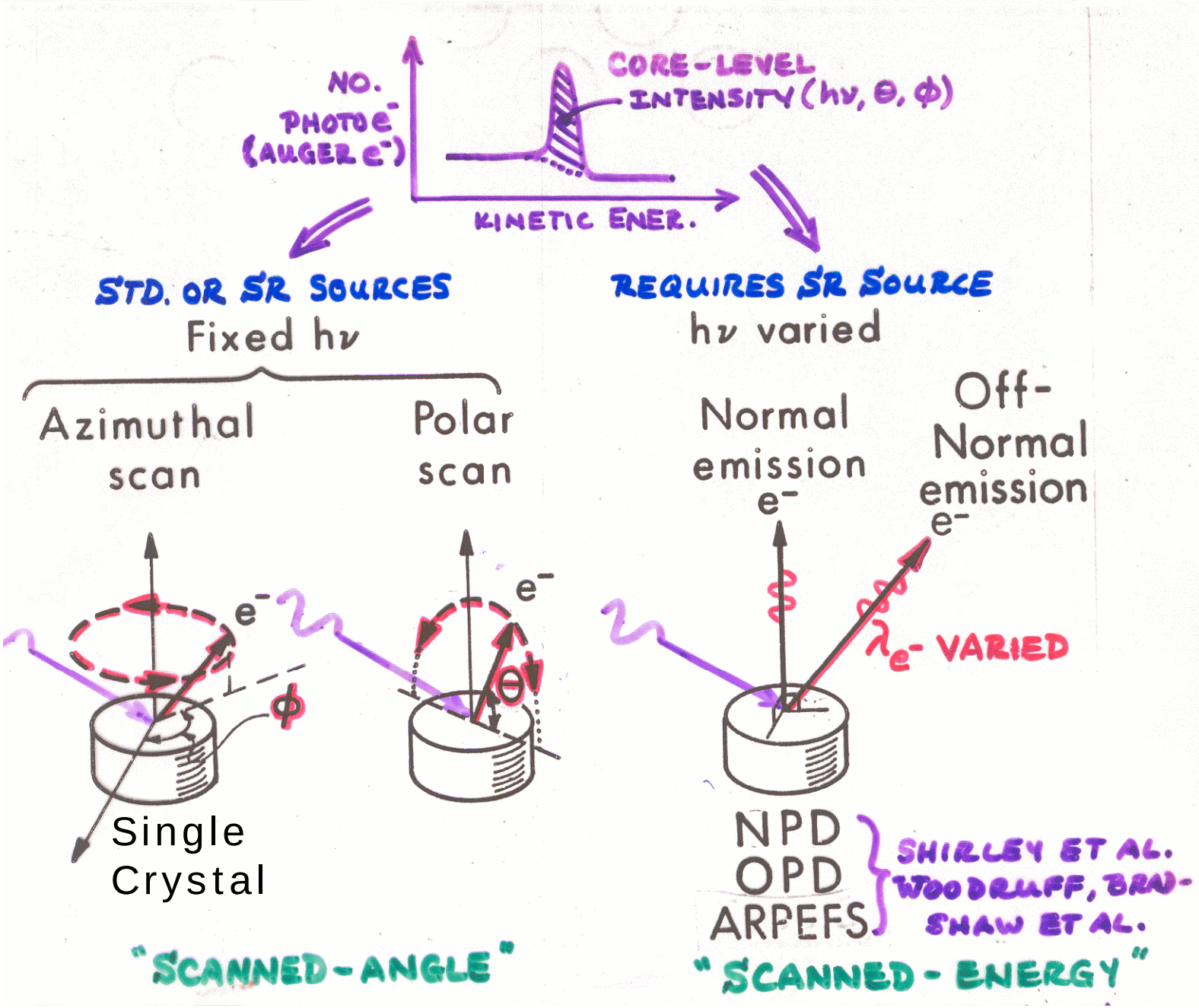

EFFECTS OF ELASTIC SCATTERING ON ANGULAR DISTRIBUTIONS: SINGLE-CRYSTAL SAMPLE→→ *PHOTOELECTRON DIFFRACTION And PHOTOELECTRON HOLOGRAPHY*

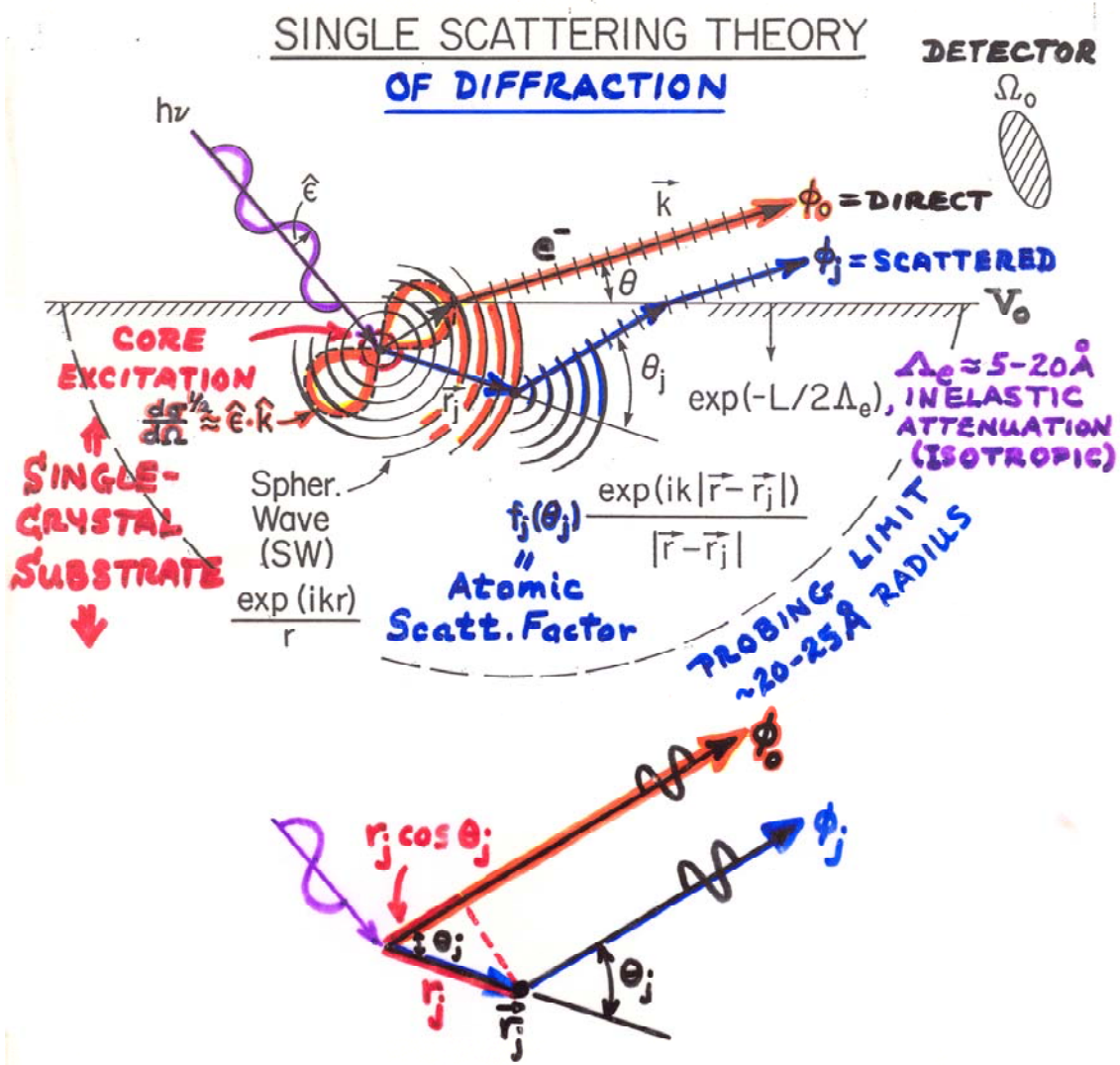

"Study of Surface Structures…"
Figure 3

Photoelectron diffraction: A Simple Picture

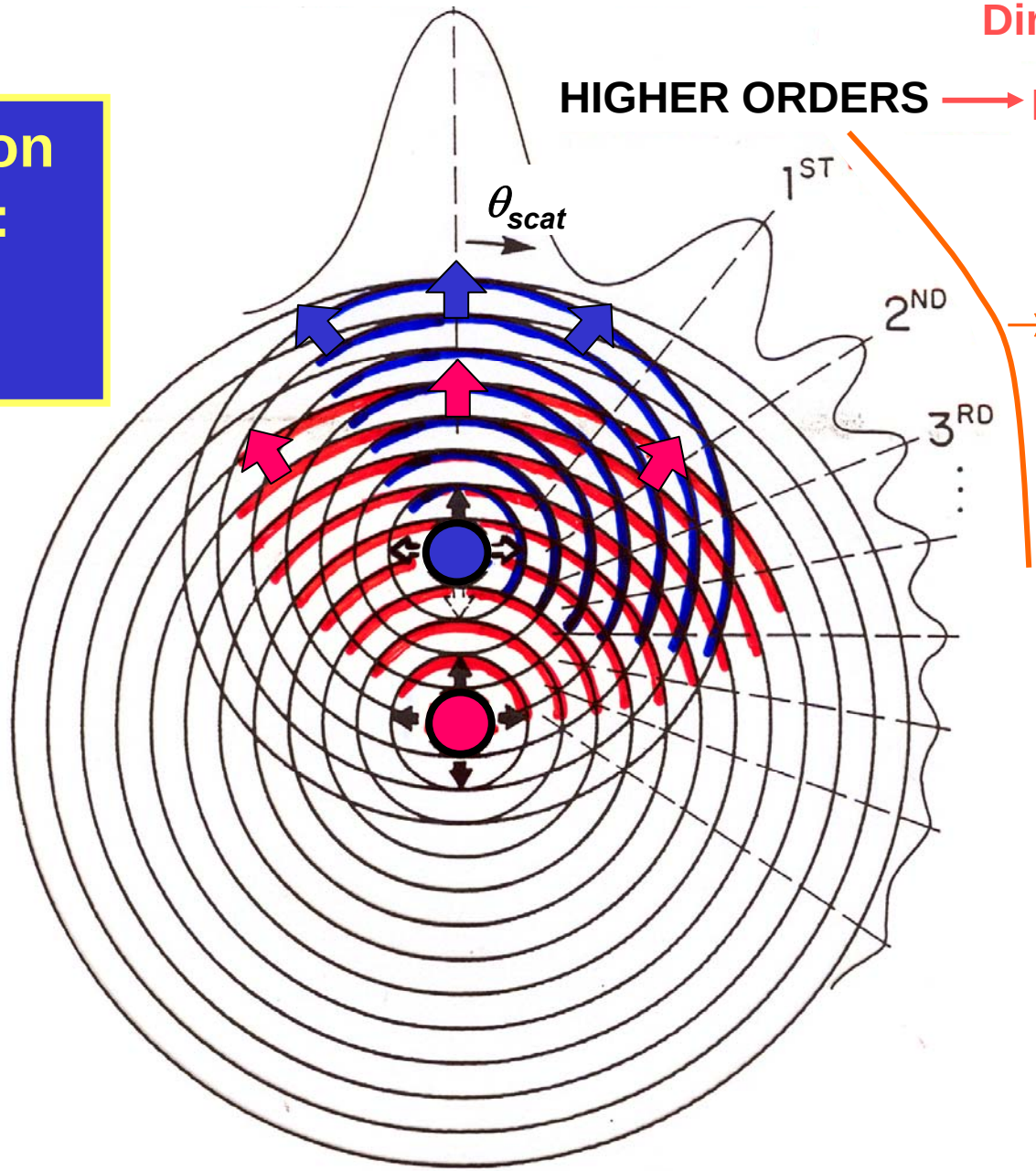

FORWARD SCATT. = "OTH ORDER" → Bond & Low-Index Directions

HIGHER ORDERS → Bond Lengths & Atomic Positions

→Holographic fringes

SCANNED-ANGLE PHOTOELECTRON DIFFRACTION

Example:

Ge(111) - Ge3d Photoelectron Hologram

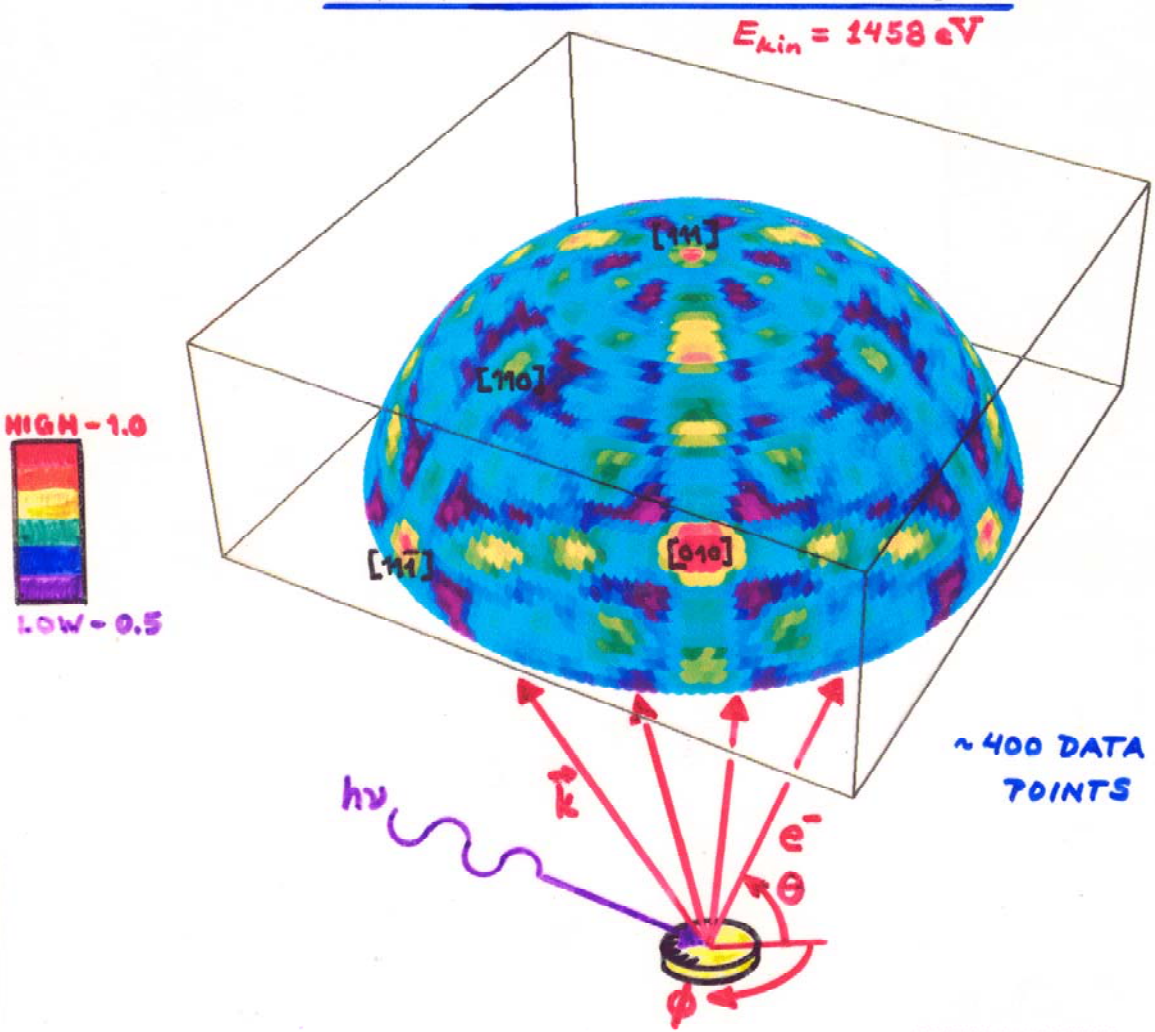

~400 DATA POINTS

TRAN ET AL., SURF. SCI. 281, 270('93) + BUDGE, YNZUNZA

SCANNED-ENERGY PHOTOELECTRON DIFF.

($\sqrt{3}\times\sqrt{3}$) AL ON Si(111)

* 41 diffraction curves χ taken from Al 2p
* $\theta = 0\sim70^\circ$, $\varphi=0\sim60^\circ$

} ~1100 DATA POINTS

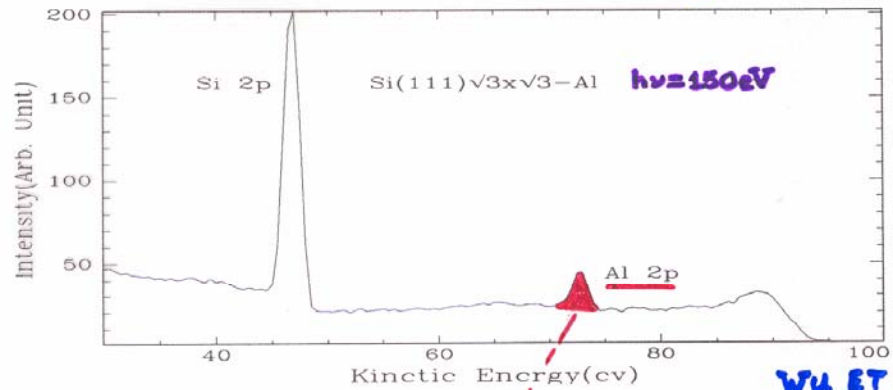

WU ET AL.,
P.R.L. 71, 261('93)
P.R.B 51, 14549('95)

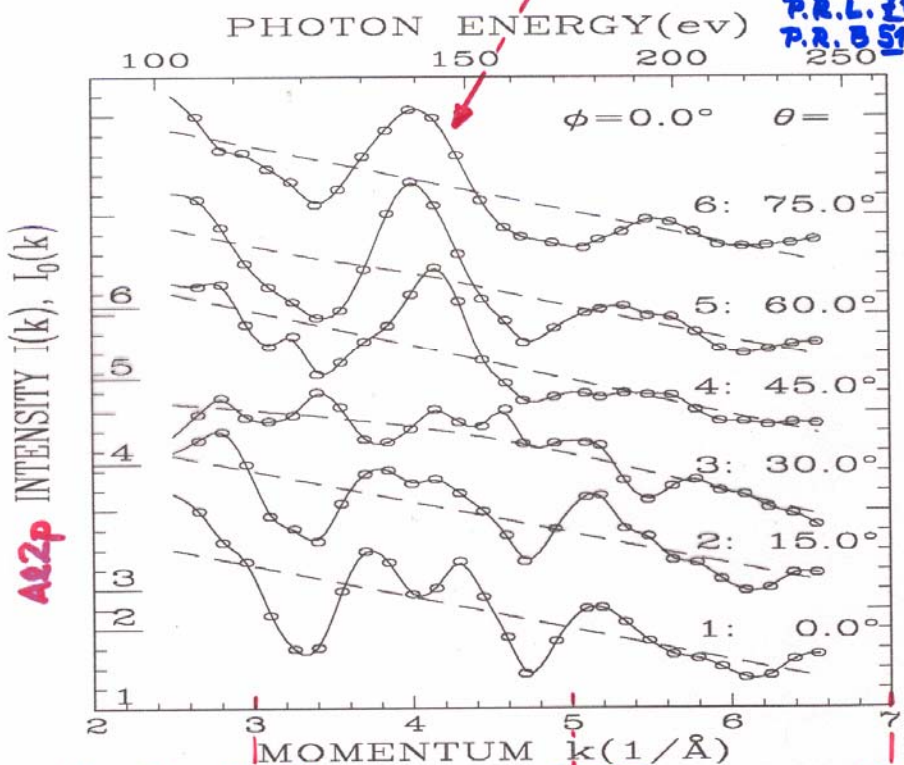

E_{kin}= 34 eV 94 eV 184 eV

Photoelectron diffraction: Simple single-scattering theory for s-subshell emission

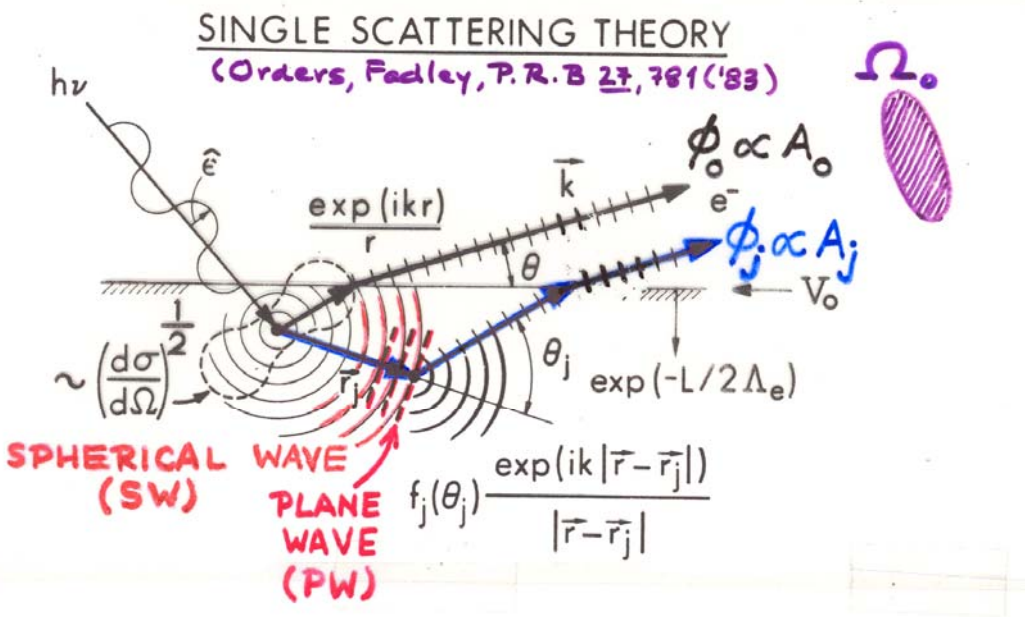

$$\chi(E \text{ or } \vec{k}) \propto \sum_j \frac{F_j(k)}{F_0} \cos\left[k r_j (1-\cos\theta_j) + \psi_j(\theta_j, k)\right]$$

(CLUSTER)

PATH LENGTH DIFFERENCE (P.L.D.)

SCATTERING PHASE SHIFT

ELASTIC e^-–ATOM SCATTERING

DEBYE-WALLER

INELASTIC e^-–e^- SCATTERING

$$F_j(k) = (\hat{\varepsilon}\cdot\hat{r}_j)\frac{|f_j(\theta_j,k)|}{r_j} W_j(\theta_j,k)\exp(-L_j/2\Lambda_e)$$

= amplitude of scattered wave

$$F_0 = (\hat{\varepsilon}\cdot\hat{k})\exp(-L_0/2\Lambda_e)$$

= amplitude of direct wave

"Study of Surface Structures…"
Figure 3

FROM SINGLE-SCATTERING THEORY:

(E.G., P.R.B 22, 6085 ('80); P.R.B 27, 781 ('83))

$$I(\vec{k}) \propto \left|\phi_0 + \sum_j \phi_j\right|^2, \quad \sum_j \text{ ON FINITE CLUSTER,}$$

$$\propto |\phi_0|^2 + \sum_j (\phi_0^* \phi_j + \phi_0 \phi_j^*) + \sum_j \sum_{j'} \phi_j^* \phi_{j'}$$

IF $\phi_j \phi_{j'}^*$ SMALL W.R.T $\phi_0^* \phi_j + \phi_0 \phi_j^*$, A NECESSARY CONDITION FOR SIMPLE HOLOGRAPHY:

$$I(\vec{k}) \propto \underset{\substack{\parallel \\ I_0}}{F_0^2} + 2F_0 \sum_j |F_j(\theta_j)| \cos\Big[k \underbrace{r_j(1-\cos\theta_j)}_{\text{PATH LENGTH DIFFERENCE}} + \underbrace{\psi_j(\theta_j, k)}_{\text{SCATTERING PHASE}}\Big]$$

$$\boxed{\chi(\vec{k}) = \frac{I(\vec{k}) - I_0}{I_0^{1/2}} \propto \left\{\sum_j |F_j(\theta_j)| \cos\Big[k r_j (1-\cos\theta_j) + \psi_j(\theta_j, k)\Big]\right\}}$$

WITH: $F_0 = (\hat{\varepsilon}\cdot\hat{k}) \exp(-L_0/2\Lambda_e)$

$= \text{amplitude of direct wave} = I_0^{1/2}$

$$|F_j(\theta_j)| = (\hat{\varepsilon}\cdot\hat{r}_j) \frac{|f_j(\theta_j)|}{r_j} W_j(\theta_j) \exp(-L_j/2\Lambda_e)$$

$= \text{amplitude of scattered wave}$

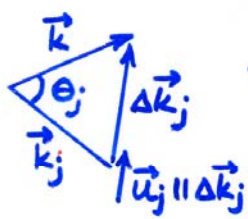

$$W_j = \exp(-\Delta k_j^2 \overline{u_j^2})$$

$$= \exp(-2k^2(1-\cos\theta_j)\overline{u_j^2})$$

LIKE EXAFS/SEXAFS, BUT THERE:

- ADD CENTRAL ATOM PHASE SHIFT δ_1
- $\psi_j \Rightarrow \pi$ FOR ALL SCATTERERS
- cos $\Rightarrow$ sin IN ANGLE INTEGRATION
- $\hat{\varepsilon}\cdot\hat{r}_j/r_j \Rightarrow \hat{\varepsilon}\cdot\hat{r}_j/r_j^2$ IN OUT/BACK PATHS

CALCULATION OF e^--ATOM SCATTERING FACTORS:

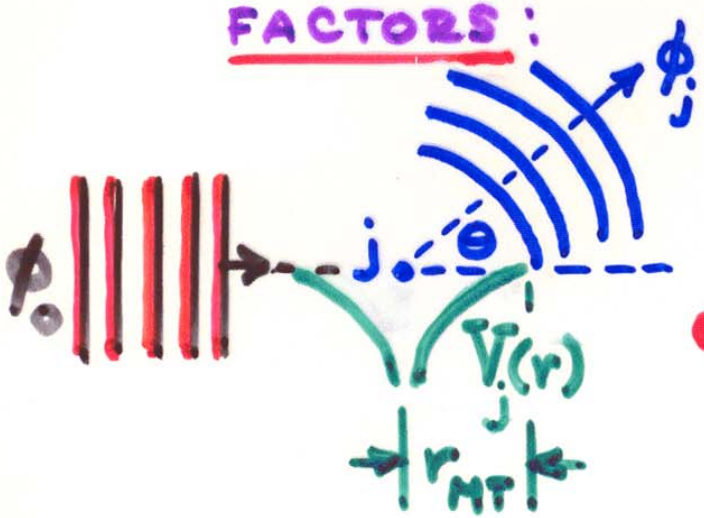

PLANE-WAVE SCATTERING:

PARTIAL-WAVE METHOD†

PHASE SHIFT

$$f_j^{PW}(\theta) = \frac{1}{k} \sum_{\ell=0}^{\ell_{max}} (2\ell+1) e^{i\delta_\ell} \sin\delta_\ell \, P_\ell(\cos\theta)$$

$$\ell_{max} \lesssim k r_{MT}$$

† ANY TEXTBOOK ON SCATTERING

ENERGY DEPENDENCE OF ELECTRON ELASTIC SCATTERING

$f(\theta) = |f(\theta)| e^{i\psi(\theta)}$

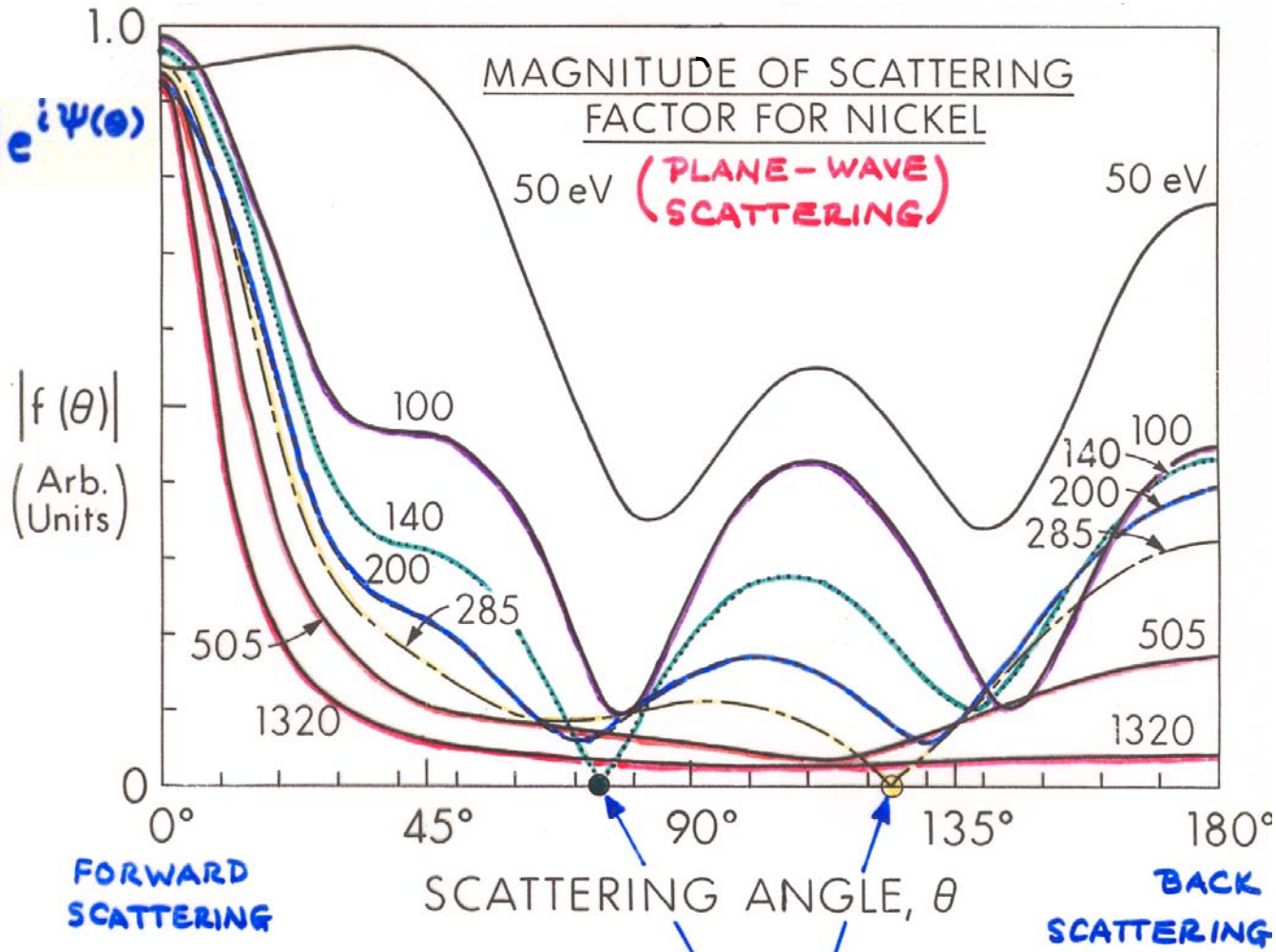

ZEROES, "GENERALIZED RAMSAUER-TOWNSEND EFFECT"

(M. SAGURTON ET AL., SURF. SCI. 182, 287 ('87))

"Study of Surface Structures…"
Figure 2

ENERGY DEPENDENCE OF ELECTRON ELASTIC SCATTERING

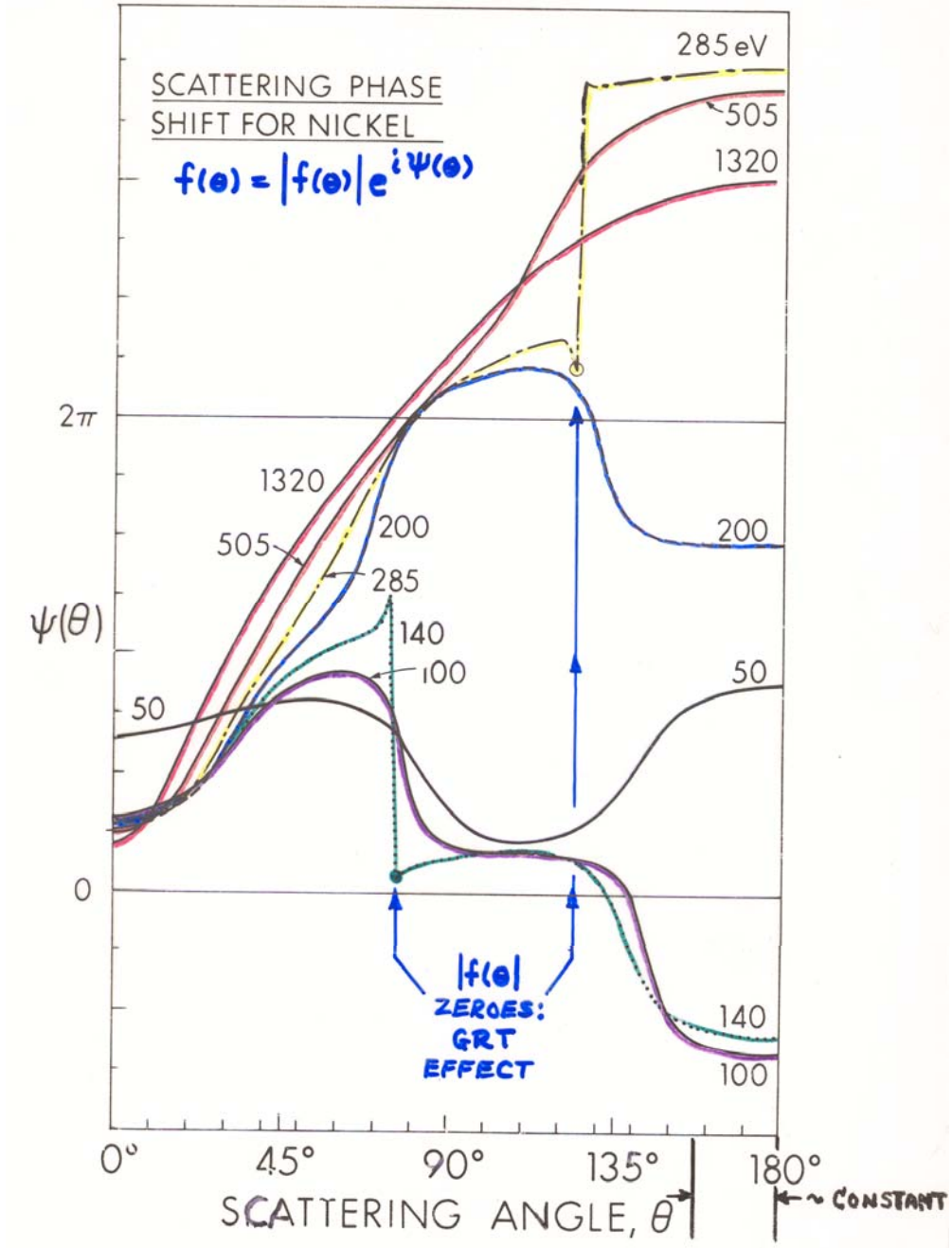

CALCULATION OF e^--ATOM SCATTERING FACTORS:

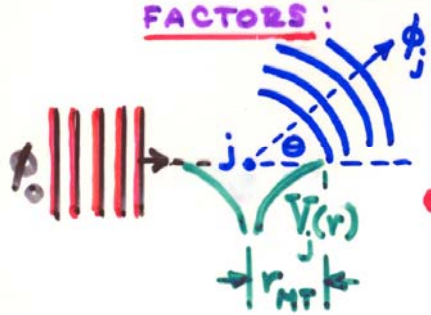

PLANE-WAVE SCATTERING:

PARTIAL-WAVE METHOD[+]

PHASE SHIFT

- $$f_j^{PW}(\theta) = \frac{1}{k}\sum_{\ell=0}^{\ell_{max}}(2\ell+1)e^{i\delta_\ell}\sin\delta_\ell P_\ell(\cos\theta)$$

$$\ell_{max} \lesssim k r_{MT}$$

[+] ANY TEXTBOOK ON SCATTERING

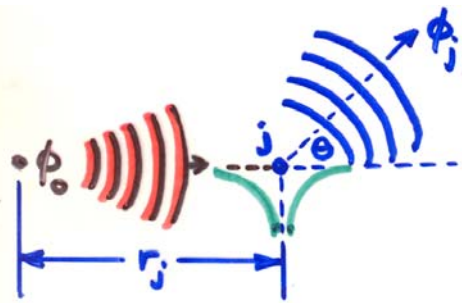

SPHERICAL-WAVE SCATTERING:

REHR-ALBERS METHOD[*]

- $$f_j^{SW}(\theta) = \frac{1}{k}\sum_{\ell=0}^{\ell_{max}}\left\{(2\ell+1)e^{i\delta_\ell}\sin\delta_\ell P_\ell(\cos\theta)\cdot \frac{[(\ell+1)C_{\ell+1}(kr_j)+\ell C_{\ell-1}(kr_j)]}{2\ell+1}\right\}$$

WITH:

$$C_\ell(kr_j) = \left[1+\frac{\ell(\ell+1)}{2(kr_j)^2}\right]e^{\frac{i\ell(\ell+1)}{2kr_j}}$$

[*] MUSTRE DE LEON ET AL., PHYS. REV. B 39, 5632 ('89)

- AND MORE ACCURATE MATRIX METHODS IN REHR, ALBERS, PHYS. REV. B 41, 8139 (1990) + FRIEDMAN, FADLEY, J. ELECT. SPECT. 51, 689 (1990)

PW vs. SW scattering

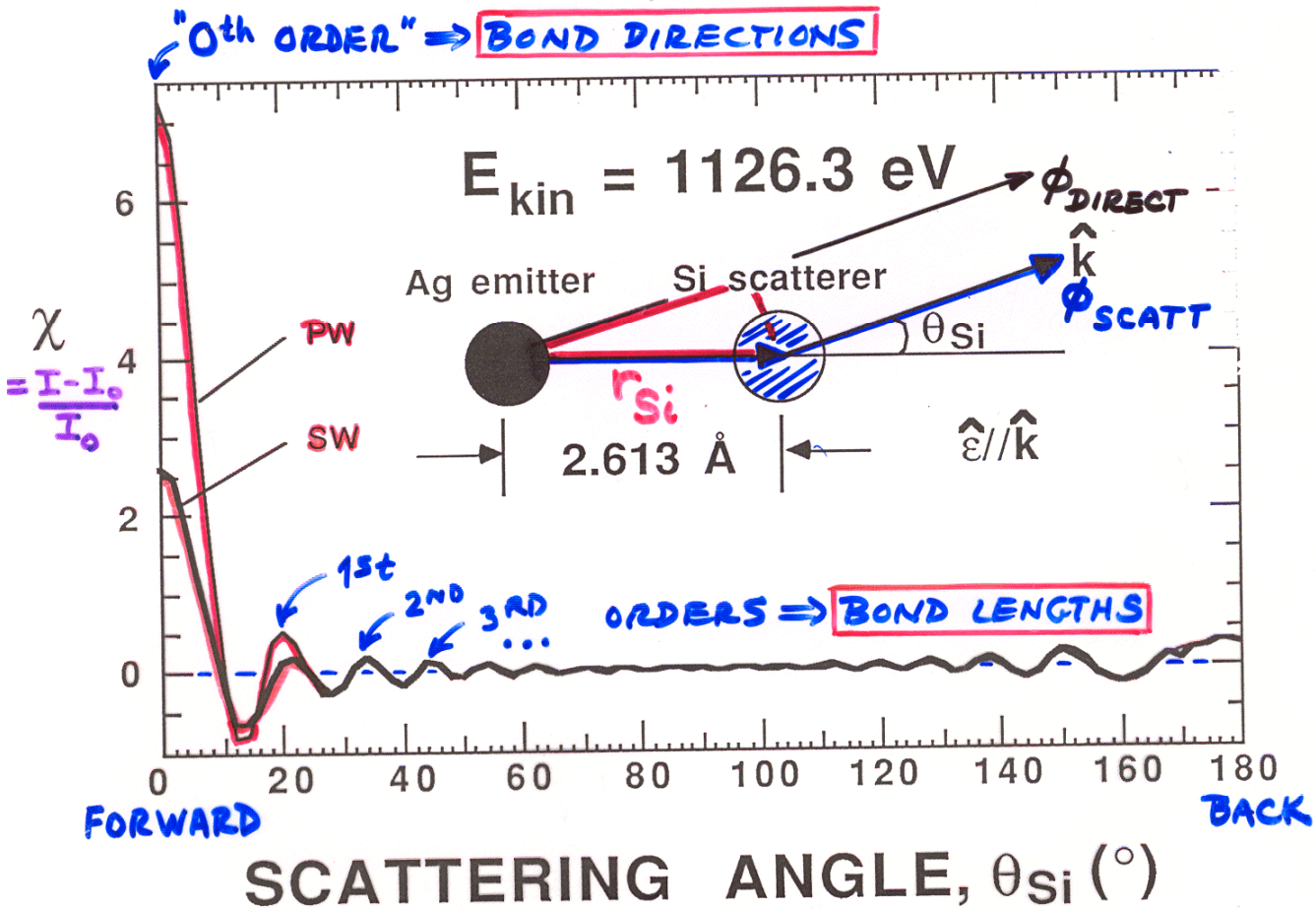

PATH LENGTH DIFFERENCE =

$$r_{Si}(1-\cos\theta_{Si})$$

ORDERS:

SCATTERING PHASE SHIFT

$$2\pi n = [k r_{Si}(1-\cos\theta_{Si}) + \psi_{Si}(\theta)]$$

Vibrational effects on diffraction

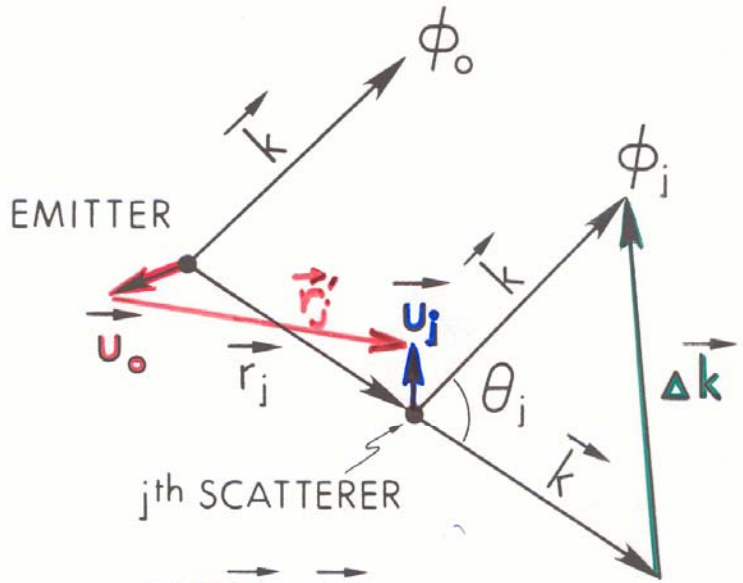

$$\vec{\sigma}_{jo} = \vec{U}_j - \vec{U}_o$$

- DW FACTOR $= e^{-\frac{1}{2}\overline{(\Delta\vec{k}\cdot\vec{\sigma}_{jo})^2}} = e^{-\frac{1}{2}\Delta k^2\overline{\sigma_{jo,\parallel}^2}}$
- $\vec{U}_j$, $\vec{U}_o$ UNCORRELATED:

  $$DW = e^{-\frac{1}{2}\overline{(\Delta\vec{k}\cdot\vec{u}_j)^2}}\, e^{-\frac{1}{2}\overline{(\Delta\vec{k}\cdot\vec{u}_o)^2}}$$

- $\vec{U}_j \approx \vec{U}_o$ IN DISTRIBUTION:

  $$DW = e^{-\overline{(\Delta\vec{k}\cdot\vec{u}_j)^2}}$$

- $\vec{U}_j$ ISOTROPIC:

  $$DW = e^{-\Delta k^2\overline{u_j^2}} = e^{-2k^2(1-\cos\theta_j)\overline{u_j^2}}$$ ← USUAL LEVEL

DECREASING ACCURACY

+ CORRELATED?

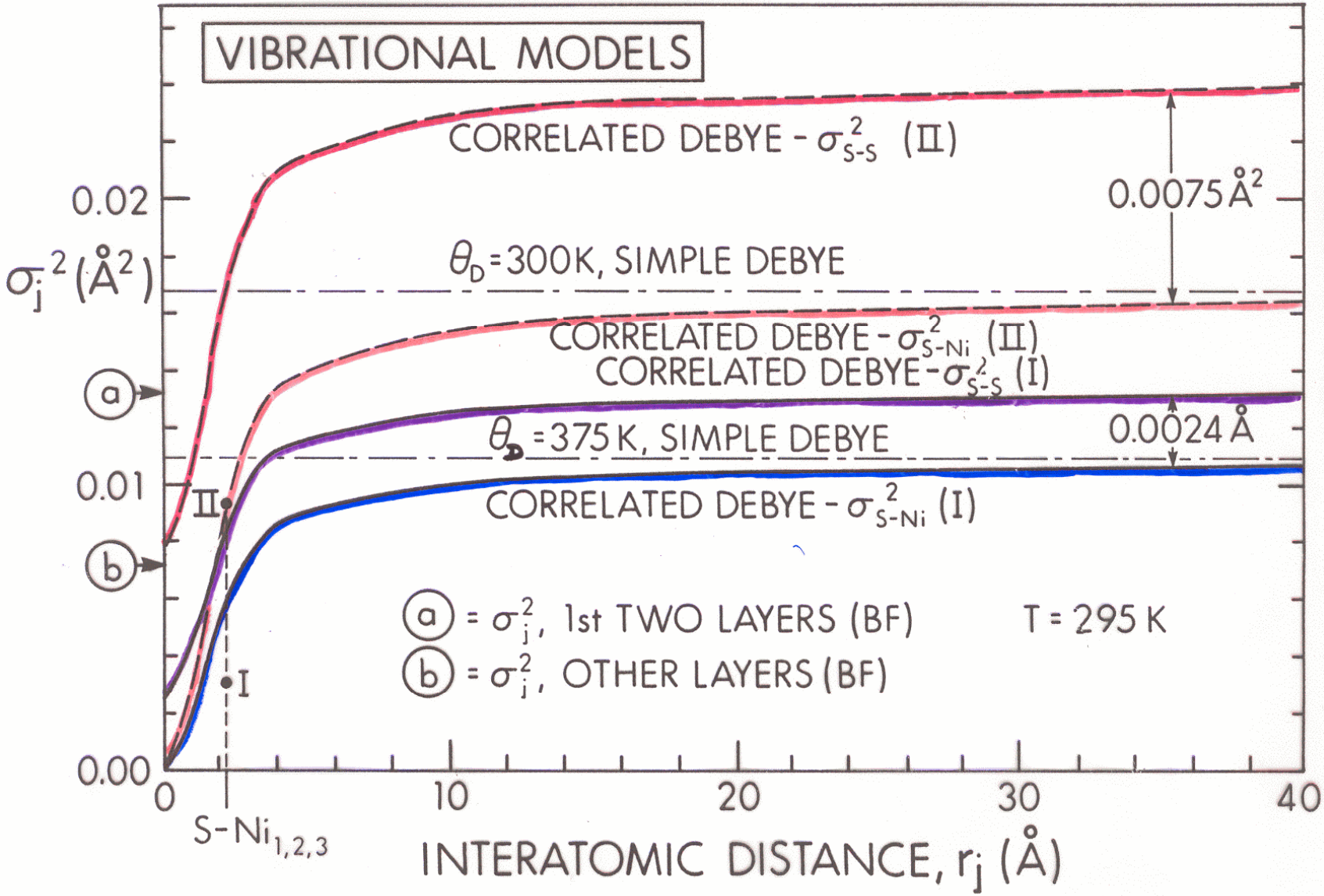

[SAGURTON, BULLOCK, FADLEY, SURF. SCI. 182, 287 (1987)]

Table 1 Debye temperature and thermal conductivity[a]

Low temperature limit of θ, in Kelvin
Thermal conductivity at 300 K, in W $cm^{-1}K^{-1}$

Li	Be											B	C	N	O	F	Ne
344	1440												2230				75
0.85	2.00											0.27	1.29				
Na	Mg											Al	Si	P	S	Cl	Ar
158	400											428	645				92
1.41	1.56											2.37	1.48				
K	Ca	Sc	Ti	V	Cr	Mn	Fe	Co	Ni	Cu	Zn	Ga	Ge	As	Se	Br	Kr
91	230	360.	420	380	630	410	470	445	450	343	327	320	374	282	90		72
1.02		0.16	0.22	0.31	0.94	0.08	0.80	1.00	0.91	4.01	1.16	0.41	0.60	0.50	0.02		
Rb	Sr	Y	Zr	Nb	Mo	Tc	Ru	Rh	Pd	Ag	Cd	In	Sn w	Sb	Te	I	Xe
56	147	280	291	275	450		600	480	274	225	209	108	200	211	153		64
0.58		0.17	0.23	0.54	1.38	0.51	1.17	1.50	0.72	4.29	0.97	0.82	0.67	0.24	0.02		
Cs	Ba	La β	Hf	Ta	W	Re	Os	Ir	Pt	Au	Hg	Tl	Pb	Bi	Po	At	Rn
38	110	142	252	240	400	430	500	420	240	165	71.9	78.5	105	119			
0.36		0.14	0.23	0.58	1.74	0.48	0.88	1.47	0.72	3.17		0.46	0.35	0.08			
Fr	Ra	Ac															

Ce	Pr	Nd	Pm	Sm	Eu	Gd	Tb	Dy	Ho	Er	Tm	Yb	Lu
						200		210				120	210
0.11	0.12	0.16		0.13		0.11	0.11	0.11	0.16	0.14	0.17	0.35	0.16
Th	Pa	U	Np	Pu	Am	Cm	Bk	Cf	Es	Fm	Md	No	Lr
163		207											
0.54		0.28	0.06	0.07									

[a] Most of the θ values were supplied by N. Pearlman; references are given the *A.I.P. Handbook*, 3rd ed; the thermal conductivity values are from R. W. Powell and Y. S. Touloukian, Science **181**, 999 (1973).

Case study: Determining the orientation of an adsorbed molecule from photoelectron diffraction at about 1 keV energy

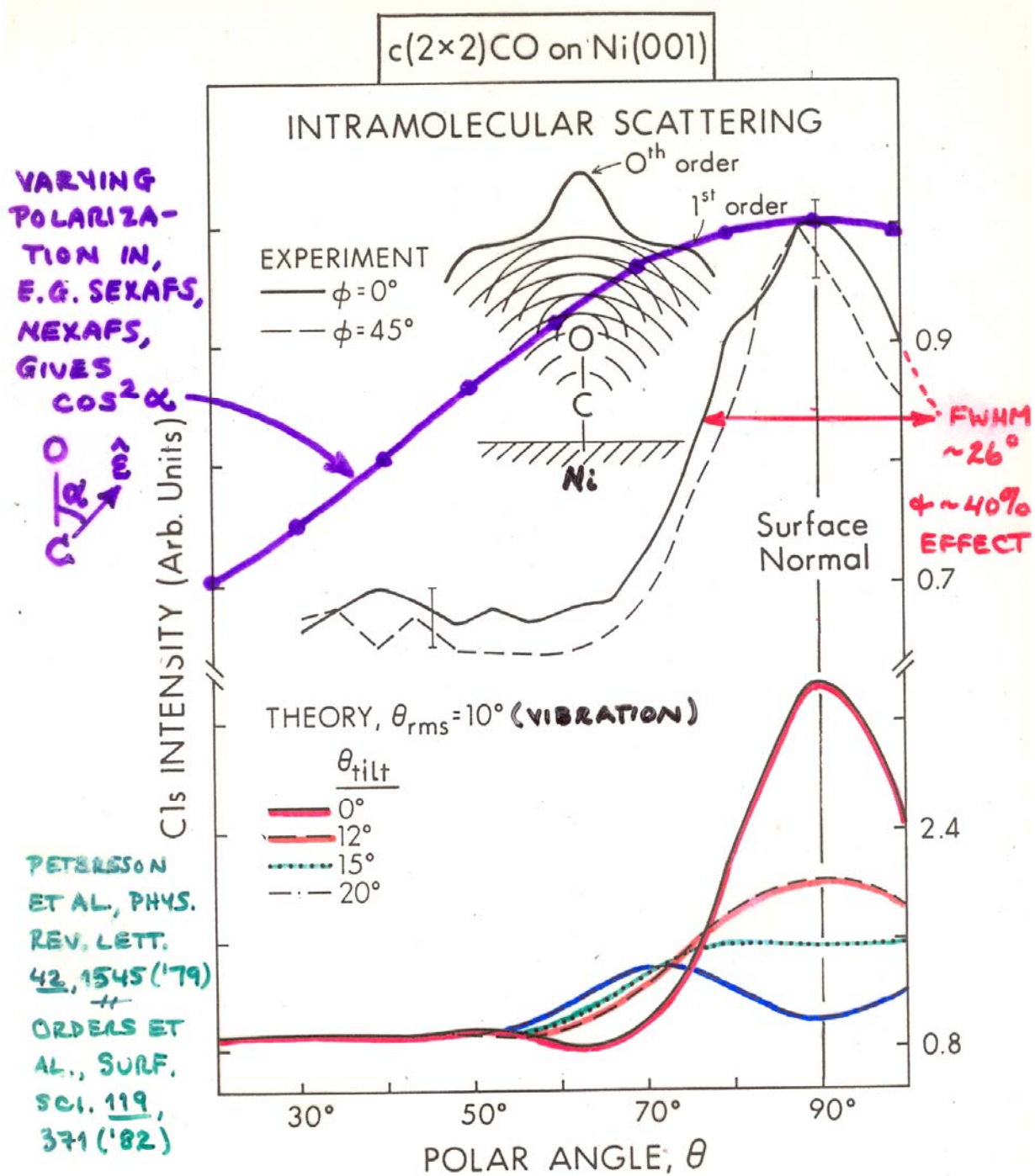

"Study of Surface Structures…"
Figure 8

TEMPERATURE-DEPENDENT ADSORBATE ORIENTATION

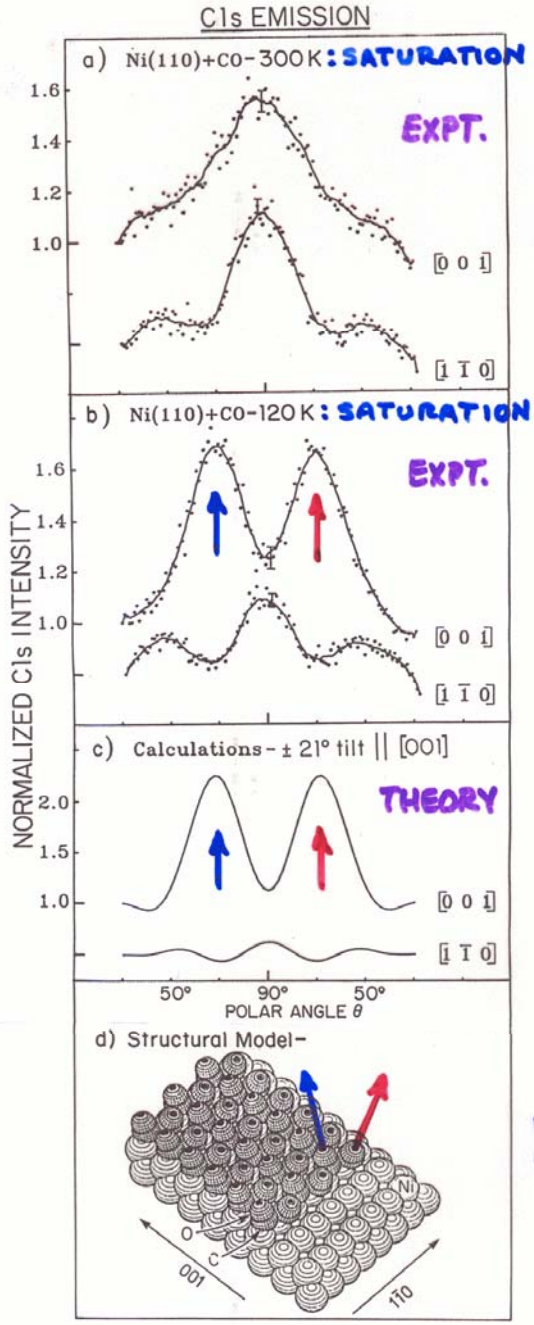

WESNER, BONZEL
COENEN, P.R.L.
60, 1045 ('88)

"Study of Surface Structures…"
Figure 12

ORIENTATION OF A HIGHLY TILTED MOLEC. ON SURFACE

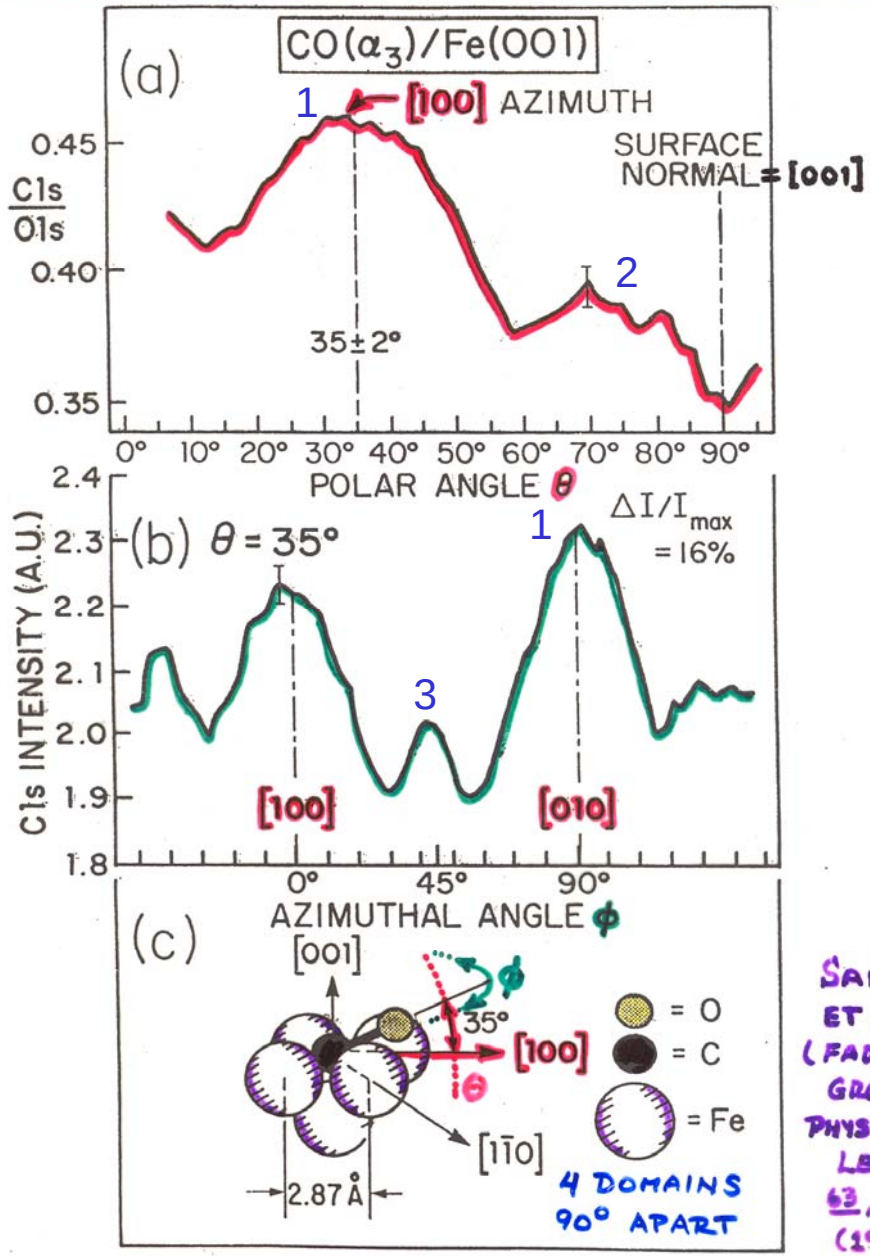

SAIKI ET AL. (FADLEY GROUP) PHYS. REV. LETT. 63, 283 (1989)

"Study of Surface Structures…"
Figure 9

CALCULATED 2π INTENSITY
CO(α_3)/Fe(001)

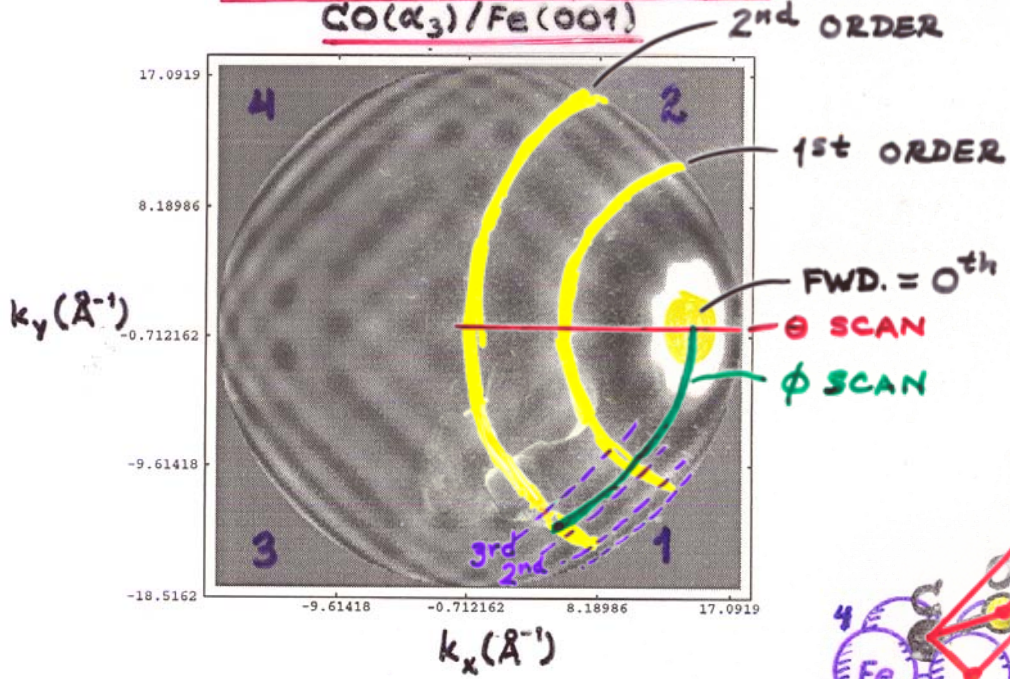

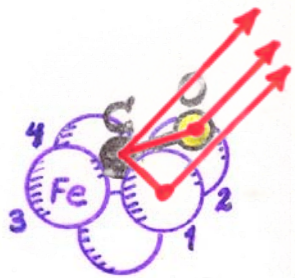

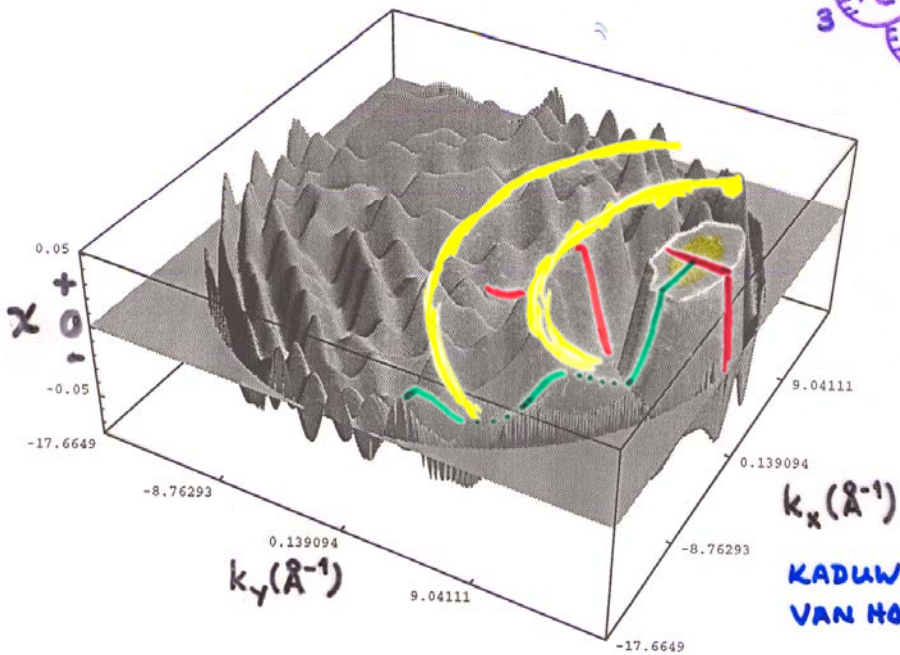

KADUWELA, BUDGE, VAN HOVE, FADLEY

Online calculation of photoelectron diffraction patterns:

EDAC output for CO/Fe(001)

Click on the figure to download data.

http://csic.sw.ehu.es/jga/software/edac/a.html

7 atoms:

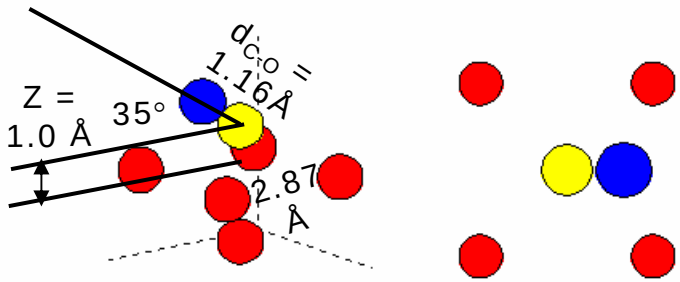

Left: representation of the cluster rocking around a line parallel to the *z* direction and passing by the **emitter (yellow atom)**. The dashed lines stand for the *xyz* axes. **Right:** top view of the cluster, where the *x*/*y* direction (not plotted) runs along the horizontal/vertical screen direction. Different atomic species have been assigned the colors **O**, **Fe**.

Oxygen 1st order diff. ring

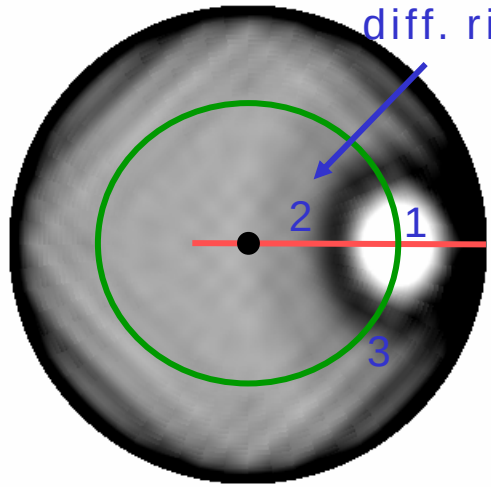

Polar scan of photoemission intensity (logarithmic scale). White/black regions correspond to high/low intensity. The orientation is the same as in the top-view of the cluster. The distance to the center of the figure is proportional to the polar angle θ. The polar angle range is (0.0, 89.0) (in degrees).

Parameters used in the calculation:

N=7 atoms
Iteration order=4
l_{max}=25
V_0=10.5 eV
Photoelecton energy=1202 eV
p-polarized light
z_0=1.435 Å
Recursion iteration method

X 4 domains rotated by 90°

Electron Diffraction in Atomic Clusters

for Core Level Photoelectron Diffraction Simulations

Created by F. Javier García de Abajo (CSIC and DIPC, San Sebastian, Spain)
in collaboration with M. A. Van Hove and C. S. Fadley (LBNL, Berkeley, and UCD, Davis, California)

This site allows performing on-line photoelectron diffraction calculations. Multiple scattering (MS) of the photoelectron is carried out for a cluster representing a solid or molecule. Select the corresponding parameters and click on the "Calculate" button below to perform the actual calculation and to produce a plot of the calculated data (a separate window pops out to display it). A numerical data table can be downloaded by clicking on the resulting plot. Click on the different parameter names in blue to see fuller explanations. Click on the "Preview Cluster" button to display the currently selected atomic cluster (but without performing a MS calculation) or the button "Download Cluster" to download the currently selected cluster. Notice that the scattering phase shifts and excitation radial matrix elements are calculated internally for each cluster configuration, so that the user does not have to provide them. Please, read the terms of use and the restrictions on input parameters before using this site for the first time.

Terms and conditions of use

Terms of use Restrictions on input parameters Password: ********

A password is only necessary for large computation times (click here for more details). Leave it blank otherwise.

Title (optional): CO/Fe(001)

Cluster definition

The cluster and the list of emitters are defined by a list of commands with the following format (click here or on the items of this list for further details):

atom symbol *x y z* layer symbol *x y z a b* α_1 α_2

surface symbol *x y z a* type emitter *x y z*

Fill in the text box with these commands according to the cluster specifications that you need. Some examples are provided by clicking here (you may cut and paste them to this page and modify them further).

```
atom O 0.95 0 1.66
atom C 0 0 1.0
surface Fe 1.435 1.435 0 2.87 bcc100
emitter 0 0 1.0
end
```

The cluster consists of a maximum of 7 atoms. (Warning: a finite number of atoms generally introduces symmetry breaking.)

The size of the cluster is determined by the distance d_{max} = 10 Å and the reference point x_0 = 0 Å, y_0 = 0 Å, z_0 = 0 Å.

See cluster shape for more details.

Plot cluster on output? ◉ Yes ○ No

Cluster shape: ◉ Parabolic ○ Spherical

Preview Cluster* Download Cluster*

Geometry of beam and analyzer

Incoming beam parameters (see figure)

Polar angle θ_i = 0 degrees

Azimuthal angle φ_i = 0 degrees

Polarization:
- ◉ p-polarization
- ○ s-polarization
- ○ RCP
- ○ LCP

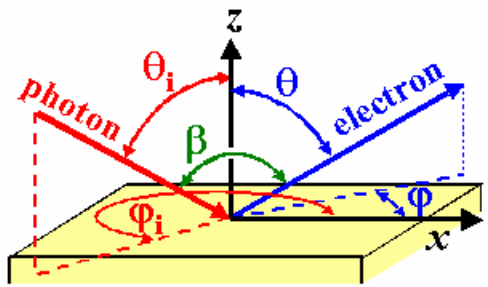

Schematic representation of the geometry

Mobility of cluster beam, and sample (click here for details):
- ◉ Only the sample moves with constant β = 90 degrees
- ○ Only the analyzer moves
- ○ Both the sample and the analyzer move

Energy and angle scanning parameters (see figure above)

The following entries will select the range of photoelectron energies and angles of emission.

Energy scans for a given emission angle can be chosen by selecting more than one energy of emission and only one polar angle and one azimuthal angle (the value of each angle is then taken as the lower limit of the selected angular range, and the value of the upper limits are disregarded). In this case, the output is a 1D plot with the photoelectron intensity as a function of photoelectron energy.

Electron energy range: 1 equally-spaced value(s) of the electron energy from 1202 eV to 1202 eV

Polar angle: 50 equally-spaced value(s) of the polar angle θ from 0 degrees to 89 degrees

Azimuthal angle: 61 equally-spaced value(s) of the azimuthal angle φ from 0 degrees to 360 degrees

Type of 2D angular representation: ○ Linear scale ◉ Logarithmic scale

Type of azimuthal of polar angular representation: ◉ Cartesian ○ Polar

Photoelectron detector half-width acceptance angle = 0 degrees. The photoelectron intensities are angle-averaged over a cone with half aperture given by this parameter.

Multiple scattering parameters

Additional solid parameters

Inner potential V_0 = 12.4 eV

Electronic edge z_0 = 1.435 Å

8.1 eV from band struct. + work function = 4.3 eV = 12.4 eV

Internal code parameters

Maximum orbital quantum number l_{max} = 25

Scattering order = 4

Iteration method: ○ Jacobi (regular MS) ◉ Recursion

Inelastic mean free path: either choose a fixed value = 17.8 Å

or (if that last entry is <0) use the TPP-2M formula with parameters ρ = 8.91 g/cm^3, N_v = 10, E_p = 35.45 eV, and E_g = 0 eV

Temperature (K) = 300 and Debye emperature (K) = 450

Table 4 Density and atomic concentration

The data are given at atmospheric pressure and room temperature, or at the stated temperature in deg K. (Crystal modifications as for Table 3.)

Atomic radius = r_{MT} = 0.5 n-n dist.

Average surface density = $\rho_S = (\rho_V)^{2/3}$

H 4K																	He 2K
0.088																	0.205 (at 37 atm)
Li 78K	Be											B	C	N 20K	O	F	Ne 4K
0.542	1.82											2.47	3.516	1.03			1.51
4.700	12.1											13.0	17.6				4.36
3.023	2.22												1.54			1.44	3.16
Na 5K	Mg											Al	Si	P	S	Cl 93K	Ar 4K
1.013	1.74											2.70	2.33			2.03	1.77
2.652	4.30											6.02	5.00				2.66
3.659	3.20											2.86	2.35			2.02	3.76
K 5K	Ca	Sc	Ti	V	Cr	Mn	Fe	Co	Ni	Cu	Zn	Ga	Ge	As	Se	Br 123K	Kr 4K
0.910	1.53	2.99	4.51	6.09	7.19	7.47	7.87	8.9	8.91	8.93	7.13	5.91	5.32	5.77	4.81	4.05	3.09
1.402	2.30	4.27	5.66	7.22	8.33	8.18	8.50	8.97	9.14	8.45	6.55	5.10	4.42	4.65	3.67	2.36	2.17
4.525	3.95	3.25	2.89	2.62	2.50	2.24	2.48	2.50	2.49	2.56	2.66	2.44	2.45	3.16	2.32		4.00
Rb 5K	Sr	Y	Zr	Nb	Mo	Tc	Ru	Rh	Pd	Ag	Cd	In	Sn	Sb	Te	I	Xe 4K
1.629	2.58	4.48	6.51	8.58	10.22	11.50	12.36	12.42	12.00	10.50	8.65	7.29	5.76	6.69	6.25	4.95	3.78
1.148	1.78	3.02	4.29	5.56	6.42	7.04	7.36	7.26	6.80	5.85	4.64	3.83	2.91	3.31	2.94	2.36	1.64
4.837	4.30	3.55	3.17	2.86	2.72	2.71	2.65	2.69	2.75	2.89	2.98	3.25	2.81	2.91	2.86	3.54	4.34
Cs 5K	Ba	La	Hf	Ta	W	Re	Os	Ir	Pt	Au	Hg 227	Tl	Pb	Bi	Po	At	Rn
1.997	3.59	6.17	13.20	16.66	19.25	21.03	22.58	22.55	21.47	19.28	14.26	11.87	11.34	9.80	9.31		
0.905	1.60	2.70	4.52	5.55	6.30	6.80	7.14	7.06	6.62	5.90	4.26	3.50	3.30	2.82	2.67	—	—
5.235	4.35	3.73	3.13	2.86	2.74	2.74	2.68	2.71	2.77	2.88	3.01	3.46	3.50	3.07	3.34		
Fr	Ra	Ac															
		10.07															
—	—	2.66															
		3.76															

Density in g cm^{-3} (10^3kg m^{-3}) ⟶

Concentration in 10^{22} cm^{-3} (10^{28} m^{-3}) ⟶

Nearest-neighbor distance, in Å (10^{-10}m) ⟶

Ce	Pr	Nd	Pm	Sm	Eu	Gd	Tb	Dy	Ho	Er	Tm	Yb	Lu
6.77	6.78	7.00		7.54	5.25	7.89	8.27	8.53	8.80	9.04	9.32	6.97	9.84
2.91	2.92	2.93	—	3.03	2.04	3.02	3.22	3.17	3.22	3.26	3.32	3.02	3.39
3.65	3.63	3.66		3.59	3.96	3.58	3.52	3.51	3.49	3.47	3.54	3.88	3.43
Th	Pa	U	Np	Pu	Am	Cm	Bk	Cf	Es	Fm	Md	No	Lr
11.72	15.37	19.05	20.45	19.81	11.87								
3.04	4.01	4.80	5.20	4.26	2.96	—	—	—	—	—	—	—	—
3.60	3.21	2.75	2.62	3.1	3.61								

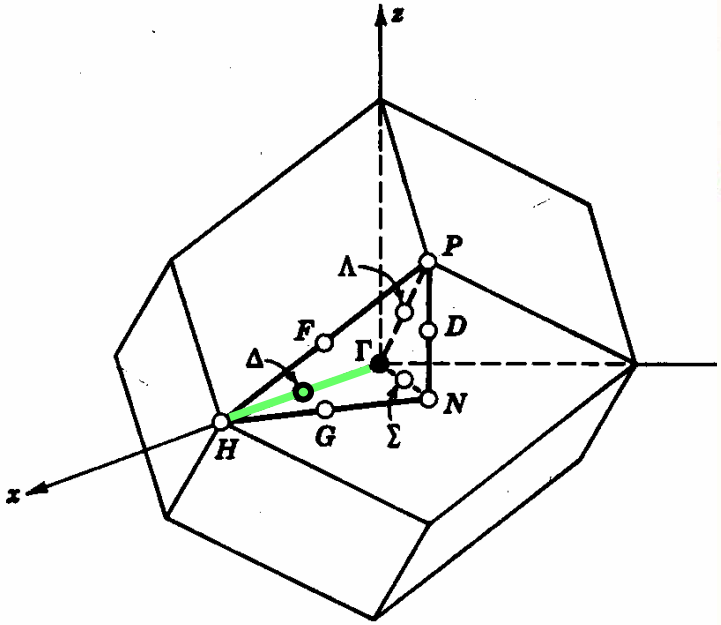

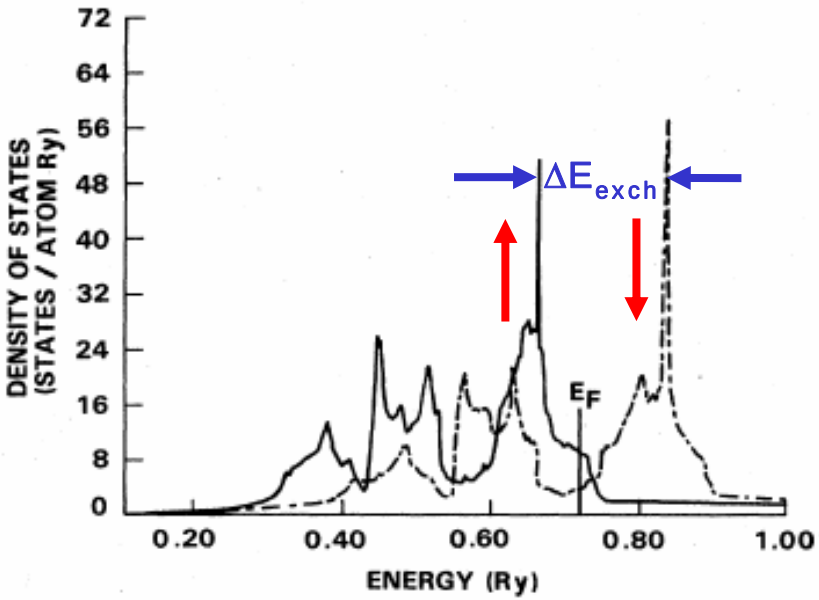

FIG. 4. Density of states at the equilibrium lattice constant of Fe for majority- (solid line) and minority- (broken line) spin states.

Hathaway et al., Phys. Rev. B 31, 7603 ('85)

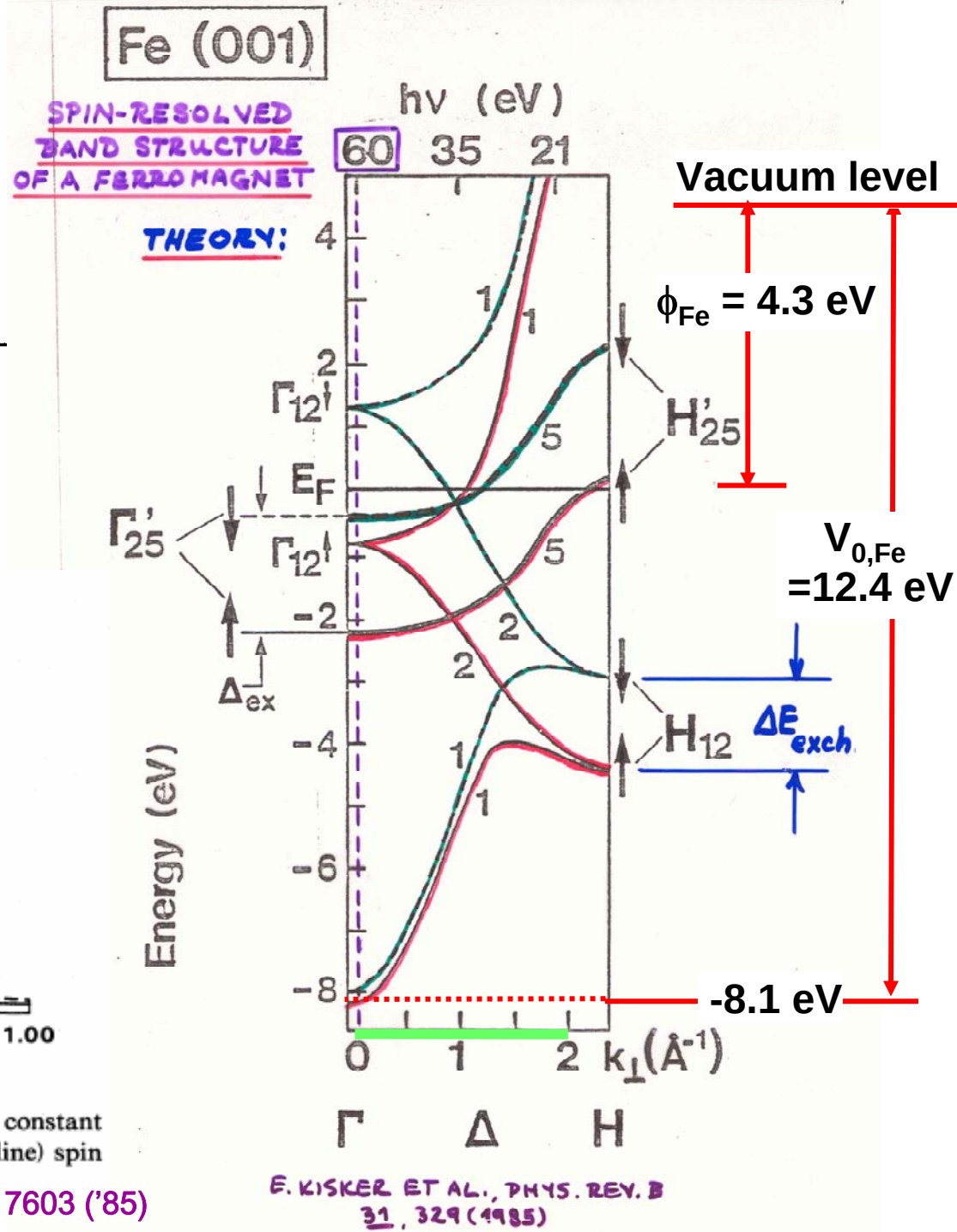

Initial core-state quantum numbers

Radial matrix elements:

- (•) Automatic: core level (e.g. 1s, 2s, 2p, etc.) = 1s
- ( ) Manual: l_0=0, R_{l0+1}=1.0, δ_{l0+1}=0.0, R_{l0-1}=0.0, δ_{l0-1}=0.0

Calculate* | Download Input File** | Reset***

COMPUTATION TIME: the CPU time needed for the calculation using the default cluster and input parameters (use Reset to recover default input) is 1.24 seconds on a Pentium III @ 733 MHz. This gives a time scale to estimate the computation time for other input parameters, keeping in mind that it scales like ~ $(n_{scat} - 1)\, N^2\, (l_{max}+1)^3$, where N is the number of atoms in the cluster and n_{scat} is the scattering order. For reference, the default values are N=48, l_{max}=6, and n_{scat}=2, for which the above number is 7.9 10^5.

IMPORTANT: READ THESE LINES BEFORE RUNNING THE CODE FOR THE FIRST TIME.

***The results will be plotted on a separate window.**

****The input file can be used to run the code locally, for which a copy of the code is needed. This can be obtained from F. Javier García de Abajo. An online version of the input-file manual is also available here.**

*****Reset all input values (including cluster specification) to the original settings.**

For comments/questions/suggestions, please contact F. Javier García de Abajo at jga@sw.ehu.es

CO/Fe(001)—Effect of CO height z above first Fe plane

2 atoms: Z = ∞

7 atoms: 1.0 Å

0.5 Å

0.0 Å

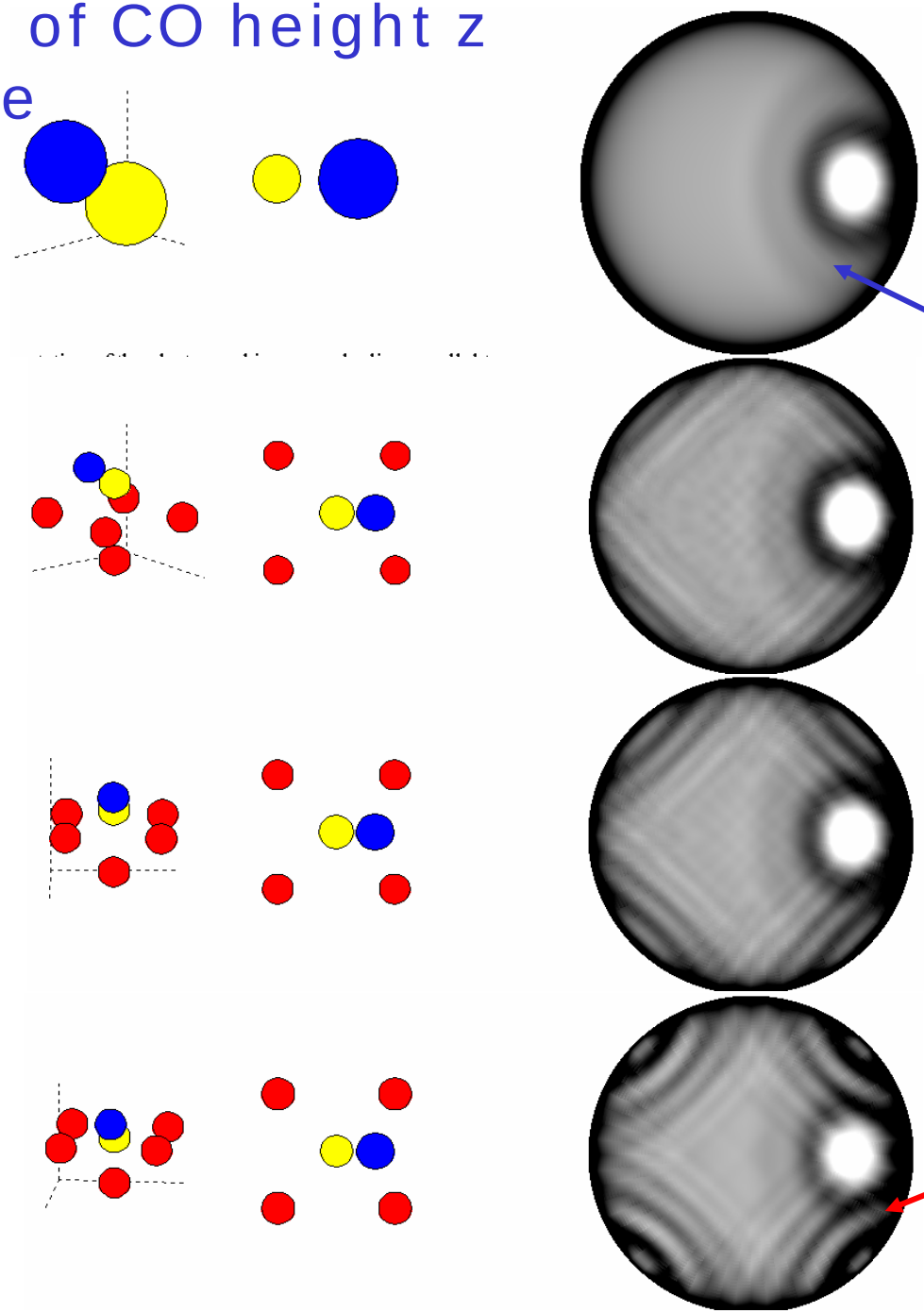

CO/Fe(001)—Effect of CO bond dist.

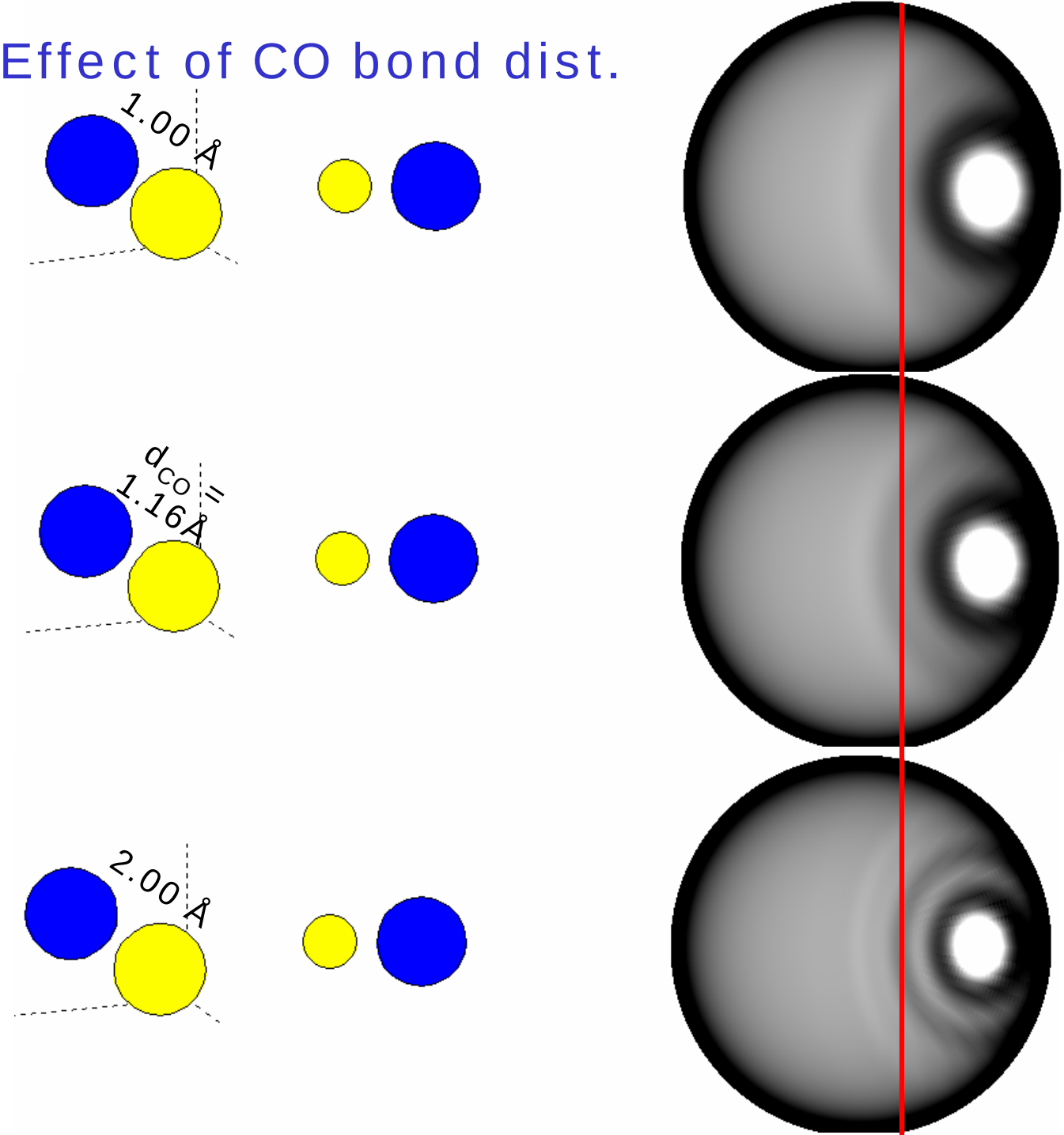

CO/Fe(001)—Effect of cluster size

19 atoms:

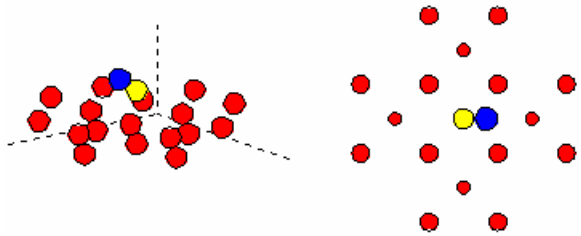

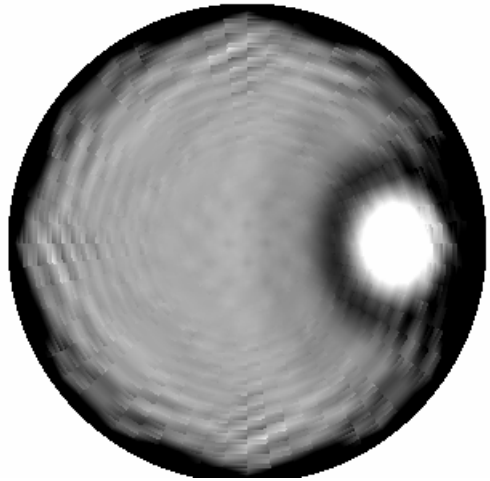

31 atoms:

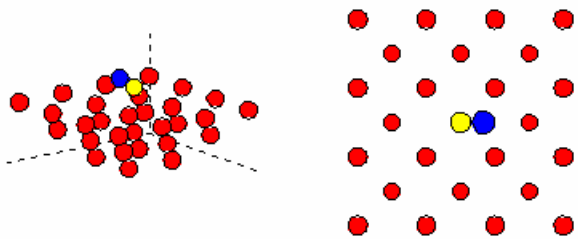

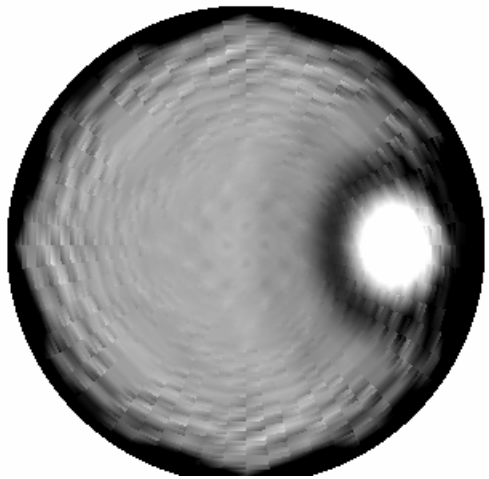

19 ≈ 31, AND SO “CONVERGED” AT 19 OR LESS

CO/Fe(001)—Effect of scattering order

Single scattering:

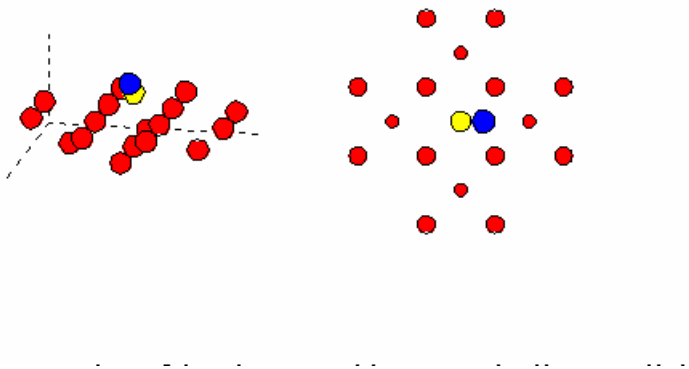

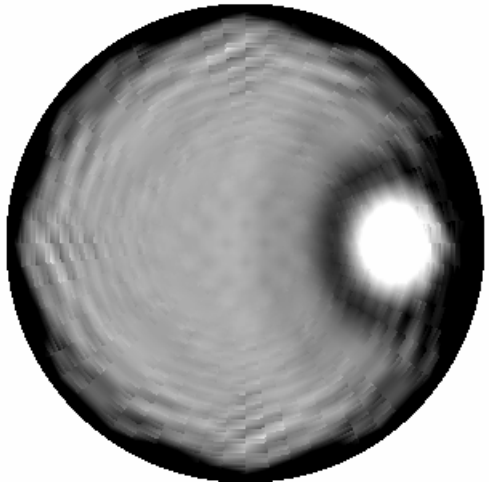

Fourth order scattering:

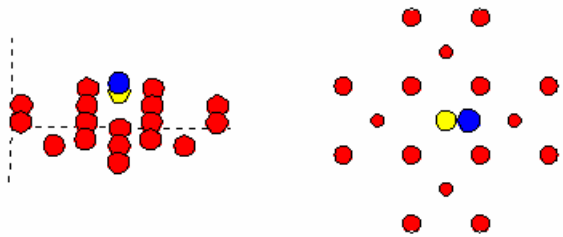

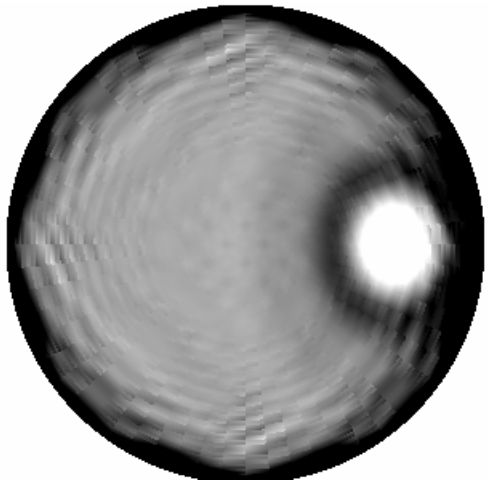

APPROX. CONVERGED AT SINGLE—FOR THIS PARTICULAR PROBLEM ONLY!

Effect of varying the polarization?: C 1s emission from CO

E_{kin} = 200 eV

Linear p polarization:

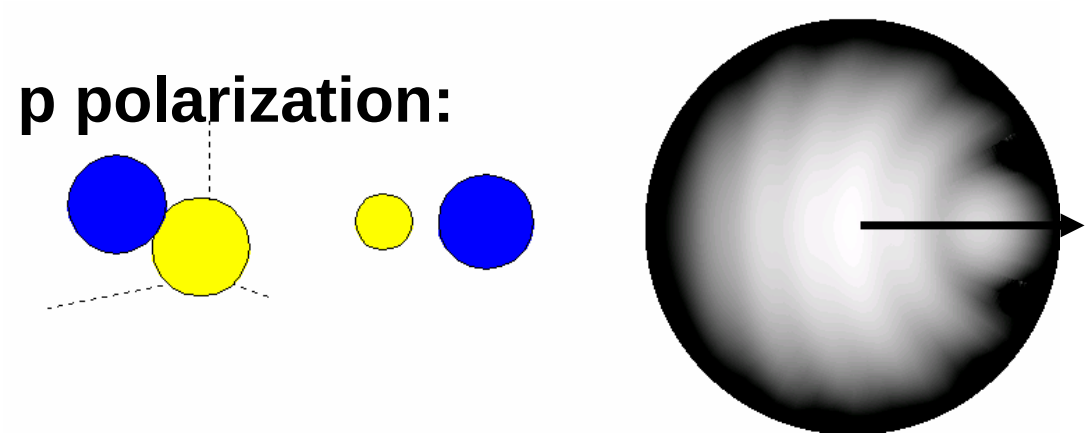

Right circular polarization:

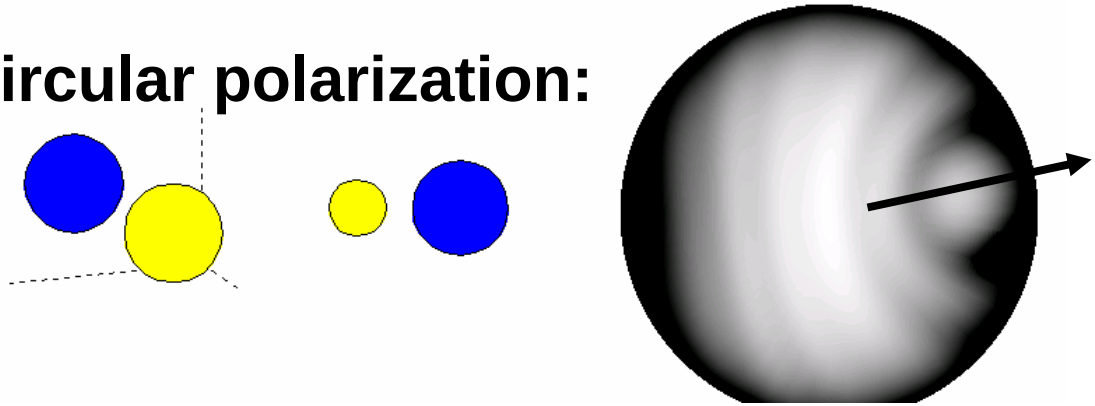

Left circular polarization:

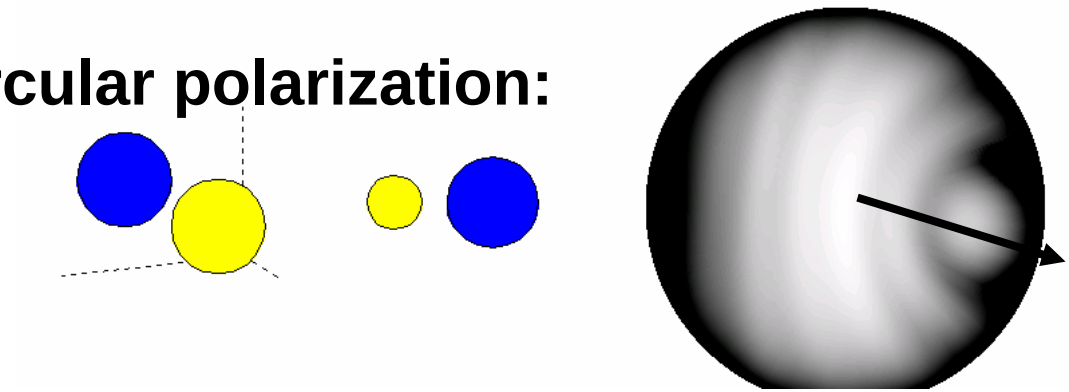

Circular dichroism in angular distributions (CDAD)—more later

4-atom Fe nearest-neighbor chain along [110]—Effect of scattering order

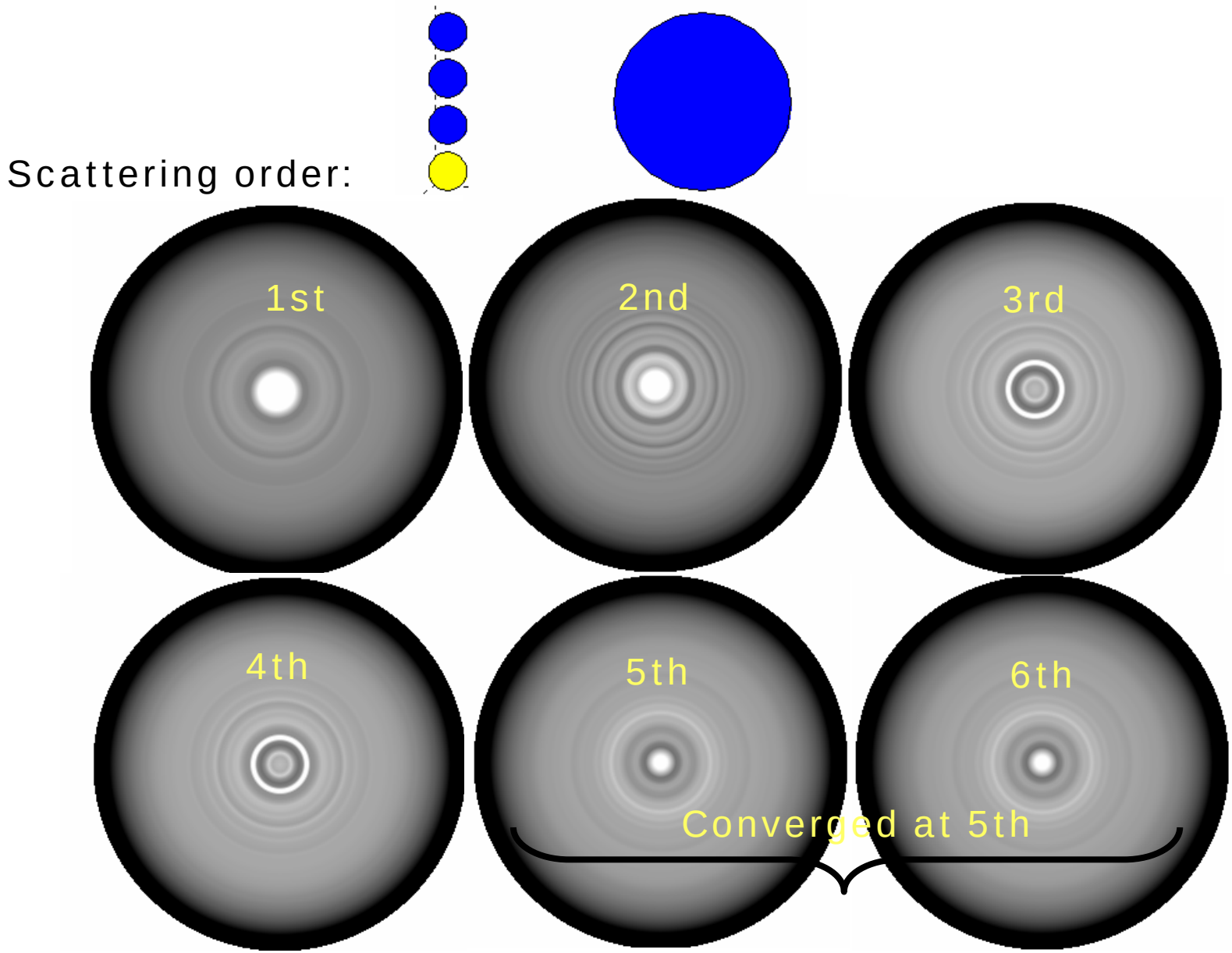

Cu nearest-neighbor chains along [110]—Effect of scattering order

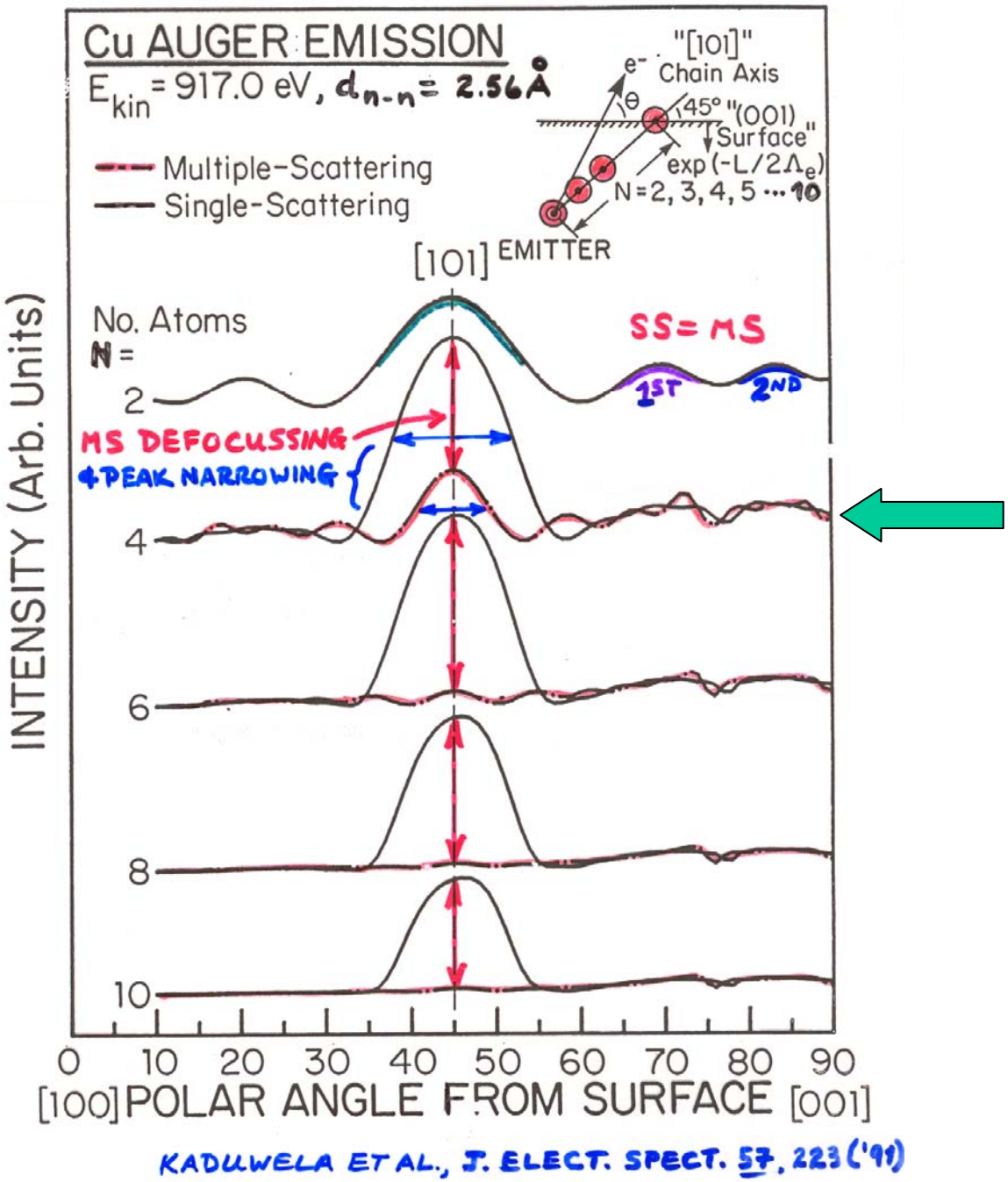

Plus cf. Figs. 6 and 7 in C.F., "The Study of Surface Structures by Photoelectron Diffraction and Auger Electron Diffraction"

Photoelectron Intensities From Different Surfaces
(Stereographic Projection)

Ni(001):Ni 2p at 636 eV

fcc
(001)

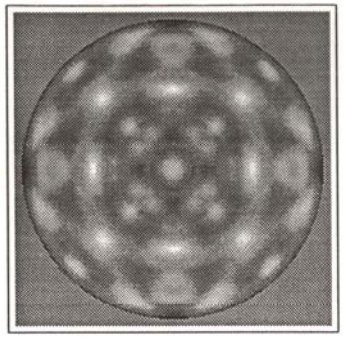

THEVUTHASAN
ET AL.

Ru(0001):Ru 3d at 1206 eV

hcp
(0001)

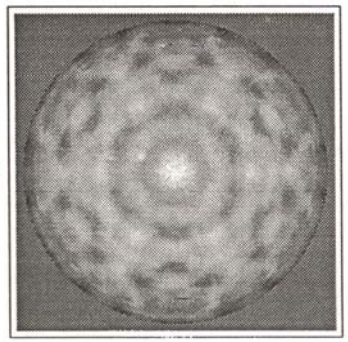

THEVUTHASAN
ET AL.

HOPG:Graphite (0001): C 1s at 946 eV

textured

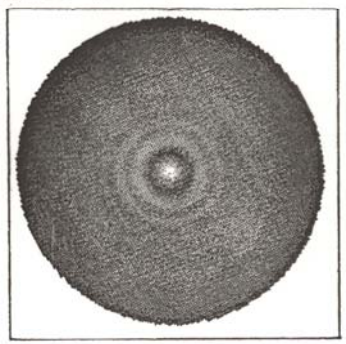

OSTERWALDER
ET AL.

Fingerprint identification of short-range atomic structure and symmetry

- Some growth modes:

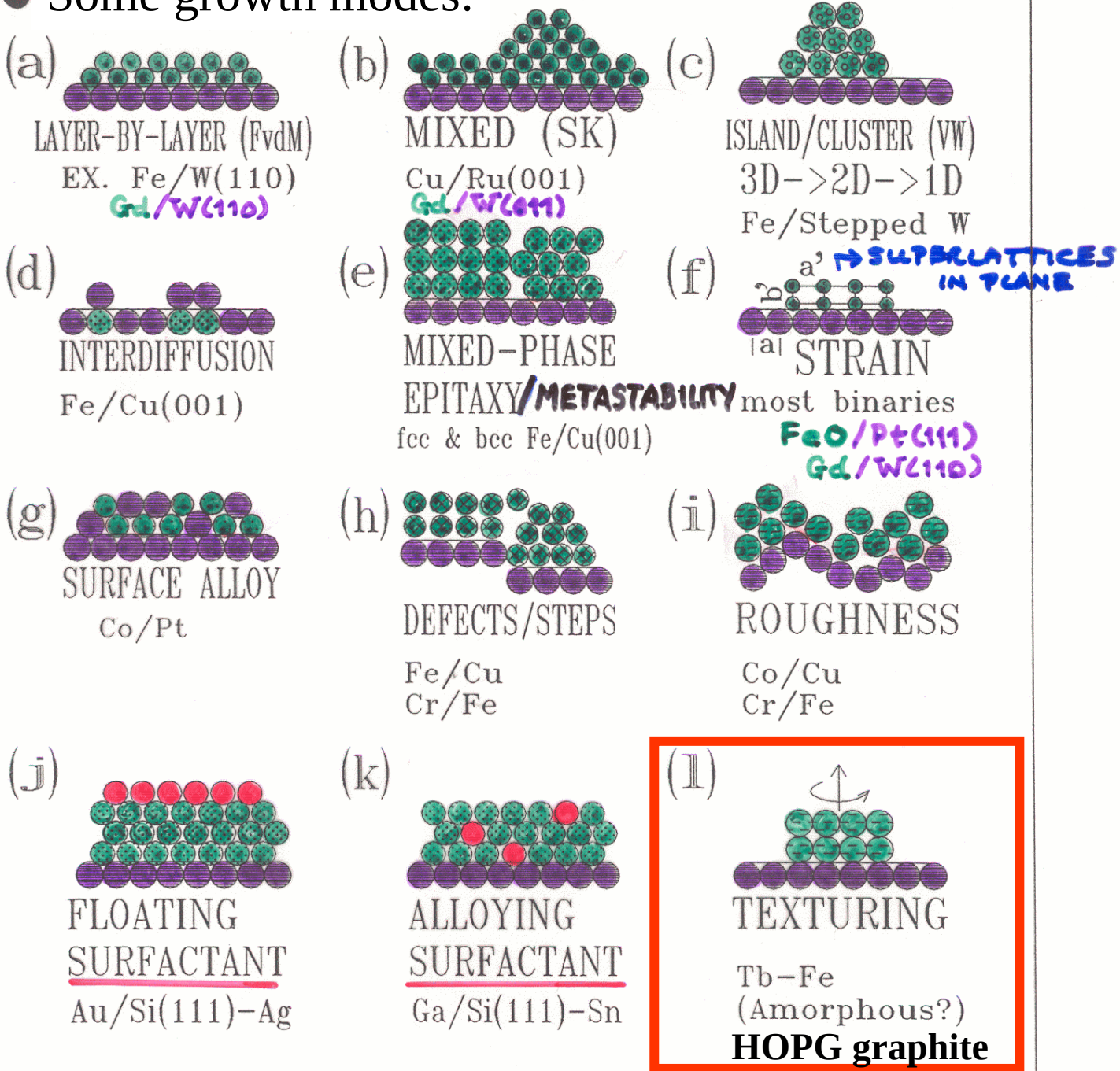

Photoelectron diffraction from W(110) interface atoms beneath an Fe overlayer

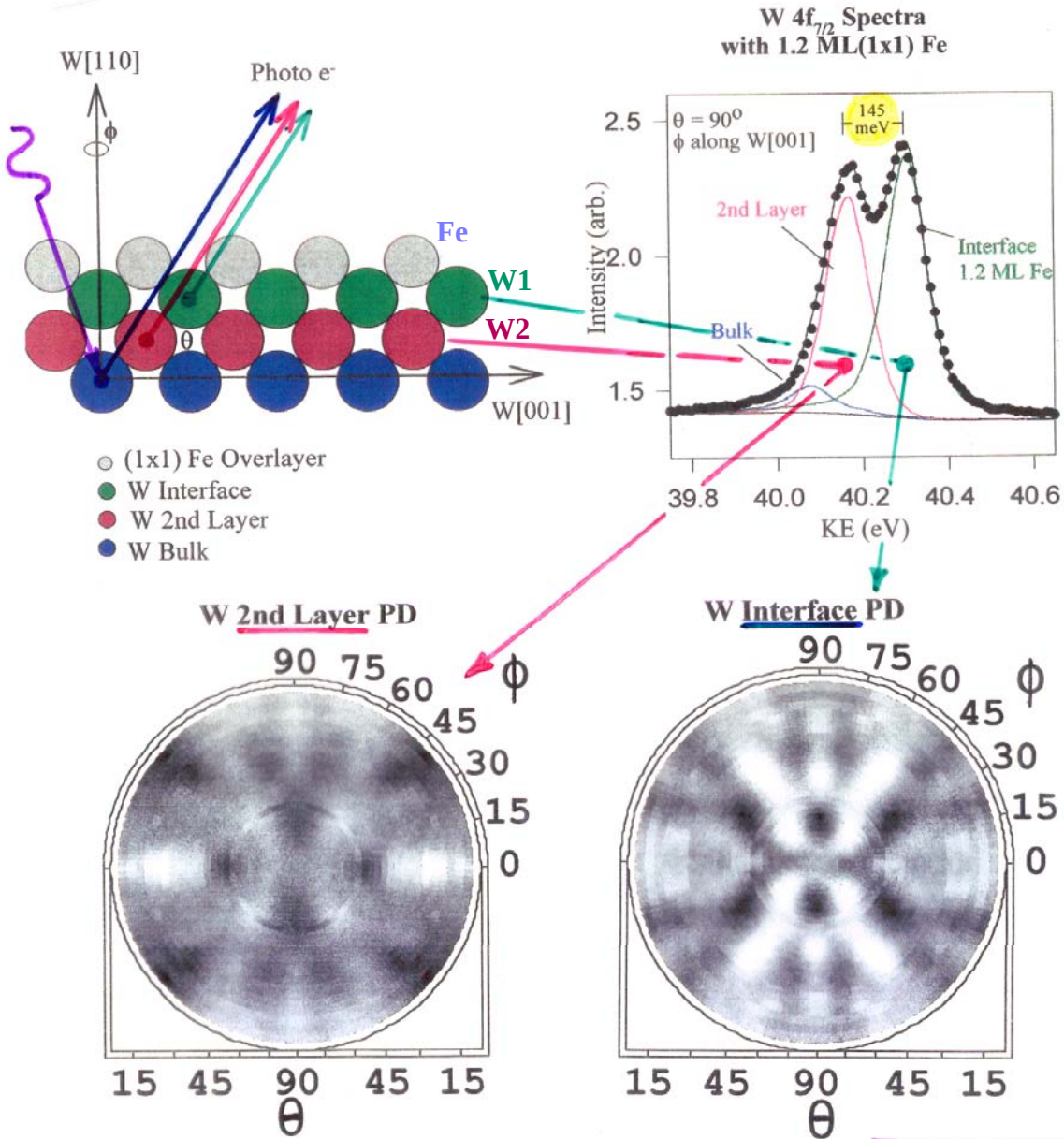

TOBER ET AL.
P.R.L.,
79, 2085 ('97)

Fe on W(110): Determination of structure by expt./theory comparison

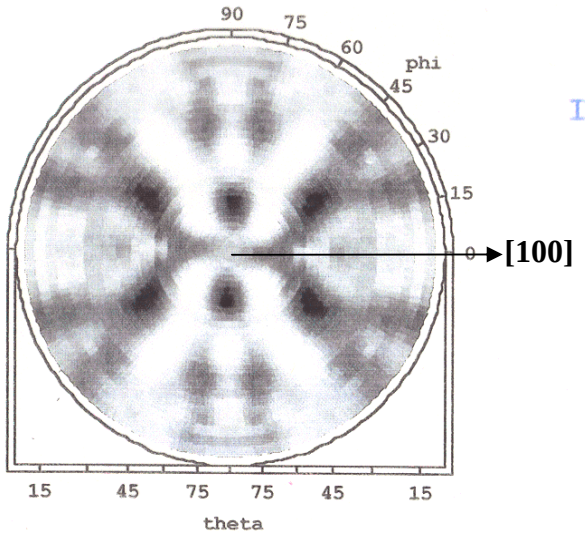

W $4f_{7/2}$
Interface Diffraction

Experiment

$h\upsilon$ = 70 eV
E_{kin} = 40 eV

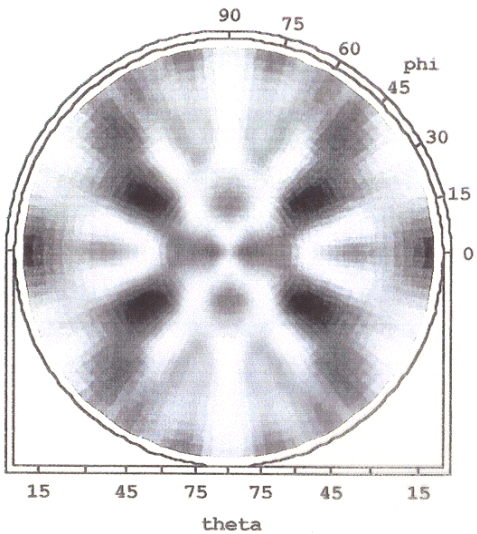

W $4f_{7/2}$
Interface Diffraction

Multiple Scattering Theory
(110 atom cluster)

E_{kin} = 40 eV
Z_{Fe} = 2.165 Å

(Bridge Site)

↳ ~ CONTINUES BULK W STRUCTURE

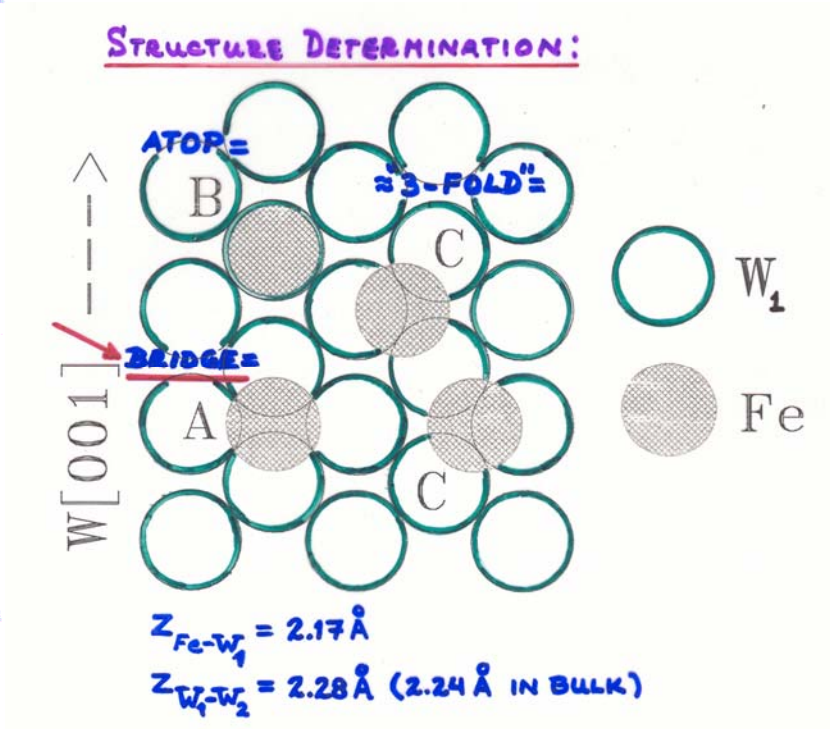

Clean W(110) 4f Surface Peak: R-Factor Analysis

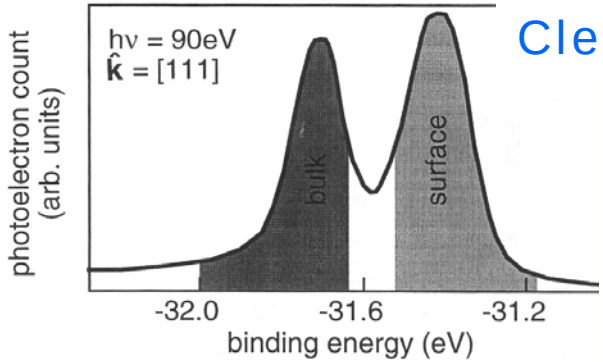

Expt.

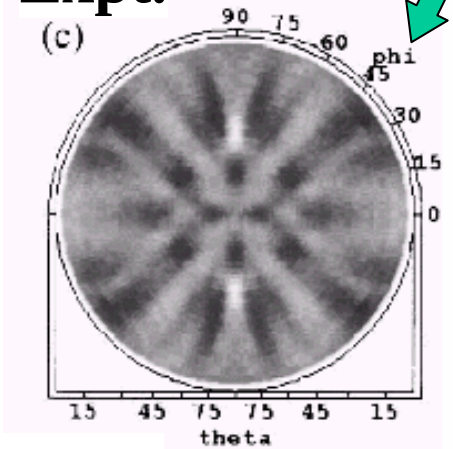

Theory

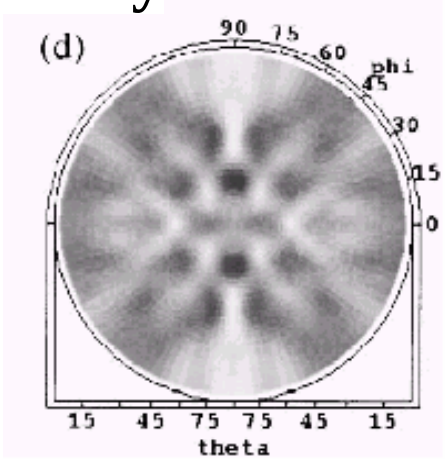

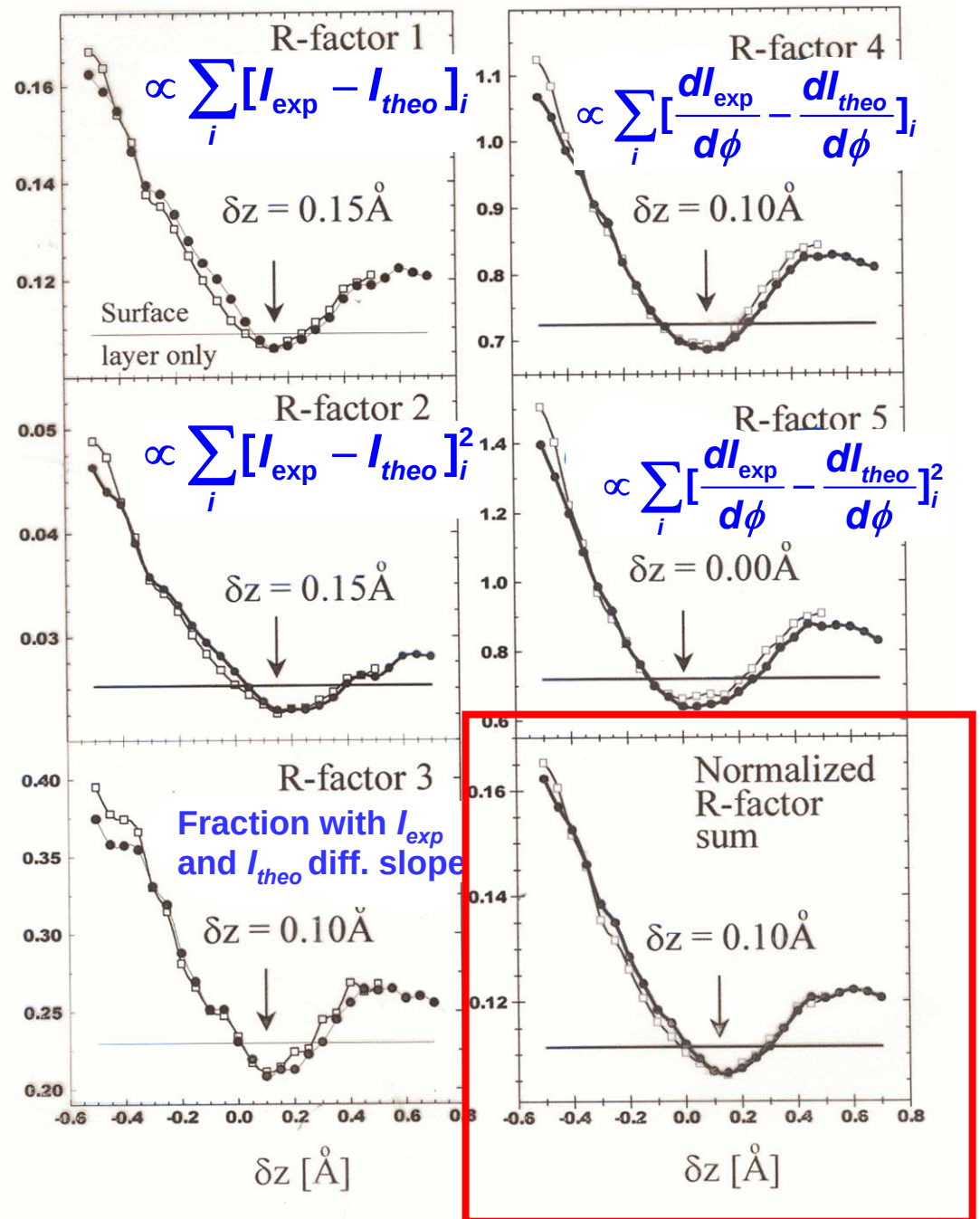

PHOTOELECTRON SPECTRA

OXIDIZED SILICON

CHEMICAL SHIFTS OF CORE LEVELS

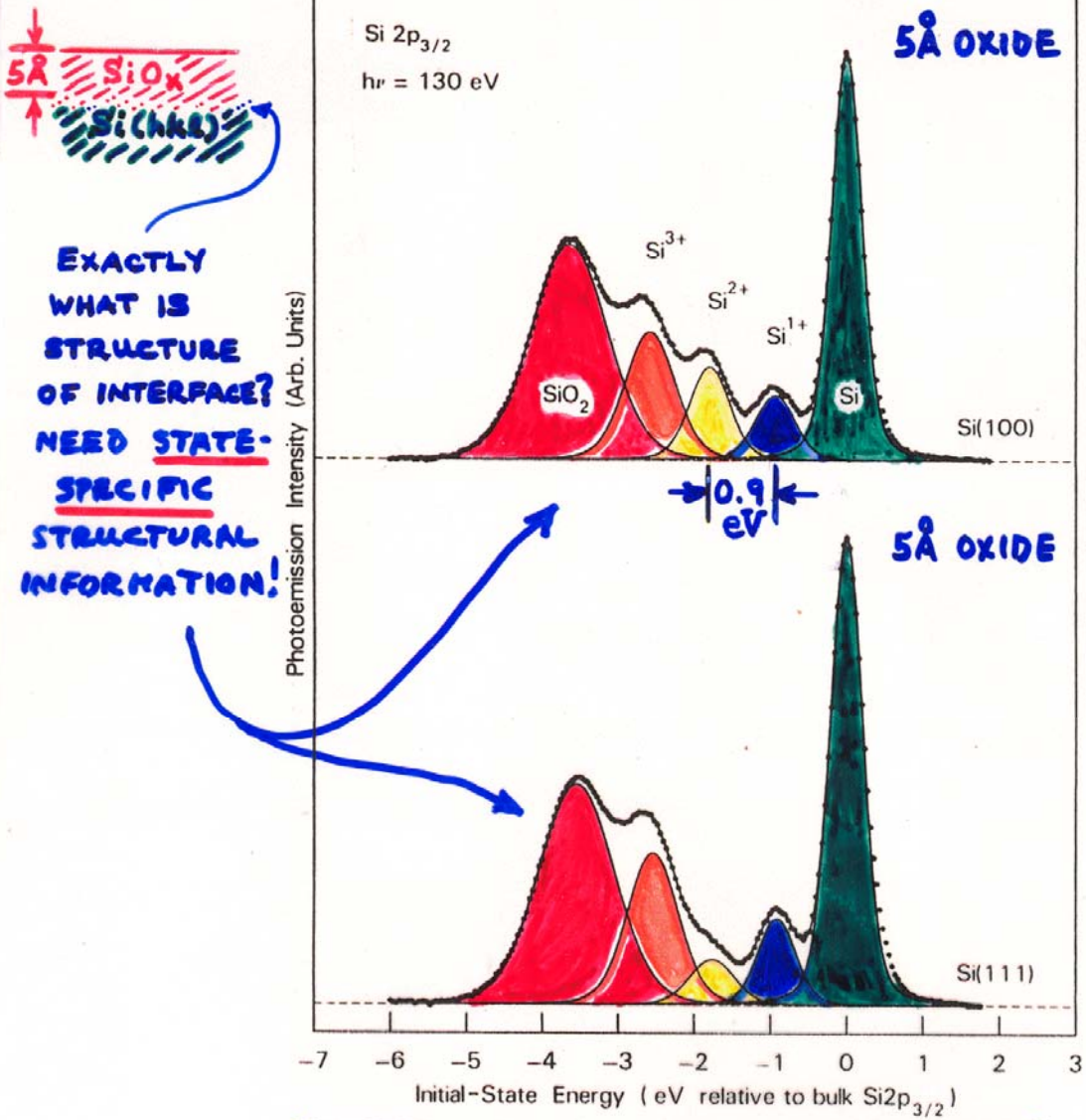

EXACTLY WHAT IS STRUCTURE OF INTERFACE? NEED STATE-SPECIFIC STRUCTURAL INFORMATION!

HIMPSEL ET AL., PHYS. REV. B, 38, 6084('90)

Case study: Interface structure of SiO_x/SiO_2

(Westphal et al.)

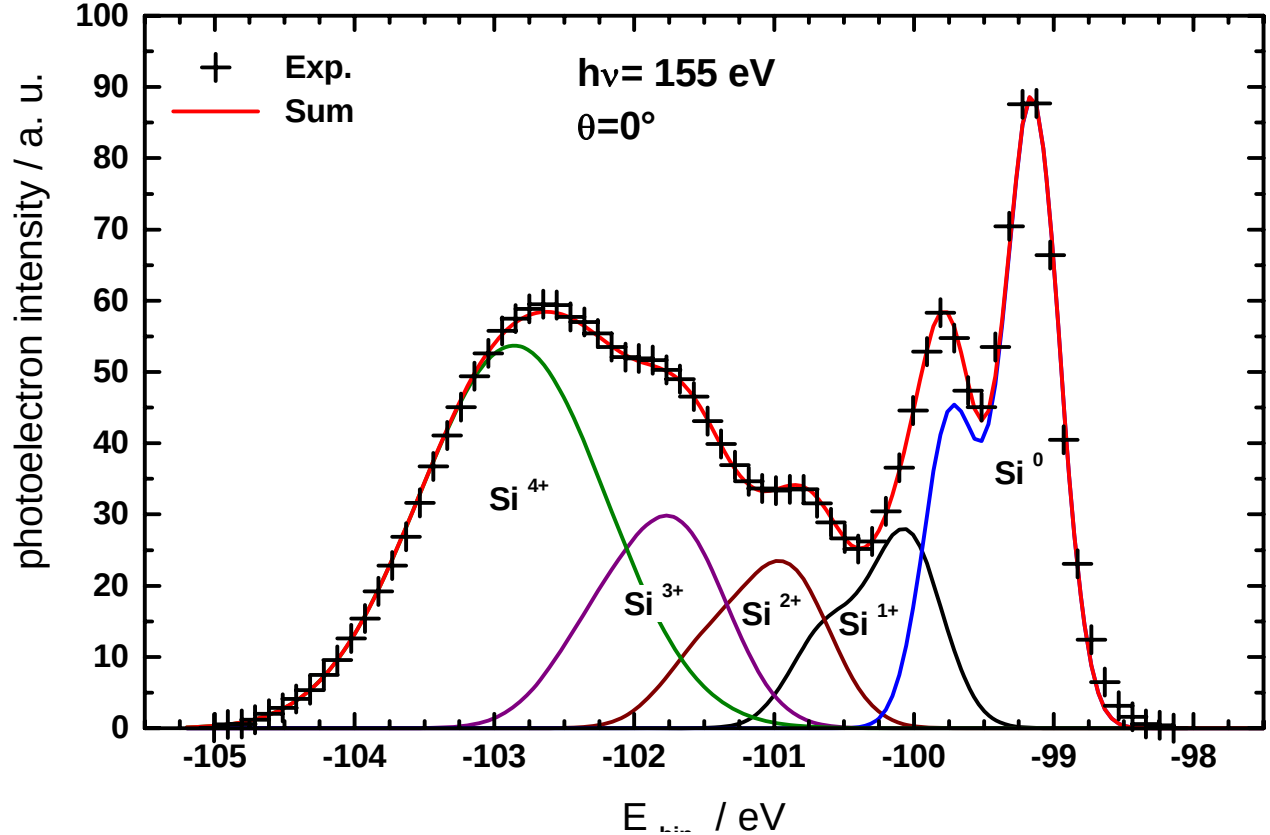

Spin-orbit-splitting	**0.58 eV**
Si^0 width	**0.48 eV**
Si^{1+} shift / width	**0.9 / 0.59 eV**
Si^{2+} shift / width	**1.74 / 0.72 eV**
Si^{3+} shift / width	**2.46 / 0.84 eV**
Si^{4+} shift / width	**3.54 / 1.42 eV**

F.J. Himpsel et al, Phys. Rev. B 38 (1988) 6084
S. Dreiner et al. (Westphal group), Phys. Rev. Lett. 86, 4068 (2001)

Experimental diffraction patterns for SiO_2/Si(100)

3000 L

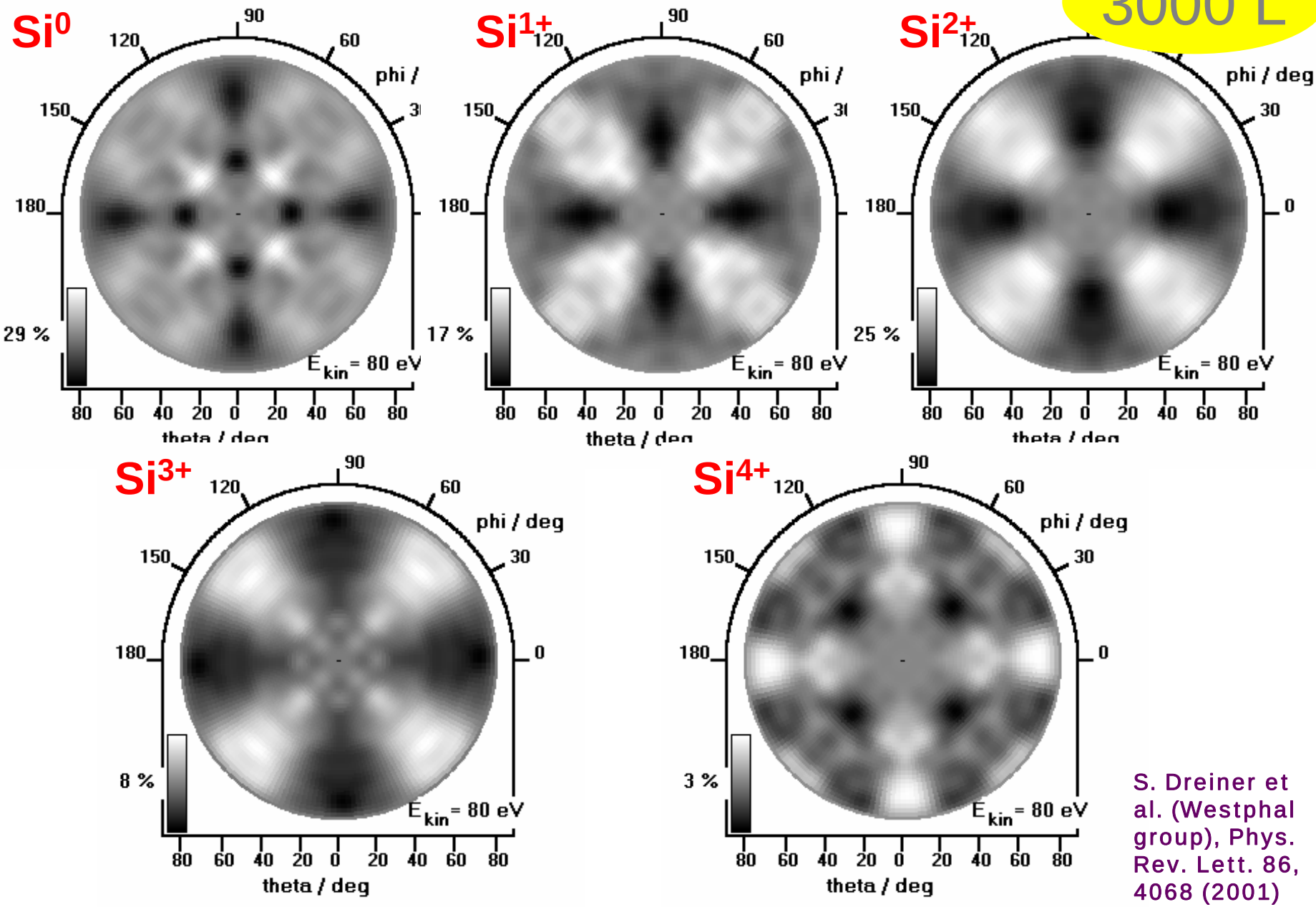

S. Dreiner et al. (Westphal group), Phys. Rev. Lett. 86, 4068 (2001)

Structure determination by R-factor analysis: SiO_x/Si(100)

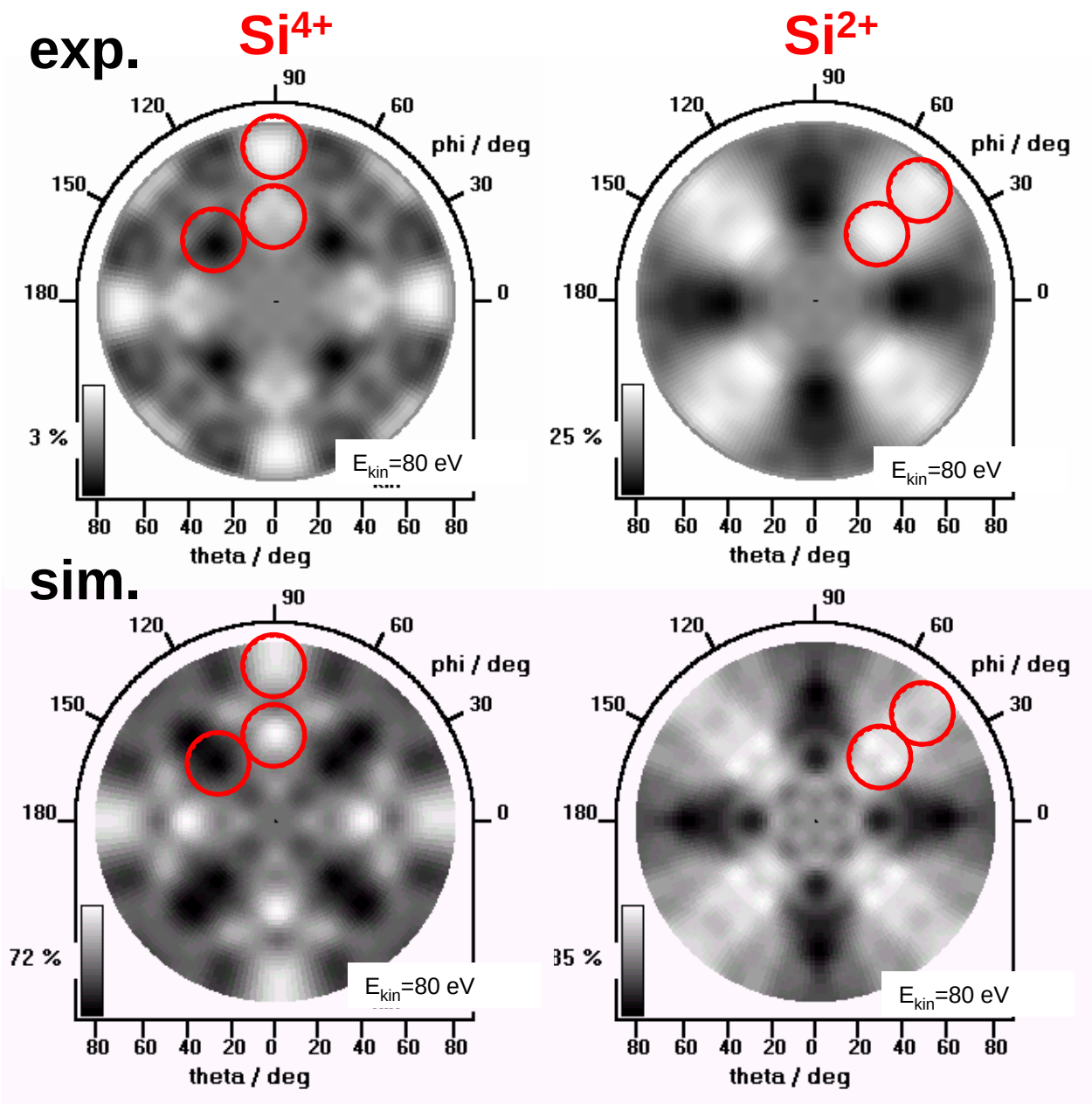

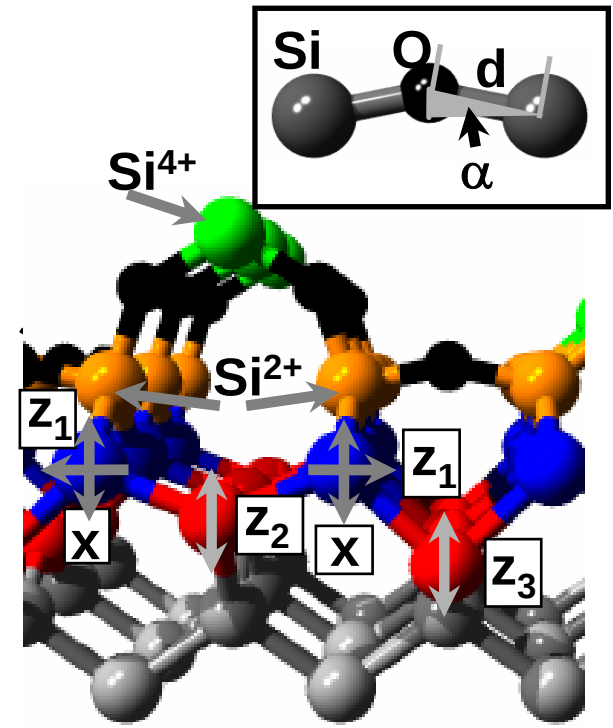

d [Å]	1,82 ± 0,02
α [°]	20 ± 1
x [Å]	0,18 ± 0,02
z_1 [Å]	-0,01 ± 0,02
z_2 [Å]	0,5 ± 0,02
z_3 [Å]	-0,27 ± 0,02
R-Faktor	0,14

Phys. Rev. Lett. 86, 4068 (2001)

+ Assignment of additional Si^{α}- and Si^{β}-components

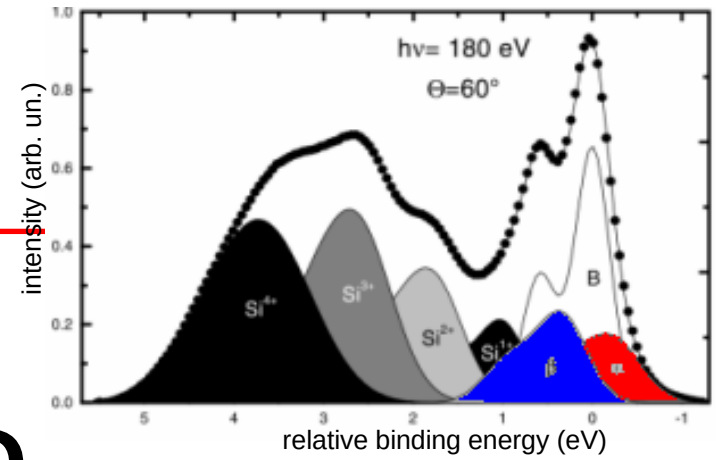

SiO_2

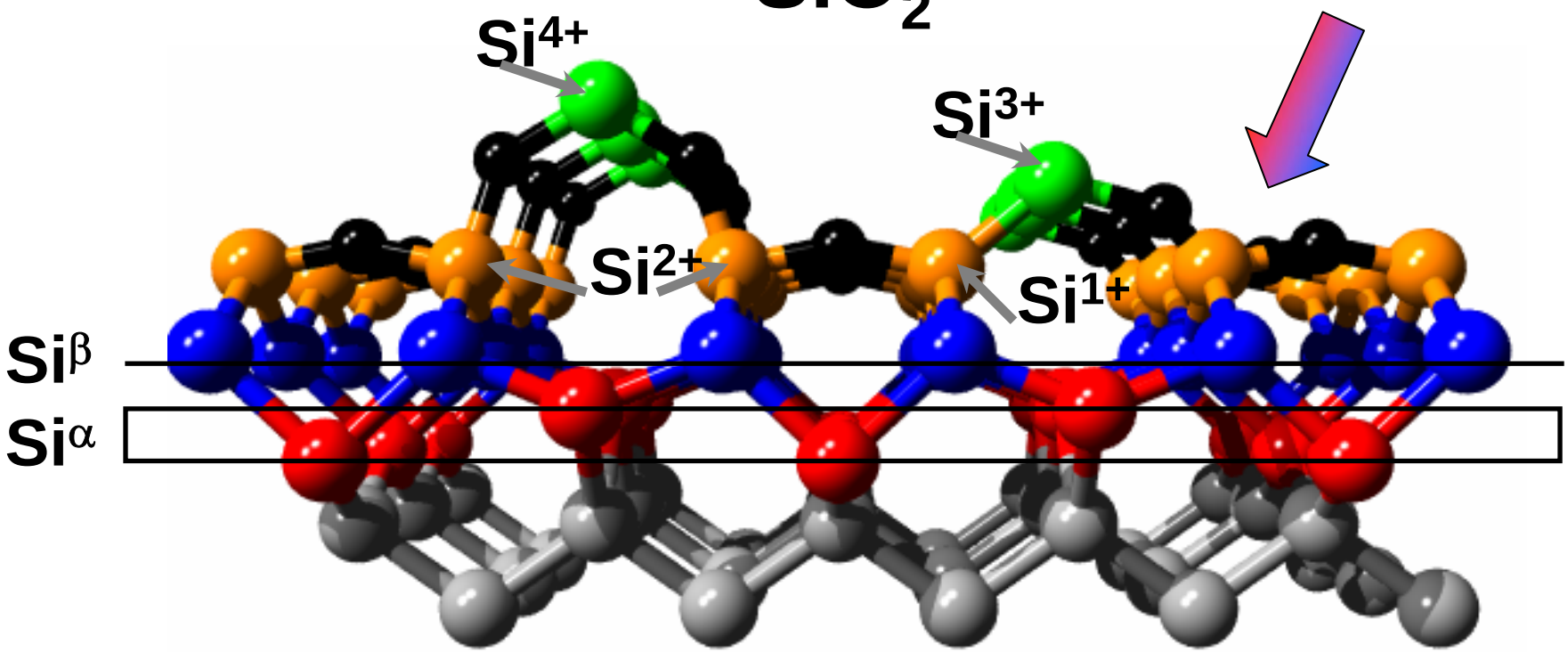

Si-bulk

S. Dreiner et al. (Westphal group)

Some Comple-mentary Surface Structure Probes

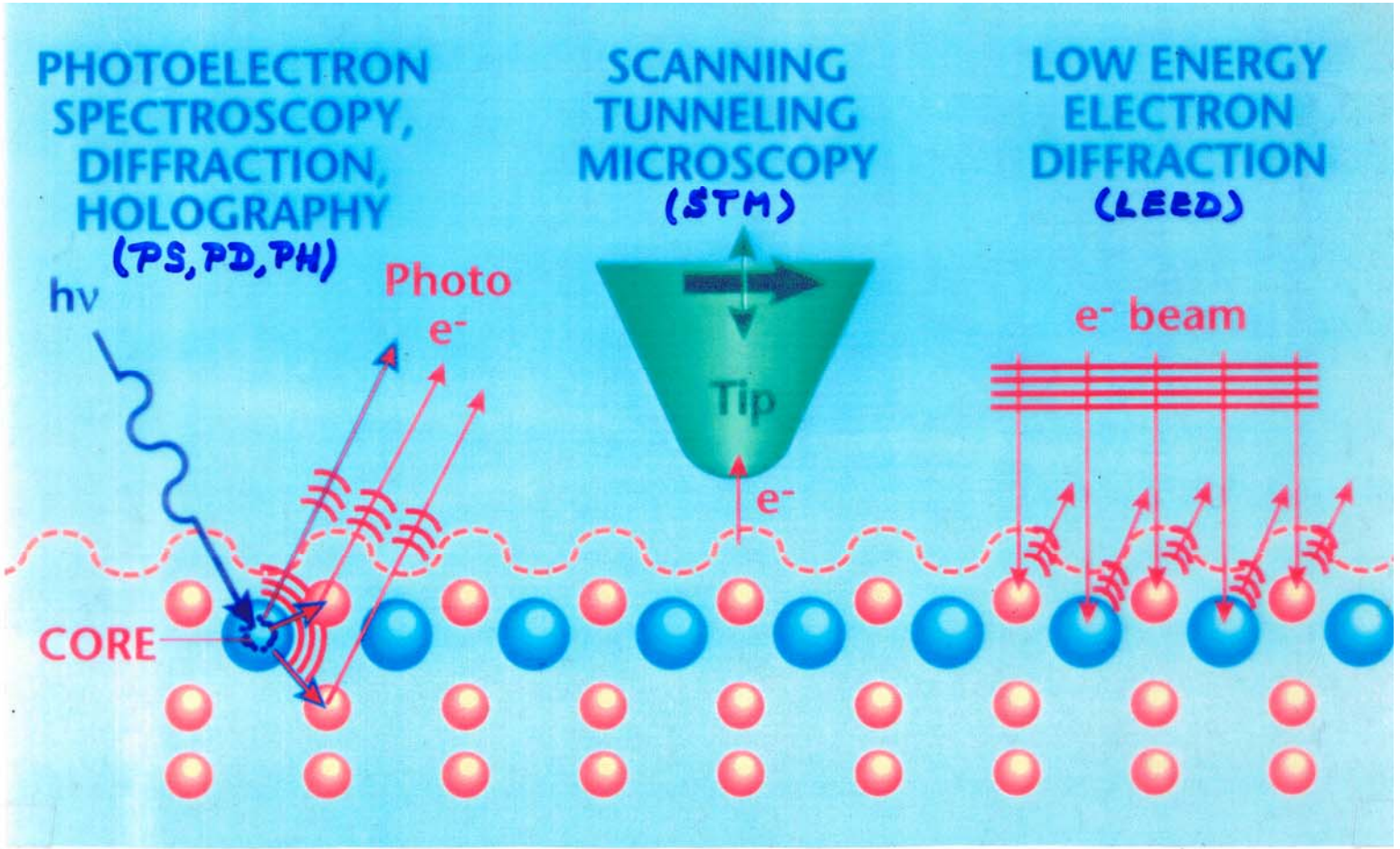

-Type of order:	Short (< 10Å)	Short, long and disorder	Long (> 100Å)
-Atom & site specific:	Yes	No	No
-Sensing depth:	5-40Å	Mostly surface D.O.S.	5-20Å
-Lateral resolution:	1 mm^2 to $(300Å)^2$	Single atom	1 mm^2 to 1 $micron^2$

Case study: 1 ML of FeO on Pt(111): A combined LEED, STM, XPD study

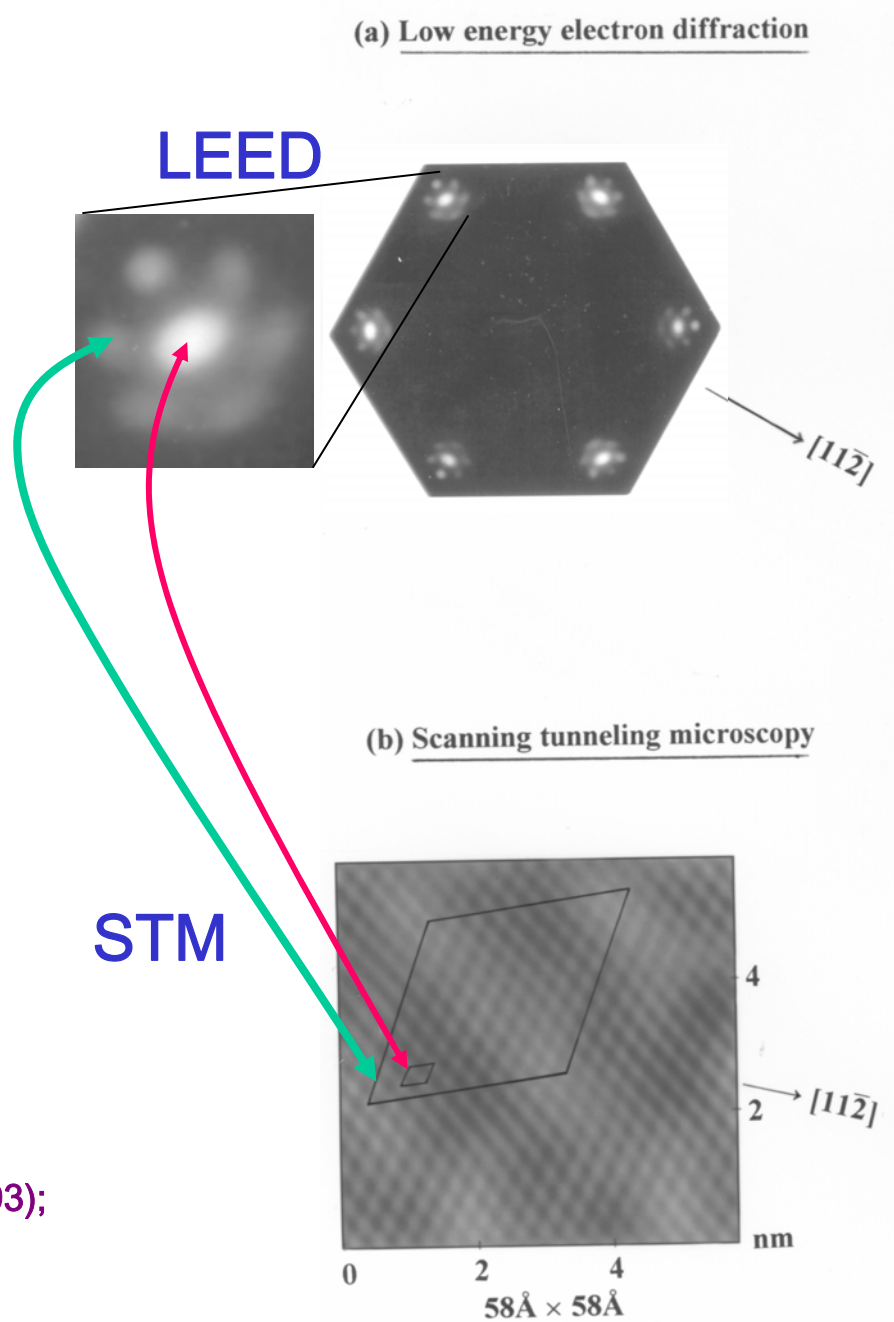

Galloway et al., Surf. Sci. 198, 127 ('93);
J. Vac. Sci. Tech. A12, 2302 ('94).
Y.J. Kim et al.,
Phys. Rev. B 55, R 13448 ('97);
Surf. Sci. 416, 68 ('98)

1 ML of FeO on Pt(111): Structural model from LEED and STM

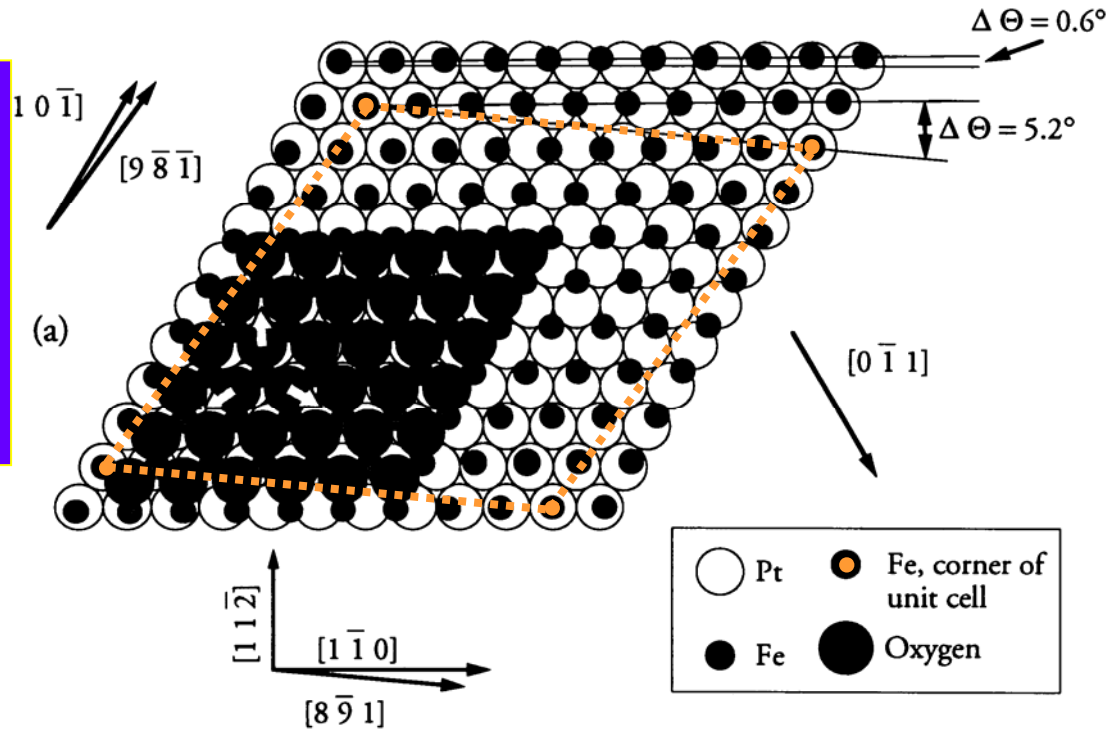

Remaining Questions:

-Is Fe or O on top?

-Fe-O interlayer spacing?

-Fe-O orientation?

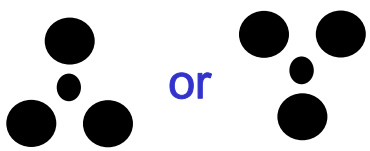

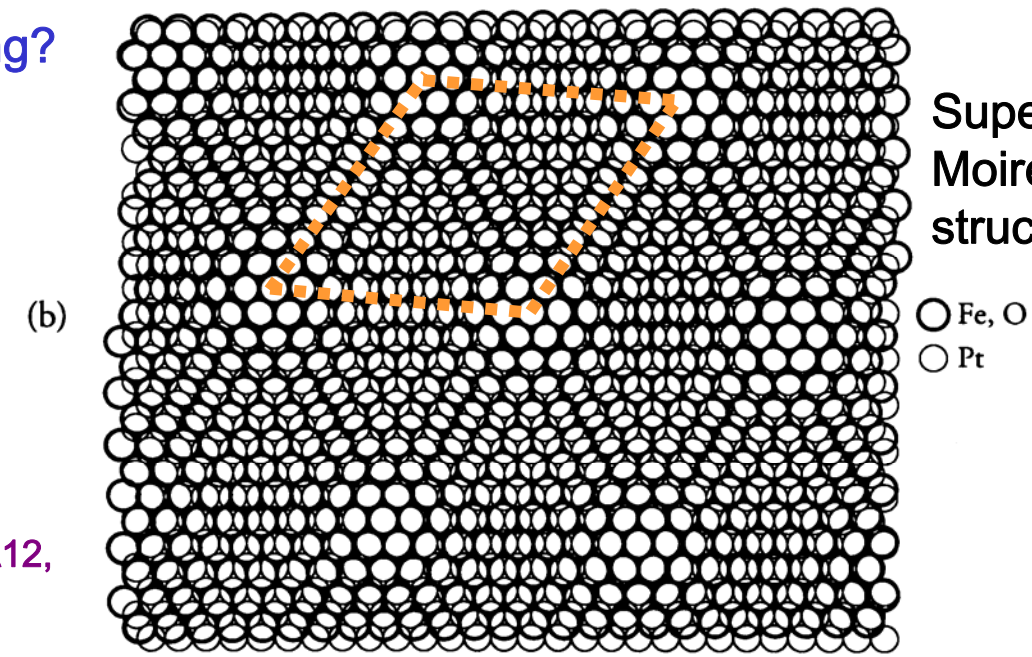

Superlattice or Moiré structure

Galloway et al., Surf. Sci. 198, 127 ('93); J. Vac. Sci. Tech. A12, 2302 ('94).

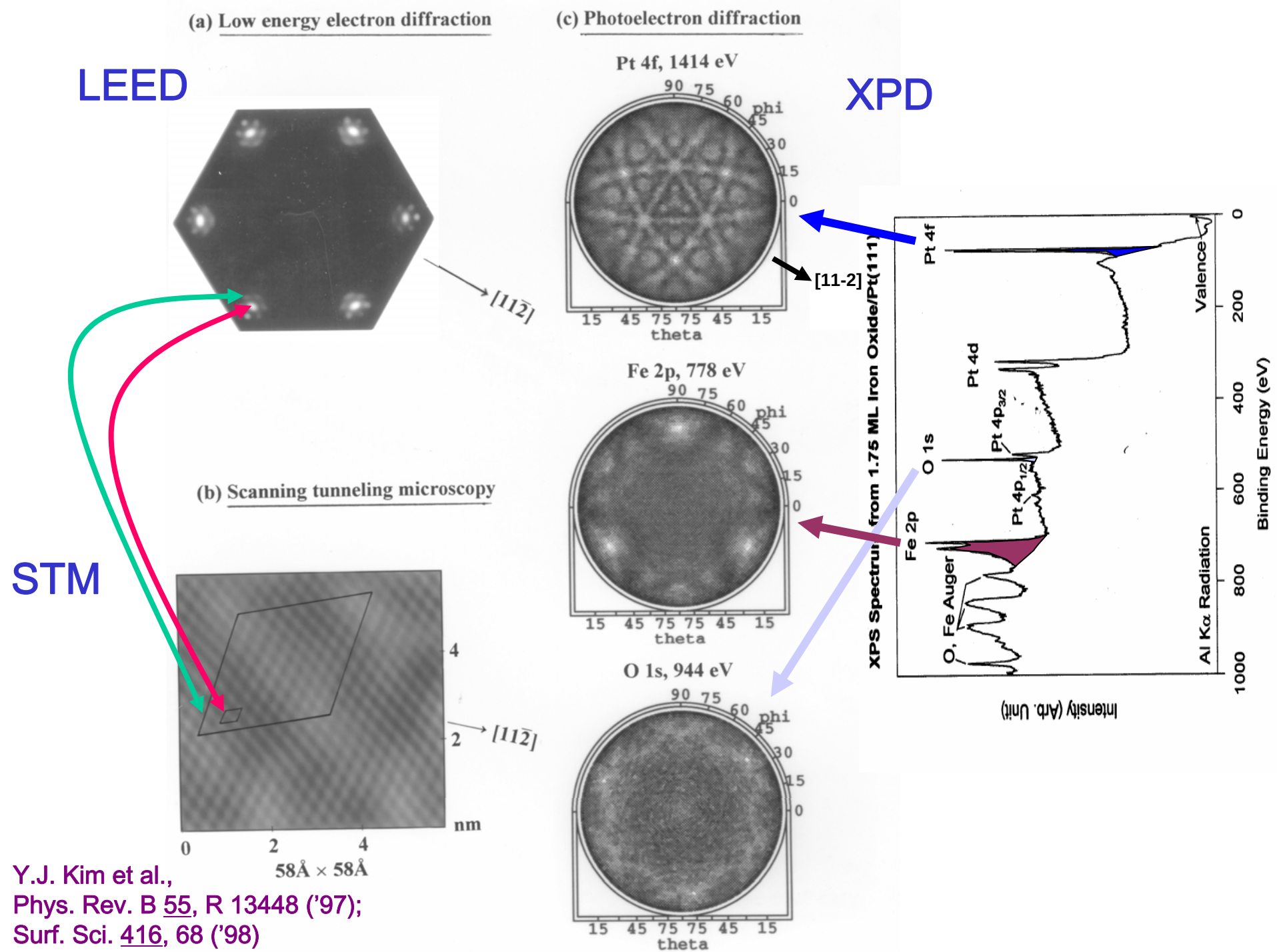

Y.J. Kim et al.,
Phys. Rev. B 55, R 13448 ('97);
Surf. Sci. 416, 68 ('98)

FeO/Pt(111)

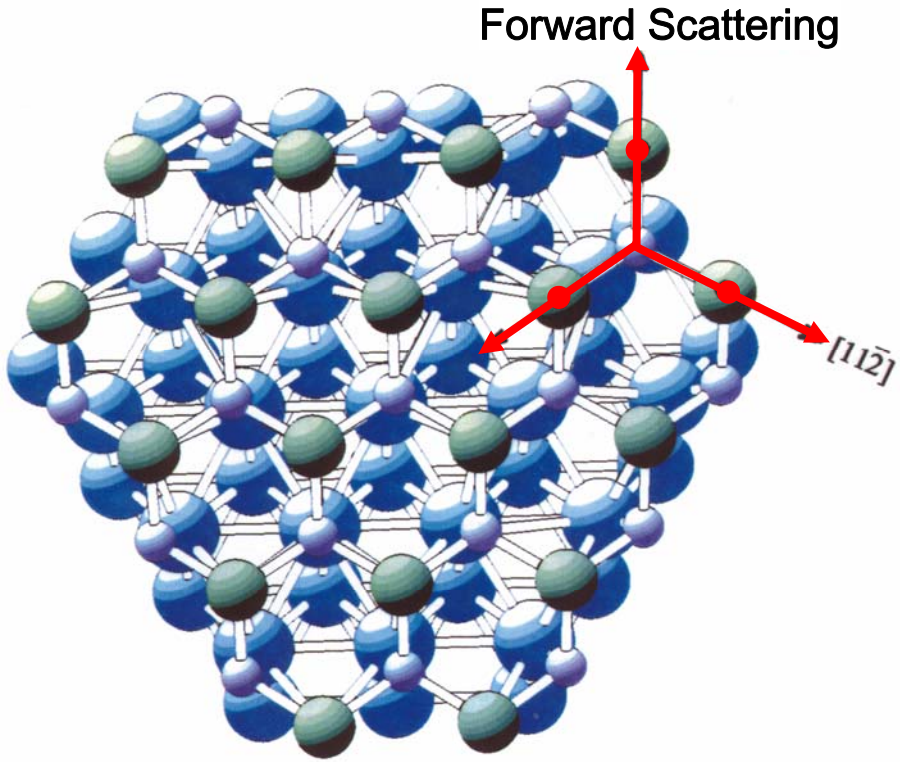
Forward Scattering
[11$\bar{2}$]

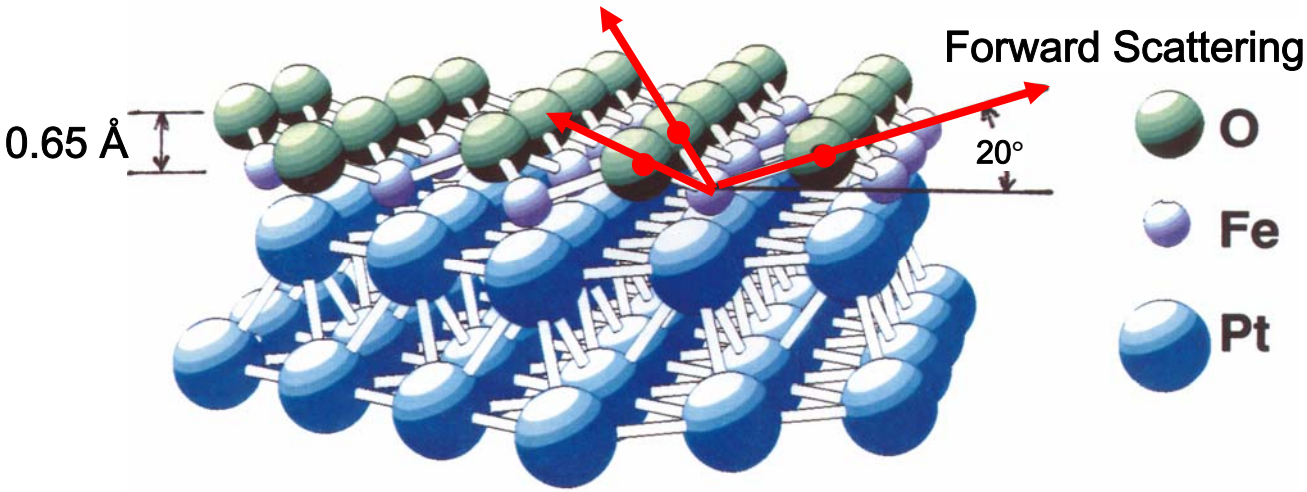
Forward Scattering
0.65 Å
20°
O
Fe
Pt

X-ray Photoelectron Diffraction: Fe 2p from 1ML FeO on Pt(111)

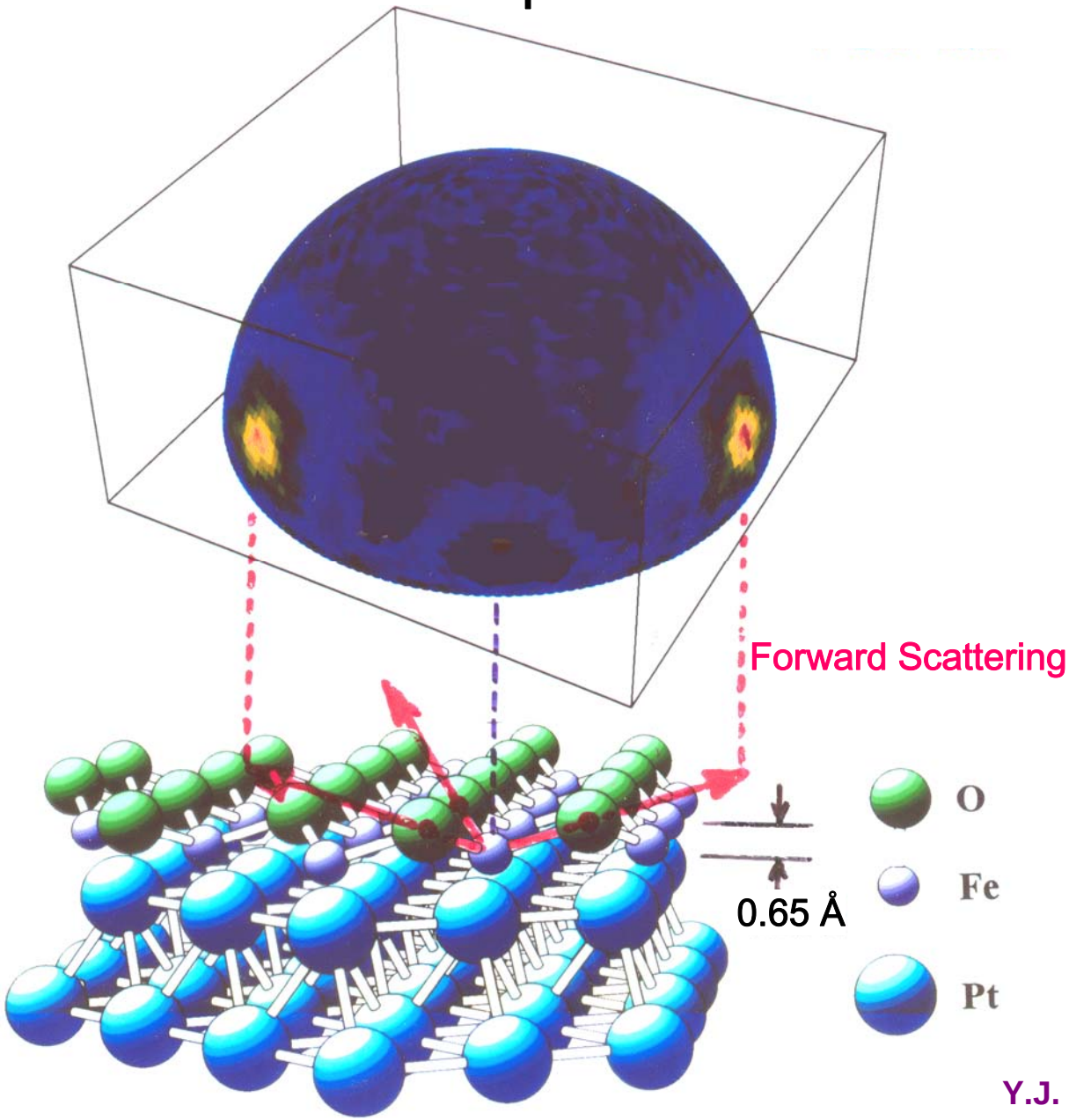

Y.J. Kim et al.
Phys. Rev. B 55, R 13448 ('97)

Permits selecting favored domain of growth—2nd layer Pt effect

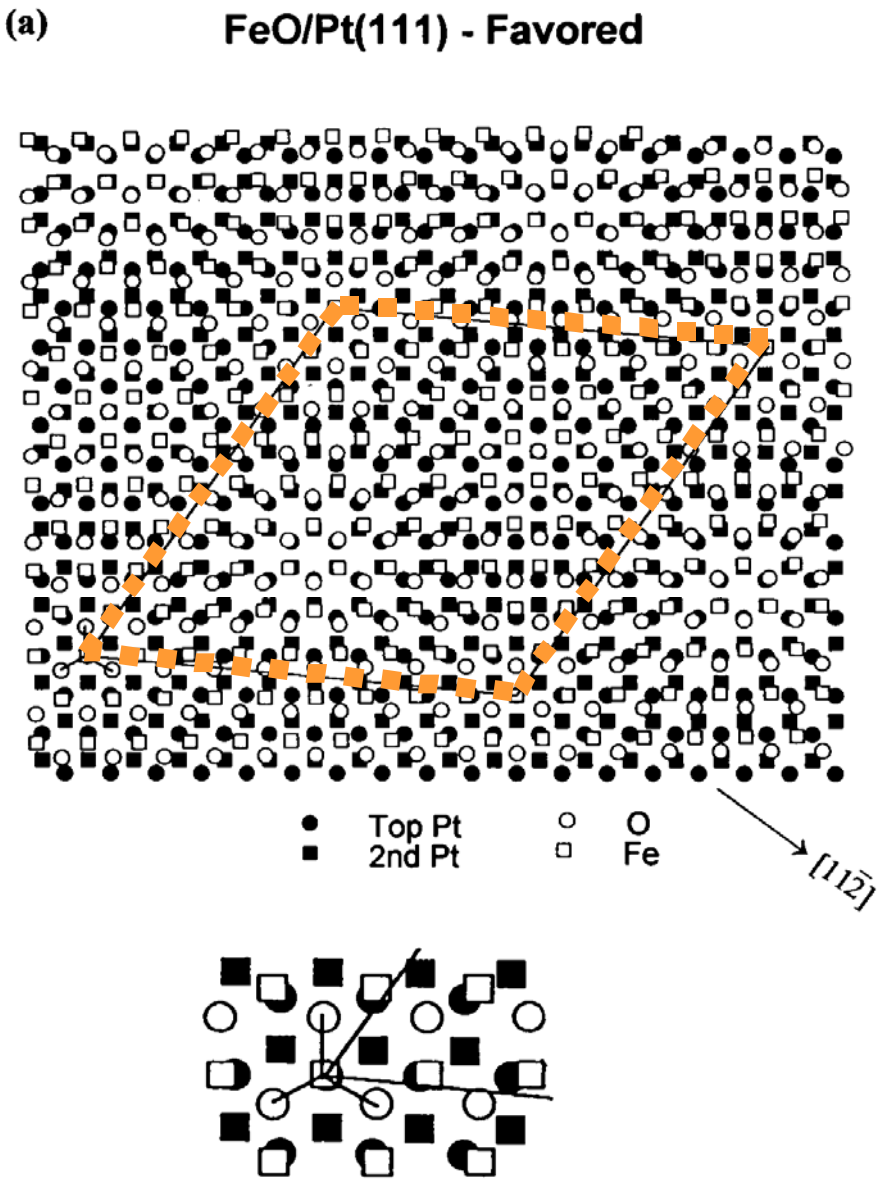

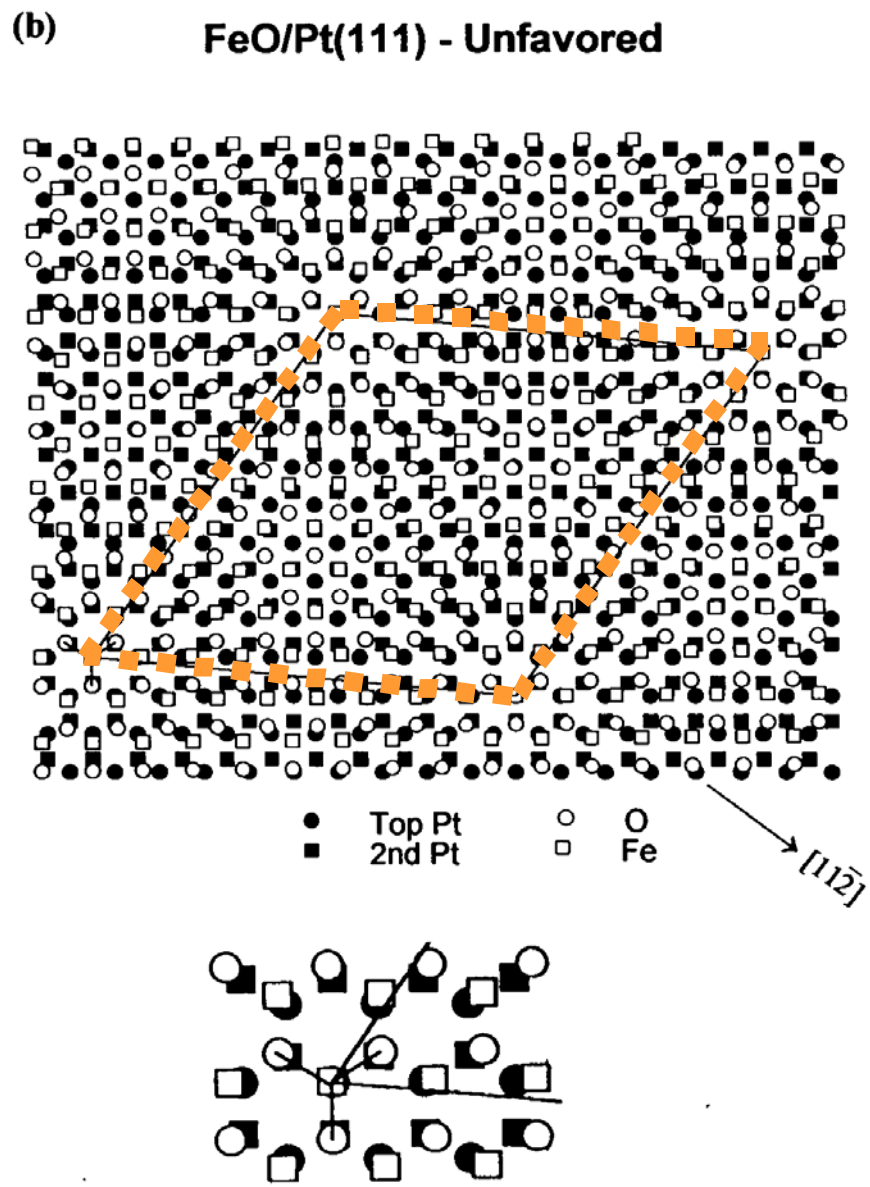

SCANNED-ENERGY PHOTOELECTRON DIFF.

($\sqrt{3}\times\sqrt{3}$) AL ON Si(111)

* 41 diffraction curves χ taken from Al 2p
* $\theta = 0\sim70^\circ$, $\varphi=0\sim60^\circ$

} ~1100 DATA POINTS

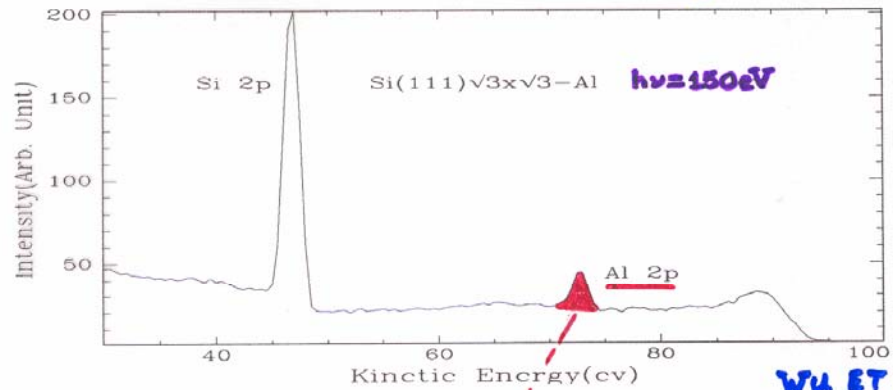

WU ET AL.,
P.R.L. 71, 261('93)
P.R.B 51, 14549('95)

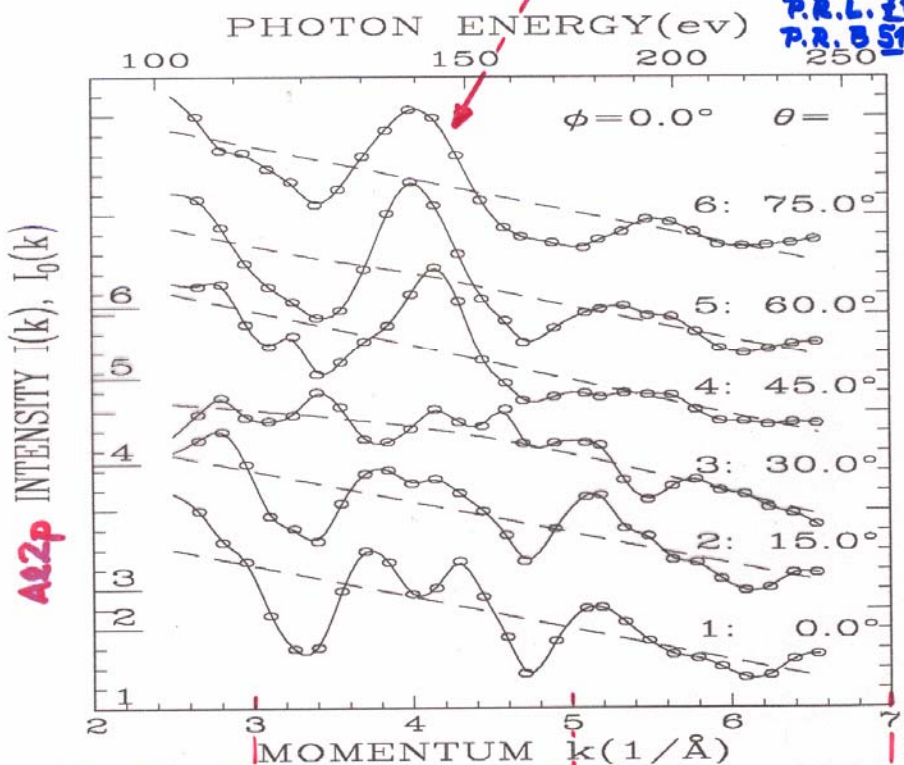

E_{kin}= 34 eV 94 eV 184 eV

Photoelectron diffraction: Simple single-scattering theory for s-subshell emission

SINGLE SCATTERING THEORY

(Orders, Fadley, P.R.B 27, 781('83))

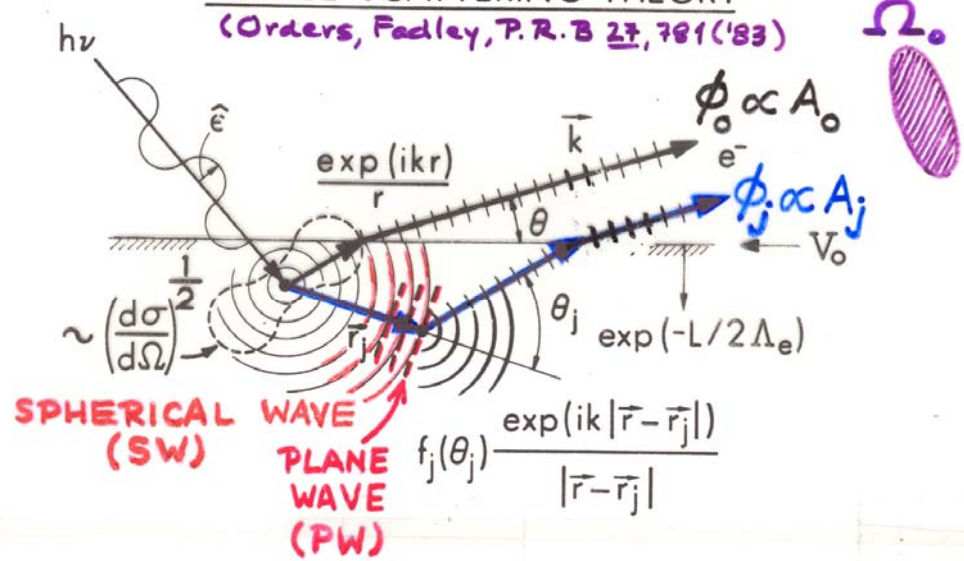

$$\chi(E \text{ or } \vec{k}) \propto \sum_j \frac{F_j(k)}{F_0} \cos\left[k r_j (1-\cos\theta_j) + \psi_j(\theta_j, k)\right]$$

(CLUSTER) Ω_0

PATH LENGTH DIFFERENCE (P.L.D.)

SCATTERING PHASE SHIFT

$$F_j(k) = (\hat{\varepsilon}\cdot\hat{r}_j)\frac{|f_j(\theta_j,k)|}{r_j} W_j(\theta_j,k)\exp(-L_j/2\Lambda_e)$$

ELASTIC e^-–ATOM SCATTERING

DEBYE-WALLER

INELASTIC e^-–e^- SCATTERING

= amplitude of scattered wave

$$F_0 = (\hat{\varepsilon}\cdot\hat{k})\exp(-L_0/2\Lambda_e)$$

= amplitude of direct wave

∴ FOURIER TRANSFORM OF $\chi(k) \Longrightarrow$ PEAKS AT ~ P.L.D. = $r_j(1-\cos\theta_j)$

PATH-LENGTH DIFF'S. FROM FOURIER TRANSFORMS*

c(2x2)S/Cr(001): 45° off normal

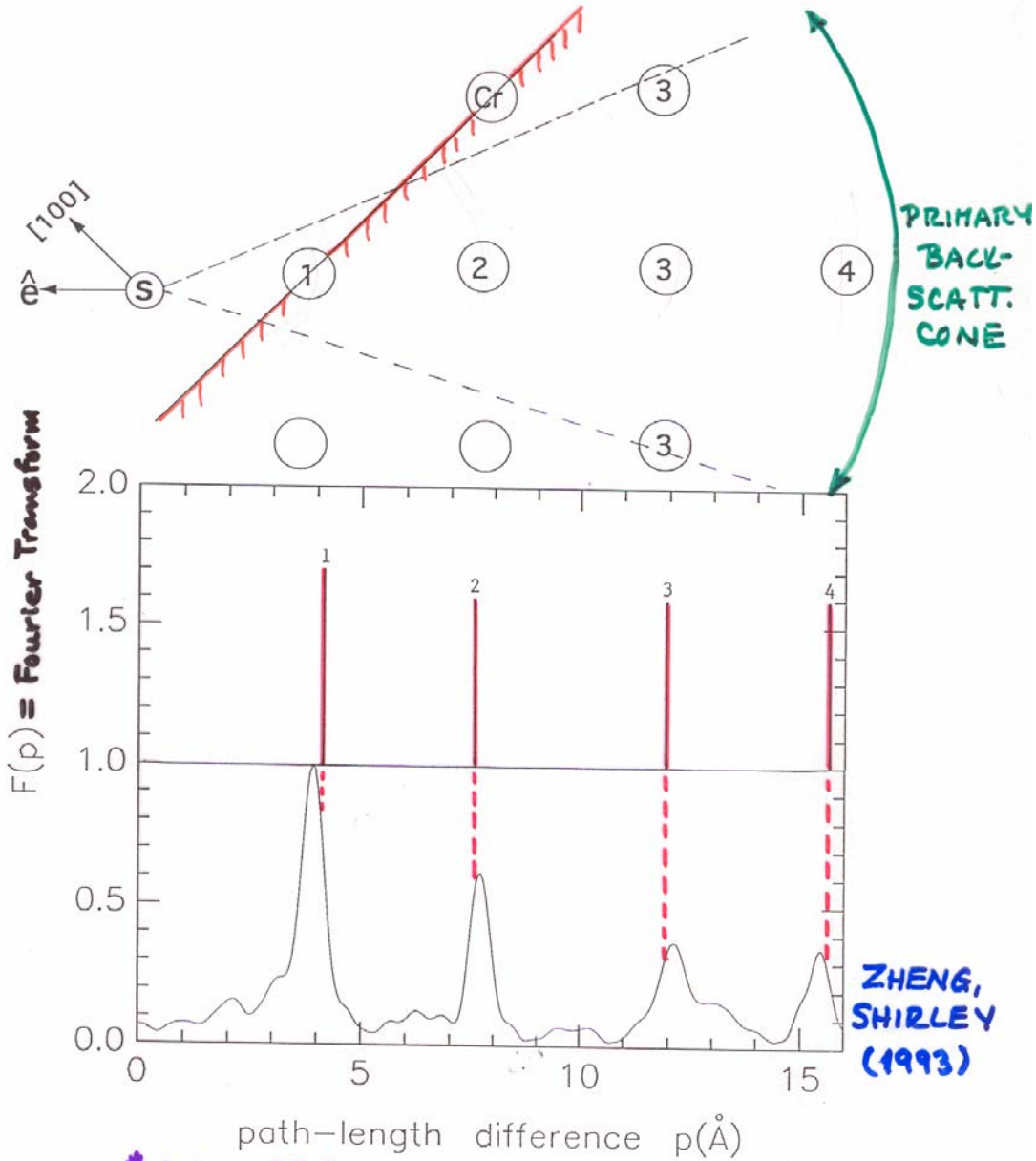

* AUTO-REGRESSIVE DATA EXTENSION

Outline

Surface, interface, and nanoscience—short introduction

Some surface concepts and techniques→photoemission

Synchrotron radiation: experimental aspects

Electronic structure—a brief review

The basic synchrotron radiation techniques:
more experimental and theoretical details

Core-level photoemission:
→ X-ray optical effects on intensities

Valence-level photoemission

Microscopy with photoemission

CALCULATION OF PHOTOELECTRON INTENSITIES—THE 3-STEP MODEL

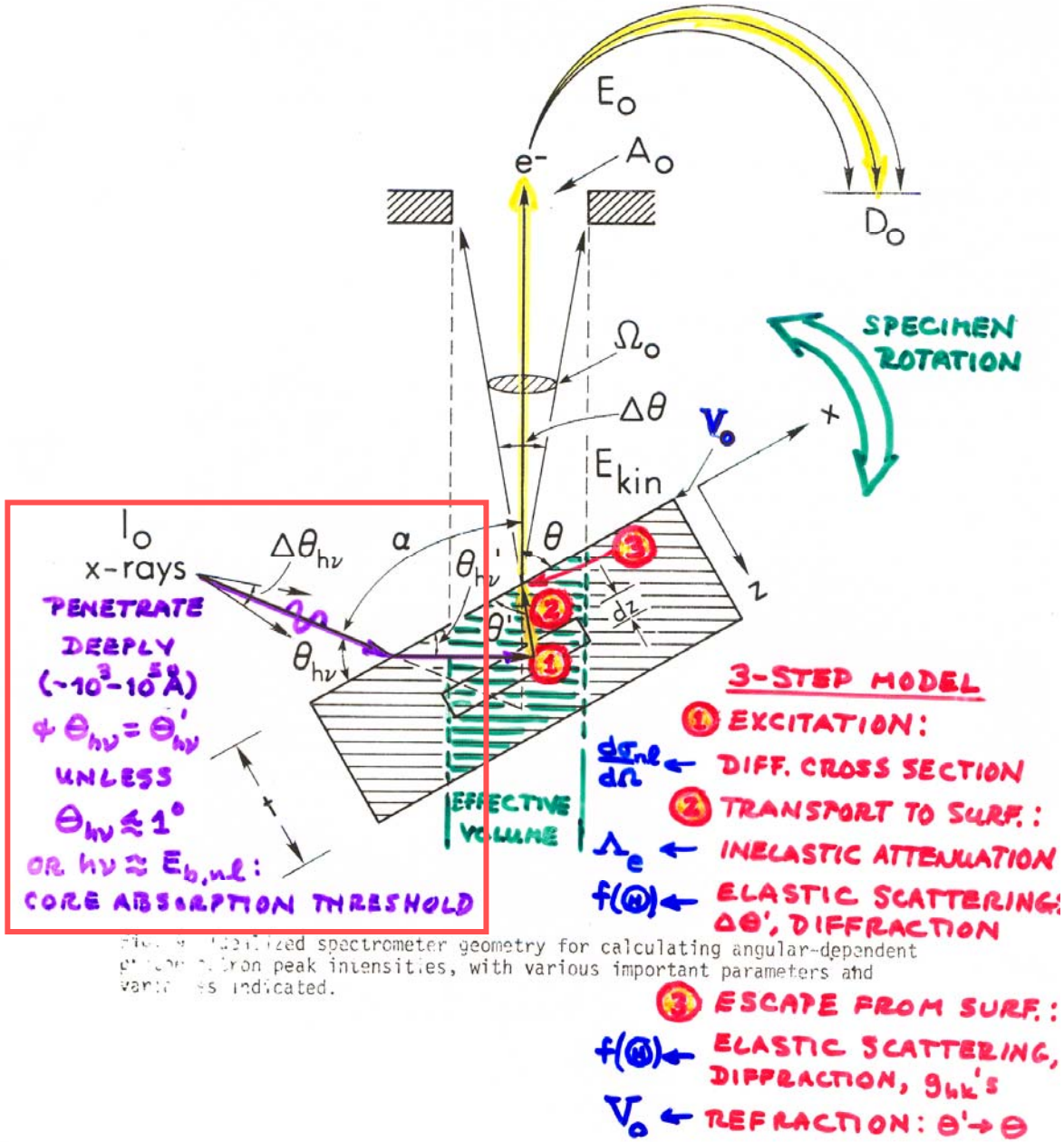

Fig. 9. Idealized spectrometer geometry for calculating angular-dependent photoelectron peak intensities, with various important parameters and variables indicated.

Some basic measurements:

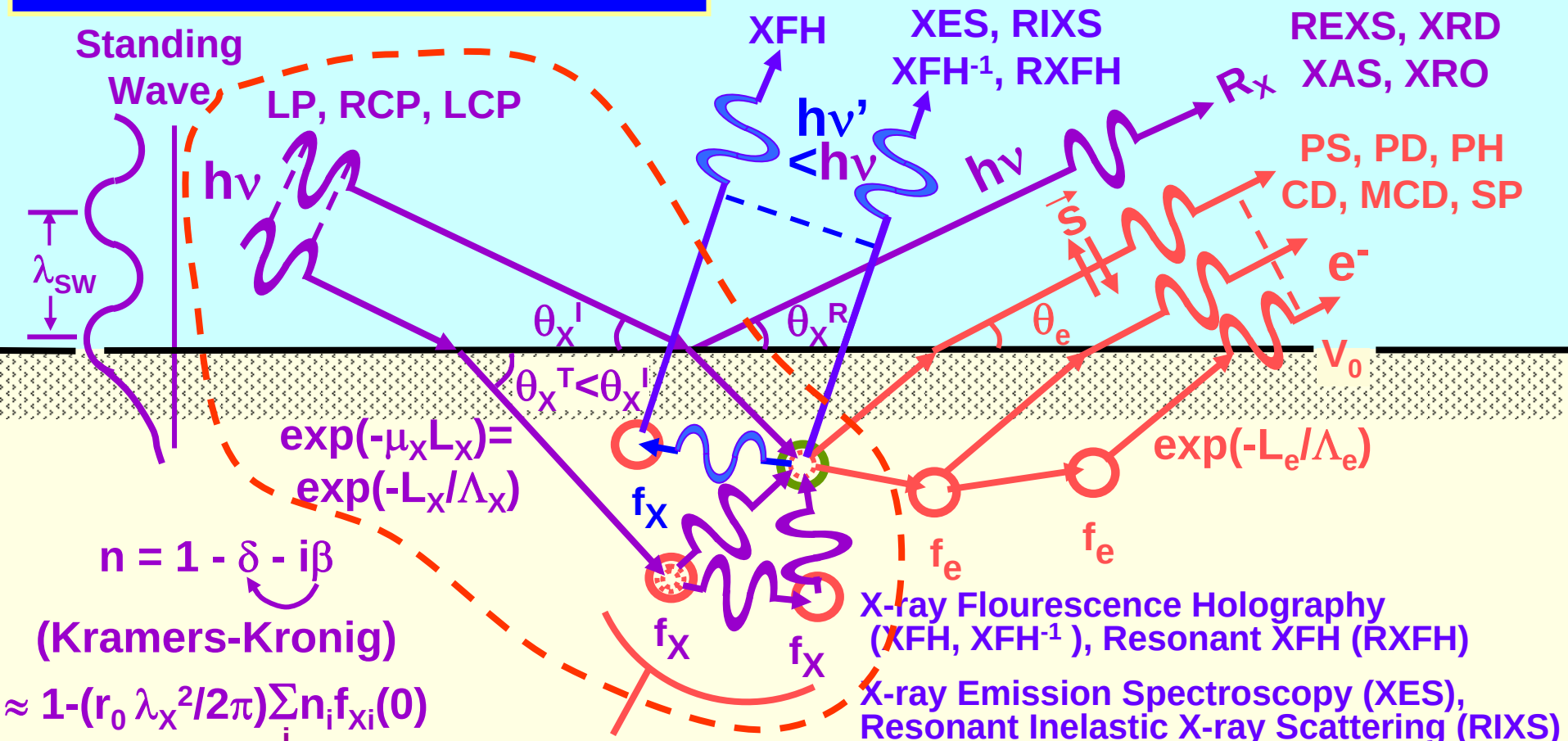

$n = 1 - \delta - i\beta$

(Kramers-Kronig)

$\approx 1-(r_0 \lambda_X^2/2\pi)\sum_i n_i f_{Xi}(0)$

$\mu_X = 4\pi\beta/\lambda_X$

$\theta_X^R = \theta_X^I$

$\lambda_{SW} = \lambda_X/(2\sin\theta_X^I)$

$\theta_{CRIT}^I = (2\delta)^{1/2}$

Multi-atom resonant photoemission (MARPE)

X-ray Flourescence Holography (XFH, XFH^{-1}), Resonant XFH (RXFH)

X-ray Emission Spectroscopy (XES), Resonant Inelastic X-ray Scattering (RIXS)

Resonant Elastic X-ray Scattering (REXS)

X-Ray Diffraction (XRD)

X-ray Absorption Spectroscopy (XAS)

X-Ray Optical measurements (XRO)

Photoelectron Spectroscopy (PS), Diffraction (PD), Holography (PH)
+ Circular Dichroism (CD), Magnetic CD (MCD), Spin Polarization (SP)

A LITTLE X-RAY OPTICS

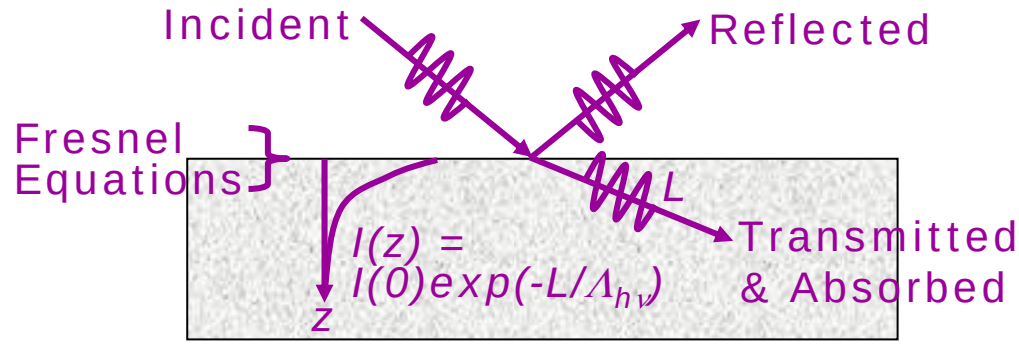

(E.G. See pp. 1-38, 1-44, 5-18-5-19 in X-Ray Data Booklet)

Index of refraction = $n = 1 - \delta - i\beta$

δ = + no. = refractive decrement << 1 (Sometimes negative through absorption resonances)

β = + no. = absorptive decrement << 1

δ and β linked by Kramers-Kronig transform

n also = $1 - (r_e/2\pi)\lambda_{h\nu}^2 \Sigma n_i f_i$(0=fwd. scatt.)

r_e = classical electron radius
$= e^2/4\pi\varepsilon_0 m_e e^2 = 2.817 \times 10^{-15}$ m
$\lambda_{h\nu}$ = x-ray wavelength

n_i = no. i atoms per unit volume

f_i = x-ray scattering factor for ith type of atom, in forward direction

Exponential absorption length = $l_{abs} = \lambda_{h\nu}/(4\pi\beta) = \Lambda_{h\nu}$

θ_{CRIT} = critical grazing angle at which reflectivity begins ($R \approx 0.20$)
$= [2\delta]^{0.5}$

Online data and calculations at:
http://www-cxro.lbl.gov/optical_constants/

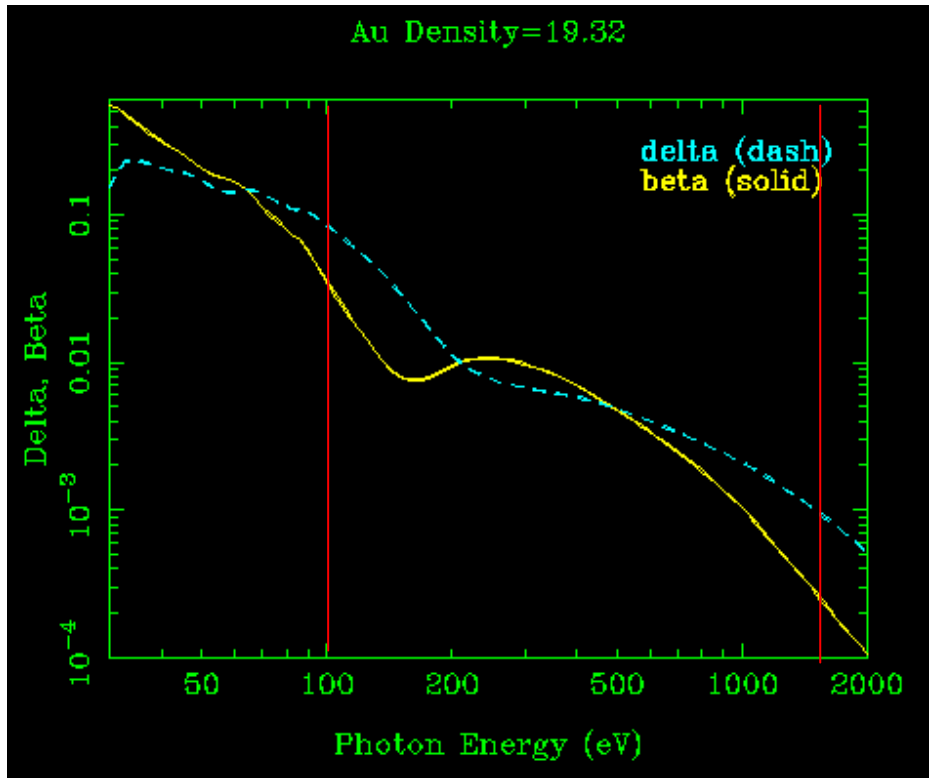

X-ray scattering factor:
$f_i = \mathrm{Re}f_i + i(\mathrm{Im}f_i)$

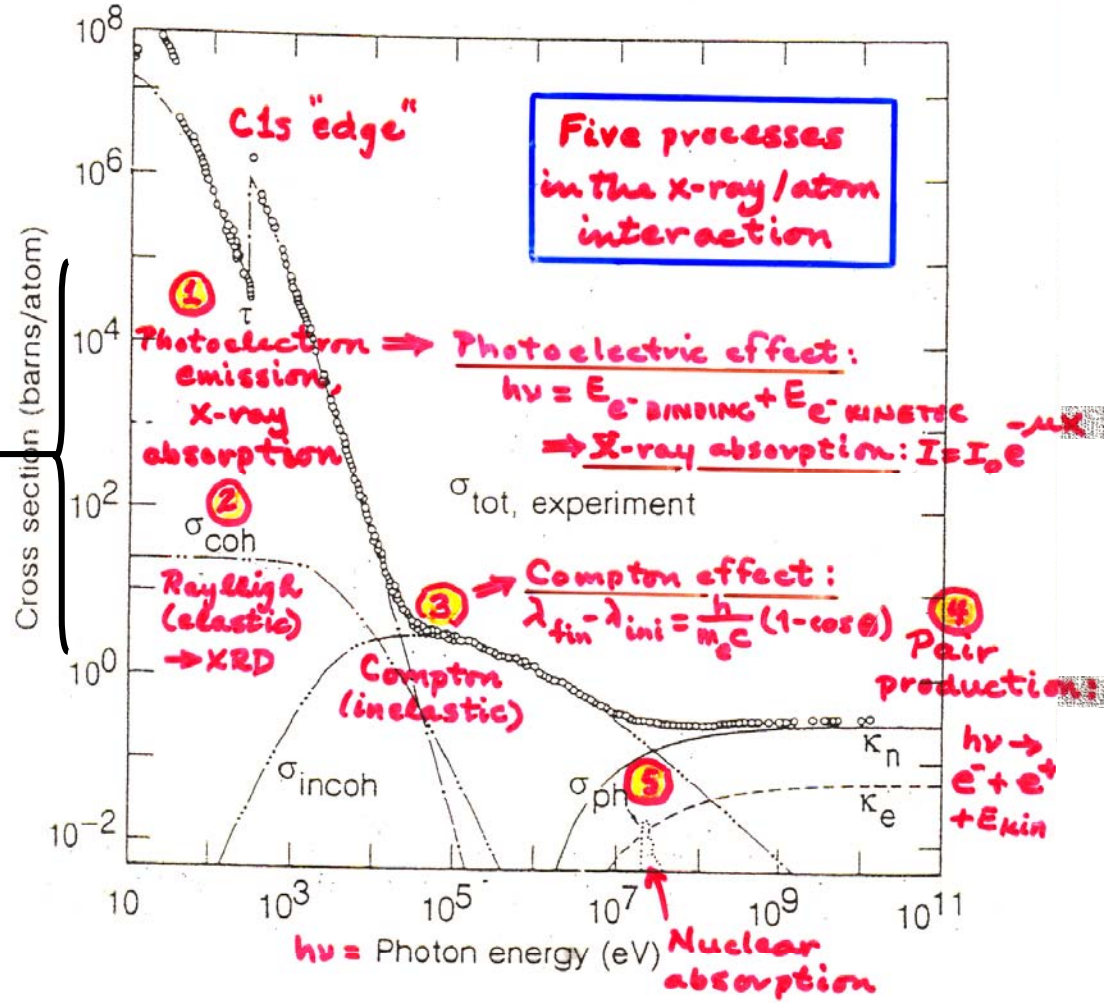

Fig. 3-1. *Total photon cross section σ_{tot} in carbon, as a function of energy, showing the contributions of different processes: τ, atomic photo-effect (electron ejection, photon absorption); σ_{coh}, coherent scattering (Rayleigh scattering—atom neither ionized nor excited); σ_{incoh}, incoherent scattering (Compton scattering off an electron) κ_n, pair production, nuclear field; κ_e, pair production, electron field; σ_{ph}, photonuclear absorption (nuclear absorption usually followed by emission of a neutron or other particle). (From Ref. 5; figure courtesy of J. H. Hubbell.)*

http://www-cxro.lbl.gov/optical_constants/

X-Ray Interactions with Matter

Website

Contents

These pages utilize *JavaScript*, but the decaffeinated versions are still available.

Reference

B.L. Henke, E.M. Gullikson, and J.C. Davis. *X-ray interactions: photoabsorption, scattering, transmission, and reflection at E=50-30000 eV, Z=1-92*, Atomic Data and Nuclear Data Tables Vol. **54** (no.2), 181-342 (July 1993).

By Eric Gullikson. Please direct any comments to EMGullikson@lbl.gov

SOME X-RAY OPTICAL EFFECTS: REDUCED PENETRATION DEPTHS AND INCREASED REFLECTIVITY AT GRAZING INCIDENCE ANGLES

θ_{CRIT} = Grazing angle at which reflectivity begins ($R \approx 0.20$)

$= [2\delta]^{0.5}$

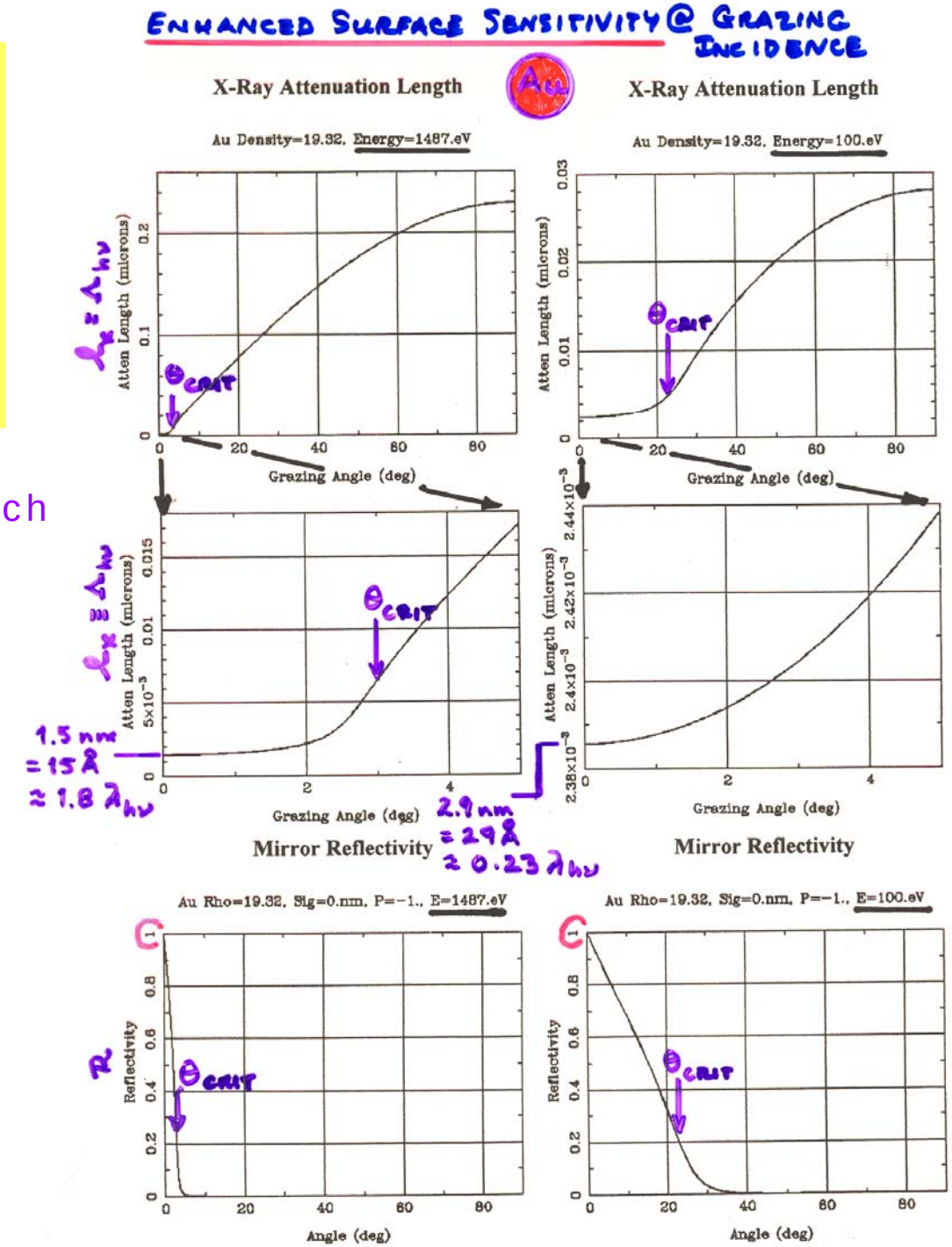

Optical constants through Mn 2p edges of MnO—Web data <u>without absorption peaks</u>

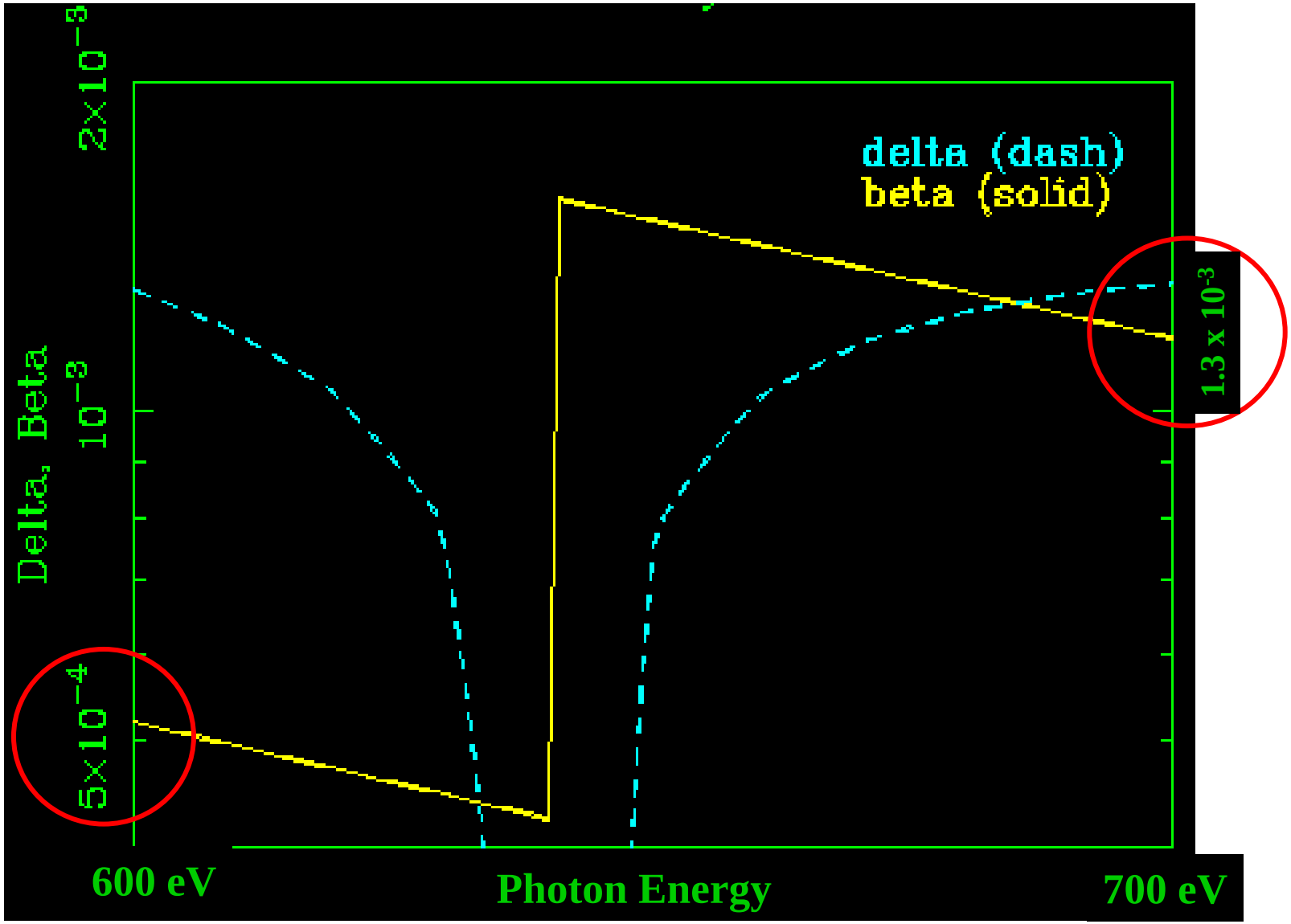

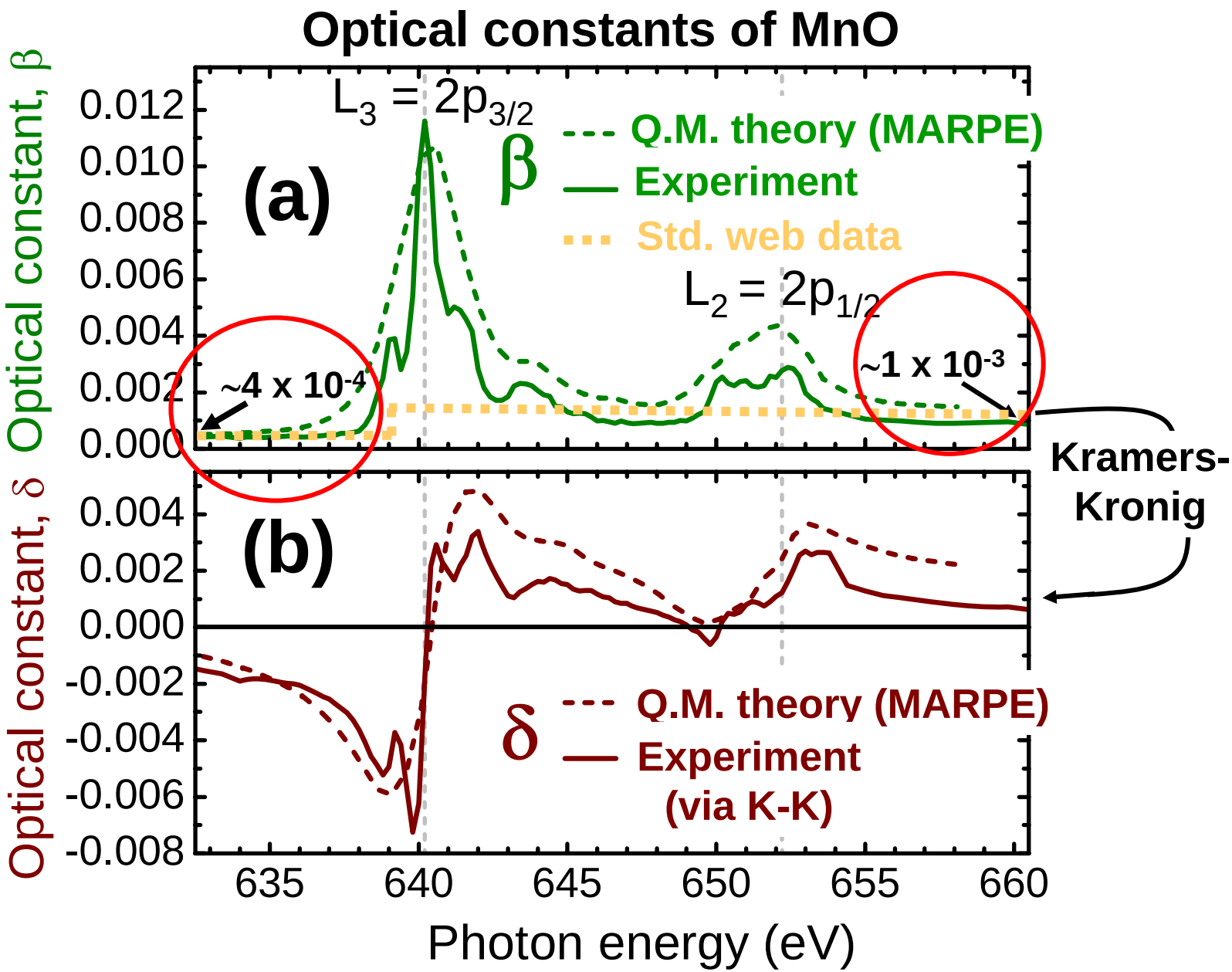
Optical constants of MnO
Optical constant, β
Optical constant, δ
(a)
(b)
L3 = 2p3/2
L2 = 2p1/2
β
δ
Q.M. theory (MARPE)
Experiment
Std. web data
Q.M. theory (MARPE)
Experiment
(via K-K)
~4 x 10-4
~1 x 10-3
Kramers-Kronig
0.012
0.010
0.008
0.006
0.004
0.002
0.000
0.004
0.002
0.000
-0.002
-0.004
-0.006
-0.008
635
640
645
650
655
660
Photon energy (eV)

X-ray optical effects through core resonances:

(a)

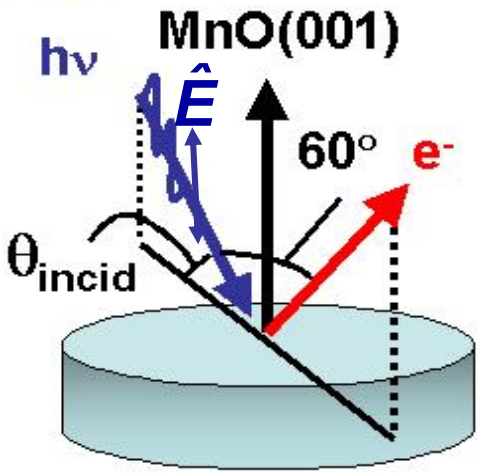

(b)

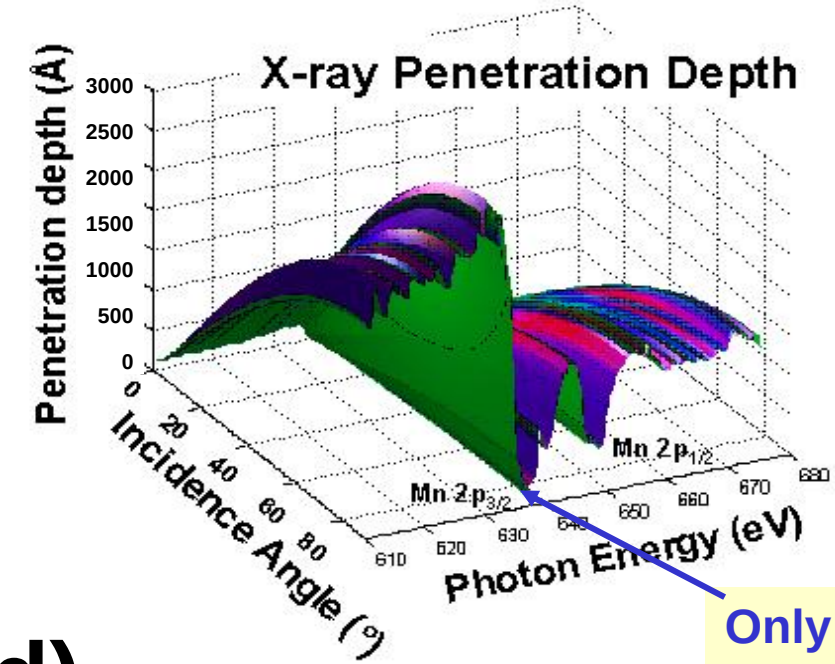

Only approx. 130 Å at normal incidence

(c)

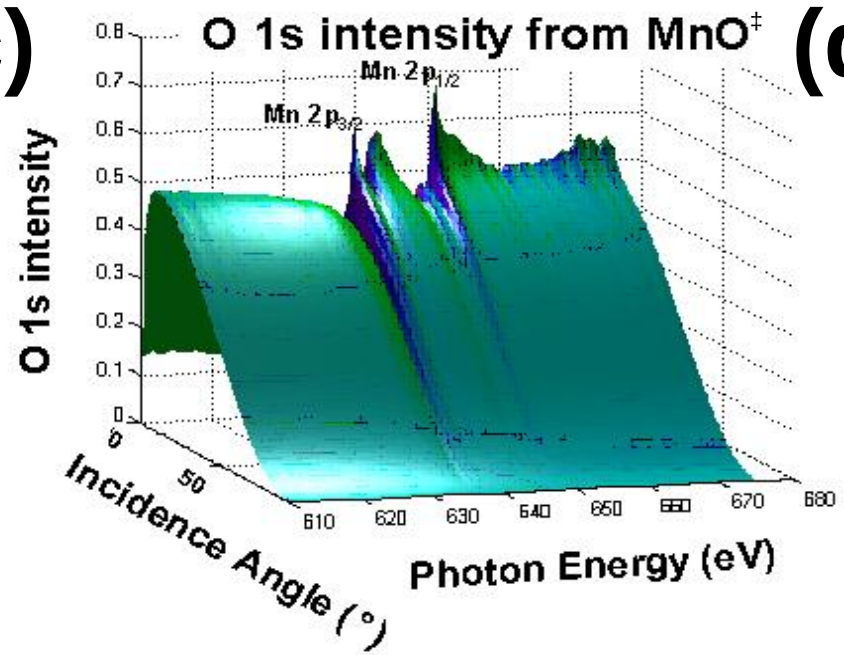

(d)

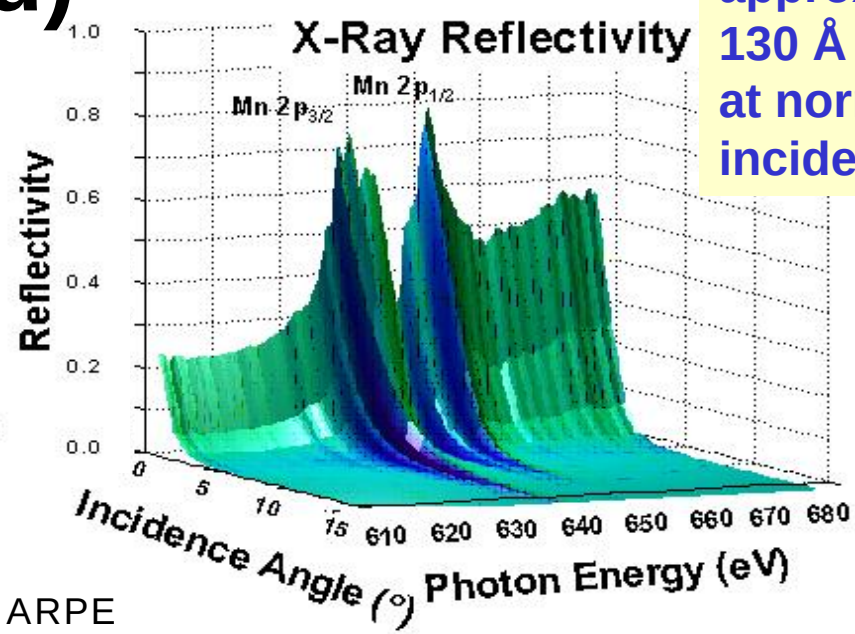

‡Aka Multi-Atom Resonant Photoemission = MARPE

Outline

Surface, interface, and nanoscience—short introduction

Some surface concepts and techniques→photoemission

Synchrotron radiation: experimental aspects

Electronic structure—a brief review

The basic synchrotron radiation techniques

Core-level photoemission
X-ray optical effects on emission→
Use of standing waves to probe buried interfaces

Valence-level photoemission

Microscopy with photoemission

Standing wave formation in reflection from a surface

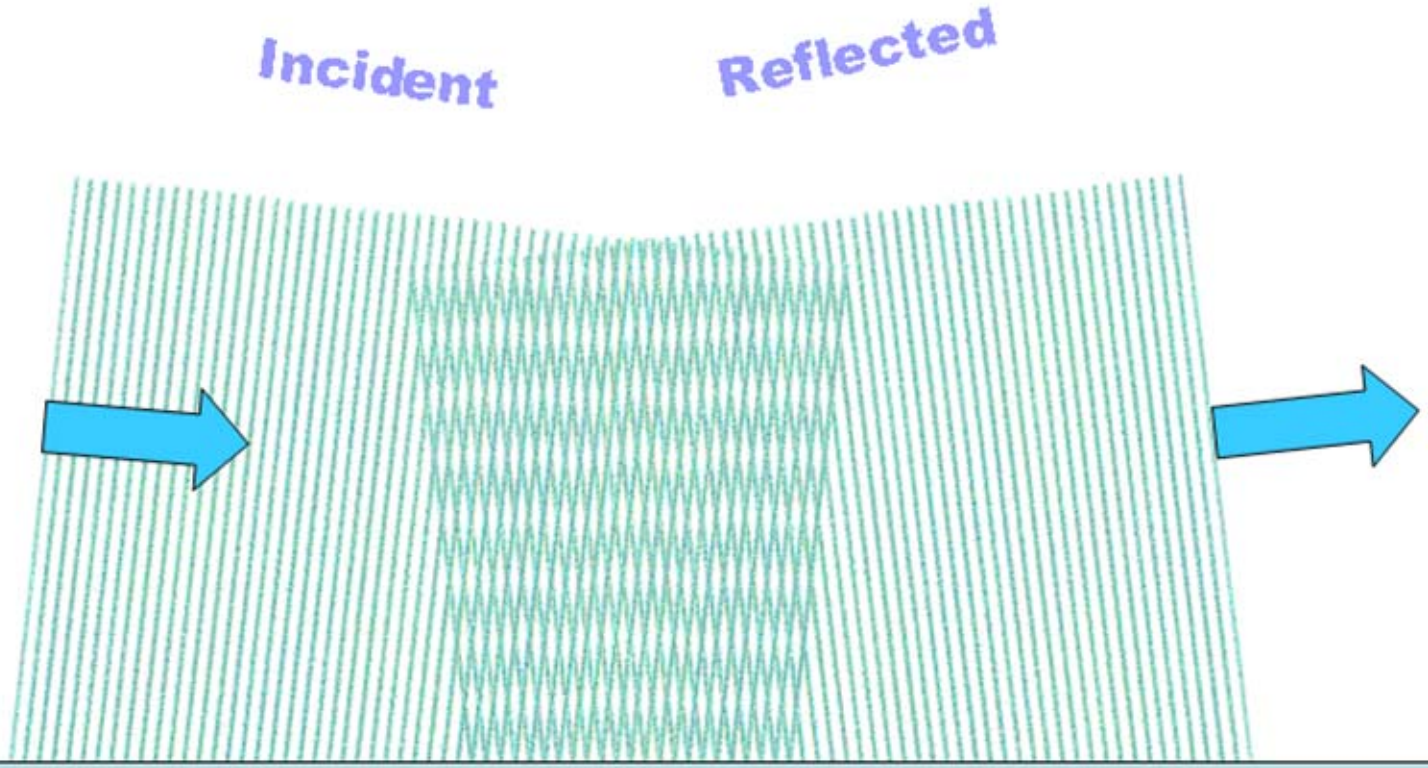

If incident angle = reflected angle (specular reflection) standing wave is <u>parallel to surface</u>

Standing wave formation:

$$I_{SW}(|E^2|) \propto |\phi_{inc} + \phi_{refl}|^2$$
$$= |\phi_{inc}|^2 + \underbrace{\phi_{inc}\phi_{refl}^* + \phi_{inc}^*\phi_{refl}}_{\text{SW modulation}} + |\phi_{refl}|^2$$

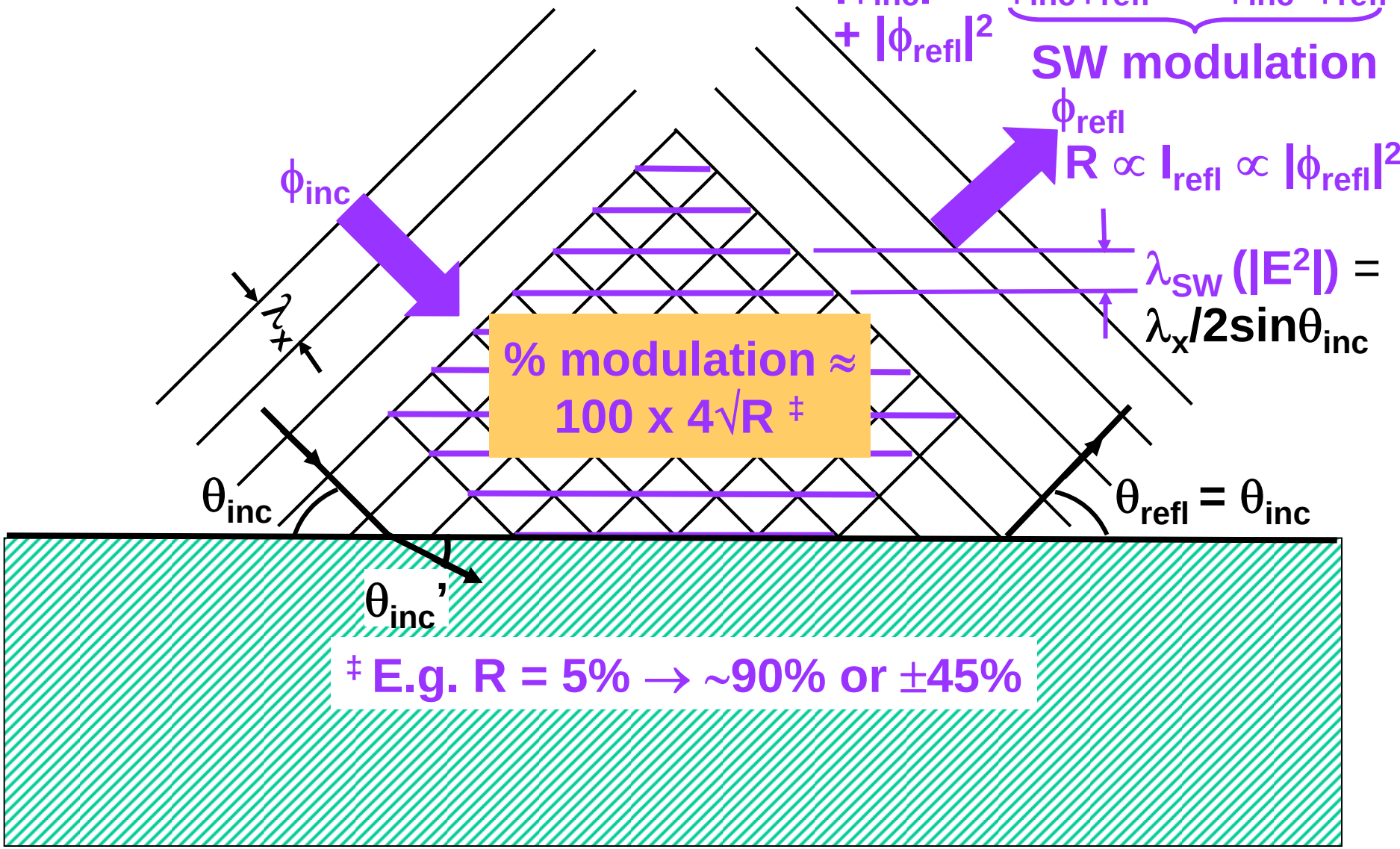

‡ E.g. R = 5% → ~90% or ±45%

Standing wave formation with a multilayer mirror:

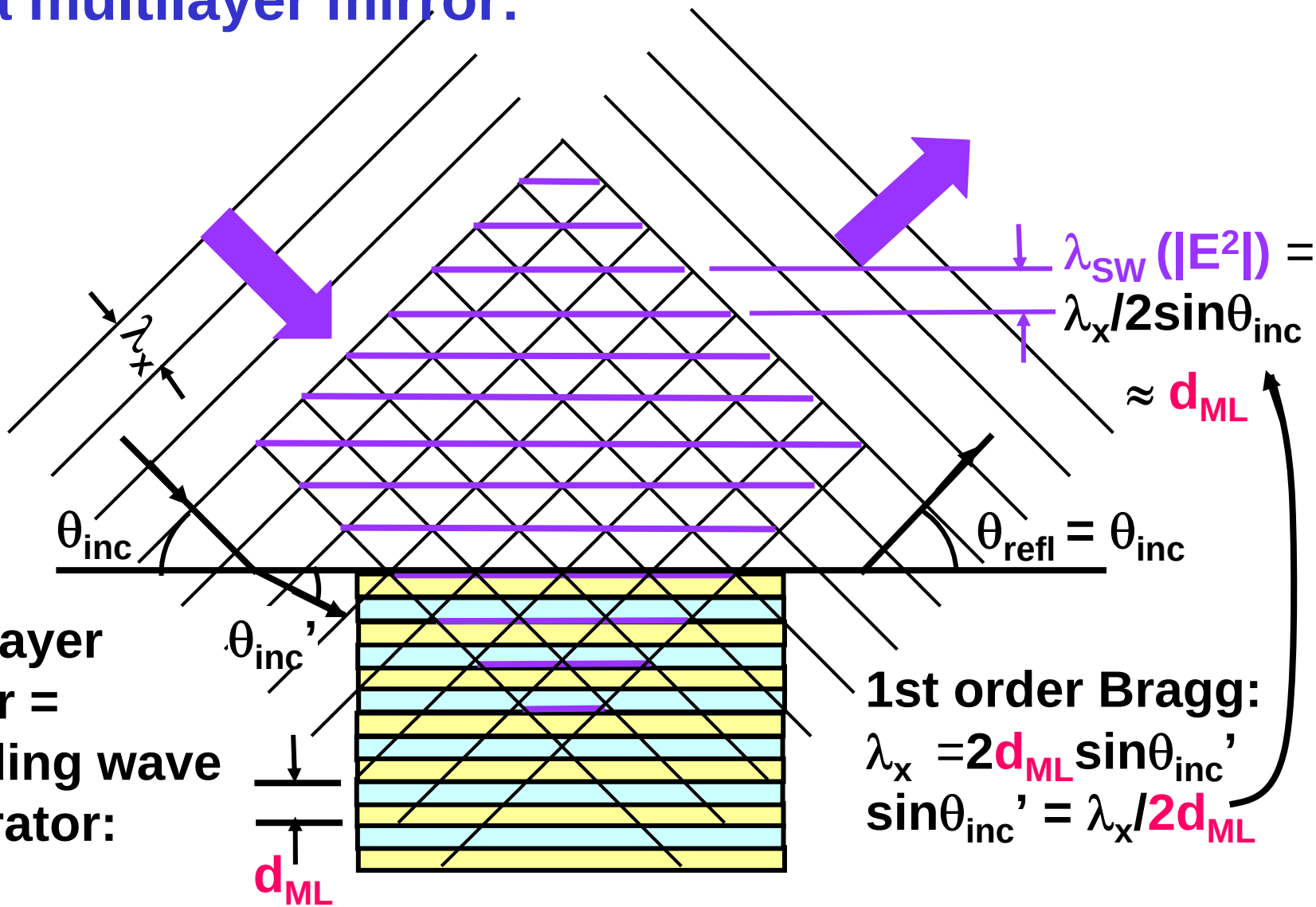

Multilayer mirror = Standing wave generator:

1st order Bragg:

$\lambda_x = 2d_{ML}\sin\theta_{inc}'$

$\sin\theta_{inc}' = \lambda_x/2d_{ML}$

PROBING BURIED INTERFACES WITH SOFT X-RAY STANDING WAVES:

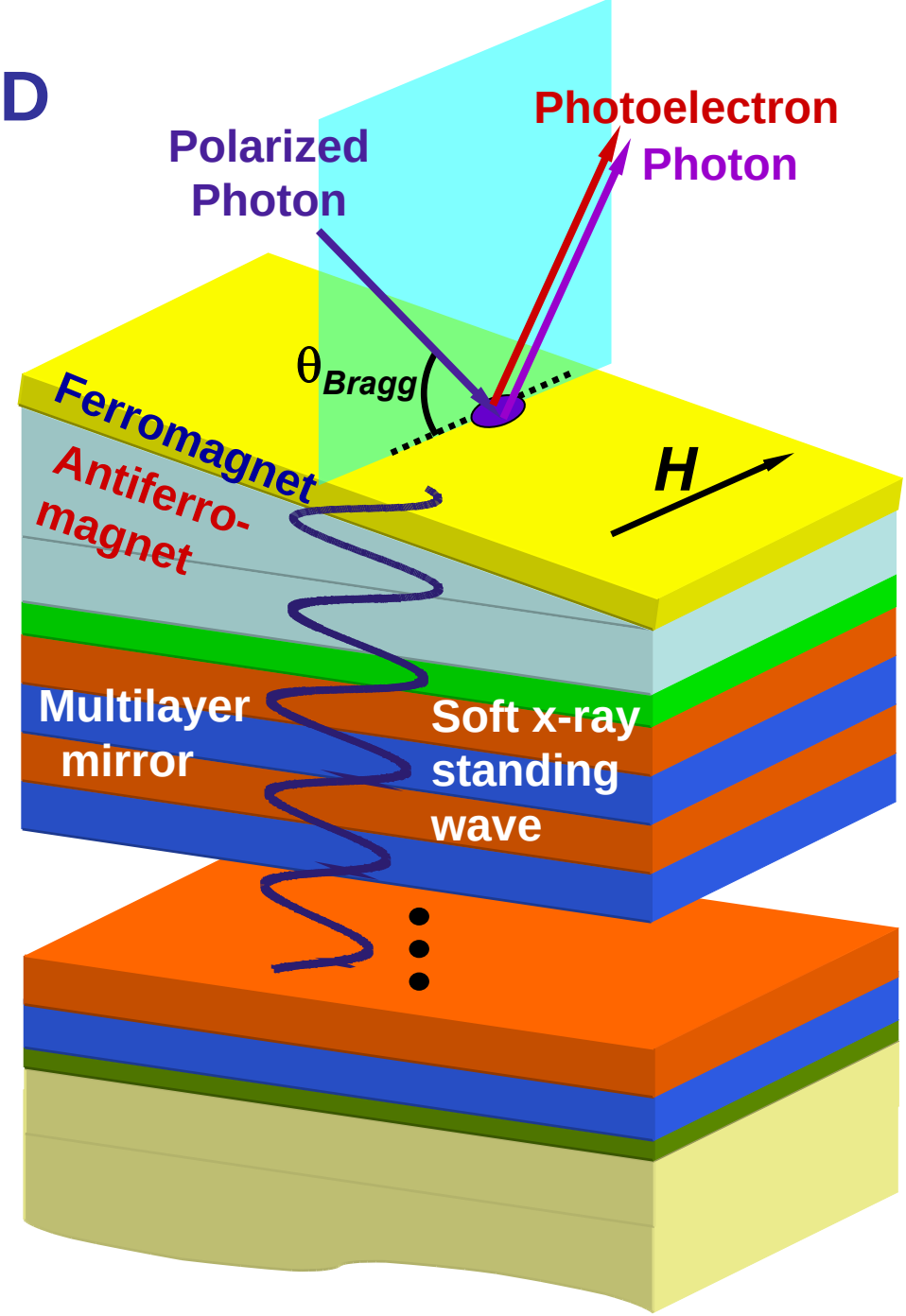

PROBING BURIED INTERFACES WITH SOFT X-RAY STANDING WAVES:

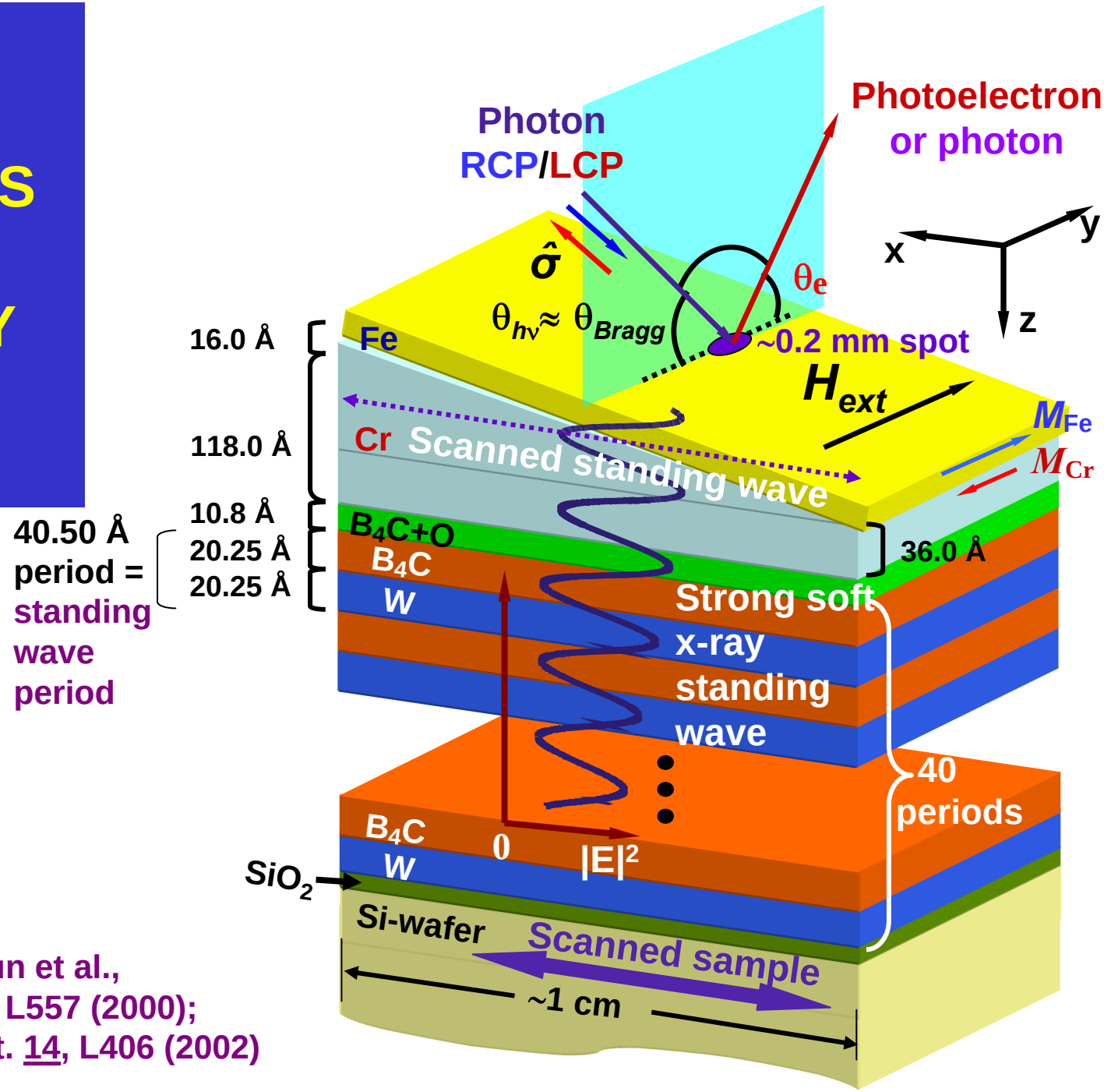

S.-H. Yang. B.S. Mun et al.,
Surf. Sci. Lett. 461, L557 (2000);
J. Phys. Cond. Matt. 14, L406 (2002)

TRANSMISSION ELECTRON MICROSCOPY IMAGE FOR Fe/Cr/MULTILAYER SWG

(Synthesis-CXRO, and Imaging-NCEM, LBNL)

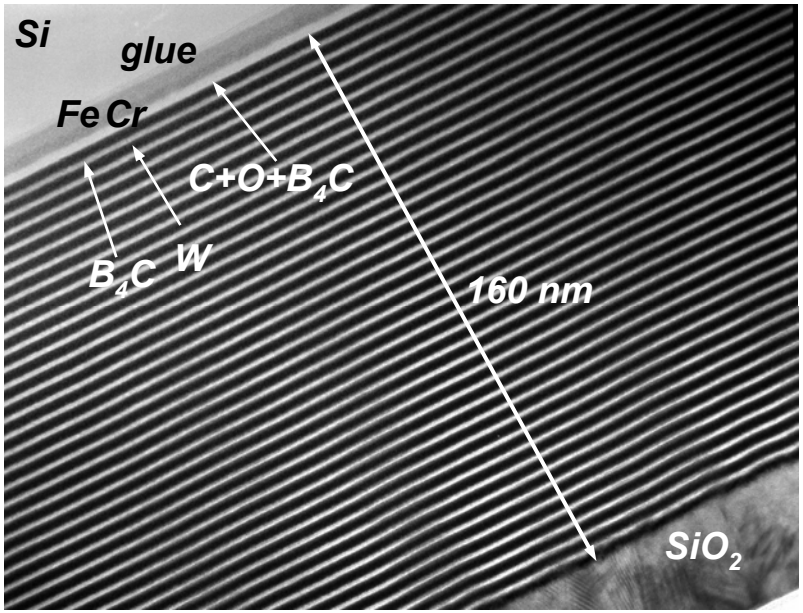

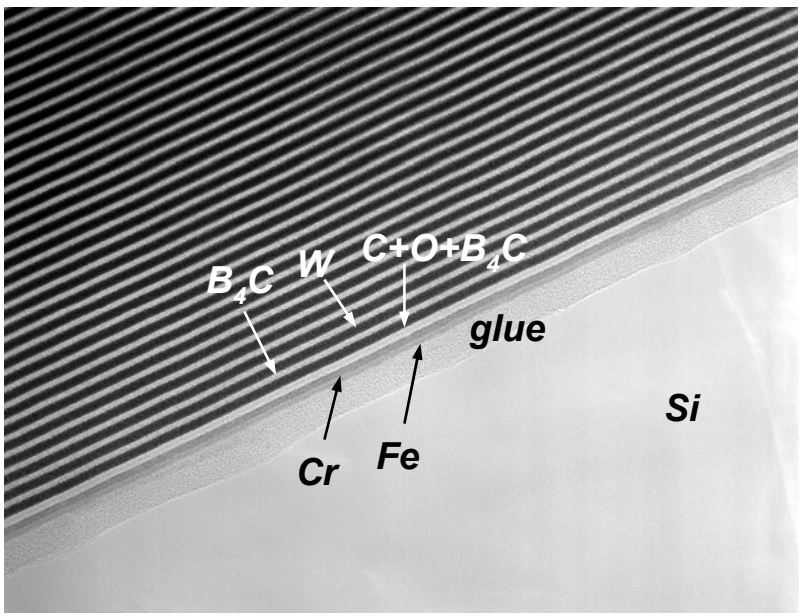

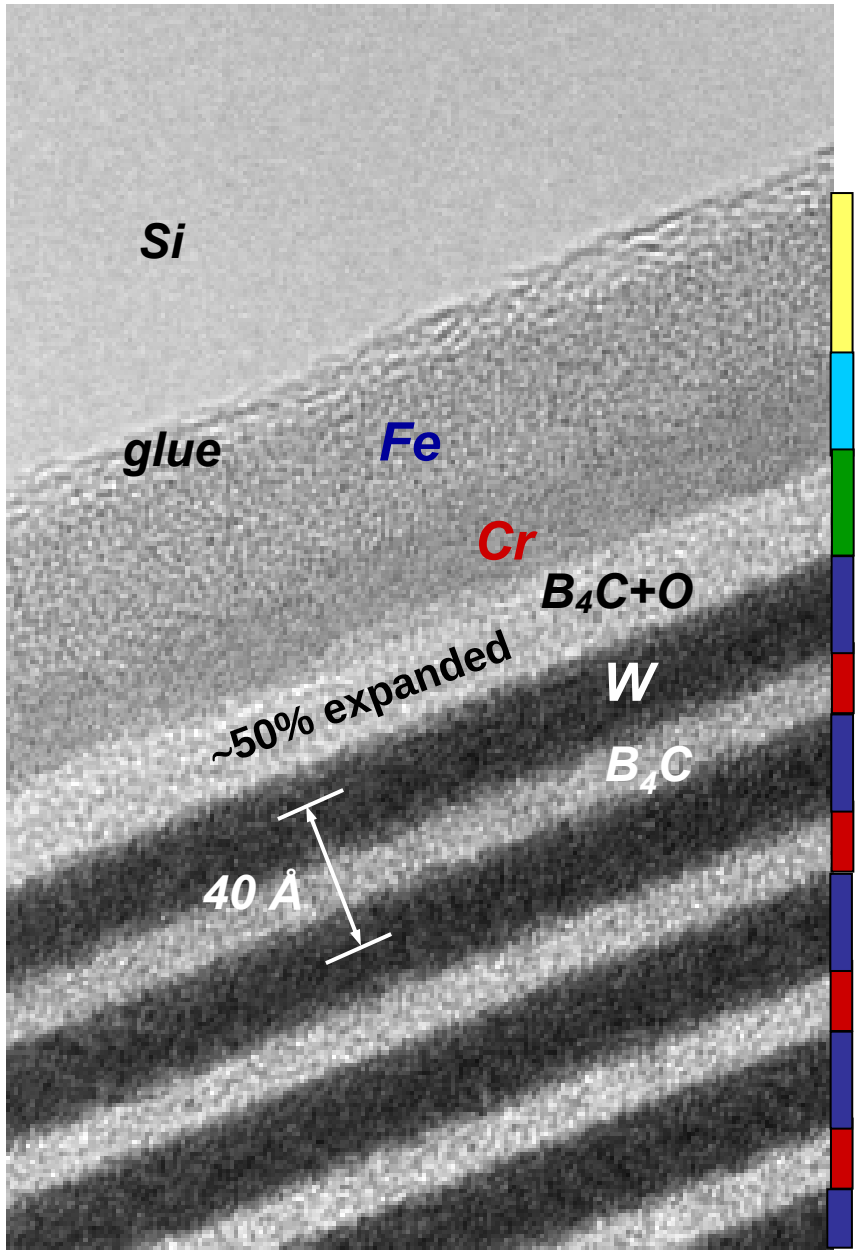

Fe & Cr 2p MCD Data from wedge (Fe/Cr)+SWG

Cr magnetization Is antiparallel to Fe; systematic variation of MCD strengths vs d_{cr}

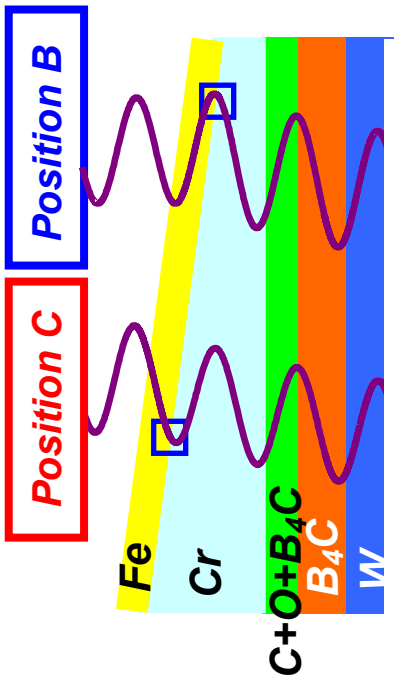

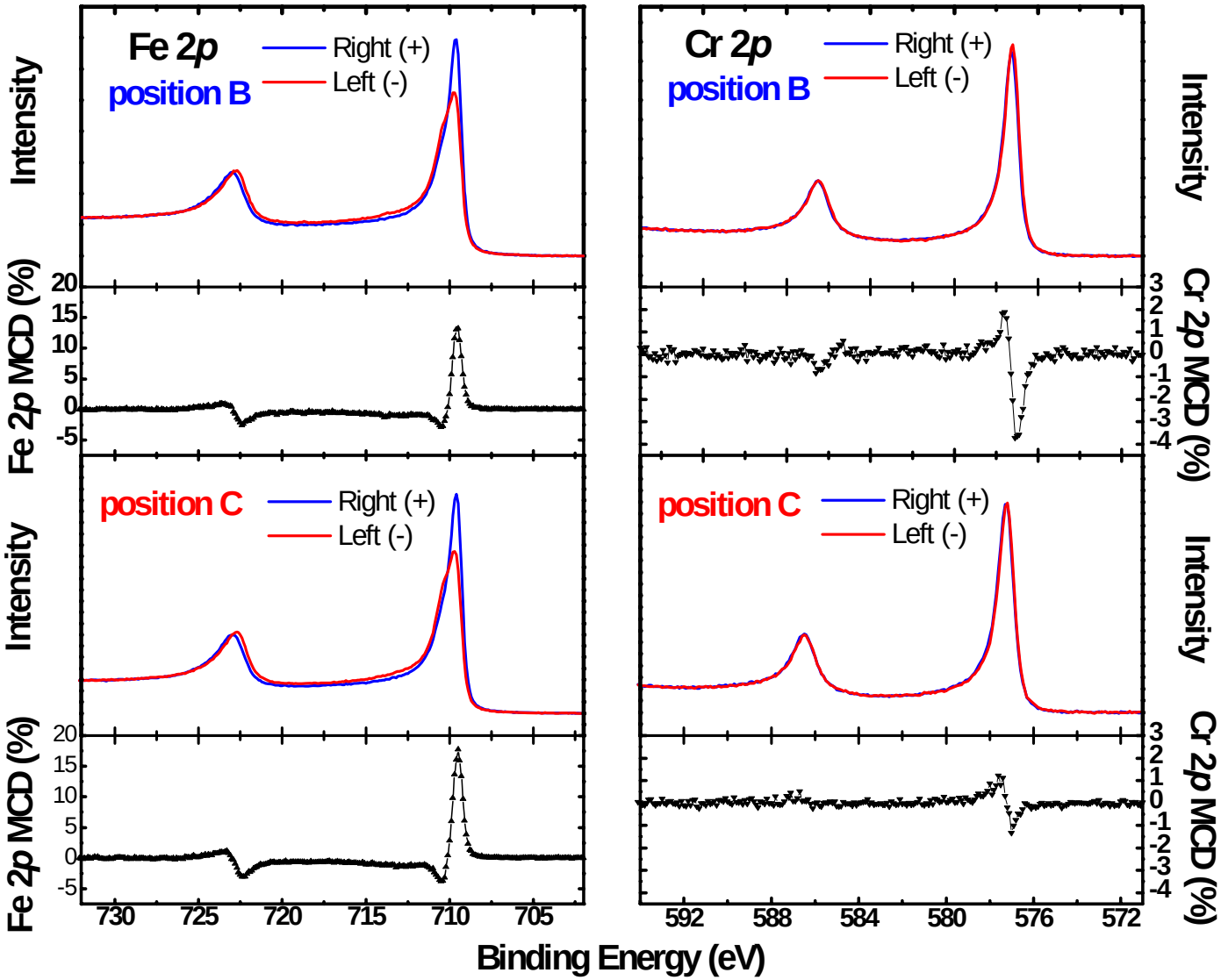

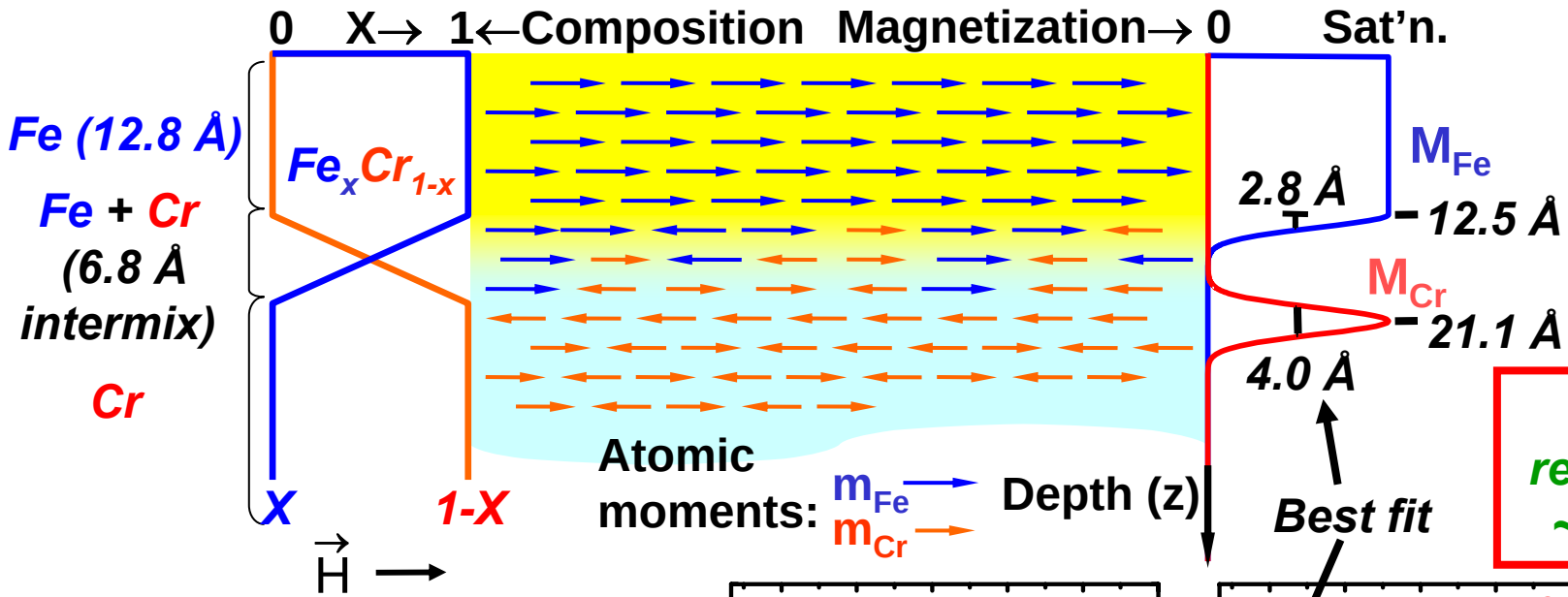

Depth-resolution ~± 2-3 Å

Non-destructive, depth-resolved det'n. of composition and magnetization profiles from standing-wave excited photoemission

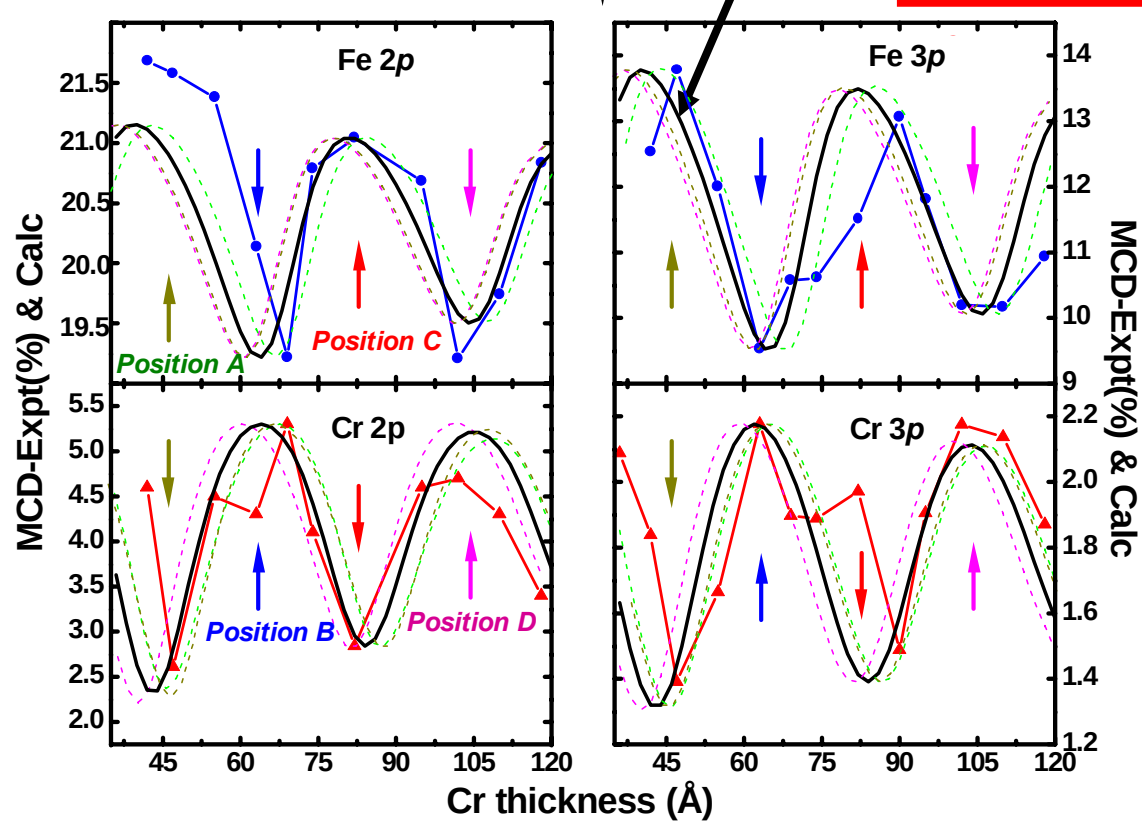

Standing-Wave Excited Spectroscopy--Future Possibilities

- Other material pairs in multilayer (B_4C/W, Al_2O_3/Pt,…) + epitaxial multilayers → epitaxial samples
- Smaller periods (to ~25-30 Å) → smaller SW period, better resolution
- Lower $h\nu_{inc}$ →higher Bragg angles→perpend. component of M
- X-ray emission→ deeper layers, more sensitivity to SW position

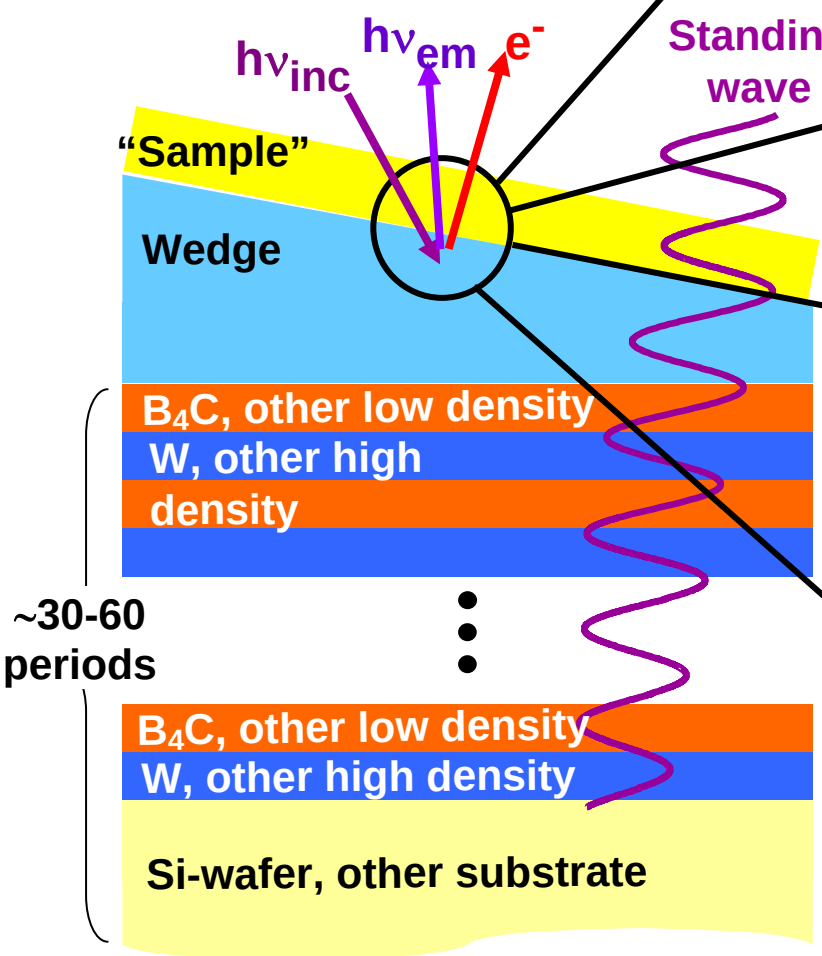

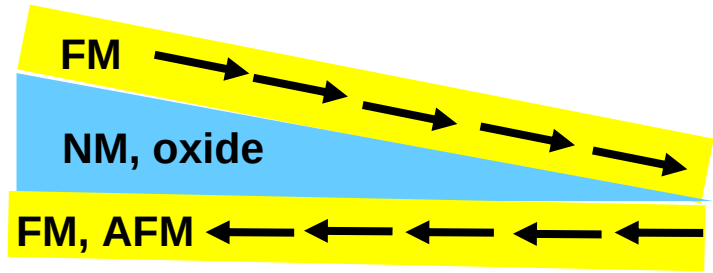

GMR, exchange biassing, tunnel junction

Ultrathin gate oxide films

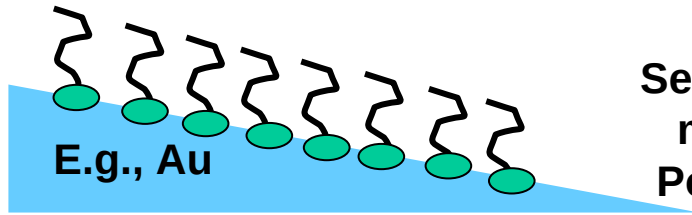

Clusters, Self-assembled monolayers, Polymer films, Liquid layers

Microscope resolution

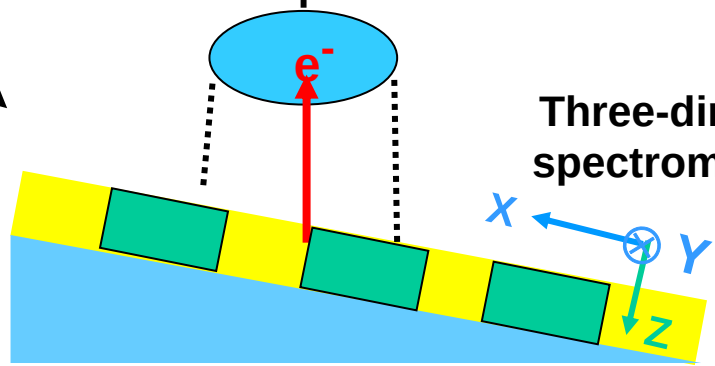

Three-dimensional spectromicroscopy

Outline

Surface, interface, and nanoscience—short introduction

Some surface concepts and techniques→photoemission

Synchrotron radiation: experimental aspects

Electronic structure—a brief review

The basic synchrotron radiation techniques:
more experimental and theoretical details

Core-level photoemission:
photoelectron (and x-ray fluorescence) holography

Valence-level photoemission

Microscopy with photoemission

CLASSIC OPTICAL HOLOGRAPHY:

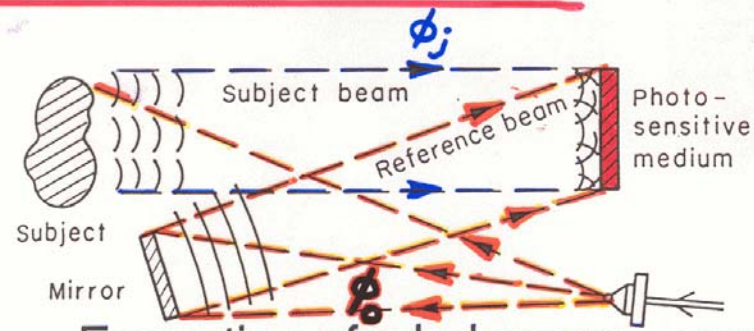

Formation of a hologram

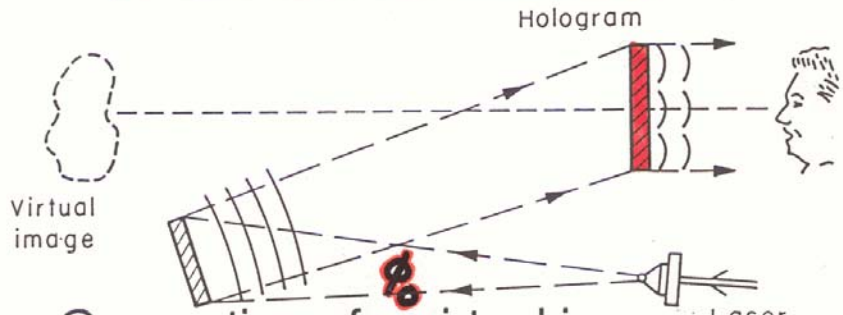

Generation of a virtual image

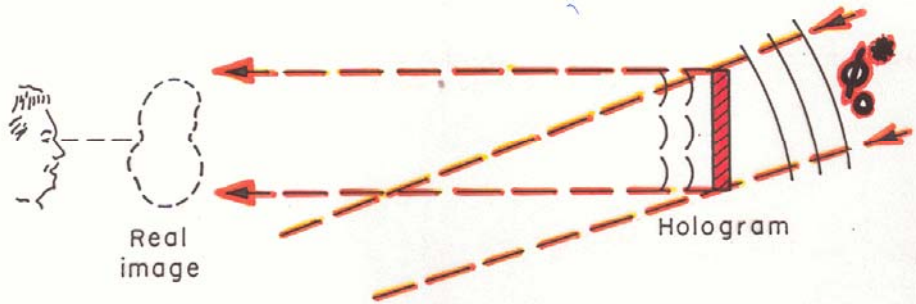

Generation of a real image

In electron emission holography, reference is outgoing spherical & conjugate is incoming spherical

Photoelectron diffraction→ holography: Element-specific short-range atomic structure

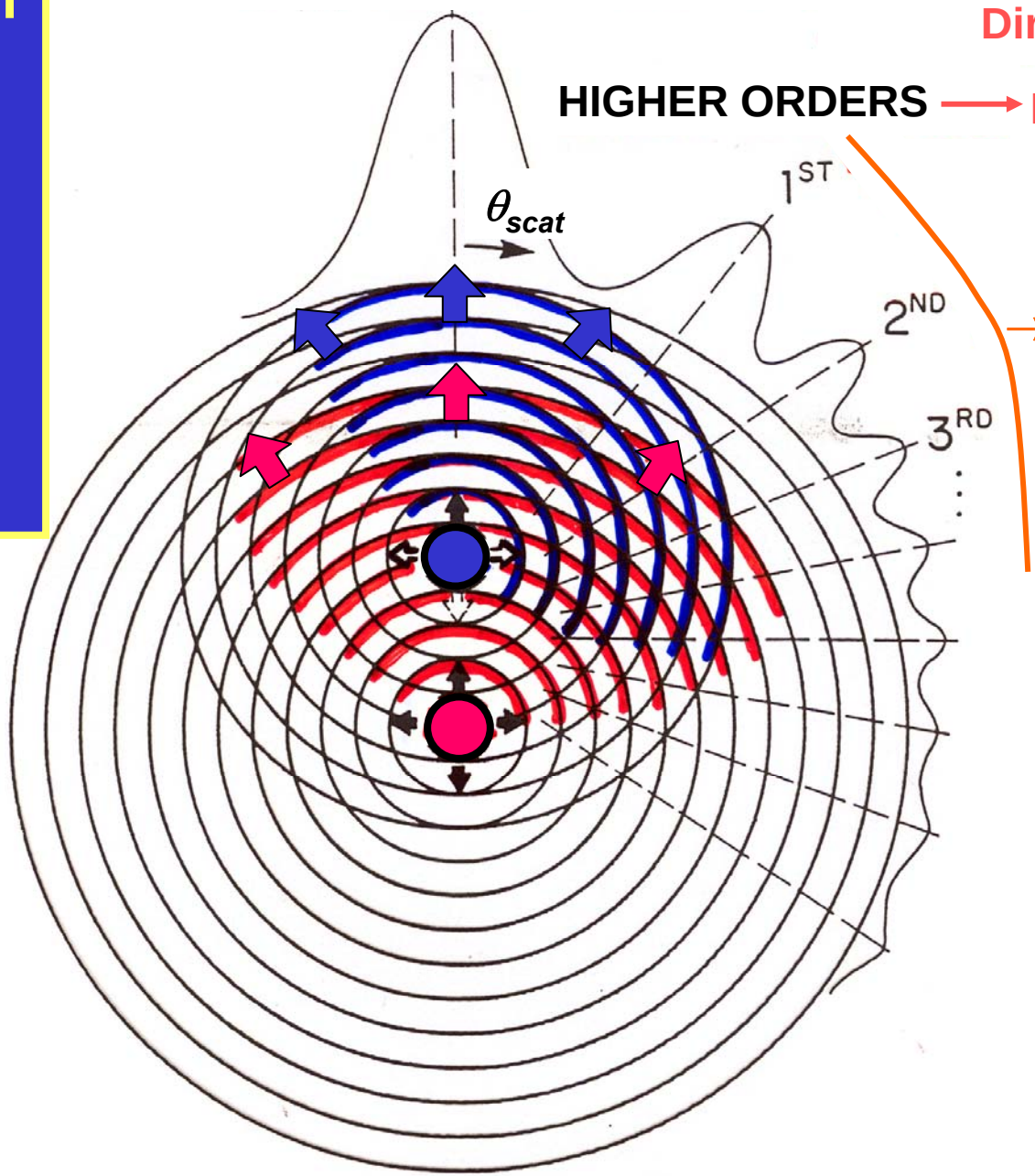

FORWARD SCATT. = "OTH ORDER" → Bond & Low-Index Directions

HIGHER ORDERS → Bond Lengths & Atomic Positions

→Holographic fringes

Principles of photoelectron and x-ray fluorescence holography:

(a) Inner source holography -direct:

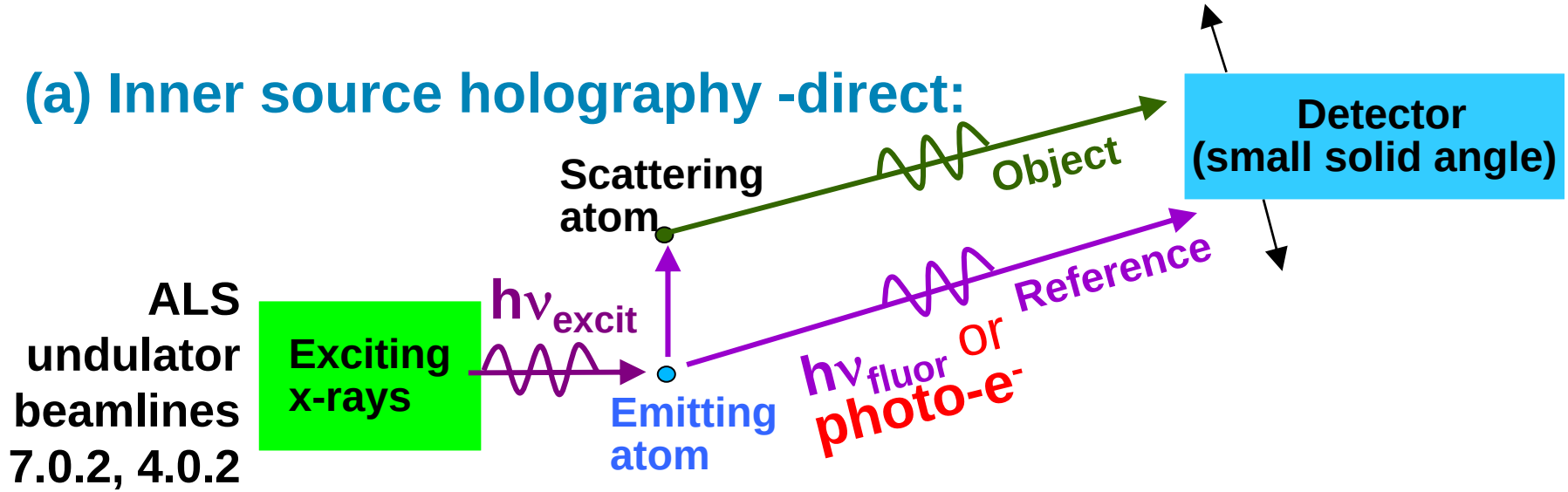

Recent overviews:
G. Faigel and M. Tegze, Rep. Prog. Phys. 62, 355 (1999)
Adams et al., Phys. Stat. Sol. (b) 215, 757 (1999)
C.S.F., M.A Van Hove, et al., J. Phys. B Cond. Matt. 13, 10517 (2001)

The basic imaging ideas
(Gabor; Helmholtz-Kirchoff; Wolf; Szöke; Barton-Tong)

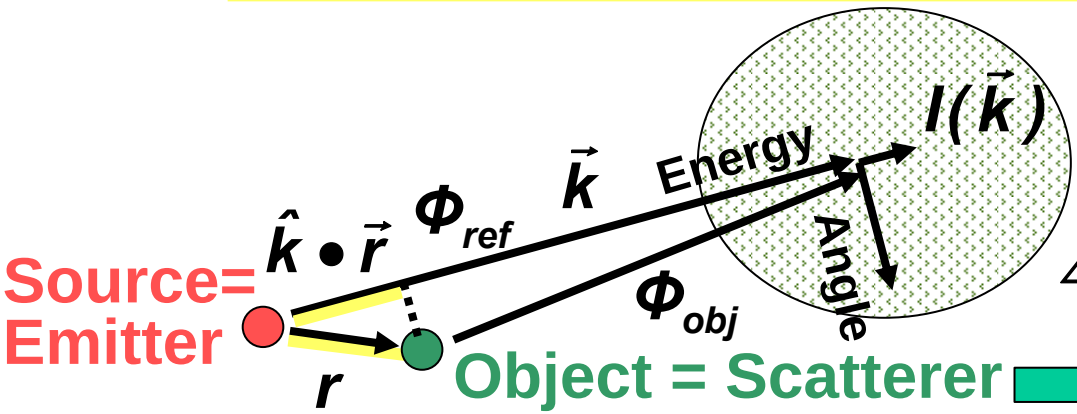

$k = 2\pi/\lambda$

3D sampled region:

$\Delta k_x \times \Delta k_y \times \Delta k_z$

Resolution:

$\Delta x \approx 1/\Delta k_x$

$\Delta y \approx 1/\Delta k_y$

$\Delta z \approx 1/\Delta k_z$

Phase difference between Φ_{ref} and Φ_{obj} $= \vec{k} \bullet \vec{r} - kr$

$$I(\vec{k}) = \left|\Phi_{ref}(\vec{k}) + \Phi_{obj}(\vec{k})\right|^2$$

Holographic interference

$$= \left|\Phi_{ref}(\vec{k})\right|^2 + \boxed{\Phi_{ref}^*(\vec{k})\Phi_{obj}(\vec{k}) + \Phi_{ref}(\vec{k})\Phi_{obj}^*(\vec{k})} + \left|\Phi_{obj}(\vec{k})\right|^2$$

Weak, ~isotropic scattering, no phase shift

$$\text{Hologram}: \quad \chi(\vec{k}) = \frac{I(\vec{k}) - I_0}{I_0} = \frac{I(\vec{k}) - \left|\Phi_{ref}(\vec{k})\right|^2}{\left|\Phi_{ref}(\vec{k})\right|^2}$$

Holographic image:

$$U(\vec{r}) = \left|\iiint \chi(\vec{k}) \exp[i\vec{k} \bullet \vec{r} - ikr]\, d^3k\right|$$

(Usual phase problem)

Inside-source PH-first adsorbate: S/Ni(100)

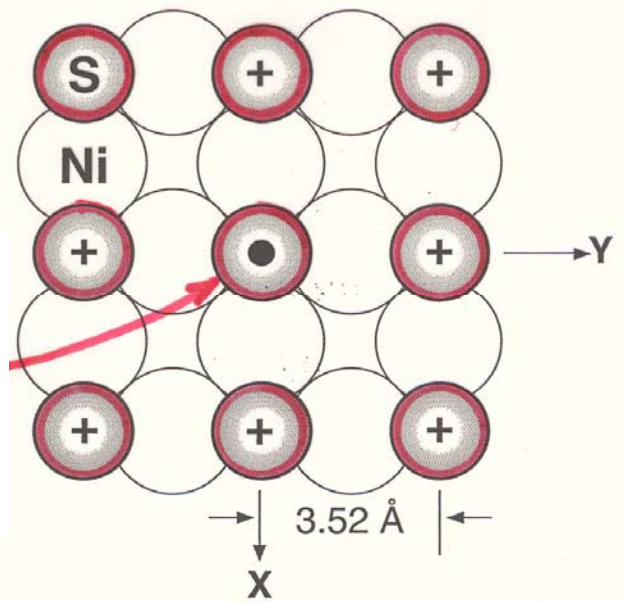

Typical S emitter
$h\nu$ = 1486.6 eV→
E_{kin} = 1327 eV

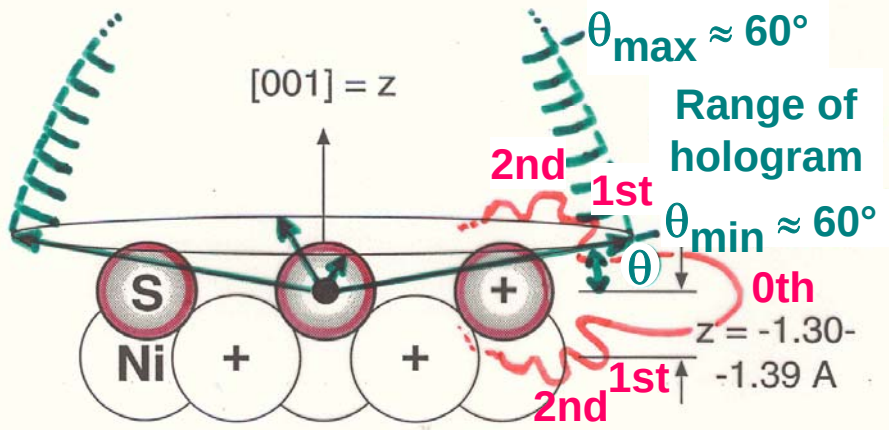

Thevuthasan et al.,
Phys. Rev. Lett. 70, 595 ('93)

Holograms: S/Ni(001)

Experiment

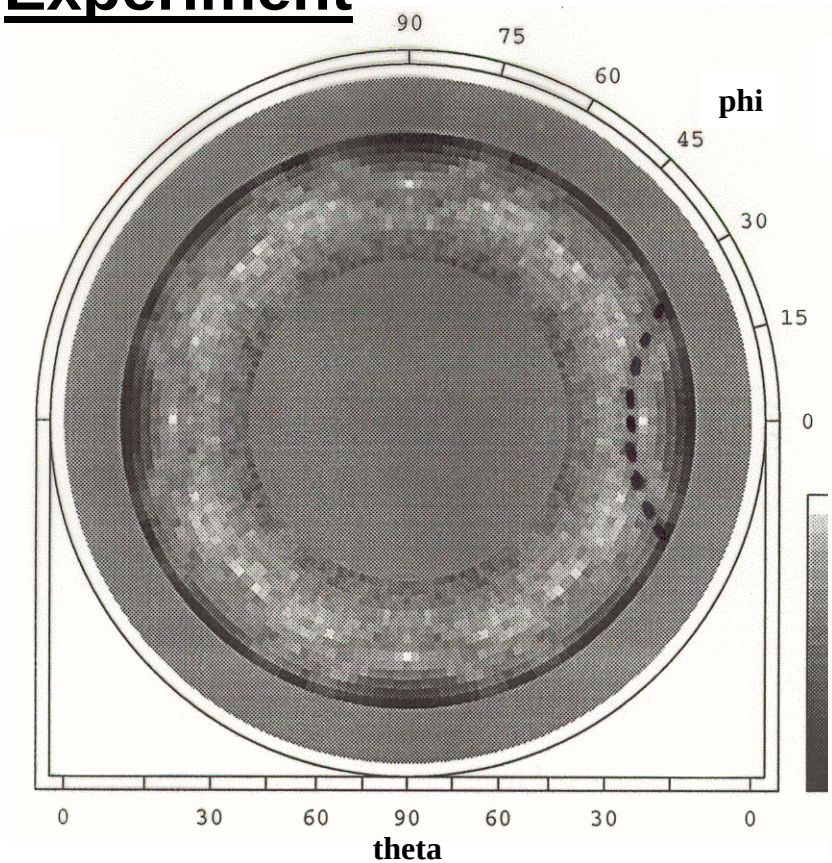

Theory

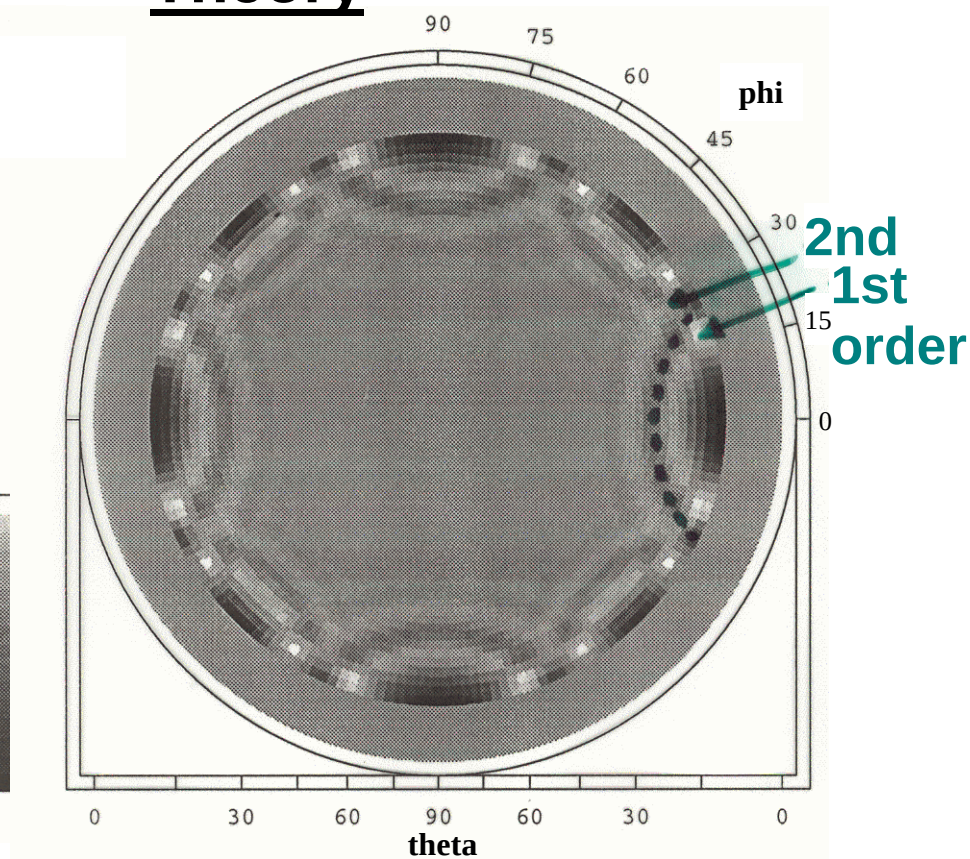

Holographic Images: S/Ni(001)

Fourier transform with scatt. wave correc. in sulfur(xy) plane

Fourier transform with scatt. wave correc. in yz plane

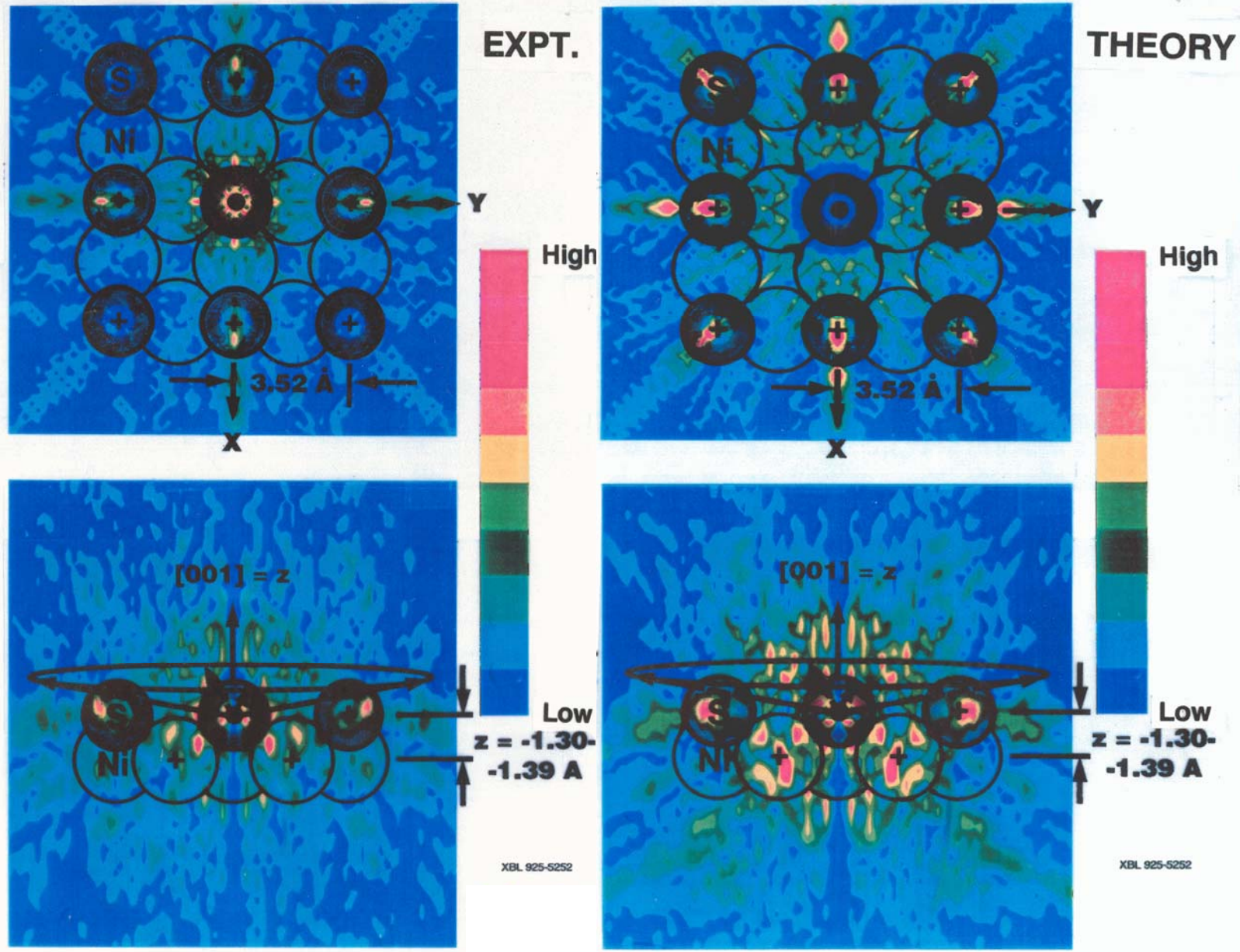

Thevuthasan et al., Phys. Rev. Lett. 70, 595 ('93)

Derivative photoelectron holography: As and Si emission from As/Si(111):

$$U(\vec{r}) = \left| \iiint \chi(\vec{k}) \exp[i\vec{k}\cdot\vec{r} - ikr] d^3k \right|$$

$$\text{with } \chi = \frac{I(\vec{k}) - I_0}{I_0}$$

and $I(\vec{k})$ from int egration of log arithmic derivative

$$L(h\nu, \hat{k}) = \frac{I(h\nu + \delta, \hat{k}) - I(h\nu - \delta, \hat{k})}{\left[I(h\nu + \delta, \hat{k}) + I(h\nu - \delta, \hat{k}) \right] \delta}$$

$$I(\vec{k}) \equiv I(k, \hat{k}) = A \int L(h\nu, \hat{k}) d^3k$$

Luh, Miller, Chiang, PRL 81, 4160 (1998)

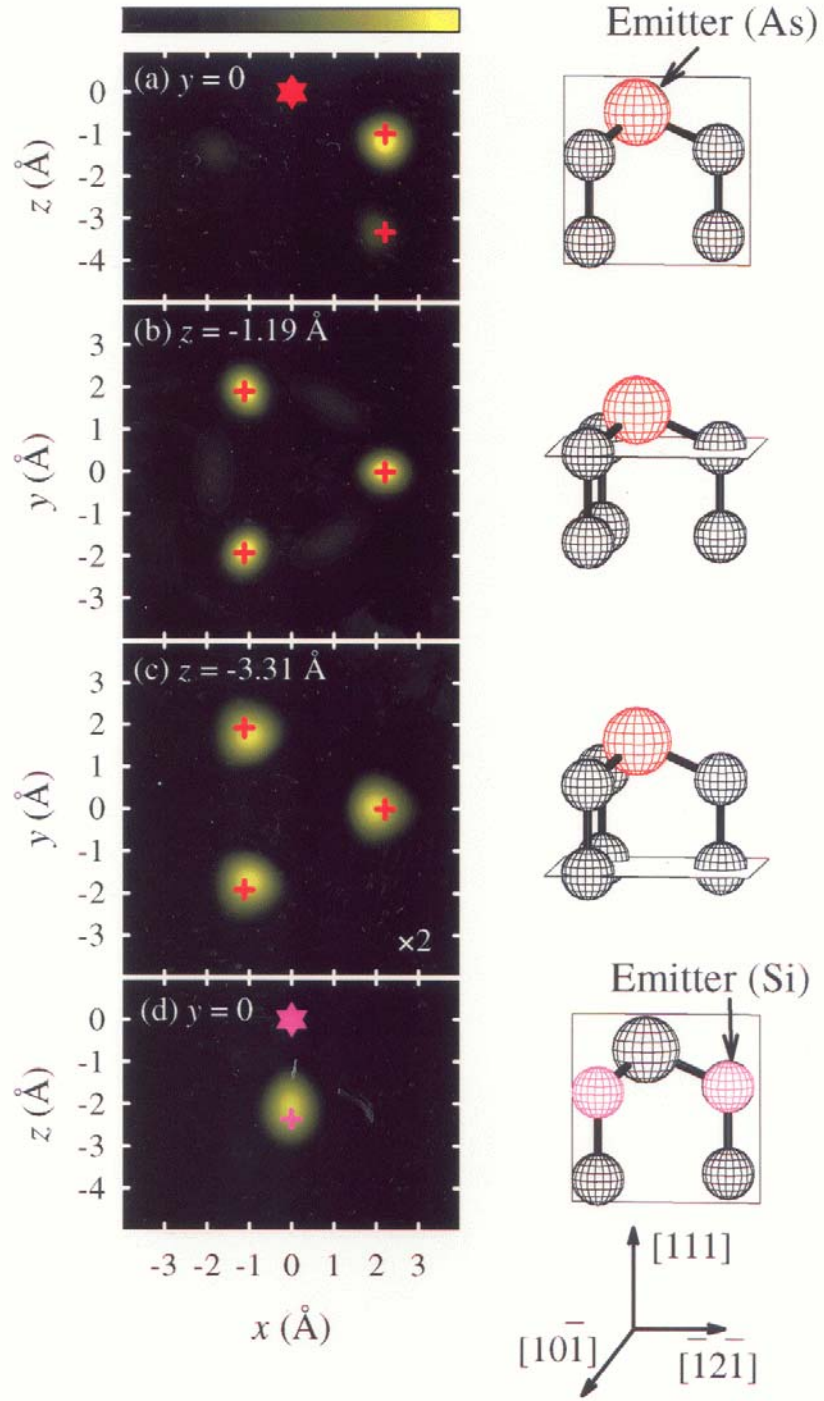

Single-atom holograms

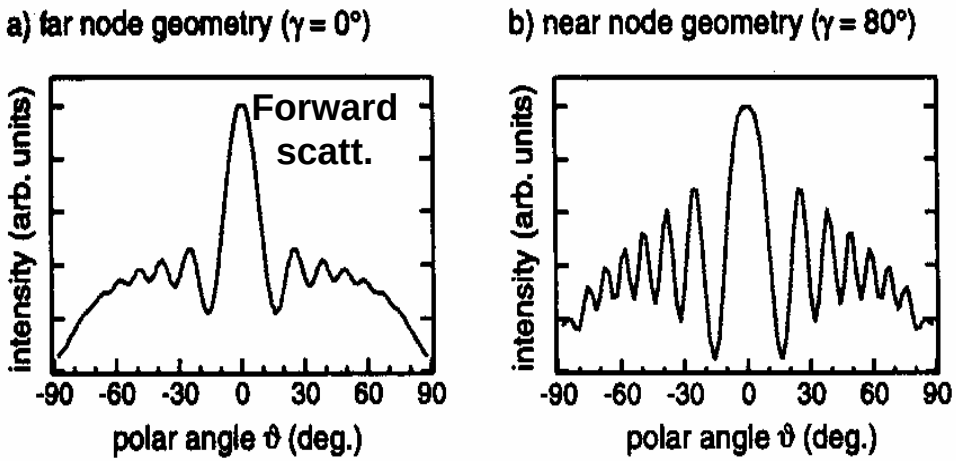

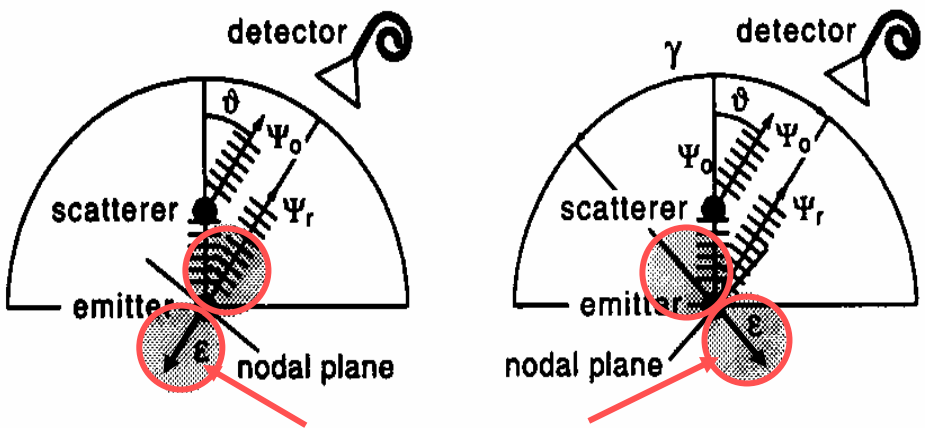

$$M(\vec{k},\vec{r}) \propto \sqrt{\text{photoe}^- \text{ cross sec.}}$$
$$= \hat{\varepsilon} \cdot \hat{k}$$

Wider et al. PRL
86, 2337 (2001)

Near-node photoelectron holography: Al 2s emission from Al(111)

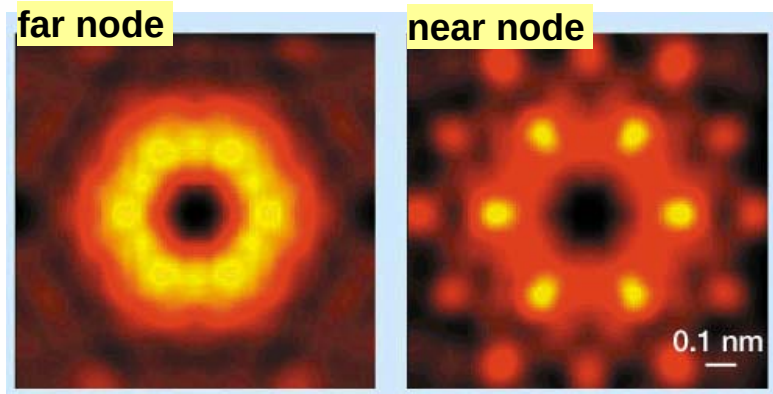

Images around
typical Al emitter

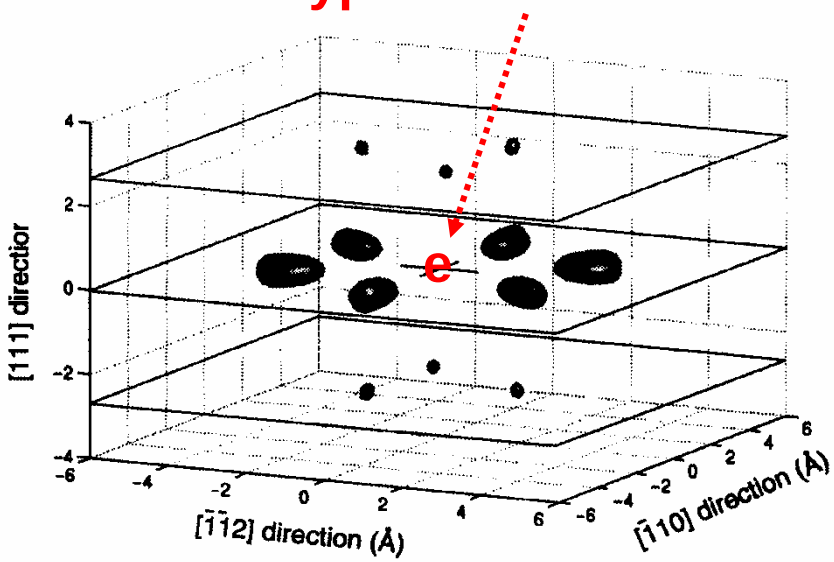

Cu 3p-Cu(001)--differential photoelectron holography

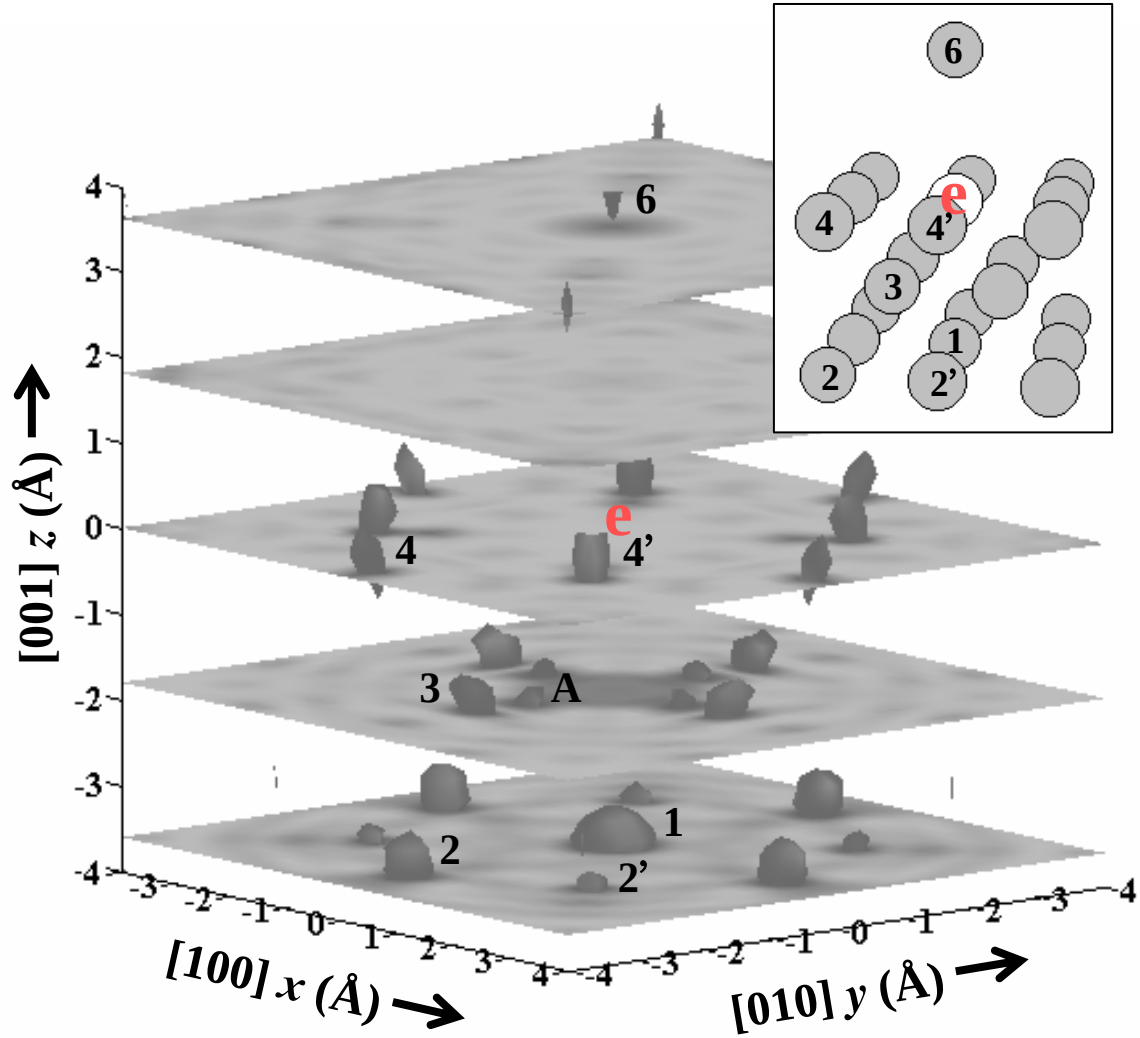

Imaging of back, side, (and fwd.) scattering atoms
(Omori et al., PRL 88, 055504 ('02) and
animations at http://electron.lbl.gov/marchesini/dph)

Principles of photoelectron and x-ray fluorescence holography:

(a) Inner source holography -direct:

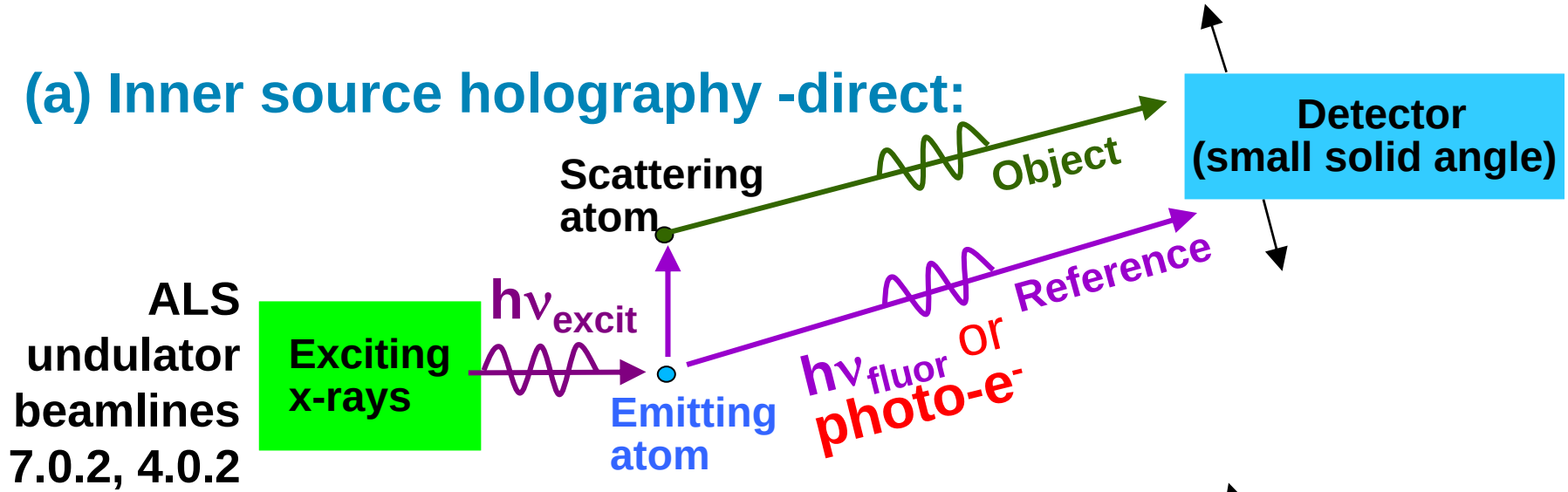

(b) Inner detector holography-inverse:

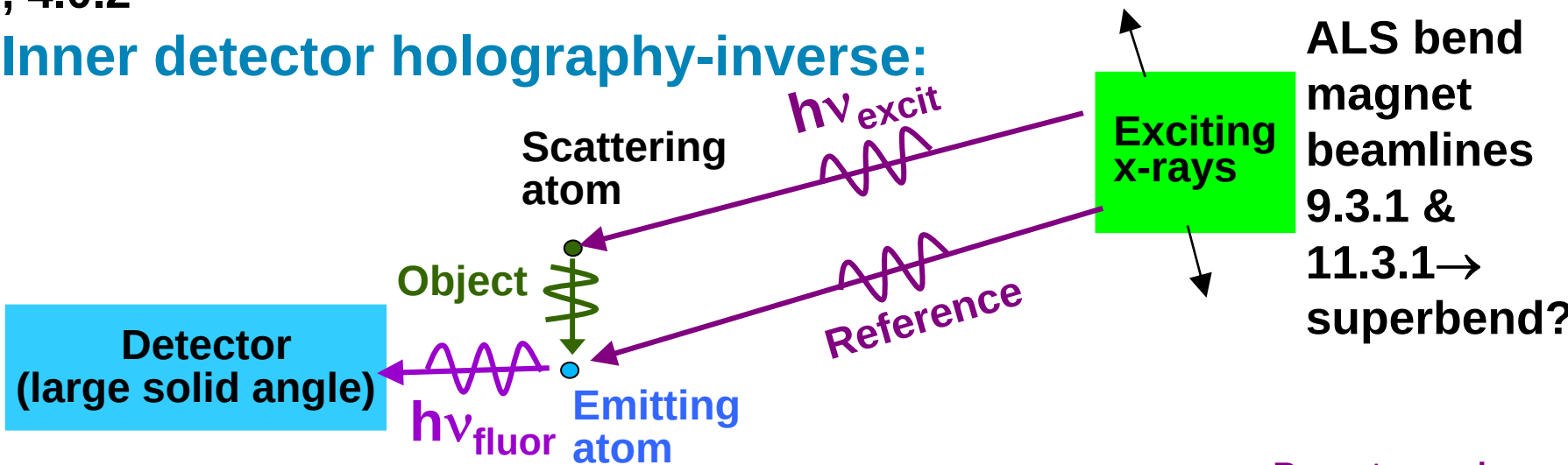

Recent overviews:

G. Faigel and M. Tegze, Rep. Prog. Phys. 62, 355 (1999)

Adams et al., Phys. Stat. Sol. (b) 215, 757 (1999)

C.S.F., M.A Van Hove, et al., J. Phys. B Cond. Matt. 13, 10517 (2001)

Inside-source XFH--the first experiment:

$\underline{Sr}TiO_3$ (100) sample
Mo x-ray tube
Excitation of Sr Kα
@ 14.1 keV with
Mo Kα @ 17.4 keV
Approx. 2 months
data accumulation
10^{10} photons counted
over 2400 pixels in θ , ϕ

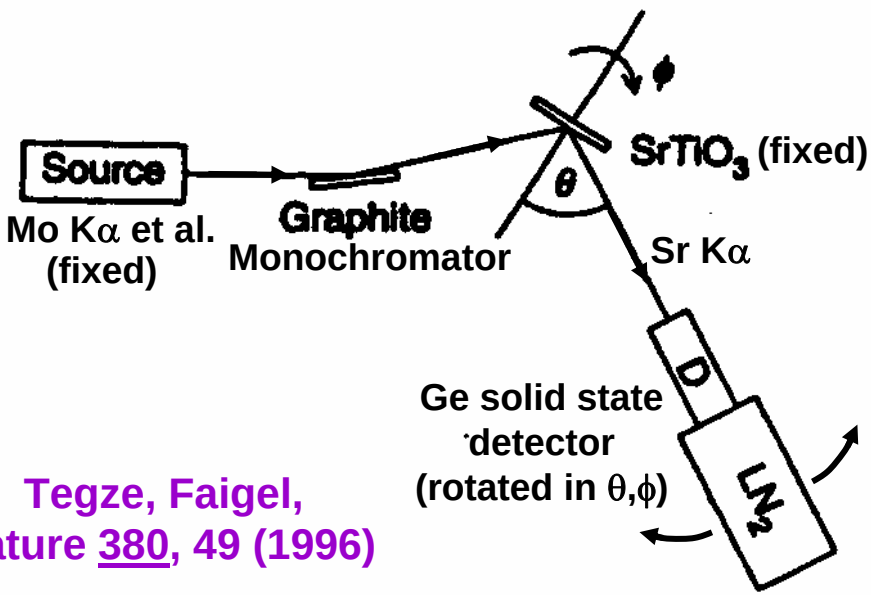

Tegze, Faigel,
Nature 380, 49 (1996)

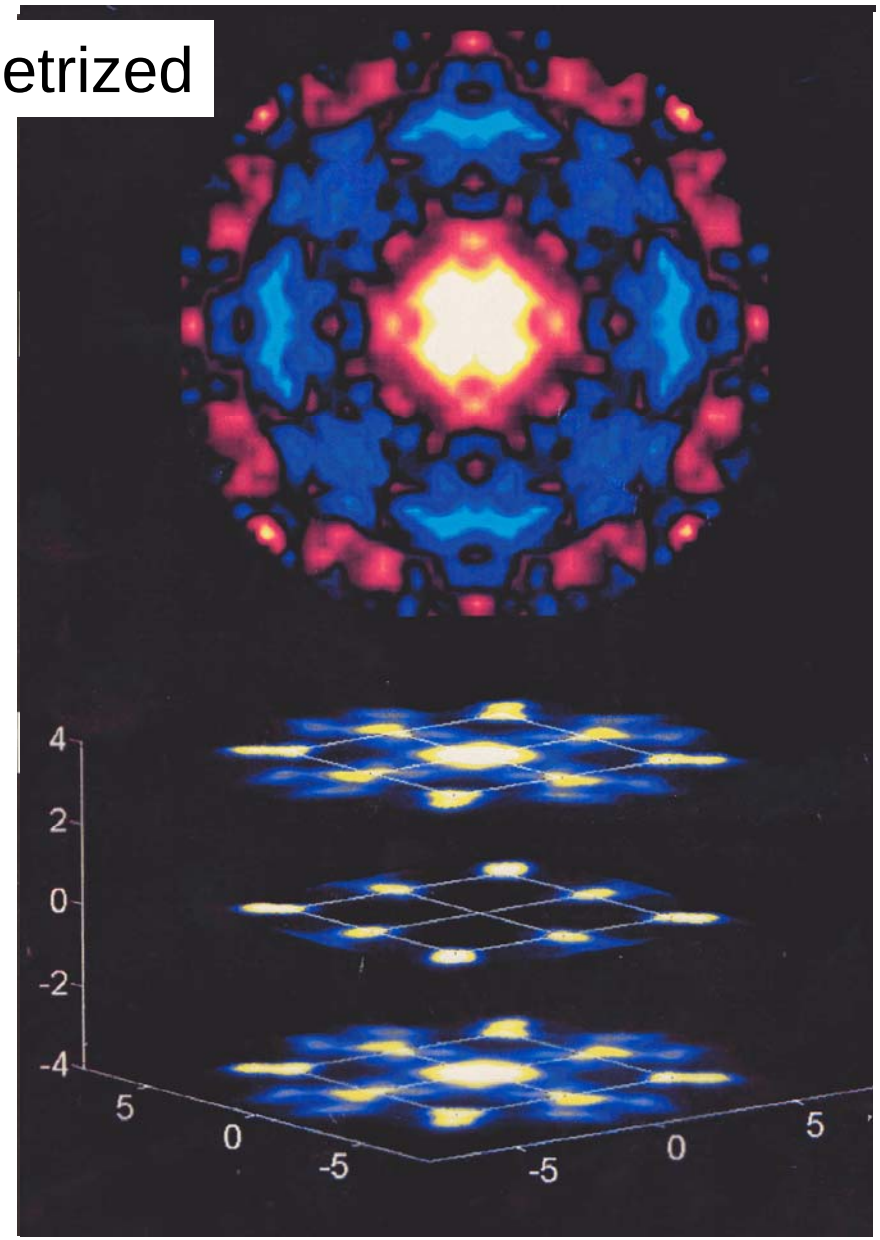

Inside-detector XFH--the first experiment:

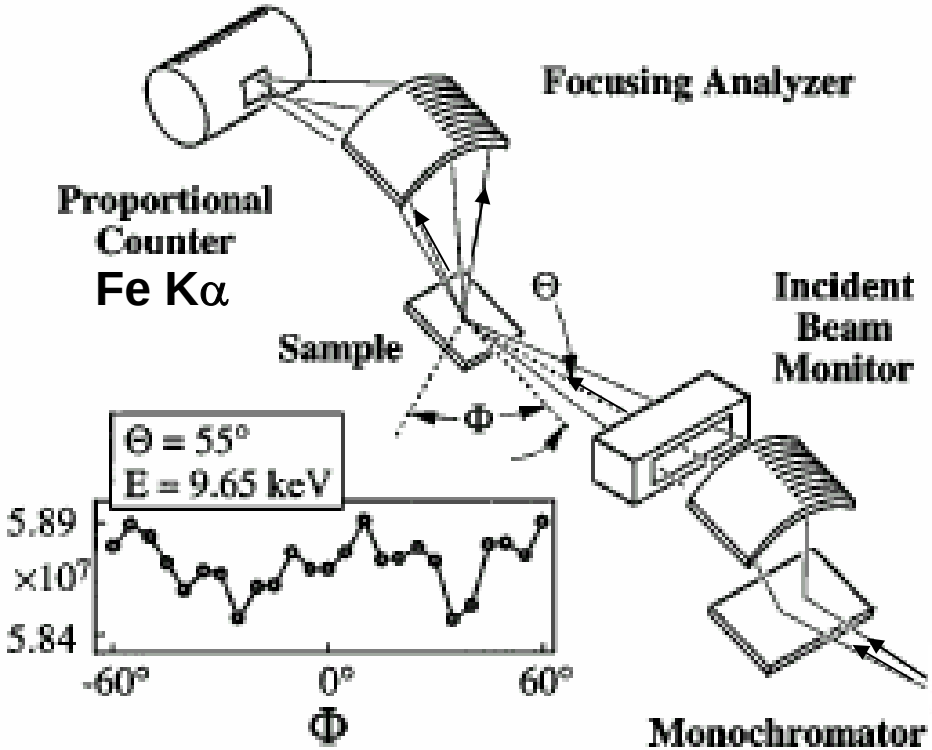

$$\frac{\Delta I}{I_0} \approx 0.5\ \%$$

Gog et al. PRL 76, 3132 (1996)

Images of Fe_2O_3

Can be multi-energy→ "MEXH"

Resolution much worse in perpendicular plane:

$$\Delta k_x = \Delta k_y >> \Delta k_z$$

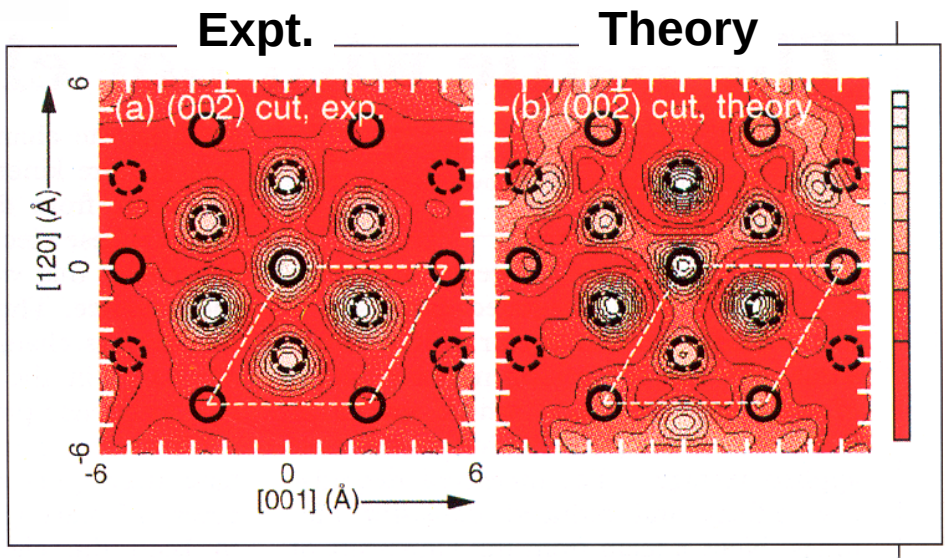

XFH at ESRF: CoO(111)

Inside source:
hν = 6.92 keV

Inside detector:
hν = 13.86 keV

Multi-energy transform

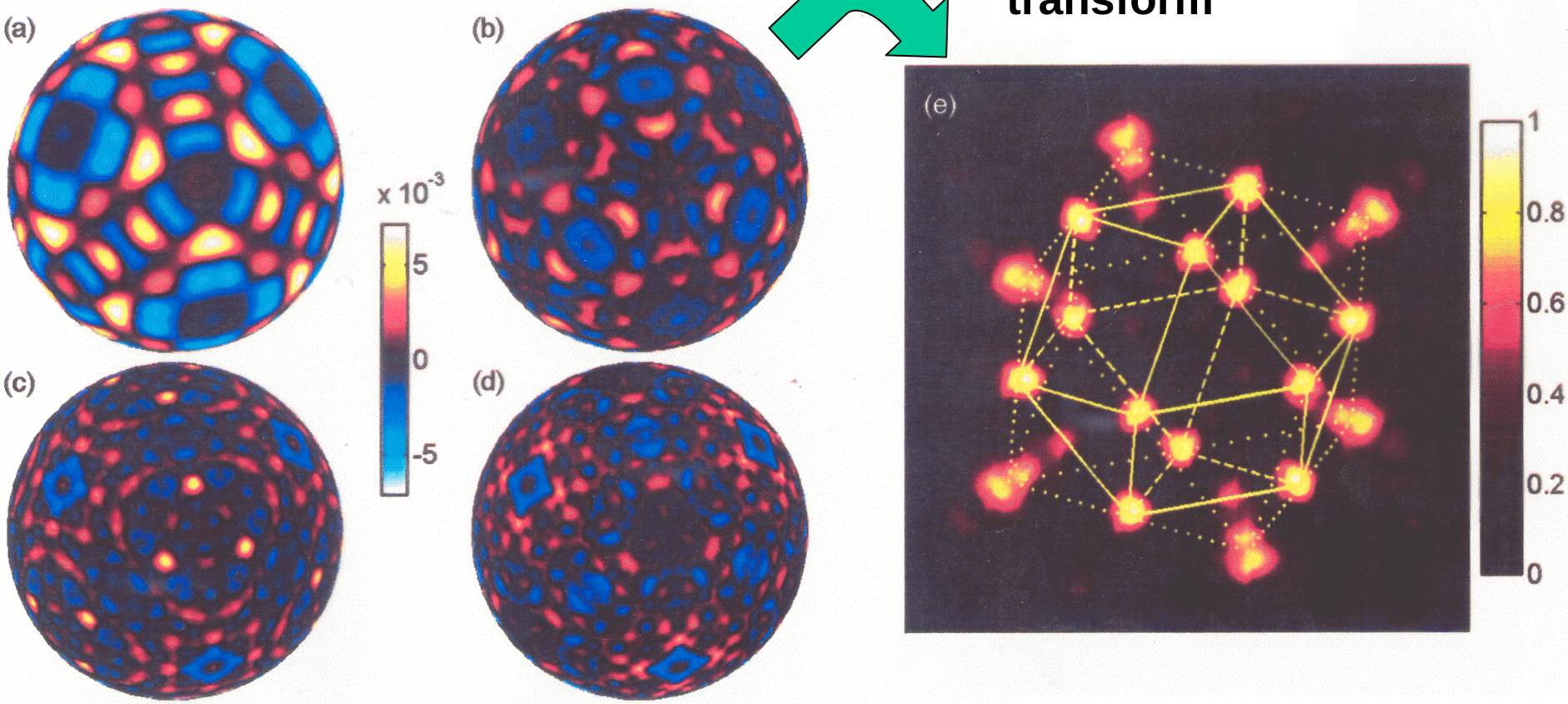

Inside detector:
hν = 17.44 keV

Inside detector:
hν = 18.92 keV

Tegze, Faigel, Marchesini et al., Phys. Rev. Lett. 82, 4847 ('99)

Multi-Energy Inside-Detector X-Ray Holography of NiO

Full hologram with Kossel lines

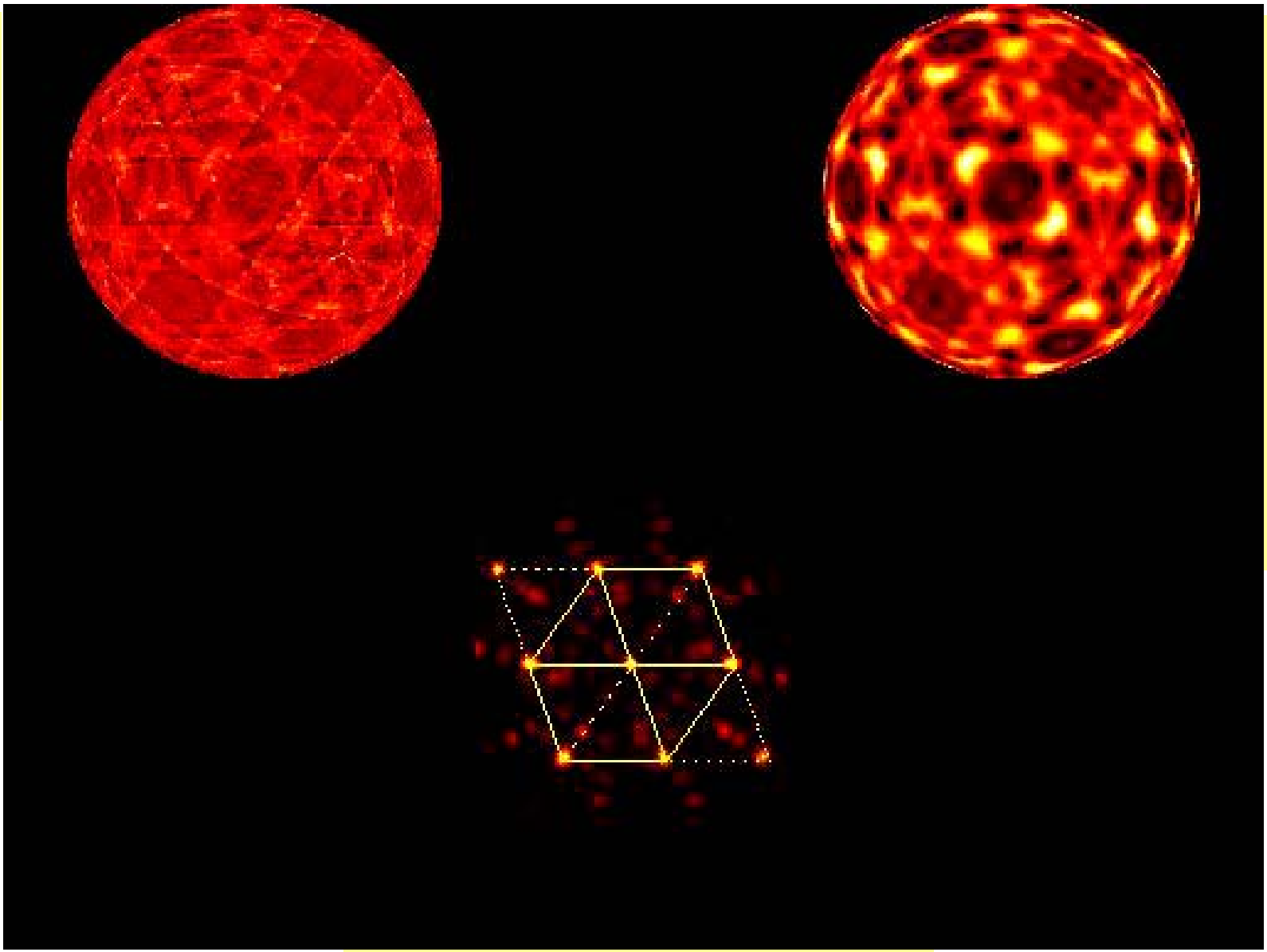

Smoothed hologram →short-range structure

Ni and weaker O images

Marchesini et al., Nature 407, 38 (2000)

XFH at ESRF: some highlights

Imaging light atoms:

Nature 407, 38 (2000)

- **O around Ni in NiO**
- **~150 O and Ni atoms imaged**

Inside detector-
Ni Kα Hologram

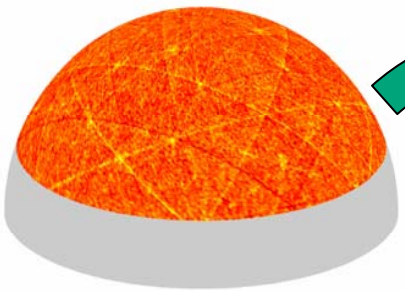

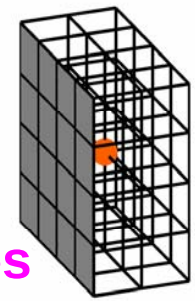

Images

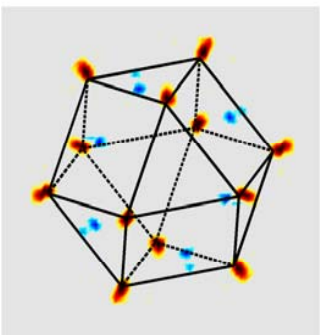

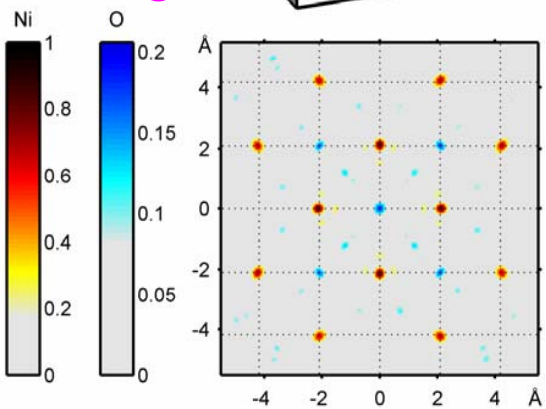

Imaging a quasicrystal:

Phys. Rev. Lett. 85, 4723 (2000)

- **method works without true periodicity**
- **neighbors around Mn in MnAlPd**
- **image of average atomic distribution**

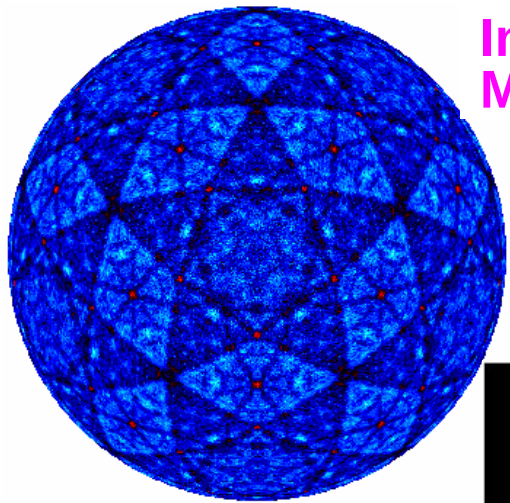

Inside detector-
Mn Kα Hologram

Image

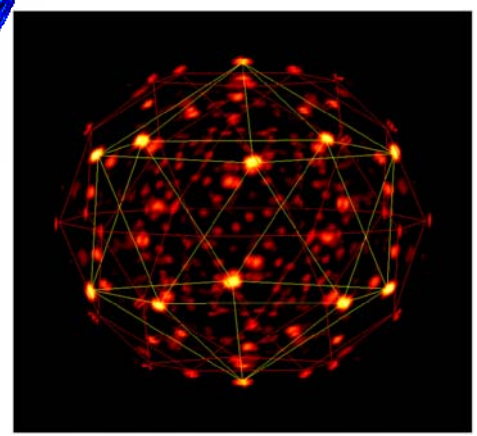

X-ray Fluorescence Holography at the ALS

(a) Experimental setup:

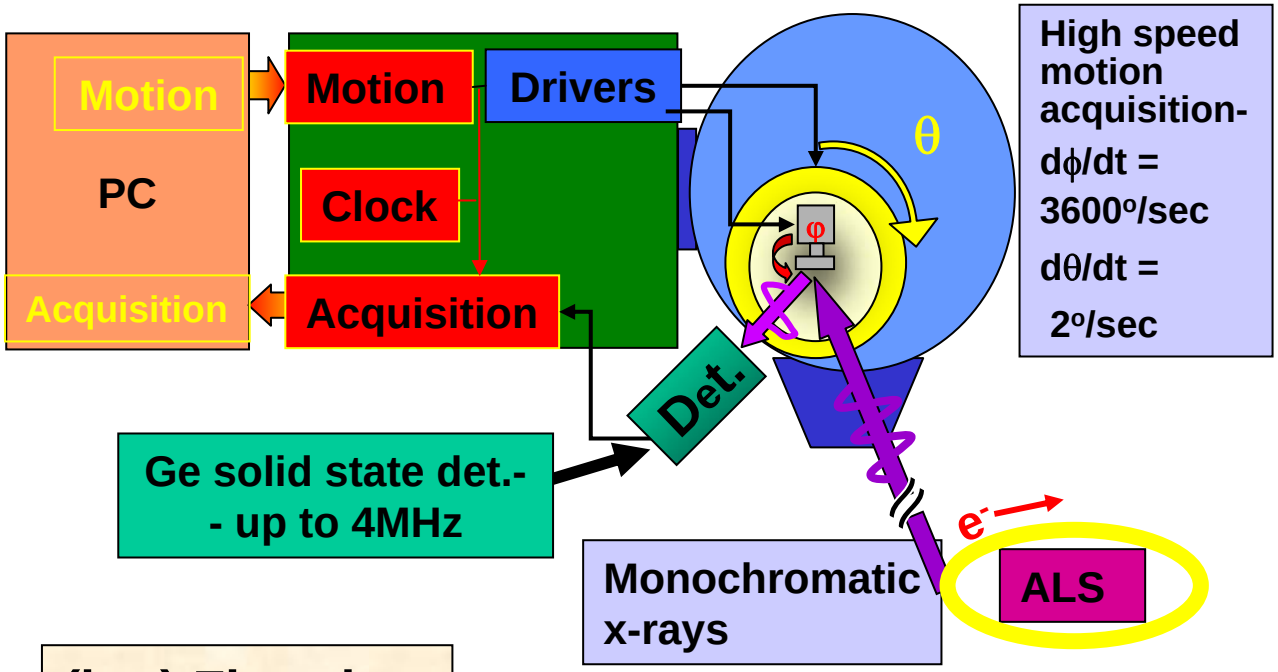

Future plans

- Sample heating/cooling-phase-transition studies
- Applications to: strongly correlated materials (CMR high-T phases), magnetic quasicrystals, bio-relevant crystals
- Development of:
  - -Resonant and dichroic XFH
  - -More efficient pixel detectors

(b-e) First data